order-disorder transitions in plastic crystals

by Chodziwa-dziwa Crossley Mjojo
BSc (MALAWI), ARACI

a thesis submitted for the
degree of Doctor of Philosophy
in the Australian National
University, Canberra

November 1975

This thesis describes original research undertaken by the author in the Australian National University. The material has not, either wholly or partially, been submitted for a degree in this or any other University. Full acknowledgement has been given wherever work from other workers, either through collaboration or the literature, is used.

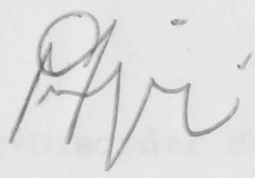

contents

acknowledgements

It was indeed very exhilarating when Prof. I.G. Ross accepted me to study under him in this university, and I am extremely thankful for the keen interest he has taken in the welfare of my family during our stay in Canberra. Committed to providing me with a diverse experience in the field of chemical physics, he invited Prof. A.N. Hambly, another eminent scientist, to join him in the supervision of my work. It is Prof. Hambly who introduced plastic crystals to the group. Together, they have provided me with one of the most stimulating supervisions that one can possibly imagine. Both of them have at one time or another taken up very powerful executive positions in the university, and Prof. Ross is currently the Pro-Vice-Chancellor of the University. Approval for official visits to other laboratories outside the university came very generously.

I am very grateful to Dr. C.K. Coogan (Div. Chem. Phys., C.S.I.R.O., Melb.) and Mr. H.K. Welsh (National Measurement Laboratory, C.S.I.R.O., Syd.) for accepting me as guest worker in their respective research groups of their laboratories, during which the work on solid-state n.m.r. and dielectric properties was carried out. I am also grateful to Mr. S. Filipczuk for arranging a day-visit to the School of Chemistry, University of Sydney, during which the dipole moment of camphoric anhydride was determined.

I am very indebted to Dr. P.A. Reynolds and Dr. D. Taylor (A.N.U.) for providing me with copies of QCFF/PI (the quantum mechanical extension of the consistent force field to π-electrons) and ORTEP (the Oak-Ridge thermal ellipsoid plot) program packages, and initiating me to their use. The former program has been used in the crystal structure calculations; and the latter, in the drawing of the predicted structures. Discussions with these people, Prof. A. Brown, Dr. Meta Sterns and Dr. R.O. Watts (A.N.U.) proved very useful. I am grateful to the staff of the A.N.U. Computer Centre who were always ready for help. Thanks are due to Miss Denis de Zwart (Stephenson & Turner Architects, Adelaide) who proof read a substantial part of the thesis.

On behalf of my family I would like to thank Dr. S.V. Boyden (A.N.U.), Dr. H.P.B. Harvey (Prince Alfred Hosp., Sydney), Dr. N. Vanzetti (Coll. of Adv. Ed., Canberra), Bob Sutton (Coll. of Adv. Ed., Tasmania) and their families for a close friendship and much assistance during our stay in Australia. Members of the first three families are God-parents for our son Dalitso Vickers Mpagwila who was born in Canberra and whose second name is after Dr. Boyden. It has been a great pleasure to be associated with the Urban Biology Group of this university which is headed by Dr. Boyden, and through which I have learned a great deal.

I would like to thank my parents, particularly Anamasina (my mother) and Paster Albert Kambuwa (my grandfather), for a lot of moral support throughout my educational career. I am very grateful to my uncle Mr. Patrick Kambuwa and my former secondary school teacher, friend and benefactor Bill Herman (Ford Foundation, N.Y., U.S.A.) who played a very crucial role both financially and morally during my secondary education

after the death of my father. Bill's assistance was deeply appreciated by my parents as it often relieved my uncle of an extra financial burden who already had a large family to attend to. It is remarkable that Bill offered his assistance whilst he was himself just a student (a postgraduate Law student in the University of Michigan). I am extremely grateful to my wife Rose for much understanding and company during the difficult period of thesis writing. She also shared a considerable amount of the computing labour (punching) involved in the preparation of the structural diagrams in chapter 5, and proof-read some chapters.

I would like to express my appreciation to Mrs Margaret Keys for her patience in the typing of the manuscript, Bob Dowhy (A.N.U.) for the preparation of most of the diagrams, and Miss Georgina Hesketh (Div. Chem. Phys., Melb.) for preparing some of the diagrams. I would like to thank all the members of the Chemistry Department for all assistance and friendship I have benefited from them.

Finally I would like to express my gratitude to Prof. J.A. Leistein (University of Malaŵi, and former colleague to Prof. I.G. Ross during their postgraduate training in the University of London), Dr. J.P. Byrne (N.S.W. Inst. of Technology, Syd.; formerly of University of Malaŵi, and former Ph.D. student of I.G. Ross) for much encouragement during my undergraduate training and establishing the necessary contact with Prof. Ross which enabled me to come to Australia. I am very grateful to the Australian Government for awarding me a fellowship under the Commonwealth Scholarship and Fellowship Plan; and to the Australian National University, for awarding me the University's Supplementary Scholarship.

thesis abstract

The thesis has two parts: experimental (chapters 2-4) and theoretical (chapters 5-8). In general, the thesis concerns itself with cooperative phenomena in molecular crystals. The following are abstracts of chapters.

1. The scope of the thesis is defined and the terminology used in the classification of phase transitions is introduced. Statistical mechanical theories of order-disorder phenomena are reviewed.

2. The phase diagrams of *d*- and *l*-camphor and camphor oxime have been re-determined using differential scanning calorimetry. Agreement with earlier measurements is good. The phase diagram of *d*- and *l*-camphoric anhydride has been determined for the first time. Primary concern was with the absence of eutectic behaviour in the phase diagram of camphor; this has been confirmed. Although the three phase diagrams are similar, there are gross differences in the fundamentals involved.

3. Dielectric studies of binary mixtures of *d*- and *l*-camphor have been carried out to supplement existing data and to construct a 'dielectric phase diagram' of camphor. Special emphasis lay on the dielectric properties preceding the solid-state rotational transition in this system. Two types of dielectric absorption mechanisms emerge, characteristic of the optical isomer and the racemic mixture. On the other hand dielectric studies of *d*- and *dl*-camphoric anhydride do not show this difference. Dielectric absorption studies have been carried out both in the rotator and non-rotator phases, to investigate d-c conductivity and Maxwell-Wagner effects in the neighbourhood of the transition.

4. The peak-to-peak linewidths of the solid-state n.m.r. spectra of *d*- and *dl*-camphoric anhydride have been studied between 80 K and 500 K. Both systems show a rapid decrease in linewidth at about 90 K due to rotation of the three methyl groups and another fall at the temperature of the rotational transition. The racemate however shows anomalous line-broadening from 160 K to a maximum at 290 K followed by a rapid fall which precedes the rotational transition.

5. The crystal structures of *d*- and *dl*-camphoric anhydride at room temperature have been calculated in order to examine the crystal packing behaviour at the most microscopic level. Calculated sublimation energies ($(\Delta E_s)_{d-}$ = 70 kJ/mole and $(\Delta E_s)_{dl-}$ = 36 kJ/mole) favour the *d*-crystal by the extent of 34 kJ/mole. A chiral discrimination energy of the same sense is also obtained for camphor from experimental sublimation energies.

6. A generalisation of two-sublattice models of fusion in atomic and molecular crystals (Lennard-Jones and Devonshire; Pople and Karasz; Amzel and Becka) has been attempted. The intention was to develop a scheme by which parameters, such as the number of sublattices and distinguishable molecular orientations, can be selected. It is found that the choice of these parameters made by Lennard-Jones and Devonshire, and by Pople and Karasz, protects the theory to some extent from some of the more difficult physical issues. A single-lattice model also emerges as another possibility in the series of models that may be called upon. Thus a single-lattice model, based on concepts from Eyring's significant structure theory of

liquids has been developed to evaluate thermodynamic properties of fusion in atomic and molecular crystals to the Bragg-Williams approximation. Predicted values of entropy of fusion are in good agreement with experimental data. These are used in conjunction with the known melting points to evaluate the mean positional disordering energies.

7. A more general statistical mechanical model for the evaluation of thermodynamic properties of solid-state rotational transitions in molecular crystals is developed, following in part the approach due to Aston. An analytical expression is obtained for the relative potential energy parameter ν_{eff}; in a single-lattice model, ν_{eff} is a measure of the relative energy barriers for the rotation of a molecule on the one hand and the simultaneous creation of a vacant site and diffusion of the molecule to the vacant site on the other. Analytical expressions connecting T_M and configurational properties of both the rotational and melting transitions are also obtained. Finally thermodynamic functions are generated for the general melting transitions in molecular crystals which involve both positional and rotational disorder simultaneously.

8. Statistical mechanical models are developed in order to provide a qualitative explanation of the binary phase diagrams of *d*- and *l*-systems of camphor-type compounds. It is shown that, in the case of camphor, the superlattice model of mixing, as developed in alloy statistics, is by itself not acceptable. More satisfactory is a combination of the superlattice and the domain models, in such a way that they are allowed to operate on the system at different composition ranges. Both models have been evaluated to the Kirkwood approximation, which in turn has been generalised to cover the case of unequal composition ($x_d \neq x_l$). The anomalous submaximum in the phase diagram of camphor, and the associated premonitory behaviour with respect to the rotational transition, around the racemic composition are attributed to short-range order effects consistent with a mutual repulsion between different optical isomers in the domain mode of mixing. The estimated critical temperature of mixing for *dl*-camphor (59 K) lies below the rotational transition temperature (205 K) and so accounts for the lack of eutectic behaviour in this system. Finally the phase diagrams of camphoric anhydride and camphor oxime are discussed.

papers delivered at conferences

Some of the work presented in the thesis has been presented at conferences by the author in the following papers.

"Order-Disorder Transitions: The Transition Energy at Constant Volume from Transition Energy at Constant Pressure", Fifth National Convention, The Royal Australian Chemical Institute, May 1974.

"Calorimetric Studies of Order-Disorder Phenomena in Camphor and Related Compounds", and "NMR (Broadline) and Dielectric Studies of Order-Disorder Phenomena in *d*- and *dl*-Camphoric Anhydride", International Crystallography Conference, Melbourne (Australia), August 1974.

list of symbols

A	the Helmholtz free energy of the system
A_C	the configurational free energy of the system
A_m	the molecular free energy of the system
A_{mi}	the Einstein free energy function with A'_{mi} and A''_{mi} corresponding to $\tilde{\nu}'_{mi}$ and $\tilde{\nu}''_{mi}$ respectively
C_{mi}	the Einstein specific heat function with C'_{mi} and C''_{mi} corresponding to $\tilde{\nu}'_{mi}$ and $\tilde{\nu}''_{mi}$ respectively
C_P	the specific heat of the system at constant pressure
$C_P(\sigma)$	the specific heat due to the rotation of molecules during the rotational transition at constant pressure
C_V	the specific heat of the system at constant volume
$C_V(\sigma)$	the specific heat at constant volume during the rotational transition
$C_V(x)$	Einstein or Debye specific heat function of the solid
$C_V(v)$	contribution to the specific heat from translational lattice vibrations and intramolecular vibrations
$D(x)$	the Debye function
$E(\rho)$	configurational energy for positional disorder
$E(\sigma)$	configurational energy for orientational disorder
$E(\rho,\sigma)$	configurational energy for orientational and positional disorder
$E(x)$	Einstein or Debye energy function of the solid
E_a	activation energy
E_{mi}	the Einstein energy function with E'_{mi} and E''_{mi} corresponding to $\tilde{\nu}'_{mi}$ and $\tilde{\nu}''_{mi}$ respectively
E_v	the energy needed to create an isolated lattice vacancy
ΔE	mean substitutional disordering energy in the superlattice model
ΔE_{dl}	mean substitutional disordering energy in the domain model
ΔE_s	sublimation energy
$\Delta E'_{eff}$	the effective mean positional disordering energy
$\Delta E'_s$	mean positional disordering energy in a crystal with fluidised vacant lattice sites

E'	the energy required to shift one molecule from one sublattice to a site on any other sublattice when all other molecules are in the initial sublattice.
E''	the energy required to move one molecule within any of the m sublattices from the initial orientation to any of the other orientations when all the other molecules are in the initial orientation.
$\Delta E''$	mean orientational disordering energy
$\Delta E_{Th}(\sigma)$	thermal (as opposed to configurational) energy change at the rotational transition
$\Delta E_{v}(\sigma)$	the configurational energy change at the rotational transition
$\Delta E_{\tilde{\nu}}$	change in Einstein thermal energy at the rotational transition
G	the Gibbs free energy of the system
ΔG_{m}	the molecular Gibbs free energy
$\Delta G(\rho)$	the molecular Gibbs free energy for positional disorder
$\Delta G_{m}(\rho)$	the molecular Gibbs free energy for orientational disorder
ΔH	the enthalpy change at a phase transition
$\Delta H(\sigma)$	enthalpy change at the rotational transition
$\underset{\sim}{H}$	the Hamiltonian of the system
k	the Boltsman constant
K_{T}	the isothermal compressibility
m	number of sublattices in a multi-sublattice model of a crystal lattice (sections 6.2 and 6.3)
	molecular mass (throughout the rest of the text)
n	number of molecular orientations in the plastic phase
n_{V}	number of fluidised vacancies
N	the avogadro number
N_{T}	total number of lattice sites = n_{V} + N, where N is number of molecules
P	pressure
Q	the partition function of the system
Q_{C}	the configurational partition function of the system
Q_{m}	the molecular partition function of the system

Q_{mG}	the molecular partition function for the gas-like molecules
Q_{mi}	the Einstein molecular partition function for the ith mode of lattice vibrations with Q'_{mi} and Q''_{mi} corresponding to the orientationally ordered and a disordered phase respectively
Q_{mS}	the molecular partition function for the solid
R	the gas constant
s	the degree of substitutional order
s_1	the degree of orientational order
S	entropy of the system
S(x)	Einstein or Debye entropy function of the solid
S_{mi}	the Einstein entropy function with S'_{mi} and S''_{mi} corresponding to $\tilde{\nu}'_{mi}$ and $\tilde{\nu}''_{mi}$ respectively
$\Delta S(\sigma)$	the observed entropy change at the rotational transition
$\Delta S_c(\sigma)$	the configurational entropy change at the plastic-phase transition
$\Delta S_{Th}(\sigma)$	the thermal entropy change at the plastic-phase transition
$\Delta S_M(\rho)$	entropy of melting
T	temperature
T_c	rotational transition temperature
$T_c^{(D)}$	the critical temperature of mixing in the domain model
$T_c^{(s)}$	the critical temperature of mixing in the superlattice model
T_M	the ordinary melting temperature
T_{MR}	the rotational melting temperature
U	the internal energy of the system
$\Delta U(\sigma)$	the internal energy change at the rotational transition
$\Delta U_M(\rho)$	the internal energy change due to positional disorder at the melting transition
$\Delta U_M(\sigma)$	the internal energy change due to orientational disorder at the melting transition
$\Delta U_M(\rho,\sigma)$	the internal energy change at the melting transition
v_m	molecular volume
V	volume
V_s	molar volume of a solid

W_c	work done by the system at the rotational transition
W_m	work done by the system at the melting transition
x	θ_E/T or θ_D/T where θ_E and θ_D are the Einstein and Debye characteristic temperatures
x_d	mole fraction of *d*-molecules in binary systems of optical isomers
Z	coordination number
α	the thermal expansivity
ε'	the relative permittivity of a dielectric
ε''	the dielectric absorption factor
ζ_ℓ	number of moles of lattice sites
κ_T	specific conductance
λ	a constant defined on page **115**
μ	the nth central moment of the configurational energy probability density function
μ_D	dipole moment
$\tilde{\nu}_{mi}$	frequency of lattice vibration with $\tilde{\nu}'_{mi}$ and $\tilde{\nu}''_{mi}$ corresponding to the orientationally ordered and disordered solids respectively
ν_{eff}	the ratio $\Delta E''_0/\Delta E'_{eff}$ and is a measure of the relative energy for the rotation of a molecule on the one hand and the simultaneous creation of a vacant site and diffusion of the molecule to the site on the other hand
$(\nu_{eff})_c$	the critical relative disordering energy corresponding to the case where both orientational and positional disordering processes occur at the same temperature
ρ	(single-lattice model) fraction of solid-like molecules
ρ_i	(multi-sublattice model) fraction of molecules in the ith sublattice
σ_j	fraction of molecules in the jth orientation
$\hat{\sigma}_1$	the equilibrium value of the fraction of molecules in the reference (initial) orientation
χ	number of moles of fluidised vacancies, $\chi = 1 - \rho$
ψ	reduced entropy function for positional and orientational disorder

$\psi(\rho)$	reduced entropy function for positional disorder
$\psi(s,x_d)$	reduced entropy function for the substitutional disorder of the binary system with a given composition x_d
$\psi(\sigma)$	reduced entropy function for the orientational disorder of the system
$\Delta\omega$	peak-to-peak linewidth of a solid-state n.m.r. spectrum

list of figures

list of tables

1 introduction

The scope of the thesis is defined and the scheme of terminology used in the thesis is introduced in this chapter. Current theories of order-disorder transitions related to rotational and melting transitions are briefly described.

"A phase transition in a molecular crystal is a little like the elephant in the fable of blind men - it shows different aspects depending on how it is approached."

- Guthrie and McCullough [1]

1.1 The Scope of the Thesis

We are concerned with two aspects of fundamental importance in molecular crystals: *the implications of molecular rotations in crystals and, in two component systems, the effects of composition on solid-state rotational phase transitions.* Our interests have extended to *melting transitions* mainly because molecular rotations are also involved in these transitions.

The *crystal statistics* concerned with *substitutional disorder* between two types of molecules is simplified by choosing molecules which have similar molecular goemetries and crystal packing behaviours. For this reason *binary systems of d- and l-compounds* (optical isomers) appeared to be suitable systems to study. We shall hereafter refer to these systems simply as *d- and l-systems* for a given compound. The choice of substances to study finally fell on camphor and its related compounds, as these compounds comprise of quasi-spherical molecules which exist as optical antipodes and begin to rotate above a certain temperature in the solid before the melting point.

The investigation has called on several techniques. Experimentally, we have employed calorimetry, dielectric studies and solid-state n.m.r. to establish the temperature ranges over which molecular rotation is activated, and the phase diagrams of the substances involved, particularly with respect to the transitions associated with molecular rotation. Theoretically, crystal packing calculations have been used to illuminate the properties of

the crystal at the most microscopic level. From these calculations, and other observations, *discrimination energies* of two of the systems studied have been deduced. Further theoretical investigations have been concerned with the statistical mechanical models for melting transitions and for solid-state transitions associated with molecular rotation. Throughout, we are concerned with the effects of coupling between substitutional disorder and rotational disorder.

1.2 The Plastic Crystal Phase

A crystalline phase in which rigid molecules are free to rotate is called the *rotator* or *plastic crystal phase*. The phase stable below the rotator phase is called the *non-rotator phase*. The phase transition connecting the (low temperature) non-rotator and (the high temperature) rotator phases is called the *rotational transition*. This transition may also be called the *non-plastic crystal-plastic crystal phase transition* or simply the *plastic phase transition*.

Crystals which form plastic crystal phases, generally known as *plastic crystals*, were first recognized by Timmermans [2], and the plastic crystal phase itself is now universally accepted as *a distinct state of aggregation of matter*. Molecules which they comprise tend to be *quasi-globular* or *quasi-cylindrical* in shape. The term plastic refers to the ease with which such crystals can be deformed under external pressure.

Important characteristics of plastic crystals are low entropies of fusion, generally of the order of the communal entropy, and relatively high melting points. Timmermans [2] explains the rotational transition as a consequence of breaking the melting process into two steps: namely, attainment of isotropy, and then liquefaction - the first step absorbs much energy and is due to the rotation of molecules. The crystal structure undergoes reorganization in terms of the packing of spheres or cylinders.

The second step (melting) is due to positional disordering and requires only small entropy change.

1.3 Chiral Molecular Discrimination Energies

Chirality (= handedness) is a well known property of molecules which are characterised by a lack of any improper rotation axis including inversion and reflection. These molecules form isomers which have different *optical activity*, and therefore are called optical isomers, distinguished as *d*- (*dextro*) and *l*- (*laevo*), according to the sense of rotation of plane polarized light (usually, of the wavelength of the sodium D-lines). The equimolar *d*-*l* mixture is referred to as a *racemic mixture*. The word *racemate*, for this racemic mixture, is reserved in this thesis for situations in which the mixture has a distinct crystal structure, so having some of the characters of a compound.

Craig *et al* [3][4] define for a pair of chiral molecules a discrimination energy equal to the difference between the interaction energies of a *d*-*d* pair and a *d*-*l* pair. Their approach is based on multipole-multipole interaction (the multipoles being so defined as to confer chirality on the interacting centres), or else on *ab initio* molecular orbital calculations in the case of very close contacts. For model molecules separated by several Ångströms, in *locked configurations*, they find discrimination energies of the order of 0.5-1.5 kJ/mole. For the closely interacting situations, represented by the isomers of 2,3-dicyanobutane [*d*-$(CH_3)(CN)HC$]-C[*d*- or *l*-$CH(CN)CH_3$)], the discrimination energy is 3 kJ/mole in favour of the *dl*-compound. Very importantly, the discrimination energies over longish distances are found to be substantially reduced in the *weakly coupled limit*, corresponding to the freely rotating molecules in the liquid or gas phases. They have found that in this limit the electrostatic discrimination energy has a leading term in the inverse seventeenth power

of the separation, and can be neglected.

Thus chiral discrimination energies vary from one state to another. In particular we would expect a relatively large discrimination energy to be active in the non-rotator phase; and a reduced discrimination energy, in the rotator phase. Consequently, the properties of the rotational transition will vary with composition in a phase diagram of a binary system of *d*- and *l*-compounds according to the sign and magnitude of the discrimination energy.

1.4 The Nature of Molecular Rotation in the Plastic Crystal Phase

Solid-state molecular rotation can be described according to two models, the *Frenkel model* and the *Pauling model*. The former views each molecule as capable of taking only certain orientations, rather than being in a continuous state of rotation as suggested by the latter. In most cases the Frenkel model is currently considered to be the most realistic [5],[6]. Each molecule is assumed to spend most of its time in one of the *energetically distinguishable allowed orientations*. This implies that the likelihood of a molecule being in a state of transit at any given instant is very small, and therefore that the thermodynamics of the system are practically insensitive to orientation dynamics [5]. The fundamental principle assumed is that the favourable orientations in the rotator phase are those for which the effective point symmetry of the molecule is the same as the symmetry of the lattice site [1] (the site group), in the space group of the rotator phase structure. It follows that the rotational transition may be treated simply as an *order-disorder transition*.

Pauling's model is quantum mechanical. Why are *quantised rotations in the plastic crystal phase* not to be expected even when the orientational disorder may be large? In a vibrating solid the barriers to rotation must change with the phase of the intermolecular vibration. An analogous

barrier to rotation exists even in the liquid. Except in the case of very small molecules like HCl in solution in non-polar solvents, we do not find evidence of quantised rotation because the collision frequency between molecules is greater than the rotation frequency. Thus in both the liquid and the plastic phase the molecule acquiring rotational energy does not have the time to perform sufficient rotations for the energy of the new state to become definite (a consequence of the Heisenberg Uncertainty Principle, $\Delta E.\Delta t \sim h$).

1.5 Statistical Theories of Fusion

There exists a functional relationship between the entropy of fusion and the fractional volume change at the melting point for simple substances (e.g. atomic crystals and plastic crystals) whose melting transitions involve positional disorder only [7]. This observation has been the basis for treating the melting transition as a positional order-disorder transition. We shall now summarise current statistical mechanical theories of fusion.

1.5.1 The Lennard-Jones and Devonshire Model [8]*

Lennard-Jones and Devonshire's (L-J-D) treatment is probably the most successful statistical mechanical theory of fusion for monatomic substances. According to this model the solid is viewed as consisting of two sublattices, symmetrically related to each other, where all the molecules are in one sublattice. Its development was inspired by statistical theories of substitutional disorder (in the 1930's) in alloys, where the two sublattices contained molecules of different types as in β-brass. The rock-salt structure also exemplifies the concept of two sublattices. The L-J-D model views the liquid as *a state of aggregation of matter in*

---

* A valuable review of these theories is presented in reference [17].

which N molecules are randomly distributed over 2N lattice sites. By matching certain theoretical parameters with experimental quantities, eminently reasonable values of thermodynamic quantities (e.g. entropy of fusion) are obtained.

1.5.2 The Pople-Karasz Model [9]*

The Pople-Karasz model is an extension of the two-sublattice model of L-J-D to cover molecular crystals. In this case the liquid is viewed as a *state of aggregation of matter in which the N molecules are randomly distributed over 2N lattice sites and 2 allowed molecular orientations.* The solid is considered as having all the molecules on one of the two sublattices and all the molecules in one of the two orientations. Pople and Karasz define a parameter ν, which is a measure of the relative heights of the potential barriers for the orientational and positional disordering of a molecule in the solid state. They find that the ordering of the two transitions (orientational and positional) depends on the value of this parameter, and for certain critical values both disordering processes occur at the same temperature, so giving rise to the ordinary melting transitions in molecular crystals. The model has been useful in increasing the conceptual understanding of plastic crystals, among other things, but has not been used for quantitative applications because of the added complications from orientational disorder.

1.5.3 The Amzel-Becka Model [10]

This model is a generalisation of that of Pople and Karasz, to include a general number of allowed orientations in the liquid and plastic phases. It is found that the critical values of the parameter ν, introduced by Pople and Karasz, varies with the number of allowed

---

* See footnote on the previous page.

molecular orientations.

1.6 Theories of the Plastic Phase Transition

The Pople-Karasz and Amzel-Becka models deal with the rotational transition in a rather general fashion. Recently theories have appeared which specialise on the rotational transition itself. We briefly describe them below.

1.6.1 The Theory of Aston [11]

This theory uses the same configurational partition function as that of Pople and Karasz for orientational disorder. Instead of using empirical force fields of the L-J-D type for the evaluation of the molecular partition function, Aston proposed an ingenious way for constructing the partition function by the use of theories of solids (e.g. Einstein theory) and spectroscopic data (e.g. I.R. and Raman spectra). We attempt a generalisation of this approach in chapter 7.

1.6.2 Reynolds' Theory [12]

In this theory, the thermal properties associated with the rotational transition are evaluated through a self-consistent model calculation between the thermal expansion and orientational disorder.

1.7 Classification of Phase Transitions

We briefly outline the scheme of nomenclature adopted for the description of phase transitions in the thesis. Details on the subject are contained in references [13],[14],[15],[16].

The scheme of classification of phase transitions that is commonly used is due to Ehrenfest. This approach is based on the mathematical properties of the Gibb's free energy function. The transition is of the nth order if $-\partial^n G/\partial T^n$ is discontinuous (where all the derivatives of order less than n are continuous). Thus a *first order transition* is

characterised by a *continuous* free energy and a *discontinuous* entropy. Similarly a *second order transition* is characterised by *continuous* free energy and entropy, and a *discontinuous* specific heat curve. Higher order transitions can be defined in a similar manner, but are not of current interest.

We have already applied a phenomenological description to the rotational transition by calling it an order-disorder transition. Order-disorder transitions are generally of second order and are referred to as *λ-transitions* from the shapes of their specific heat curves. Amzel and Becka [10] find that these transitions are of first order for n > 2 where n is the number of allowed orientations in the plastic phase. Ubbelohde, however, recommends the description of phase transitions that is based on whether or not the Gibbs free energy is *continuous* during the transition. According to this terminology a *continuous transition* is characterised by a continuous change of one phase into another where the free energy in the *transition region* is not characteristic of either the high- or the low-temperature phase. This leads to his observation that such a transition would be characterised by the coexistence of *domains* (sub-crystalline units) of the two phases in the transition region. This model has been useful in explaining the increase in conductivity and the hysteresis phenomena commonly observed in continuous transitions. He then defines *discontinuous transitions* as those which are characterised by a sharp intersection of the free energy curves of the two distinct polymorphs stable above and below the transition. These transitions may occur when the two structures stable above and below the transition are so different that the transformation requires the breaking of bonds and the reconstruction of the units into the other crystal. Usually the high-temperature structure is more symmetrical than the low-temperature form. This type of transition is called a *reconstructive transition*.

Transitions can also be described according to whether or not they occur isothermally. Thus *isothermal transitions* are those which are characterised by a sharp rise in specific heat. First order transitions tend to be isothermal. *Non-isothermal transitions* are those which occur over a wider temperature range. Continuous transitions (or transitions of higher orders) tend to be non-isothermal.

Returning to Ubbelohde's theory of continuous transitions, we note the emphasis on the *cooperative nature* of these transitions. He observes that a transition of this type never occurs unless the structures of the polymorphs stable above and below the transition are closely related. He observes further that in a discontinuous transformation the prominence of any pre-transition phenomena associated with it often depends on the degree of similarity of structures between the two phases. Thus discontinuous transitions may have both first and second order characteristics where the former occurs after the pre-transition phenomena which in turn may be associated with the latter. In general, order-disorder transitions (particularly those accompanied with a large thermal expansion) tend to show both first and second order characteristics. The treatment due to Aston and followed later in the thesis, takes this aspect into account. We observe that from a statistical mechanical point of view, the coexistent domains in a continuous transition may be attributed to short-range order effects.

1.8 A New Symbolism

An attempt is made to develop a new symbolism that reduces the mounting confusion in the usage of certain symbols which have acquired specific meanings in statistical mechanics for the description of order-disorder phenomena. For example it is customary to use S as an order parameter as well as entropy in the same text. However, we have preserved s for the degree of order.

calorimetric studies of order-disorder phenomena in camphor and related compounds

2

This chapter reports studies of the binary phase diagrams of d- and l-systems of camphor, camphoric anhydride and camphor oxime using the method of differential scanning calorimetry. Emphasis is placed on the rotational transitions in these systems.

2.1 Introduction

The object of the work described here was to provide informative surveys of the thermal properties of camphor, camphoric anhydride and camphor oxime in temperature regions which contain phase transitions. Our interest was in the solid-state rotational transitions which exhibit λ-transition characteristics and account for the order-disorder phenomena observed in these systems. How these solids are capable of undergoing the transition can perhaps be revealed by an inspection of the general shape of the molecules involved (Fig. 2.1). Differential scanning calorimetry was used for the measurements (Perkin-Elmer Model 1B instrument).

2.2 Differential Scanning Calorimetry (DSC)

The method of *differential scanning calorimetry* (DSC) is a modification of *differential thermal analysis* (DTA). The latter had its origins in Le Chatelier's studies on the composition of clays as early as 1887 [15]. The principle involved consists simply of recording the temperature difference between the sample and a thermally inert reference, while the temperature of the environment is programmed. This approach is sometimes called an *adiabatic* or *enthalpy-controlled calorimetry* [18] because the enthalpy is the independent variable, and the temperature the dependent variable. It has been observed [18] that the basic principle of scanning analytical instrumentation involves treating an intensive parameter as an independent variable and an extensive parameter as the dependent variable; and this arrangement is reversed in DTA simply for convenience. This makes the DTA inferior to DSC where the arrangement is in accord to the instrumental criteria. The existence of endothermic and exothermic changes in the case of DTA is indicated by negative or positive peaks respectively (Fig. 2.2).

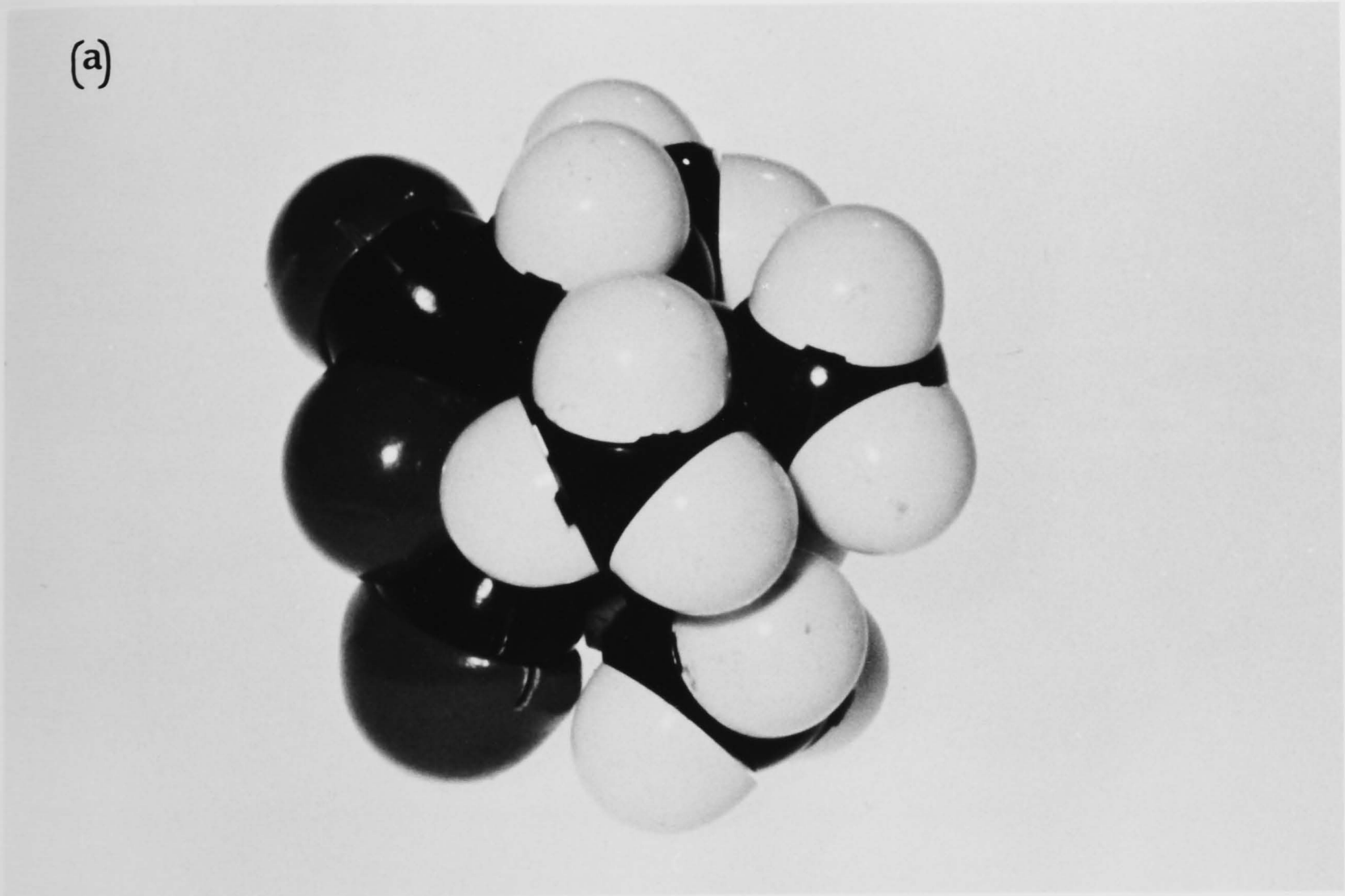

Fig. 2.1: Some representatives of molecules which form plastic phases; (a) camphoric anhydride, (b) methane. Methane is used as a model plastic crystal in the statistical mechanical theories of rotational and melting transitions in chapters 6 and 7.

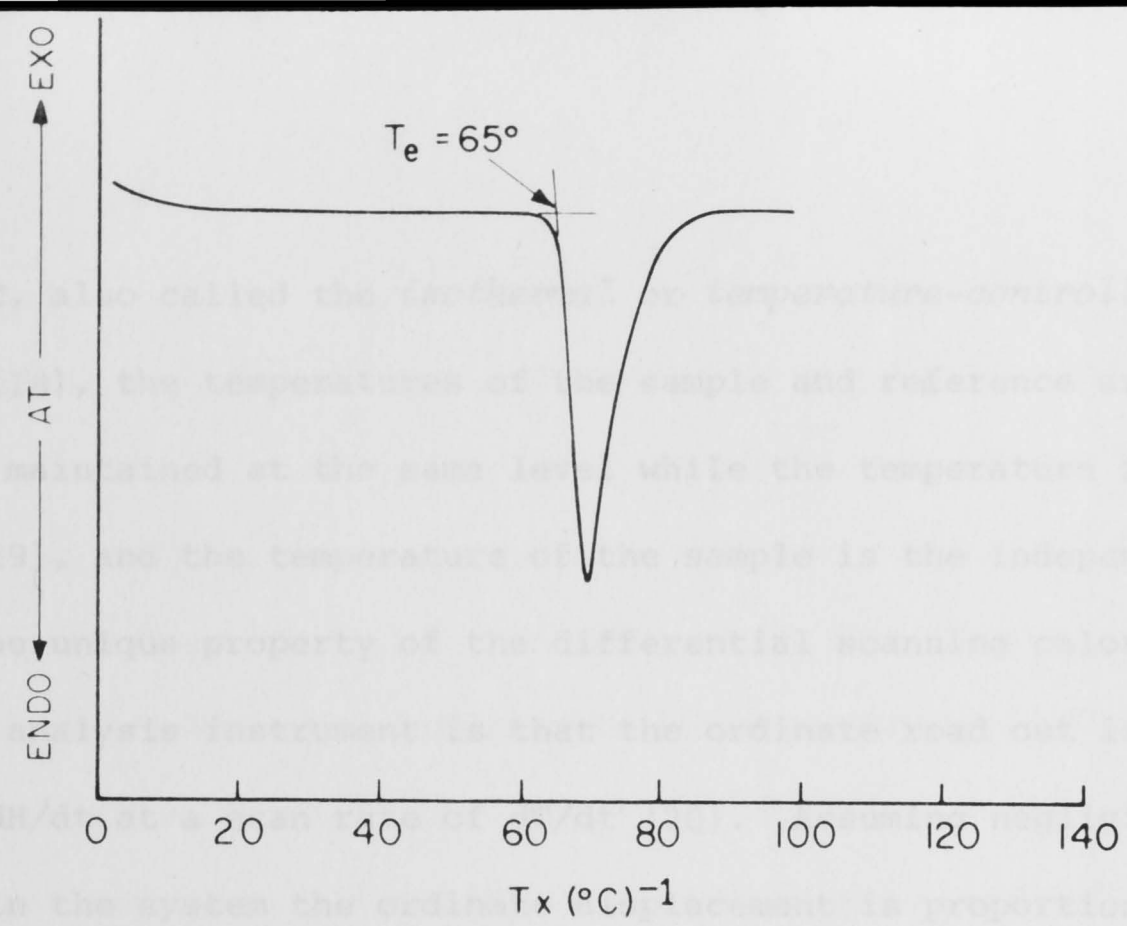

Fig. 2.2: A typical DTA thermogram. Reproduced from [21].

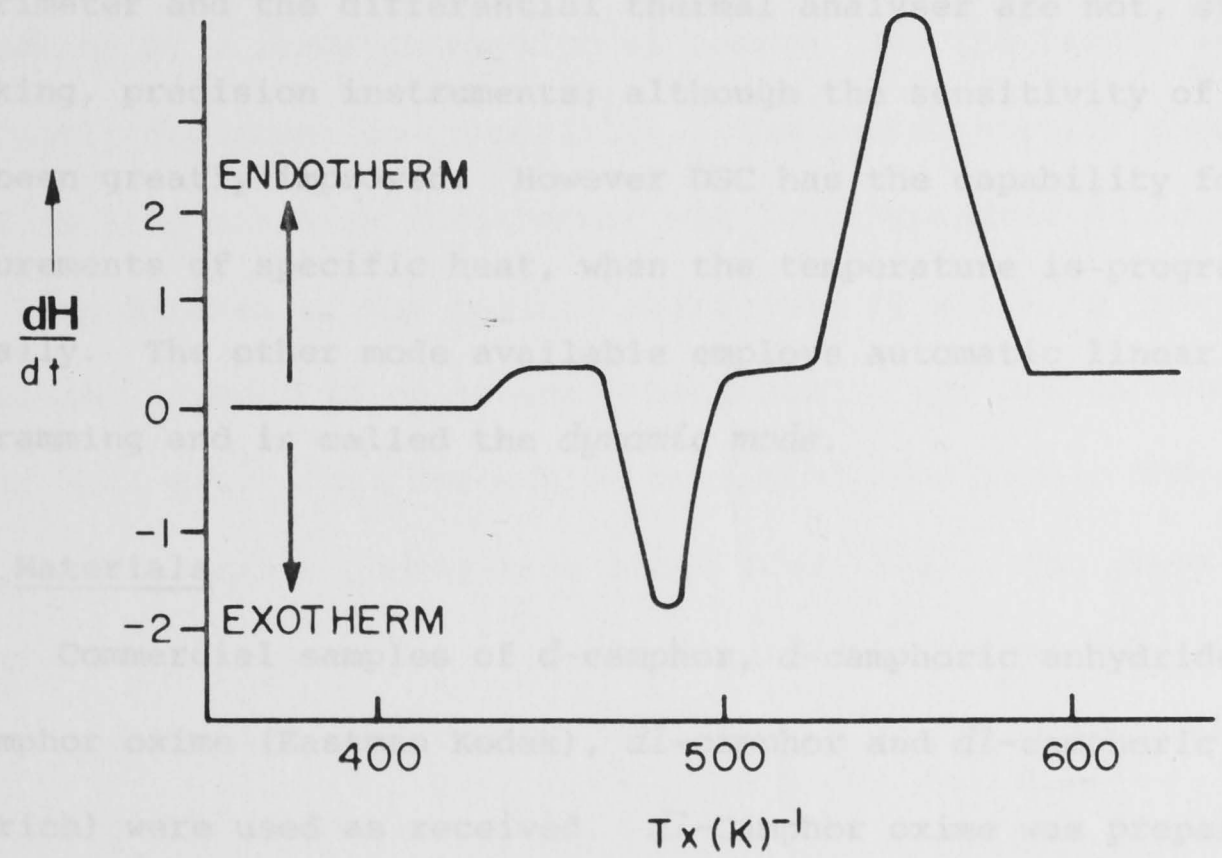

Fig 2.3: A standard format for DSC thermogram publication. Reproduced from [22].

In DSC, also called the *isothermal* or *temperature-controlled calorimetry* [18], the temperatures of the sample and reference are continuously maintained at the same level while the temperature is programmed [19], and the temperature of the sample is the independent variable. The unique property of the differential scanning calorimeter as a thermal analysis instrument is that the ordinate read out is directly to dH/dt at a scan rate of dT/dt [20]. Assuming negligible thermal lag in the system the ordinate displacement is proportional to the specific heat function dH/dT where the proportionality constant is the scan rate. In endothermic or exothermic transitions the thermogram consists of positive or negative peaks respectively (Fig. 2.3). Integrations of the calibrated peak areas give the transition energies.

Both DSC and DTA involve non-equilibrium measurements. This aspect leads to a reduction in precision and a possibility of confusion of kinetic and thermodynamic effects. Thus the differential scanning calorimeter and the differential thermal analyser are not, strictly speaking, precision instruments; although the sensitivity of the former has been greatly improved. However DSC has the capability for precision measurements of specific heat, when the temperature is programmed manually. The other mode available employs automatic linear temperature programming and is called the *dynamic mode*.

2.3 Materials

Commercial samples of *d*-camphor, *d*-camphoric anhydride and *d*-camphor oxime (Eastman Kodak), *dl*-camphor and *dl*-camphoric anhydride (Aldrich) were used as received. *dl*-Camphor oxime was prepared from *dl*-camphor by a standard synthetic method [23].

2.4 Experimental

Calorimetric experiments were conducted via the dynamic mode of the DSC. The temperature reading of the instrument was calibrated with standards of known melting points. The area response (Joule.cm^{-2}) was calibrated using the heat of fusion of indium of 99.999% purity. The areas under the endotherms were integrated with a planimeter. The DSC has a standard sensitivity range of 4.184×10^{-3} J/sec to 0.1339 J/sec as full scale deflection on a standard 10 millivolt potentiometer recorder and noise level of 2%.

2.5 The Phase Diagram of a Binary System of *d*- and *l*-Camphor

The phase diagram of *d*- and *l*-camphor (Fig. 2.4) has been reported by Schäfer and Wagner [24]. Because of the necessary symmetry only one half of the phase diagram was actually measured; the other was constructed as its mirror image. There are three solid phases: III, ordered; II and I rotationally disordered. The rotational phase transition III → II is accompanied by a large absorption of energy, and the transition temperature is strongly dependent on composition. The reconstructive phase change II → I is less markedly endothermic and less dependent on composition. Phase I terminates at the melting point (450 K) which is independent of composition. There is no eutectic behaviour. Our DSC thermograms for the III - II rotational transition consisted of a single endothermic peak over the entire composition range (Fig. 2.5). The phase diagram in the III - II region, so measured (Fig. 2.6)*, agrees well with that of Schäfer and Wagner. The transition energies run more or less in step with transition temperatures.

X-Ray measurements (Table 2.1), carried out for us by Dr. Meta Sterns, show phase II to be hexagonal close packed, and phase I face-centred cubic. Anderson *et al* [25], from X-ray diffraction patterns, found the III - II rotational transition in *d*-camphor to be accompanied

---

* The energy axes in the phase diagrams of *d*- and *l*-camphor and camphoric anhydride are incorrectly defined in the abstracts of papers presented by the author at the International Crystallography Conference held in Melbourne

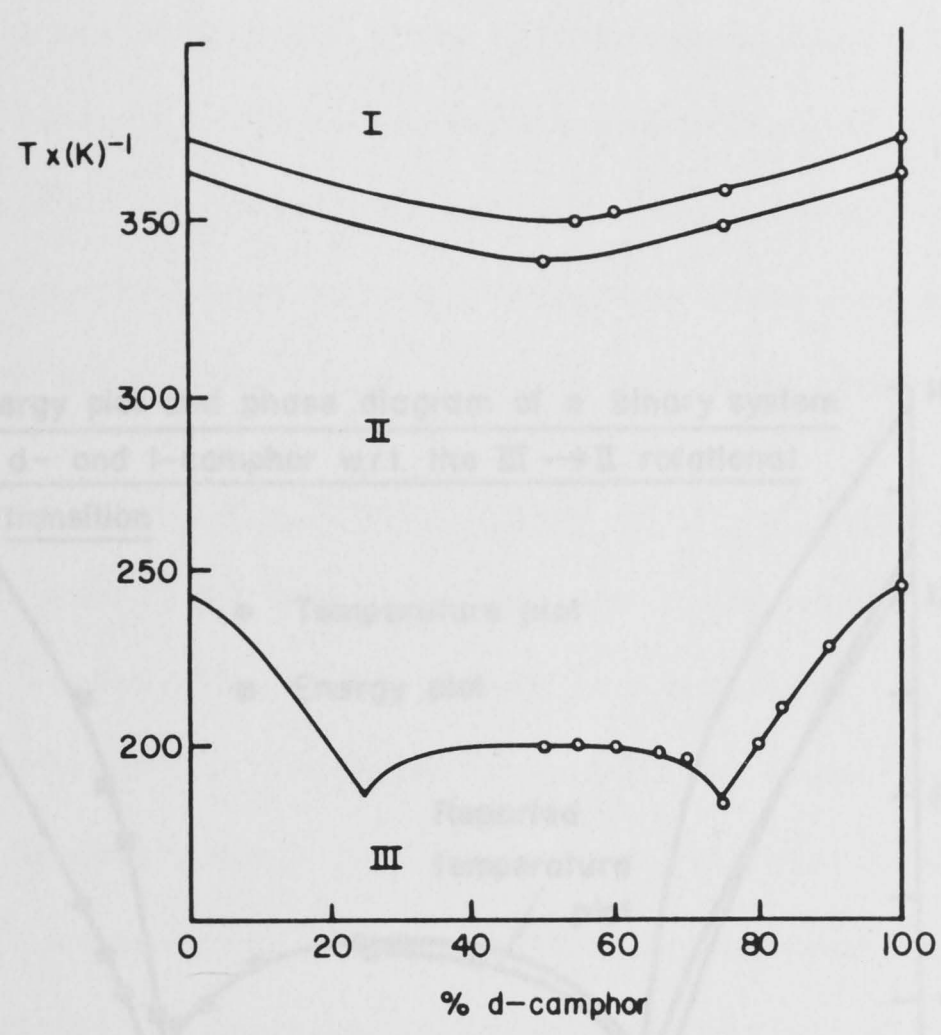

Fig 2.4: PHASE DIAGRAM OF d- AND l-CAMPHOR

(SCHÄFER ET AL Z ELECTROCHEM. 62,328,(1958))

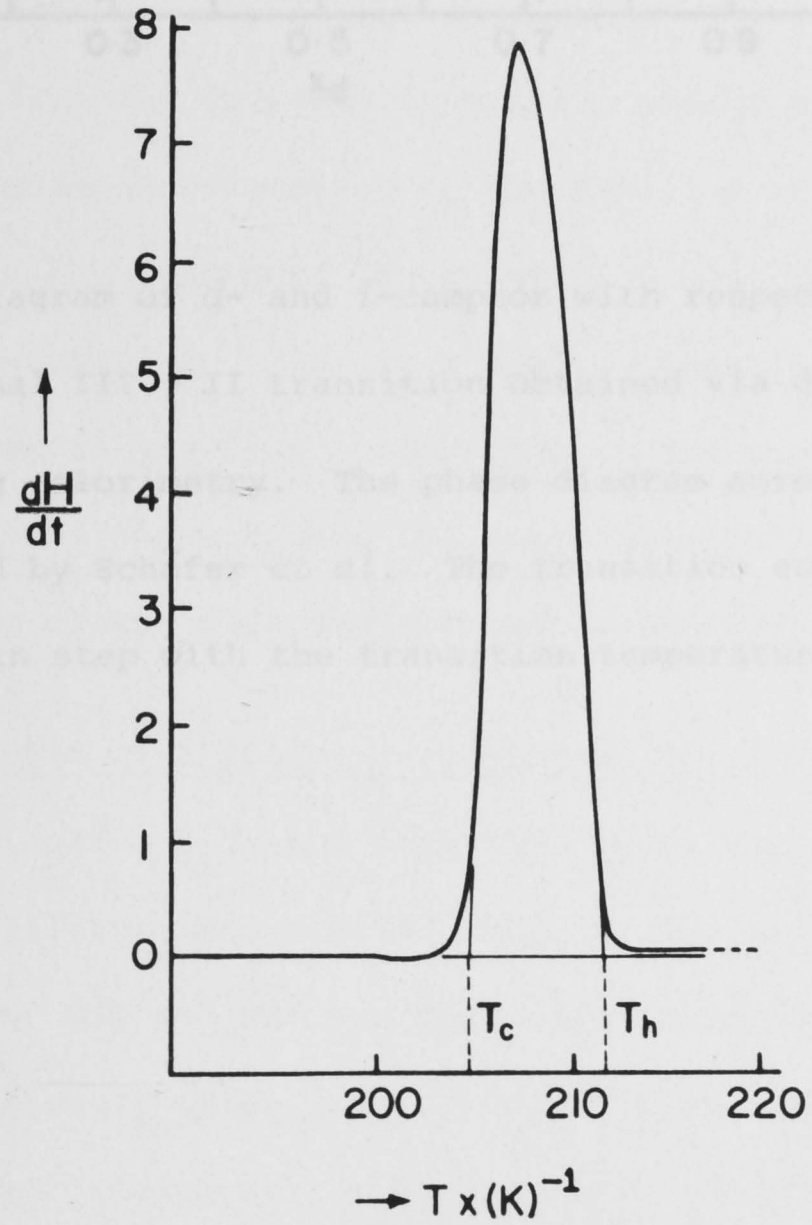

Fig 2.5: A THERMOGRAM OF CAMPHOR

(Australia), August 1974 (page 214). The energy diagrams were corrected to the form presented in the thesis during the presentation of the paper.

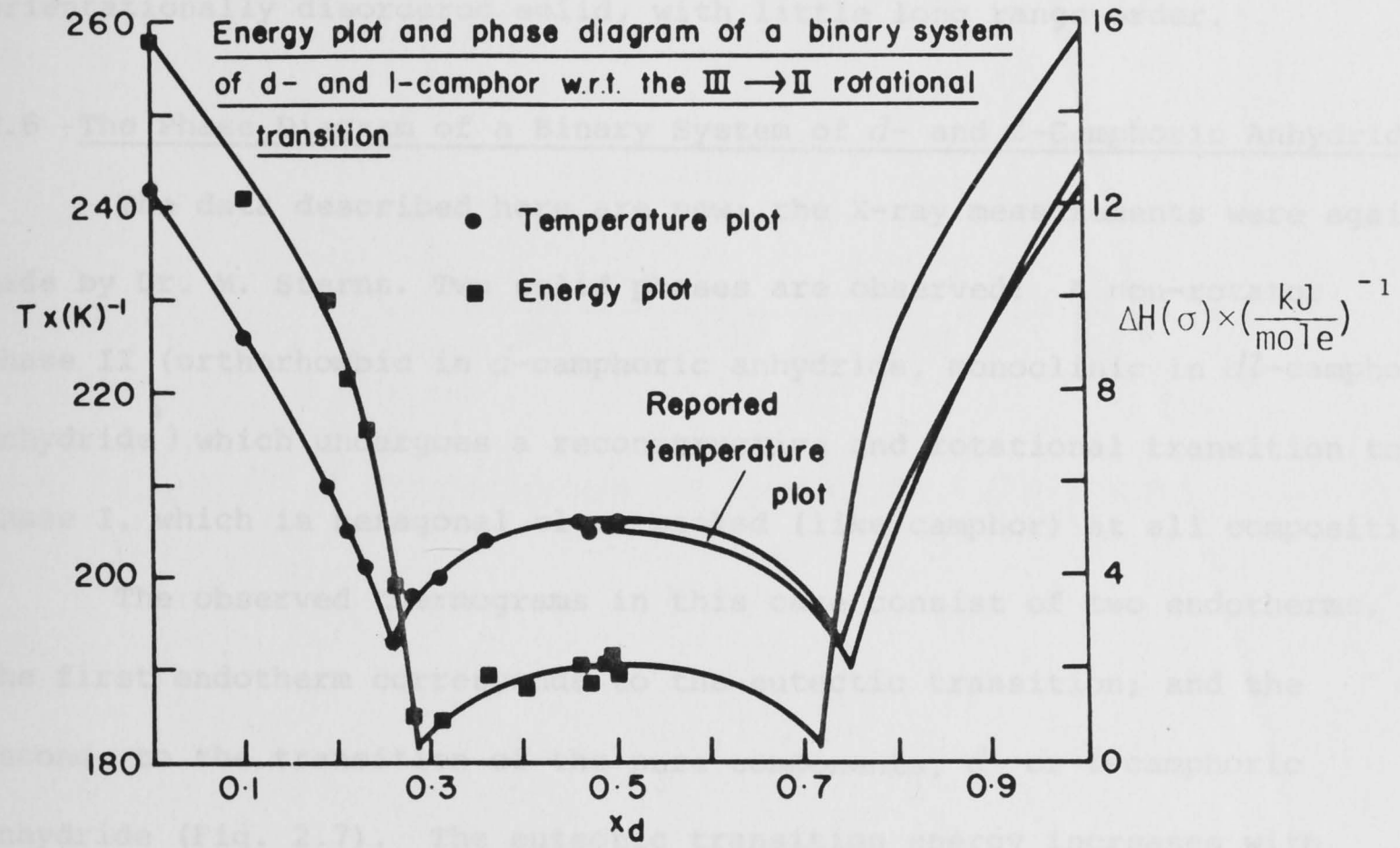

Fig 2.6: Phase diagram of *d*- and *l*-camphor with respect to the rotational III → II transition obtained via differential scanning calorimetry. The phase diagram agress with that reported by Schäfer *et al*. The transition energy $\Delta H(\sigma)$ varies in step with the transition temperature.

by a reconstructive transition from a tetragonal phase III, but in *dl*-camphor they found no evidence of such a sharp change. Rather there was a gradual change of the principal lattice spacings over a wide temperature range. They identify phase III of *dl*-camphor (measured at 77 K) as an orientationally disordered solid, with little long range order.

2.6 The Phase Diagram of a Binary System of *d*- and *l*-Camphoric Anhydride

The data described here are new; the X-ray measurements were again made by Dr. M. Sterns. Two solid phases are observed: A non-rotator phase II (orthorhombic in *d*-camphoric anhydride, monoclinic in *dl*-camphoric anhydride*) which undergoes a reconstructive and rotational transition to phase I, which is hexagonal close packed (like camphor) at all compositions.

The observed thermograms in this case consist of two endotherms. The first endotherm corresponds to the eutectic transition; and the second, to the transition of the pure components, *d*- or *l*-camphoric anhydride (Fig. 2.7). The eutectic transition energy increases with mole fraction of *d*-camphor according to the familiar lever rule until it becomes practically the only peak, at about 0.35 mole fraction. The resultant phase diagram, Fig. 2.8, is a simple eutectic binary phase diagram with respect to the II → I transition. The melting point which terminates the rotator phase I, and the total rotational transition energy (eutectic plus that of the pure components) are independent of composition.

2.7 The Phase Diagram of a Binary System of *d*- and *l*-Camphor Oxime

The phase diagram of *d*- and *l*-camphor oxime was determined by Adriani [26] by a dilatometric method. Miss A. Tom has re-determined the phase diagram by DSC and the new phase diagram agrees well with that obtained dilatometrically (Fig. 2.9). For *d*- or *l*-camphor oxime there are again two phase transitions: a II → I rotational transition, which is accompanied by a large absorption of energy, and melting. A low energy III → II transition occurs for certain mixtures about the

---

* Since *dl*-camphoric anhydride has a unique crystal lattice, we shall hereafter refer to it as the racemate as opposed to racemic mixture.

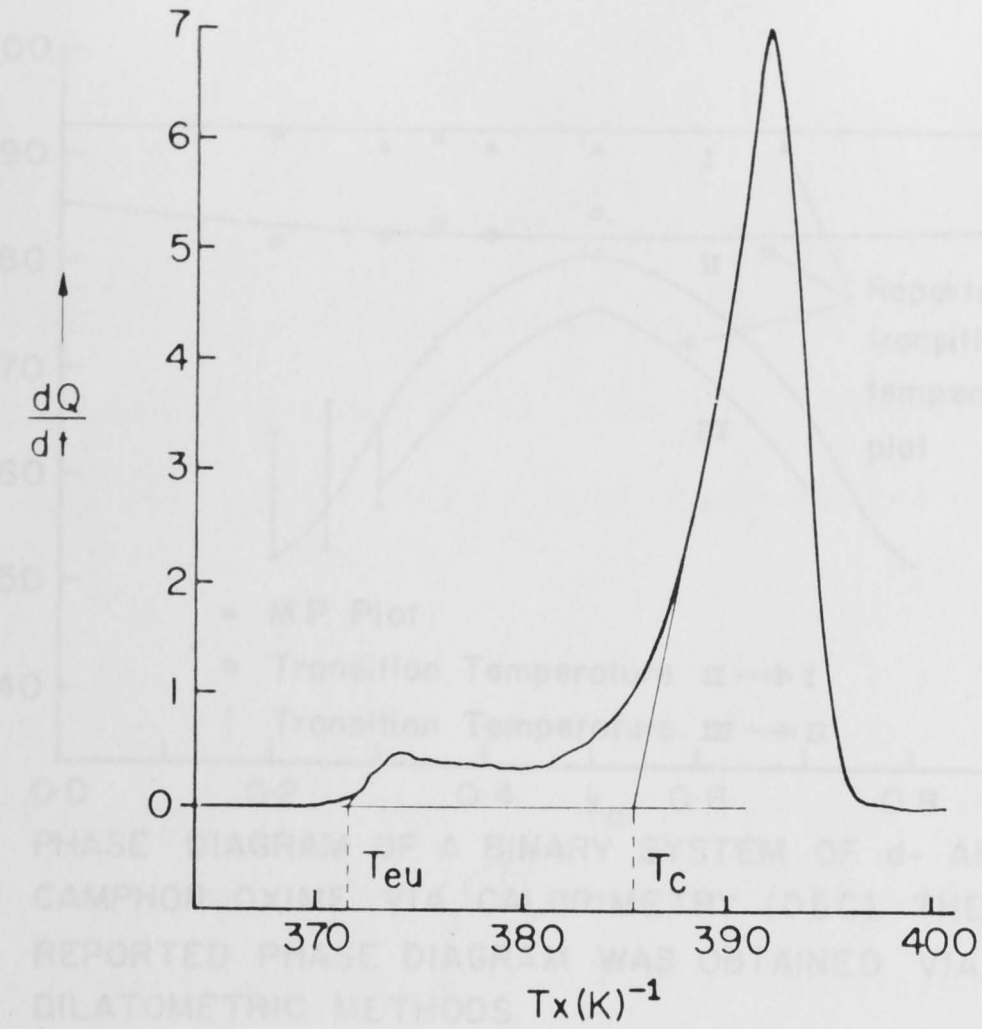

Fig 2.7: A THERMOGRAM OF CAMPHORIC ANHYDRIDE.

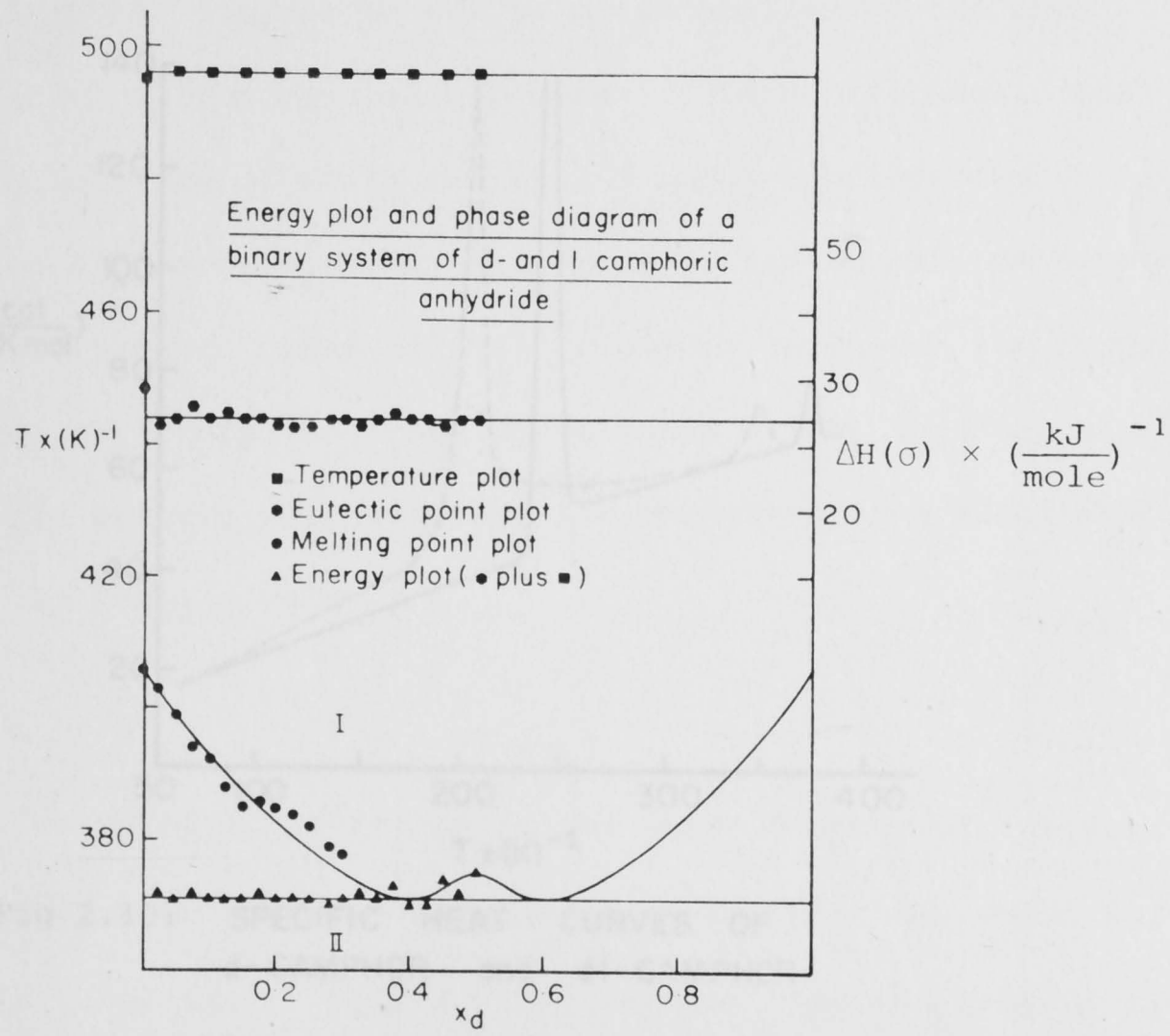

Fig 2.8: Phase diagram of *d*- and *l*-camphoric anhydride. $\Delta H(\sigma)$ is the rotational transition energy.

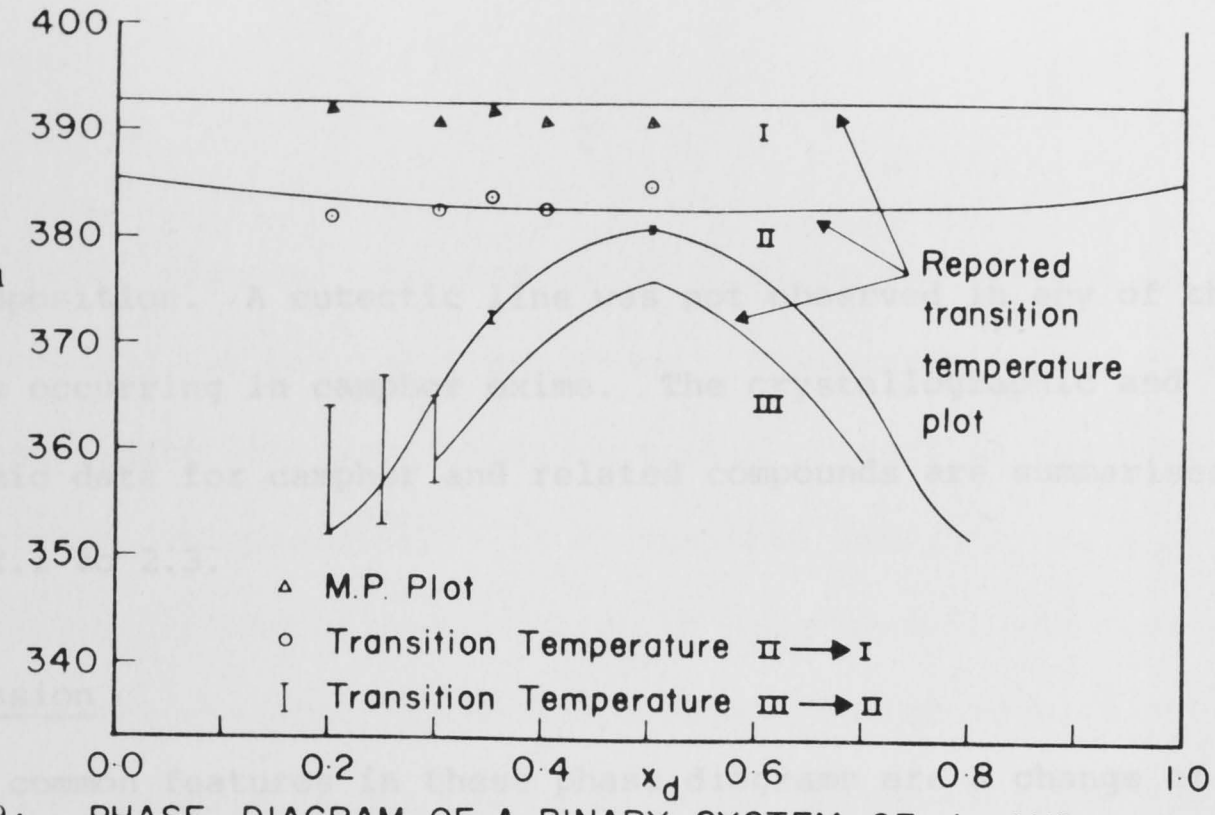

Fig 2.9: PHASE DIAGRAM OF A BINARY SYSTEM OF d- AND l-CAMPHOR OXIME VIA CALORIMETRY (DSC). THE REPORTED PHASE DIAGRAM WAS OBTAINED VIA DILATOMETRIC METHODS.

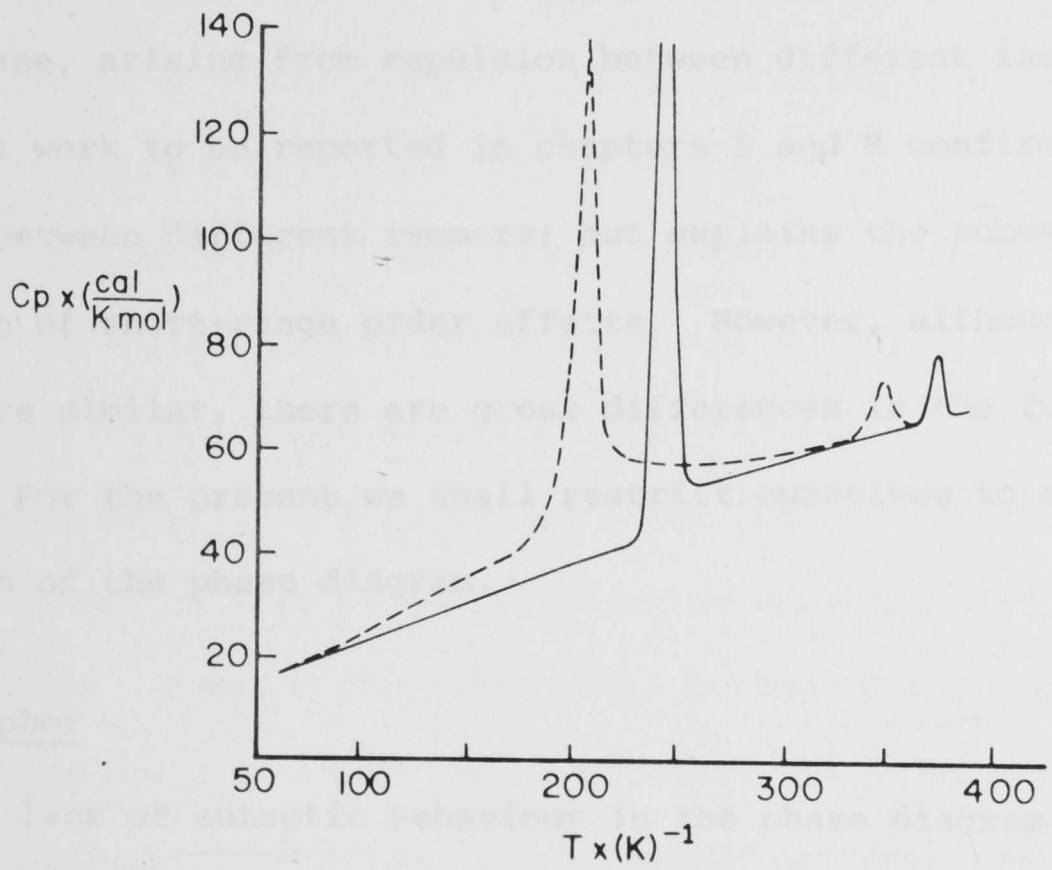

Fig 2.10: SPECIFIC HEAT CURVES OF d-CAMPHOR and dl-CAMPHOR

(SCHÄFER ET AL Z ELECTROCHEM 62,328, (1958))

racemic composition. A eutectic line was not observed in any of the transitions occurring in camphor oxime. The crystallographic and thermodynamic data for camphor and related compounds are summarised in tables 2.1 to 2.3.

2.8 Discussion

The common features in these phase diagrams are a change of molecular packing at the rotational transition particularly with regard to the optical isomers, and the existence of a more or less pronounced submaximum, normally attributed to compound formation. The interpretation of these diagrams is at present the subject of opposing views, particularly with regard to camphor. The first is that due to Schäfer *et al* [24] who postulate the existence of a pseudo-racemic compound, implying the existence of a discrimination energy in favour of the racemate. The second view is that of Anderson and Slichter [25], who suggest that the submaximum on the phase diagram is due to metastability of the non-rotator phase, arising from repulsion between different isomers. Our theoretical work to be reported in chapters 5 and 8 confirms the repulsion between different isomers; but explains the submaximum as a consequence of short-range order effects. However, although the phase diagrams are similar, there are gross differences in the fundamentals involved. For the present we shall restrict ourselves to a qualitative description of the phase diagram.

2.8.1 Camphor

The lack of eutectic behaviour in the phase diagram of camphor implies the existence of a complete range of solid solutions above and below the III-II transition. This further implies that the discrimination energy present in this system is not significant enough to cause phase separation at the rotational transition. It is found from work to appear later that the submaximum on the phase diagram can be attributed to

short-range order effects. The situation is different for the II - I reconstructive and the melting transitions. These transitions occur between phases where the discrimination energy present in the non-rotator phase has either diminished (II - I) or vanished (melting) as a result of the averaging effects of the rotation of molecules in the rotator phases. These observations appear compatible with the results of model calculations of discrimination energies in the locked-up limit (cf. the non-rotator phase) and the weakly coupled limit (cf. the rotator phase) carried out by Craig *et al* [3].

The variation of the rotational transition energy with composition is now considered. Schäfer and Wagner determined the total entropy changes for a number of compositions ranging from *d*-camphor to *dl*-camphor from 0 K to about 378 K (just before the melting point) and found them invariant with composition within experimental error. Camphor, like other substances which form plastic crystals, shows smaller than usual entropy changes above the rotational transition. Thus the variation of the rotational transition energy, which is accompanied by a decrease in entropy of transition with increasing *d*-camphor concentration, may be explained by postulating a premonitory phenomenon which introduces disorder in the system before the transition, and so decreases the entropy change in the final stages of the transition. This premonitory phenomenon may be in a form of co-operative lattice defect formation which stabilises the crystal against lattice strains caused by distortion of the lattices. These distortions could be due to the substitution of a *d*-camphor molecule by an *l*-camphor molecule, in a *d*-camphor crystal lattice. Premonitory behaviour in *dl*-camphor and other mixtures of *d*- and *l*-camphor have been detected by calorimetry, NMR and dielectric studies. Fig 2.10 shows results of specific heat measurements for *d*- and *dl*-camphor reported by Schäfer and Wagner where a gradual pre-

transitional rise in the specific heat for the *dl*-mixture can be seen relative to that of the optical isomer. This observation could be seen to correspond to the observation made by Anderson *et al* that long-range orientational disorder is sustained to very low temperatures in the racemic mixture. More evidence for premonitory behaviour in these systems will be found in the next two chapters.

The minima of energy and temperature plots (Fig. 2.6) in the *d*- and *l*-camphor system, do not coincide. The two points are significantly separate even if experimental errors are taken into account - the magnitude of the uncertainty in energy required to make the two minima coincident is very much larger (by a factor of 200) than the uncertainty in energy assessed from experimental errors. Kimorov *et al* [27] made a similar observation in the nitrogen-oxygen system. They attributed the effect to a large strain energy arising from the distortion of the crystal.

2.8.2 Camphoric Anhydride

The eutectic behaviour observed in this system may be attributed to a significant discrimination energy that destabilises the crystal of the racemate relative to that of the optical isomers. We return to this subject in subsequent chapters, in particular chapter 8, where a theoretical discussion of this phase diagram is given.

No premonitory behaviour of the type observed in camphor is detected in the camphoric anhydride system. The only anomaly observed has been detected by NMR studies to be reported in the next chapter.

The difference in the molecular packing between the optical isomer and the racemate is of particular importance in this thesis. We note from table 2.1 that the optical isomer packs more efficiently than the racemate, yet the cell parameters of the two systems are very similar, and table 2.2 shows another monoclinic cell which can be picked from the same *dl*-lattice. This new unit cell shows a stronger resemblance

to that of the isomer. The racemate cell at room temperature may therefore be viewed as resulting from a change of the space group from the $P2_12_12_1$ of the optical isomer to $P2_1/c$ of the racemate crystal accompanied by a monoclinic distortion that changes one of the right angles of the orthorhombic lattice to an obtuse angle of 92°. We recall this observation in later chapters.

2.8.3 Camphor Oxime

Relatively very little work has been carried out on this system. The transitions occur at relatively high temperatures and the absence of eutectic behaviour suggests the existence of a complete series of solid solutions. X-Ray diffraction data obtained by A. Tom has produced evidence for a reconstructive phase transition connecting phases III and II around the racemate composition. Above this transition the patterns for *d*- and *dl*-camphor oxime crystals became similar at the same temperature. This explains why a similar transition is not observed in the case of the optical isomer. However this diffraction pattern resembles only qualitatively the -pattern at room temperature. Another pattern emerged above the II - I transitions; but this time was independent of composition.

The fact that the III - II reconstructive transition is observed around the racemic composition suggests a relatively small discrimination energy which has negligible effects on the packing of molecules at low concentrations of the minority isomer. It would seem that this discrimination energy becomes negligible in the expanded lattice so that the racemate crystal resorts to the crystal system of the optical isomer in phase II.

Table 2.1: Crystallographic data for camphor and related compounds (provided by Dr M. Sterns, except where otherwise noted)

Substance	Non-Rotator Phase		Rotator Phase	
	Crystal System	Cell Dimension (Å)	Crystal System	Cell Dimension (Å)
d-Camphor			II hexagonal	a =7.14*(295K)* z = 2 c =11.72 V = 517Å^3 c/a=1.64 v_m = 259Å^3
			I face centred cubic	a =10.1*(380K)* z = 2 V = 1030Å^3 v_m = 258Å^3
			T_c (II→I) = *374K*	
dl-Camphor			II hexagonal	a =7.05*(295K)* z = 2 c =11.50 V = 476Å^3 c/a=1.63 v_m = 238Å^3
			T_c (II→I) = *350K*	
d-Camphoric anhydride	Orthorhombic $P2_12_12_1$	a=10.9*(295K)* z = 4 b=13.1 V = 920Å^3 c=6.44 v_m=230Å^3	hexagonal	a =7.25*(413K)* z = 2 c =11.76 V = 535Å^3 c/a=1.62 v_m = 268Å^3
dl-Camphoric anhydride	Monoclinic $P2_1/c$	a=6.44*(295K)* z = 4 b=11.56 V = 944Å^3 c=13.99 v_m=236Å^3 β=115.0°	hexagonal	a =7.25*(386K)* z = 2 c =11.76 V = 535Å^3 c/a=1.62 v_m = 268Å^3
*Camphor oxime	Monoclinic $P2_1$	a=12.17 Z=2 b=11.82 c=7.19 β=100.8°		

* Data from reference [28], both the temperature and phase are not specified.

Table 2.2: An alternative set of unit cell parameters for the *dl*-camphoric anhydride lattice at room temperature (non-rotator phase).

Crystal System	Unit Cell Parameters (Å)
Monoclinic $P2_1/n$	a = 6.44 Z = 4 b = 11.56 V = 944 Å^3 c = 12.69 v_m = 236 Å^3 β = 92°

Table 2.3: Thermodynamic quantities associated with transitions in camphor and related compounds.

Substance	Transition	$T_c \times (K)^{-1}$	$\Delta H \times (\frac{kJ}{mole})^{-1}$
d-camphor	III → II	242 ± 1	16 ± 1
	[a] II → I	374	0.23 ± 0.02
	[b] melting	452	5.3
dl-camphor	III → II	206 ± 1	1.9
	[a] II → I	350	0.23 ± 0.02
	[b] melting	449	
d-camphoric anhydride	II → I	406 ± 1	29 ± 2
	melting	495 ± 1	8.7 ± 0.1
dl-camphoric anhydride	II → I	375	24 ± 2
	melting	495 ± 1	8.7 ± 0.1
d-camphor oxime	II → I	383	13.3
	melting	389	1.8
dl-camphor oxime	III → II	375	3.0
	II → I	380	11.2
	melting	388	1.2

[a] Reference [24].

[b] Reference [29].

3

dielectric studies of order-disorder phenomena in camphor and camphoric anhydride

This chapter reports the results of dielectric studies of the rotational transition in d- and l-systems of camphor and camphoric anhydride. These are then contrasted with the calorimetric results reported in the previous chapter. Particular emphasis is placed on premonitory behaviour before the transition, on hysteresis and on the increase in conductivity associated with the transition.

3.1 Acknowledgment

The writer spent some weeks at the National Measurement Laboratory, C.S.I.R.O., Sydney where the work described in this chapter was carried out in association with Mr. H.K. Welsh. The subsequent data-processing has proceeded collaboratively, and some of the figures were devised by Mr. Welsh, and drawn at C.S.I.R.O. The annotation HKW is used in the text where it is necessary to quote work that is not the present writer's.

3.2 Introduction

Yager and Morgan [30] were among the first to use dielectric measurements for the study of the rotational transitions in camphor derivatives. In this chapter we report on the dielectric properties of *d*- and *l*-systems of camphor and camphoric anhydride. This work supplements results of other workers. Our work consists mainly of low temperature measurements. Particular interest lies in premonitory phenomena, conductivity effects and hysteresis associated with the rotational transitions in these systems. Although the dielectric properties of most of the systems studied here have already received some attention in the literature, *dl*-camphoric anhydride has not been studied before.

3.3 Theory

We briefly summarise some essential features of the theory of dielectrics [31],[32],[33],[34].

We are concerned with the dielectric permittivity ε, defined for a static macroscopic field $\underset{\sim}{E}$ by

$$\varepsilon_0 = \underset{\sim}{D}/\underset{\sim}{E} = 1 + 4\pi\underset{\sim}{P}/\underset{\sim}{E} \qquad (3.1)$$

($\underset{\sim}{D}$ = displacement, $\underset{\sim}{P}$ = polarization). In an alternating field the

polarization lags behind the applied field. The component of the displacement current which is in phase with the field, the loss current, is a measure of the absorption of energy by the dielectric. The out of phase component is the charging current. The two current vectors define a loss angle δ which may also be defined in terms of the dynamic relative permittivity ε' and the dielectric loss factor ε'':

$$\tan \delta = \varepsilon''/\varepsilon' \qquad (3.2)$$

In addition to dielectric loss due to absorption, which can be designated ε'' (Debye), there are losses due to other sources. The most important in molecular solids are due to *interfacial polarization*, commonly called the Maxwell-Wagner polarization. These occur in a heterogeneous material when phases of different dielectric properties form interfaces. The dielectric loss arising from this source can be designated ε''(M-W). Dielectric loss due to conduction ε''(d-c) is also observed if some conducting impurity is present in the molecular solid. This type of loss is related to the frequency of the alternating field f and the specific d-c conductance of the material κ by the following equation.

$$\varepsilon''(\text{d-c}) = 1.8 \times 10^{12} \kappa/f \qquad (3.3)$$

This kind of dielectric loss is readily identified from the nature of its frequency dependence; e.g. it has a maximum value as $f \to 0$. ε''(d-c) is identified from the slope of a log ε'' vs. log f plot. Therefore a heterogeneous dielectric material may have the total observed loss given by:

$$\varepsilon''_{obs} = \varepsilon''(\text{Debye}) + \varepsilon''(\text{M-W}) + E(\text{d-c}) \qquad (3.4)$$

In general the dielectric factors are defined in terms of a *complex permittivity* as follows:

$$\varepsilon^* = \varepsilon' - i\varepsilon'' \qquad (3.5)$$

where according to Debye theory

$$\varepsilon' = \varepsilon'_\infty + \frac{\varepsilon'_0 - \varepsilon'_\infty}{1 + \omega^2\tau^2}$$

and

$$\varepsilon'' = (\varepsilon'_0 - \varepsilon'_\infty)\ \frac{\omega\tau}{1 + \omega^2\tau^2}$$

where $\omega = 2\pi f$ is the angular frequency of the applied oscillating field and τ is the relaxation time of the system, characterising the decay of the polarization when the electric field is removed.

Provided the relaxation process of the dielectric can be described by one relaxation time a maximum in the dielectric loss factor occurs when $\omega\tau = 1$, i.e. the condition of resonance. Thus from equation (3.5) we have the following equation for the maximum dielectric loss factor.

$$\varepsilon''_{max}(\text{Debye}) = \tfrac{1}{2}(\varepsilon'_0 - \varepsilon'_\infty) \qquad (3.6)$$

For dielectric materials which can be characterised by a distribution of relaxation times the Debye model does not apply and a number of methods have been developed to deal with those situations but they will be omitted in the present discussion. The frequency of maximum absorption is related to the energy barrier E_a for dipolar re-orientation and the relationship is assumed to be of the form of the Arrhenius equation.

$$f_{max} = A \exp\left(\frac{-E_a}{RT}\right) \qquad (3.7)$$

The variation of the rotative permittivity with temperature for a dielectrically isotropic material is given in the following equation due to Fröhlich.

$$\varepsilon_0 - \varepsilon_\infty = \frac{4\pi N}{3\varepsilon}\ \frac{3\varepsilon_0}{3\varepsilon_0 + n^2}\ \frac{\langle \underset{\sim}{m} \cdot \bar{\underset{\sim}{m}} \rangle}{kT} \qquad (3.8)$$

where $\underset{\sim}{m}$ is the moment of a unit cell; $\bar{\underset{\sim}{m}}$ is the average moment of a

macroscopic spherical region surrounding the unit cell when the moment of the latter is fixed at $\underset{\sim}{m}$; N is the number of unit cells per unit volume; n is the refractive index of the dielectric and ε is a constant whose value depends on the system of units used. Fröhlich applied equation (3.8) to the simple case in which the unit cell contains two polar molecules where each molecule can take any one of two orientations of different energies and obtained the following equation.

$$\varepsilon_0 - \varepsilon_\infty = \frac{4\pi N'}{3\varepsilon} \frac{3\varepsilon_0}{2\varepsilon_0 + n^2} \frac{8\sigma(1 - \sigma)}{kT} \underset{\sim}{\mu} \cdot \overline{\underset{\sim}{\mu}} \qquad (3.9)$$

where N' is the number of dipoles per unit volume; σ is the probability of the molecule taking the direction which is energetically unfavourable; $\underset{\sim}{\mu}$ is the dipole moment of the molecule and $\overline{\underset{\sim}{\mu}}$ is related to the average moment of the media.

Equation (3.9) is simply a model for order-disorder phase transitions in molecular crystals. Thus when $\sigma = 0$, $\varepsilon_0 = \varepsilon_\infty$ and when $\sigma \rightarrow \frac{1}{2}$, with rise in temperature, the value of ε_0 increases (since ε_∞ is assumed to have a constant value). After the limiting value of $\sigma = \frac{1}{2}$ is reached $\varepsilon_0 - \varepsilon_\infty$ decreases with increasing temperature. Thus the rotational transition temperature can be detected by a rise in the value of the relative permittivity during the transition, followed by a decrease of its value in the plastic crystal phase.

3.4 Experimental

Samples of camphor, camphoric anhydride from the same sources as in calorimetric experiments reported in the preceding chapter were purified by recrystallisations from benzene and dried under vacuum. Measurements employed a Thompson bridge [35] network, with a frequency range of 5 Hz to 10 MHz.

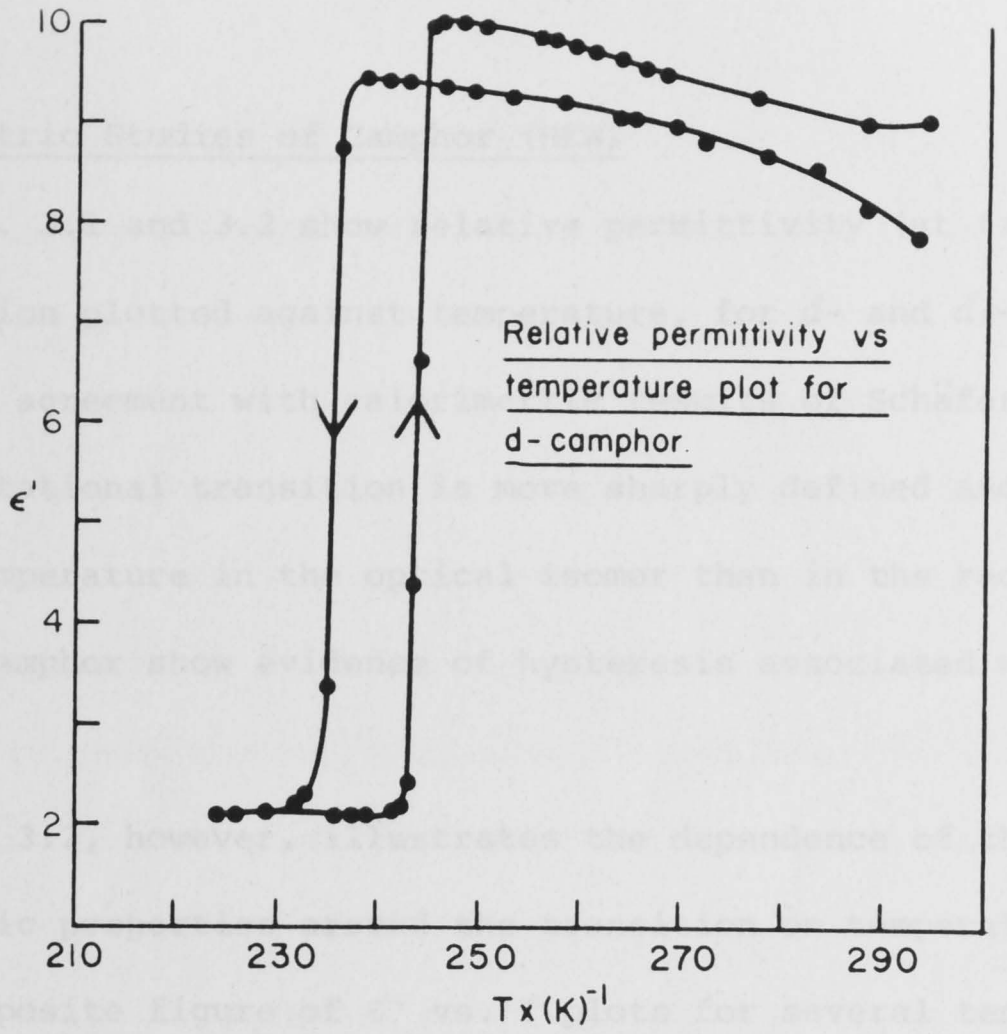

Fig 3.1: The variation of the relative permittivity with temperature in *d*-camphor. The rotational transition is sharply defined and is associated with marked hysteresis.

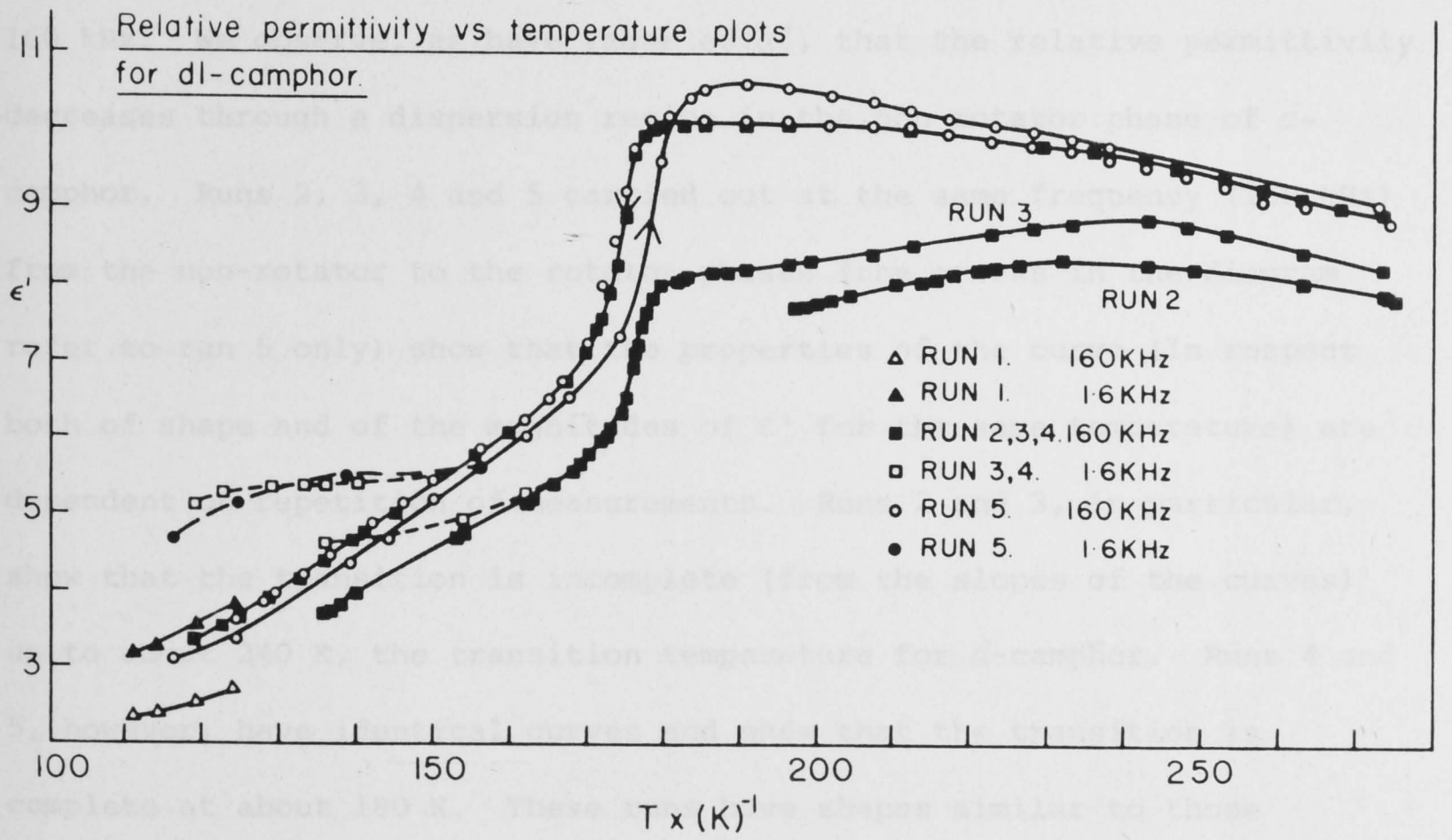

Fig 3.2: The variation of the relative permittivity with temperature in *dl*-camphor. The figure illustrates the dependence of the reproducibility of dielectric properties around the transition on temperature recycling. The rotational transition occurs over a wide temperature range. Hysteresis is also observed.

3.5 Dielectric Studies of Camphor (HKW)

Figs. 3.1 and 3.2 show relative permittivity (at frequencies below the absorption plotted against temperature, for *d*- and *dl*-camphor. It is seen, in agreement with calorimetric results of Schäfer *et al* [24], that the rotational transition is more sharply defined and occurs at a higher temperature in the optical isomer than in the racemate. Both *d*- and *dl*-camphor show evidence of hysteresis associated with the transition.

Fig. 3.2, however, illustrates the dependence of the reproducibility of dielectric properties around the transition on temperature re-cycling. It is a composite figure of ε' vs. T plots for several temperature cycles at two frequencies (1.6 and 160 kHz) on one sample; not all the cycles were completely recorded. The runs carried out at the low frequency were conducted in the non-rotator phase only and this frequency, as will be seen later, lies in the dielectric absorption region. Consequently runs conducted at this frequency have larger values of ε' than those at 160 kHz. We observe, as have Yager *et al*, that the relative permittivity decreases through a dispersion region in the non-rotator phase of *d*-camphor. Runs 2, 3, 4 and 5 carried out at the same frequency (160 kHz) from the non-rotator to the rotator phases (the arrows in the diagram refer to run 5 only) show that the properties of the curve (in respect both of shape and of the magnitudes of ε' for the same temperature) are dependent on repetition of measurements. Runs 2 and 3, in particular, show that the transition is incomplete (from the slopes of the curves) up to about 240 K, the transition temperature for *d*-camphor. Runs 4 and 5, however, have identical curves and show that the transition is complete at about 180 K. These runs have shapes similar to those reported by Yager *et al*, and Williams and Smyth [36]. Thus it would seem that several temperature cycles through the transition are required

before reproducibility of results is achieved.

The phase diagram of *d*- and *l*-camphor with respect to the rotational transition only has been repeated from our dielectric measurements and is shown in fig. 3.3. It will be seen that the dielectric phase diagram has generally shifted to lower temperatures relative to the calorimetric phase diagram. A similar observation was made in the NMR studies of the same phase diagram by Anderson and Slichter [25]. However the shape of the calorimetric phase diagram more closely resembles the dielectric phase diagram than the NMR phase diagram. The transition temperatures for the optical isomer from both calorimetric and dielectric measurements are the same within experimental error, but both of these temperatures are different from the NMR transition temperature for the same composition. The minima 0.25 and 0.75 are common in the three phase diagrams; but the curve from the 0.75 to 0.50 in the case of the NMR phase diagram differs from corresponding curves on the other two phase diagrams depicted in fig. 3.3 in that it is virtually a straight line.

Figures 3.4 and 3.5 show dielectric absorption in *d*- and *dl*-camphor respectively with corresponding Arrhenius plots. The runs indicated in figure 3.5 correspond to those reported in figure 3.2 at 1.6 kHz. Thus the dielectric loss factor and the relative permittivity increased as the measurements were repeated on the same sample. Neither the potential energy barrier nor the pre-exponential parameter changed appreciably with the re-cycling of measurements (as reflected by the consistency of the co-ordinates of the Arrhenius plot). These parameters are summarised in table 3.1. It is also observed that the dielectric absorption is much greater and broader in the racemic mixture than in *d*-camphor. In *d*-camphor, the absorption is more of the Debye-type. This is in agreement with the results of Rossiter [37].

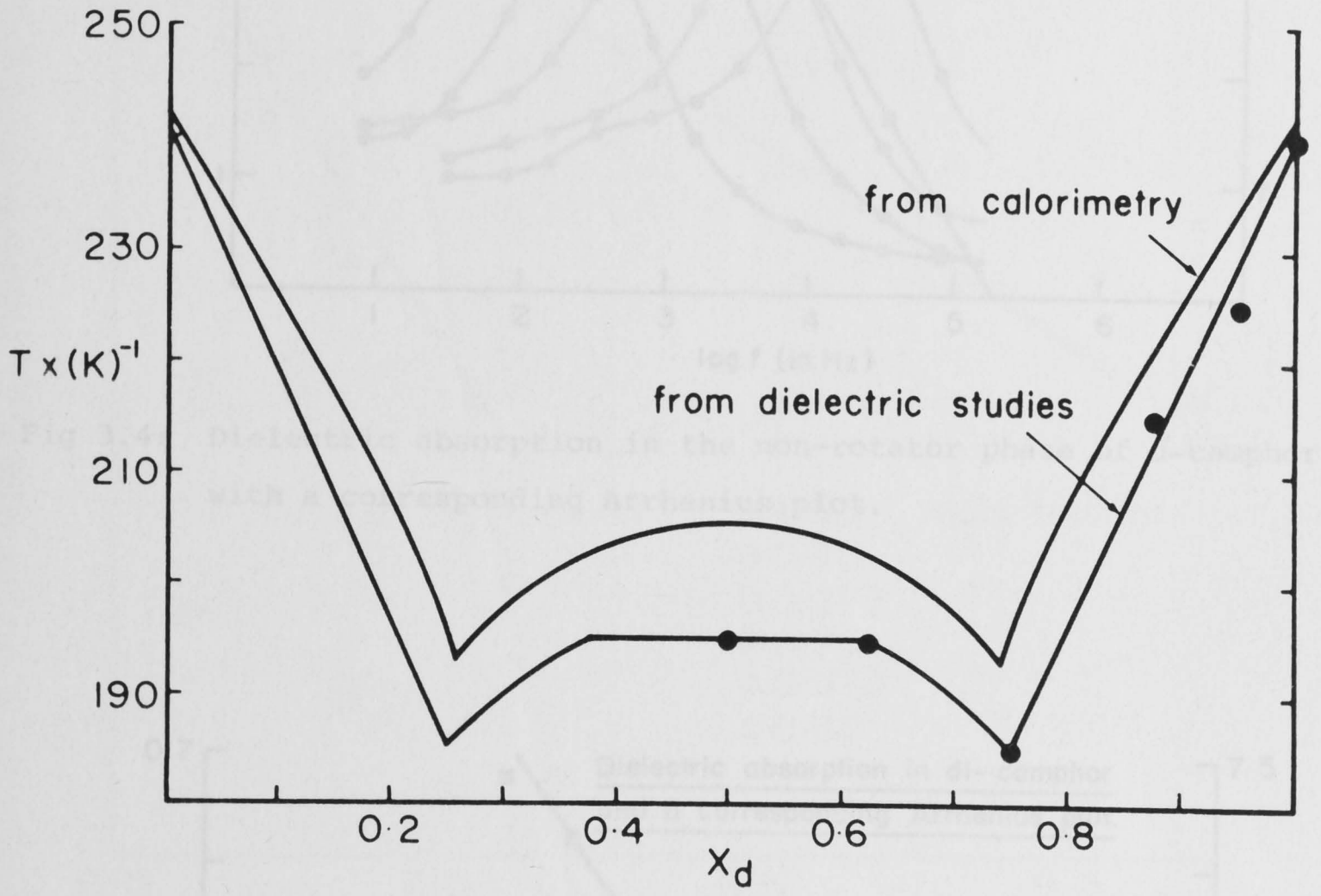

Fig 3.3: The phase diagram of d- and l-camphor as determined from dielectric studies. The phase diagram has the same pattern as the one obtained from calorimetry but occurs at relatively lower temperatures.

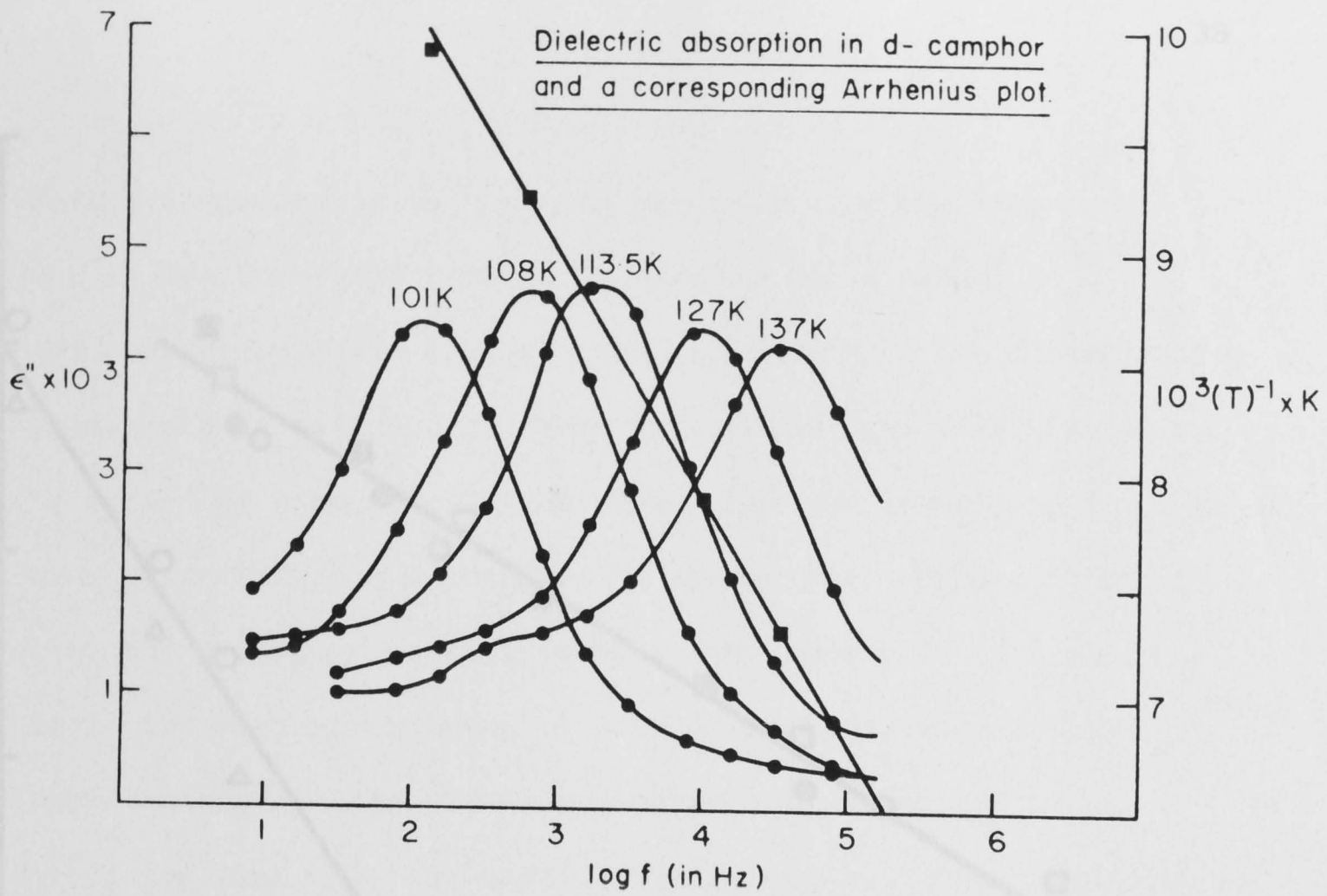

Fig 3.4: Dielectric absorption in the non-rotator phase of *d*-camphor with a corresponding Arrhenius plot.

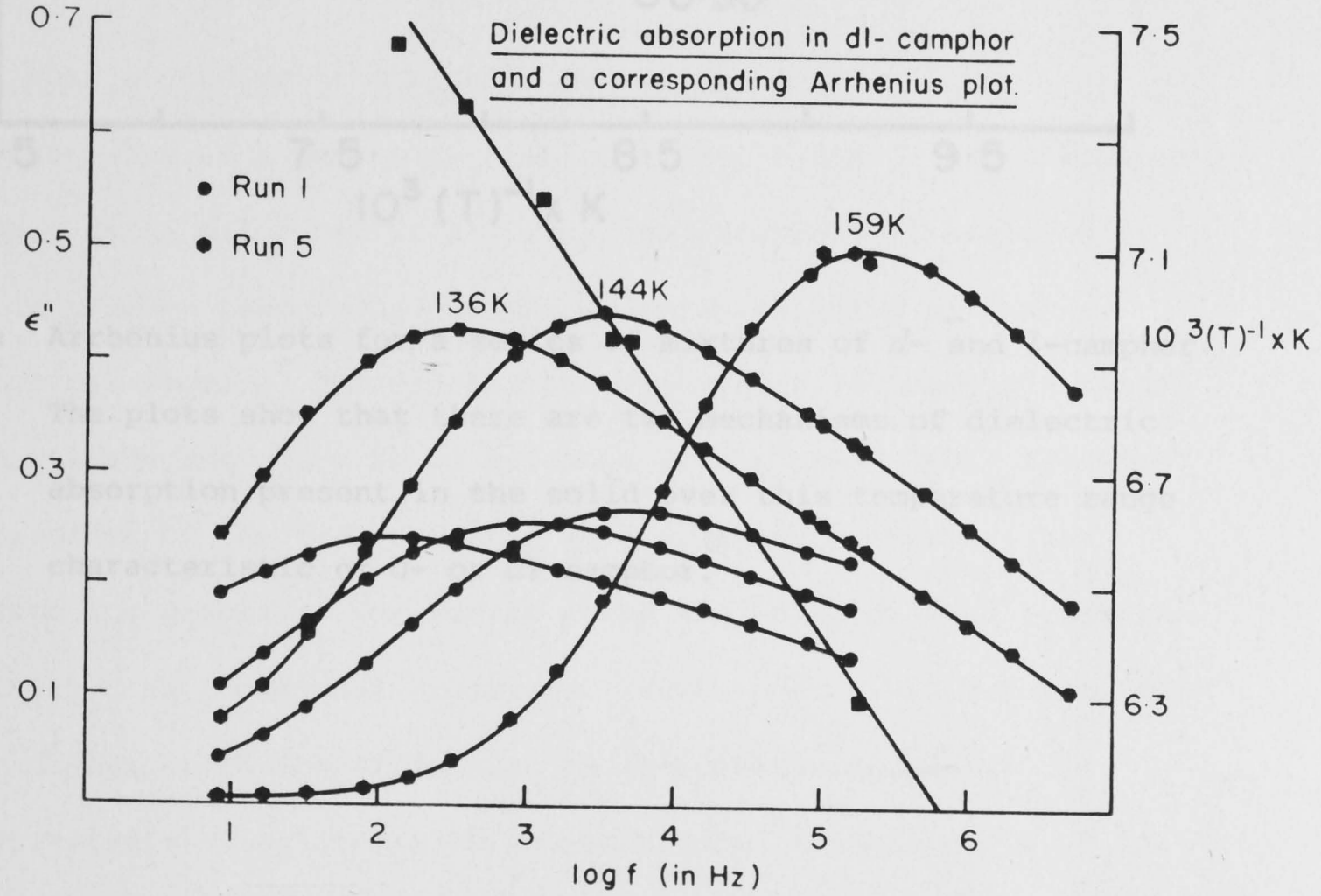

Fig 3.5: Dielectric absorption in the non-rotator phase of *dl*-camphor with a corresponding Arrhenius plot.

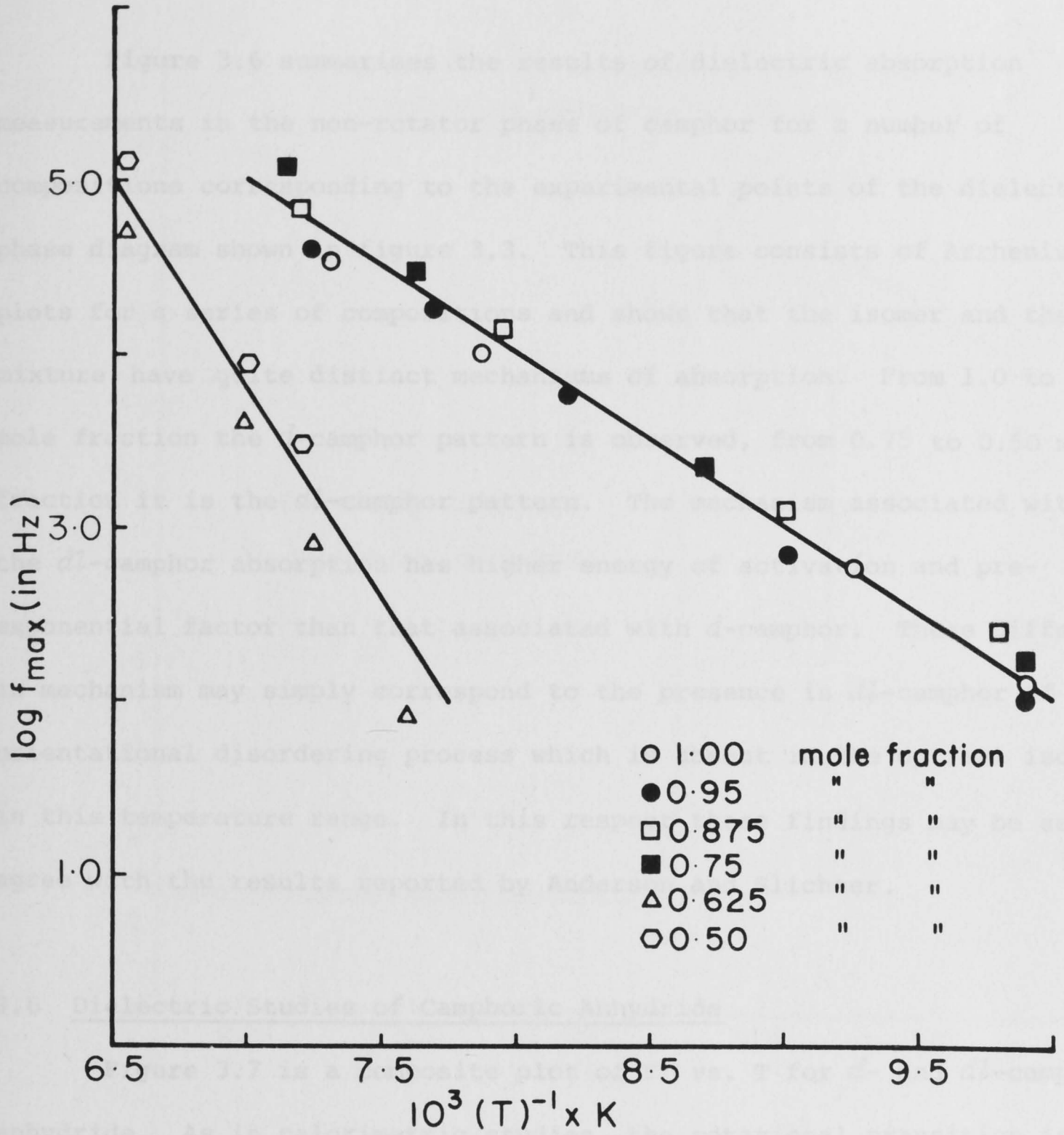

Fig 3.6: Arrhenius plots for a series of mixtures of *d*- and *l*-camphor. The plots show that there are two mechanisms of dielectric absorption present in the solid over this temperature range characteristic of *d*- or *dl*-camphor.

Figure 3.6 summarises the results of dielectric absorption measurements in the non-rotator phase of camphor for a number of compositions corresponding to the experimental points of the dielectric phase diagram shown in figure 3.3. This figure consists of Arrhenius plots for a series of compositions and shows that the isomer and the *dl*-mixture have quite distinct mechanisms of absorption. From 1.0 to 0.75 mole fraction the *d*-camphor pattern is observed, from 0.75 to 0.50 mole fraction it is the *dl*-camphor pattern. The mechanism associated with the *dl*-camphor absorption has higher energy of activation and pre-exponential factor than that associated with *d*-camphor. These differences in mechanism may simply correspond to the presence in *dl*-camphor of an orientational disordering process which is absent in the optical isomer in this temperature range. In this respect these findings may be seen to agree with the results reported by Anderson and Slichter.

3.6 Dielectric Studies of Camphoric Anhydride

Figure 3.7 is a composite plot of ε' vs. T for *d*- and *dl*-camphoric anhydride. As in calorimetric studies, the rotational transition is shifted to a lower temperature in the racemate relative to that of the optical isomer. The transition temperature is sharply defined for both systems and there is no evidence of any premonitory behaviour in the racemate of the type observed in *dl*-camphor. However, as judged from the slopes of the curves after the major rise in relative permittivity, the rotational transition occurs over a wider temperature range in *dl*-camphoric anhydride than in *d*-camphoric anhydride.

Hysteresis associated with the rotational transition in *d*- and *dl*-camphoric anhydride has been investigated by HKW and figures 3.8 and 3.9 summarise the results. It is observed that hysteresis is more evident in the racemate than in the optical isomer.

Figures 3.10 and 3.11 show the dielectric absorption observed in

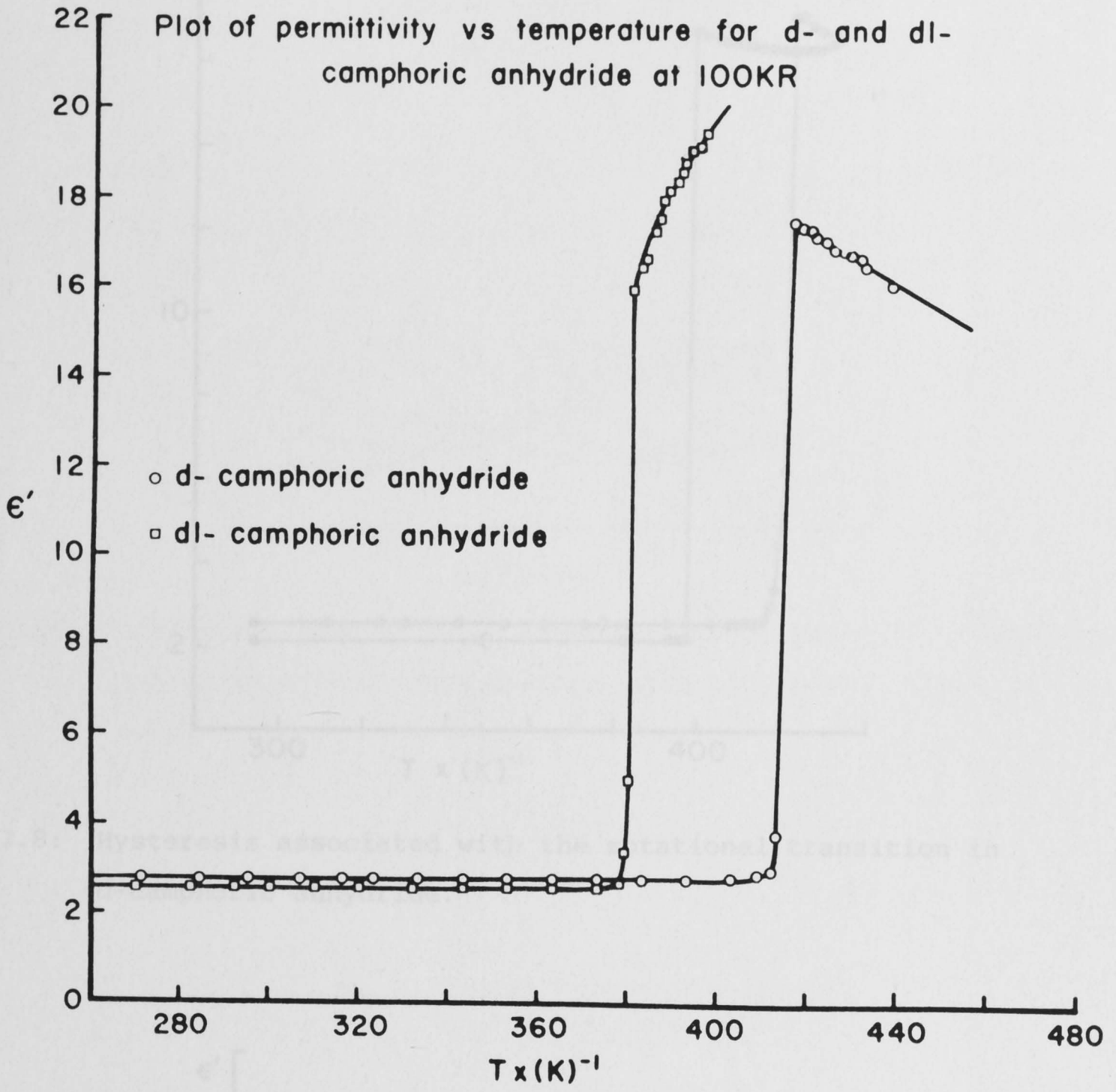

Fig 3.7: The variation of the relative permittivity with temperature in *d*- and *dl*-camphoric anhydride. The rotational transition is sharply defined in both substances, although it occurs over a wider temperature range in the racemate than in the optical isomer.

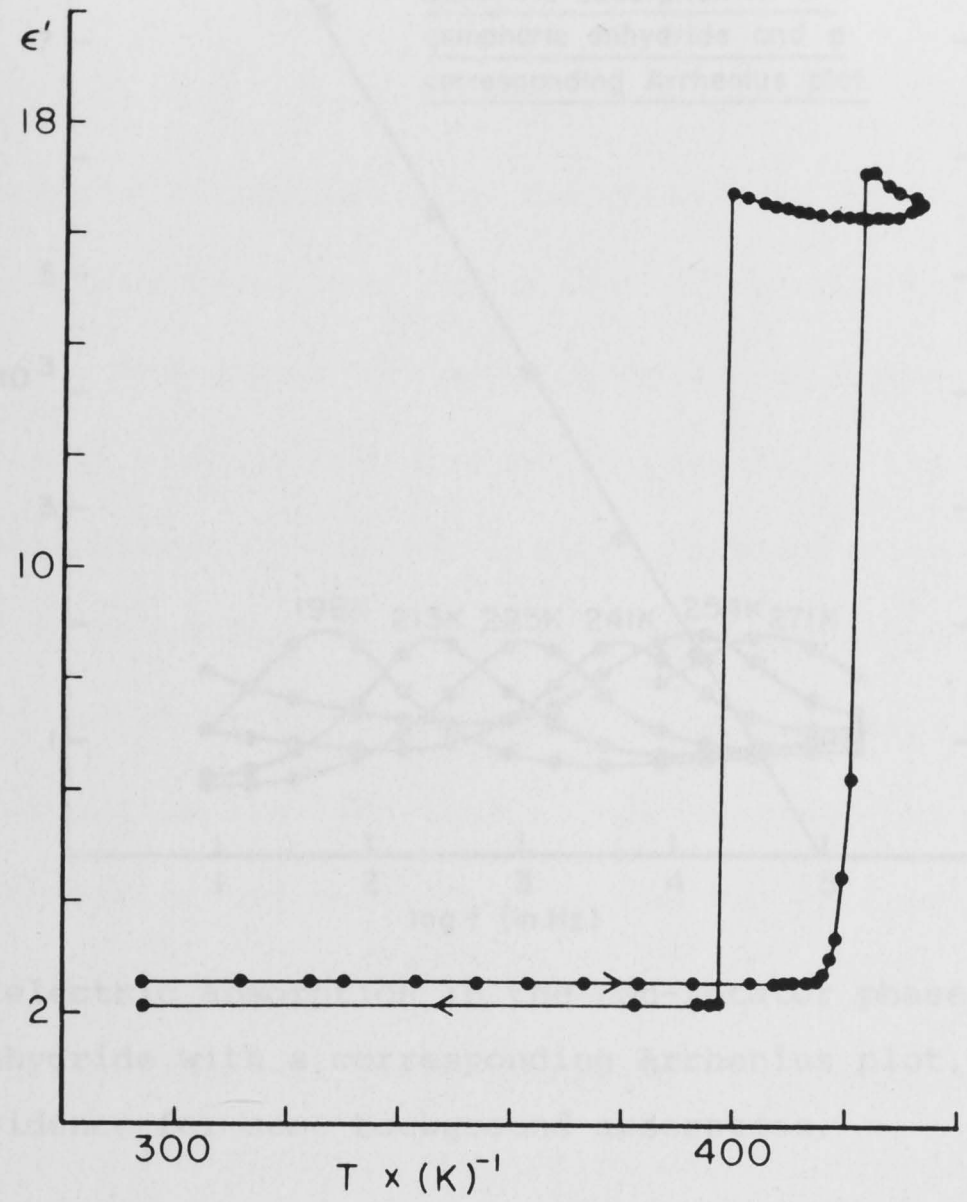

Fig 3.8: Hysteresis associated with the rotational transition in *d*-camphoric anhydride.

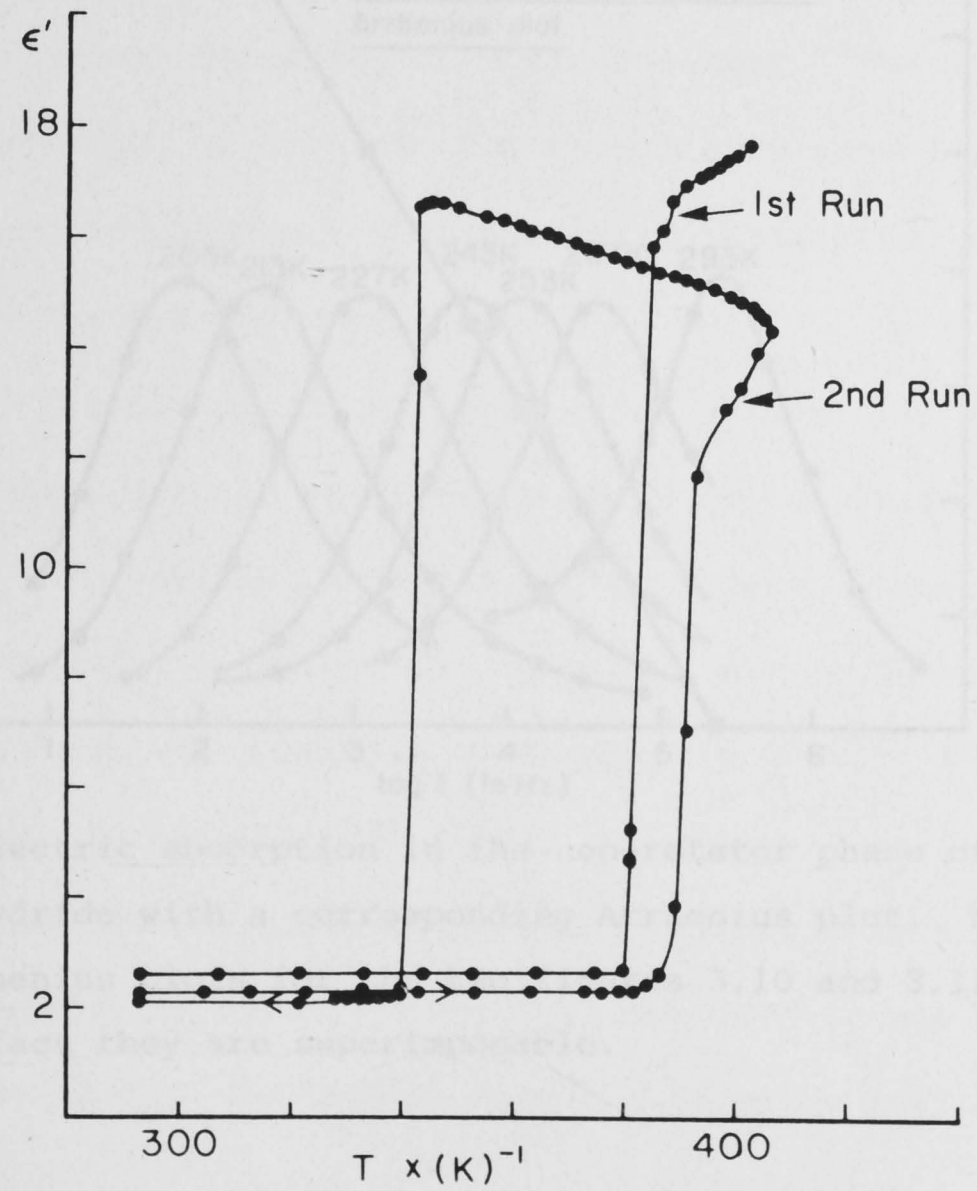

Fig 3.9: Hysteresis associated with the rotational transition in *dl*-camphoric anhydride.

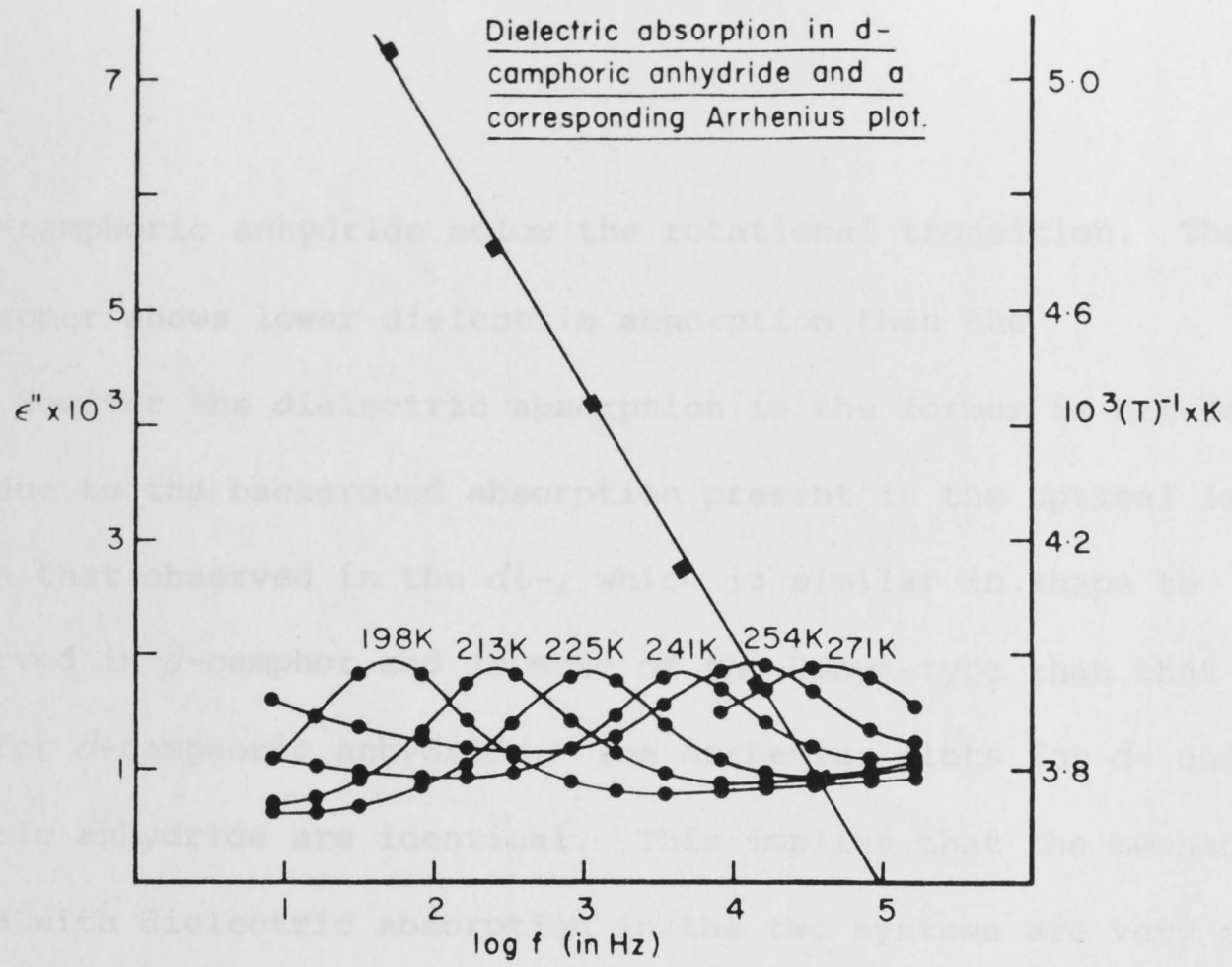

Fig 3.10: Dielectric absorption in the non-rotator phase of *d*-camphoric anhydride with a corresponding Arrhenius plot. There is evidence for some background absorption.

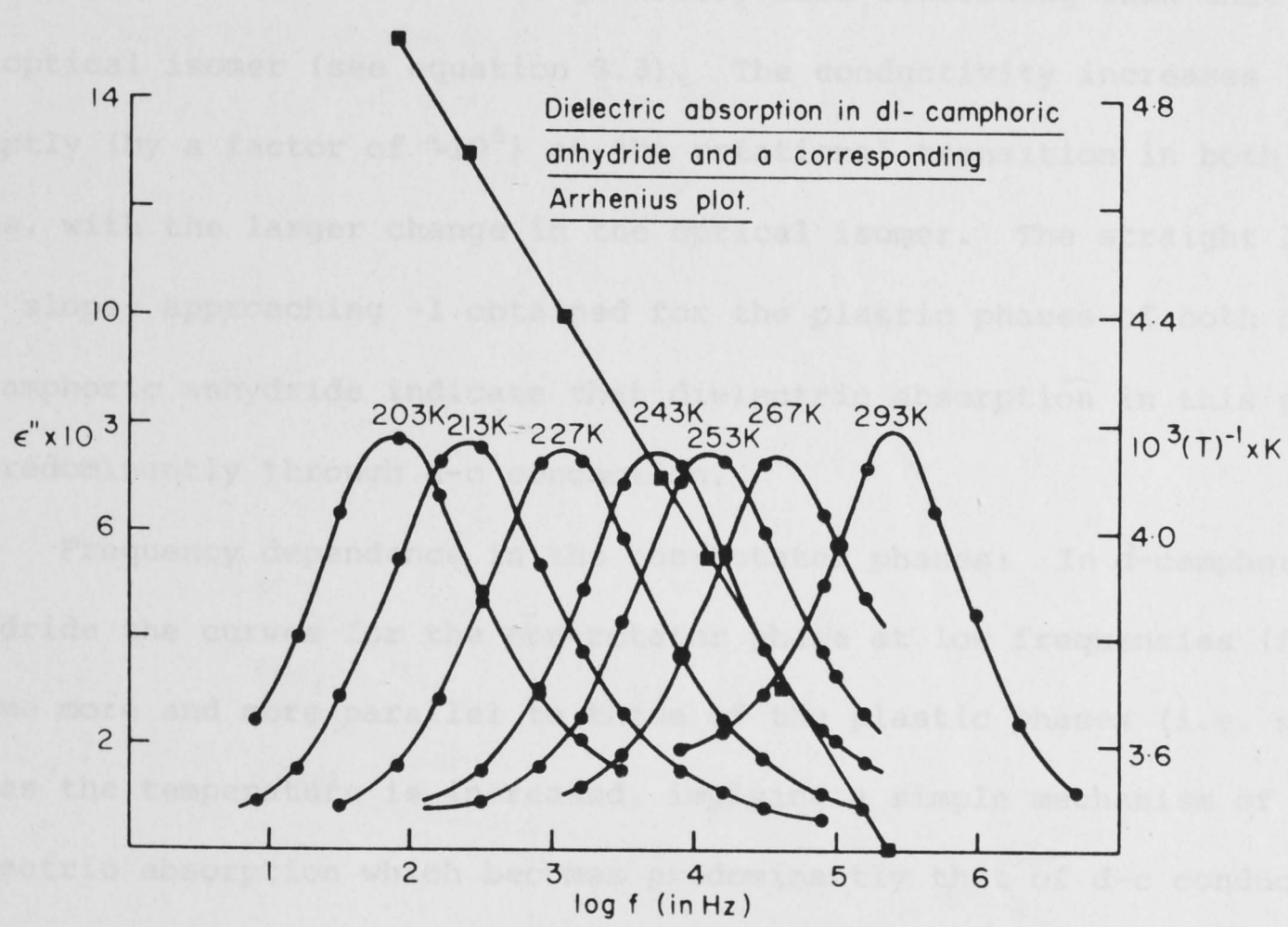

Fig 3.11: Dielectric absorption in the non-rotator phase of *dl*-camphoric anhydride with a corresponding Arrhenius plot. Note that the Arrhenius plots for the two figures 3.10 and 3.11 are parallel; in fact they are superimposable.

d- and *dl*-camphoric anhydride below the rotational transition. The optical isomer shows lower dielectric absorption than the racemate. However the dielectric absorption in the former is broader (perhaps due to the background absorption present in the optical isomer only) than that observed in the *dl*-, which is similar in shape to that observed in *d*-camphor and is more of the Debye-type than that observed for *d*-camphoric anhydride. The Arrhenius plots for *d*- and *dl*-camphoric anhydride are identical. This implies that the mechanisms associated with dielectric absorption in the two systems are very similar, in contrast with the situation in camphor.

Figures 3.12 and 3.13 (HKW) summarise results of studies carried out to investigate a dielectric absorption due to d-c conduction and interfacial polarization (the Maxwell-Wagner absorption). The non-rotator phase of the racemate is generally more conducting than that of the optical isomer (see equation 3.3). The conductivity increases abruptly (by a factor of $\sim 10^5$) at the rotational transition in both cases, with the larger change in the optical isomer. The straight lines with slopes approaching -1 obtained for the plastic phases of both *d*- and *dl*-camphoric anhydride indicate that dielectric absorption in this phase is predominantly through d-c conduction.

Frequency dependence in the non-rotator phases: In *d*-camphoric anhydride the curves for the non-rotator phase at low frequencies ($f \to 0$) become more and more parallel to those of the plastic phases (i.e. slope $\to$ -1) as the temperature is increased, implying a simple mechanism of dielectric absorption which becomes predominantly that of d-c conduction as the temperature is raised. The situation, however, is different in *dl*-camphoric anhydride where a complicated frequency dependence of the dielectric absorption is found, of the type observed in the Maxwell-Wagner system. The presence of the Maxwell-Wagner absorption may imply the

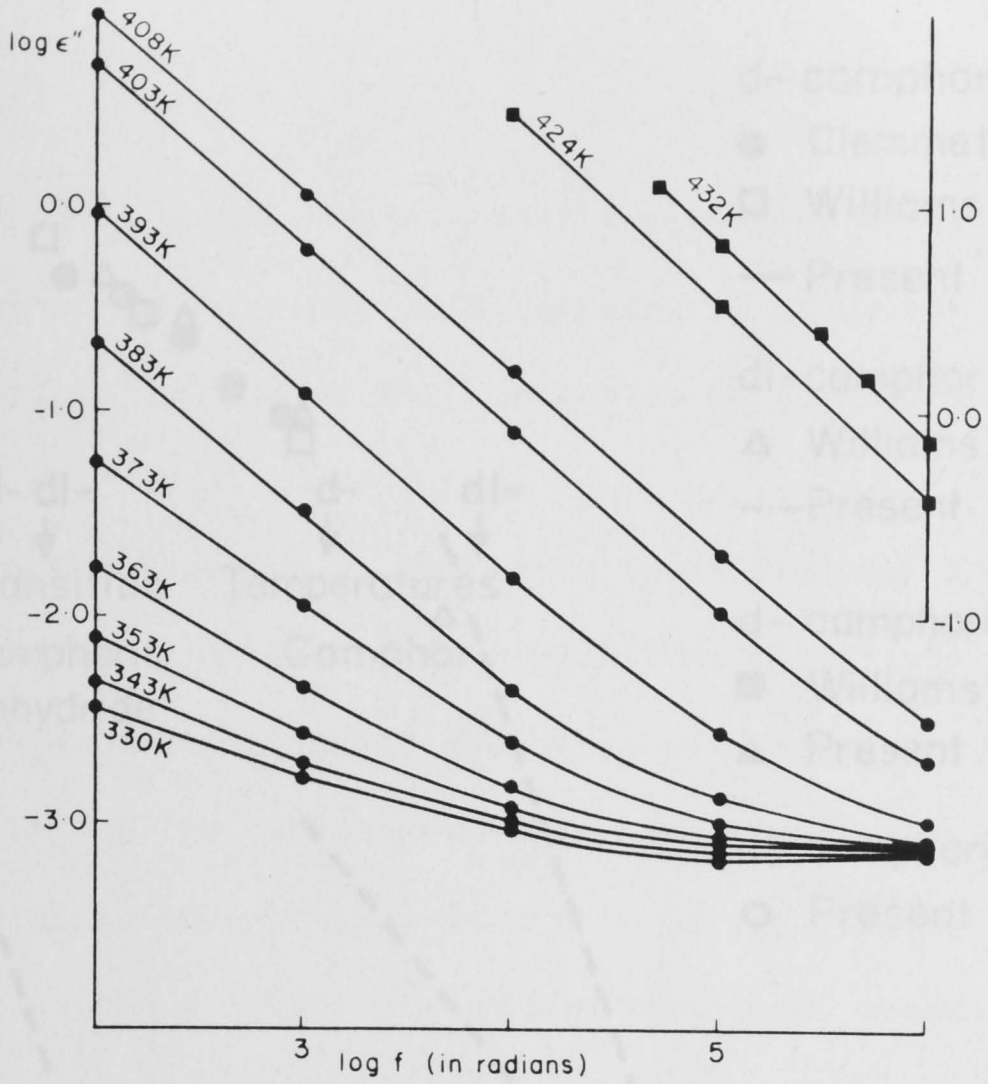

Fig 3.12: The variation of d-c conductivity and M-W absorption in the neighbourhood of the rotational transition in *d*-camphoric anhydride. The solid circles refer to the log ε" scale on the left hand side of the plot; and the solid squares, to the right hand side of the plot.

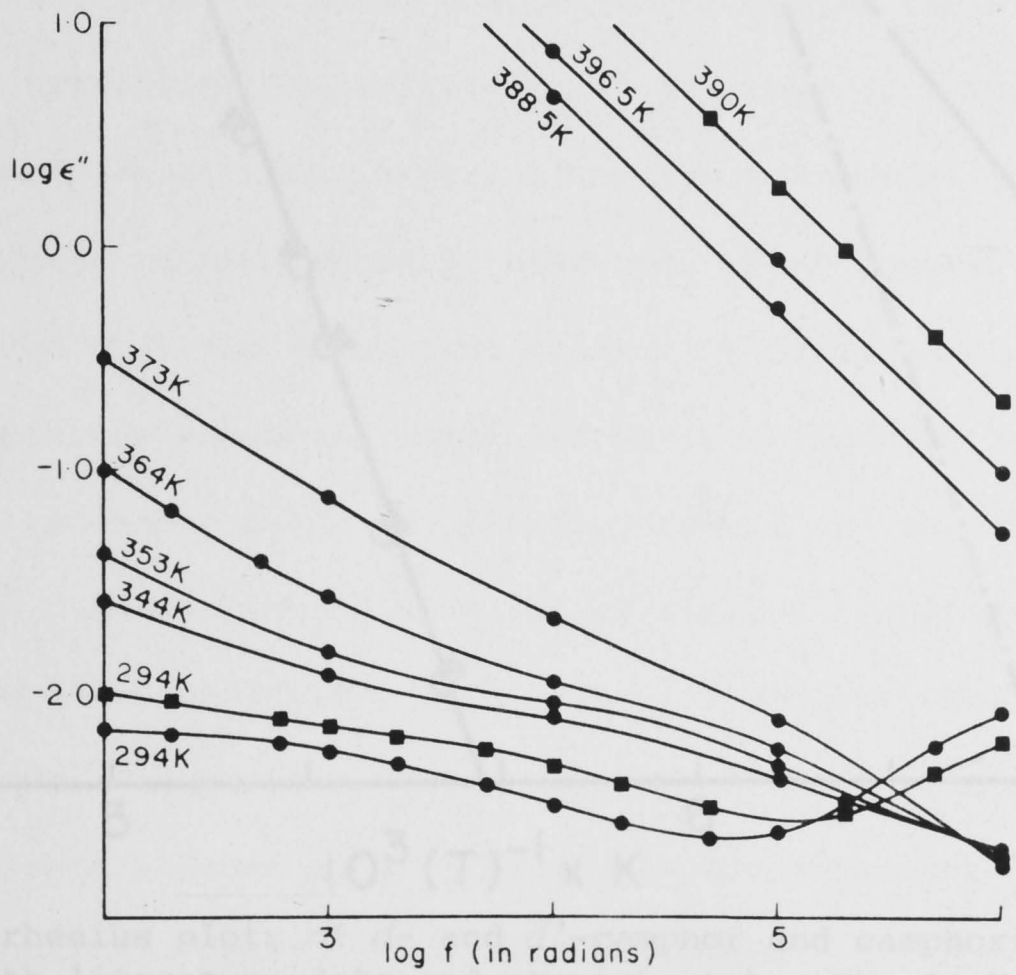

Fig 3.13: The variation of d-c conductivity and M-W absorption in the neighbourhood of the rotational transition in *dl*-camphoric anhydride. The figure also illustrates the effect of purification, solid squares and solid circles refer to results obtained before and after recrystallisation in benzene respectively.

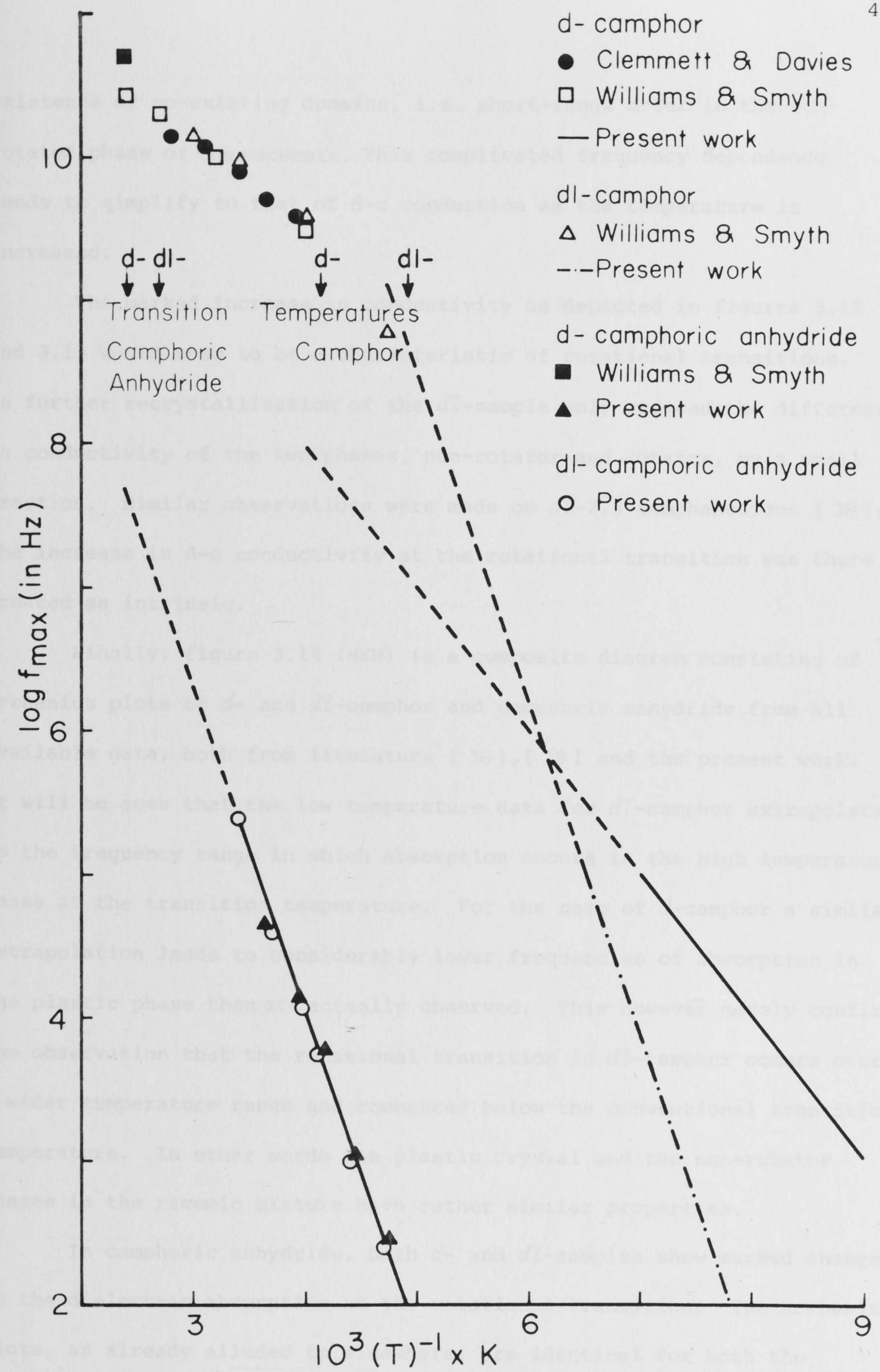

Fig 3.14: Arrhenius plots of *d*- and *dl*-camphor and camphoric anhydride from both literature data and present work. The Arrhenius plots for *d*- and *dl*-camphor non-rotator phases are different; but those of their plastic phases are very similar. The Arrhenius plot for *dl*-camphor non-rotator phase extrapolate to those of the plastic phases in *d*- and *dl*-camphor. The Arrhenius plots for *d*- and *dl*-camphoric anhydride non-rotator phases are identical; and both do not extrapolate to the result obtained in *d*-camphoric anhydride rotator phase.

existence of co-existing domains, i.e. short-range order in the non-rotator phase of the racemate. This complicated frequency dependence tends to simplify to that of d-c conduction as the temperature is increased.

The marked increase in conductivity as depicted in figures 3.12 and 3.13 would seem to be a characteristic of rotational transitions, as further recrystallisation of the *dl*-sample only reduced the difference in conductivity of the two phases, non-rotator and rotator, by a small fraction. Similar observations were made on *dl*-2,3-camphanedione [38]; the increase in d-c conductivity at the rotational transition was there treated as intrinsic.

Finally, figure 3.14 (HKW) is a composite diagram consisting of Arrhenius plots of *d*- and *dl*-camphor and camphoric anhydride from all available data, both from literature [36],[39] and the present work. It will be seen that the low temperature data for *dl*-camphor extrapolate to the frequency range in which absorption occurs in the high temperature phase at the transition temperature. For the case of *d*-camphor a similar extrapolation leads to considerably lower frequencies of absorption in the plastic phase than are actually observed. This however merely confirms the observation that the rotational transition in *dl*-camphor occurs over a wider temperature range and commences below the conventional transition temperature. In other words the plastic crystal and the non-rotator phases in the racemic mixture have rather similar properties.

In camphoric anhydride, both *d*- and *dl*-samples show marked changes in the dielectric absorption at the rotational transition. The Arrhenius plots, as already alluded to elsewhere, are identical for both the racemate and optical isomer. Thus, unlike camphor, the non-rotator phase of *dl*-camphoric anhydride is orientationally ordered below the rotational transition temperature.

Table 3.1: A summary of Arrhenius plot parameters, some representative conductivity values and dipole moments for camphor and camphoric anhydride.

substance	non-rotator phase			rotator phase	$\mu_D \times (D)^{-1}$
	$A \times (c/s)^{-1}$	$E_a \times (kJ/mol)^{-1}$	$\kappa_T \times (Ohm.cm)$	[a] $\kappa_T \times (Ohm.cm)$	
d-camphor (HKW)	1.6×10^{11}	17.4 (*101-137 K*)			[b] 2.7
dl-camphor (HKW)	7.2×10^{21}	50.3 (*134-159 K*)			
d-camphoric anhydride	2.1×10^{13}	44.2 (*198-271 K*)	3.5×10^{-14} (*295 K*)	0.55×10^{-8} (*432 K*)	[c] 5.41
dl-camphoric anhydride	1.9×10^{13}	44.4 (*203-293 K*)	7.9×10^{-14} (*295 K*)	1.67×10^{-8} (*390 K*)	

(a) Determined from dielectric absorption data obtained by the author.

(b) Reference [30].

(c) Determined by the author during a short visit to the School of Chemistry, University of Sydney in association with Mr S. Filipczuk. The measurements involved the refractivity method, with benzene as the solvent. Details of the apparatus used are found in reference [40].

3.7 Conclusions

Dielectric studies of the rotational transition in *d*- and *l*-systems of camphor and camphoric anhydride reveal certain basic differences and similarities in the physical properties of the two systems. The important common feature is the increase in d-c conductivity at the rotational transition. This feature however is rather well known in plastic crystals and has been attributed by Ubbelodhe [14] to the co-existence of domains of different phases (i.e. interfacial polarization effects of the Maxwell-Wagner type) during the transition. However the phenomenon of d-c conduction in molecular crystals is still not well understood and the domain theory just referred to does not answer all the questions. For example, at high temperatures when the rotational transition is complete the plastic phase still maintains high values of d-c conductivity although the presence of co-existing phases may not be observed (e.g. the high temperature plots in figures 3.12 and 3.13).

The fundamental difference in the properties of these systems is that both *d*- and *dl*-camphoric anhydride show similar physical properties before the rotational transition, whilst *d*- and *dl*-camphor have different properties (e.g. *dl*-camphor is orientationally disordered over a wide temperature range with most of the transition occurring at an intermediate temperature generally taken to be the transition temperature). This difference accounts for difficulties which Anderson *et al* reported in obtaining a crystal structure for the non-rotator phase of *dl*-camphor. On the other hand a crystal structure is obtainable for the low temperature phase of *dl*-camphoric anhydride.

4

solid-state n.m.r. studies of *d*- and *dl*-camphoric anhydride

This chapter reports results of n.m.r. (solid-state) studies of d- and dl-camphoric anhydride and is the final chapter on experimental work. Again emphasis is placed on the rotational transition with a particular interest on any premonitory phenomena associated with the transition.

4.1 Acknowledgement

The author spent some months at the Division of Chemical Physics, C.S.I.R.O., Melbourne where the work described in this chapter was carried out in association with Dr C.K. Coogan.

4.2 Introduction

This chapter attempts to establish the temperature ranges over which the rotational transition occurs in *d*- and *dl*-camphoric anhydride. Up to this point in this thesis no evidence has emerged for premonitory behaviour associated with this transition in camphoric anhydride. Calorimetric and dielectric studies both indicate that the rotational transition is sharply defined in these systems. We shall now present evidence for a premonitory phenomenon in *dl*-camphoric anhydride using solid-state n.m.r. measurements. This phenomenon is believed to be a new kind of observation.

4.3 Theory

We briefly summarise the essential features of the theory of solid-state n.m.r. [32],[41],[42],[43].

We are concerned with the dynamic properties of magnetic dipoles under the influence of an orthogonal static magnetic field H_0 and, at right angles, an oscillating r-f field with amplitude H_1 ($H_0 > H_1$). In order to solve the dynamic equations that result (the *Bloch equations*) it is convenient to view the precession of magnetic moments from a system of coordinates which is rotating about the static magnetic field with an angular velocity ω. The *magnetisation* (magnetic moment per unit volume) is then broken down into two major components relative to the static magnetic field: the *longitudinal* and *transverse* magnetisation. The former is concerned with the coupling between *Zeeman transitions* (transitions between different quantum states associated with nuclear

spins, under a magnetic field) and those of the lattice phonons, the spin-lattice coupling. Thus the relaxation time T_1 associated with the longitudinal magnetisation is called the *longitudinal* or *spin-lattice relaxation time*, where $T_{1\rho}$ is normally used to denote this quantity in the rotating frame of reference. The time constant for the decay of the transverse magnetisation is called the *transverse* or *spin-spin relaxation time*, T_2. This type of relaxation process causes *line broadening* as the interacting spins acquire different precessional phases which give rise to a modulation of the effective magnetic field at a given nuclear site and therefore a variation of the condition of resonance with position in the lattice. Consequently T_2 is related to the line-width.

The r-f field is treated as a linearly polarised field $H_x = 2H_1\cos\omega t$ and the transverse magnetisation is resolved into in-phase and out-of-phase components with respect to the linearly polarised field. This is done by simply defining a *complex Bloch* susceptibility (complex transverse magnetisation per unit r-f field) as follows.

$$\chi^* = \chi' - i\chi'' \tag{4.1}$$

The *in-phase* χ' and *out-of-phase* χ'' *Bloch susceptibilities* are given by the following equations.

$$\chi' = \tfrac{1}{2}\chi_0\omega_0\frac{T_2\Delta\omega}{L(\Delta\omega)} \tag{4.2}$$

$$\chi'' = \tfrac{1}{2}\chi_0\omega_0\frac{T_2}{L(\Delta\omega)} \tag{4.3}$$

where

$$L(\Delta\omega) = 1 + \gamma^2H_1{}^2T_1T_1 + T_2{}^2(\Delta\omega)^2 \tag{4.4}$$

χ_0 is the static susceptibility and γ is the gyromagnetic ratio. It is

found that *power absorption* A (the rate of energy absorption by the nuclear spin system) is related to χ'' as follows.

$$A = 2\omega H_1^2 \chi'' \tag{4.5}$$

This implies that χ'' is the absorptive part of the susceptibility; and χ' is the dispersive part. The component χ' of the susceptibility changes the inductance of a circuit; and χ'' changes the resistance. Thus it is possible to measure χ' or χ'' separately (see reference [44] for details) in which case we observe the *dispersive* or *u-mode*, and the *absorptive* or *v-mode* respectively.

We are particularly concerned with the absorption mode. From equation (4.5) power absorption is a maximum when $\omega = \omega_0$ and $L(\Delta\omega) = 1 + \gamma^2 H_1^2 T_1 T_2$ for a given H_1. The quantity $1/(1 + \gamma^2 H_1^2 T_1 T_2)$ is called the *saturation factor* and is responsible for *saturation broadening* at high r-f fields when power absorption becomes independent of the r-f field. Under normal conditions the r-f field is made so small that the term $\gamma^2 H_1^2 T_1 T_2$ is negligible compared to unity and power absorption is proportional to the r-f field. In this case $L(\Delta\omega) \simeq 1 + T_2^2 (\Delta\omega)^2$. Thus the half-width of the resonance at half power is given by

$$(\Delta\omega)_{\frac{1}{2}} = 1/T_2 \tag{4.6}$$

Under these conditions the corresponding line shape function is Lorentzian and has the same form as χ''.

To enhance sensitivity for the detection of the resonance line an audio-frequency modulation of the scanning magnetic field is employed. The modulated signal, under appropriate conditions, is proportional to the slope of the n.m.r. signal and gives rise to *derivative* or *peak-to-peak line width* (fig. 4.1). This line width is identical to that at

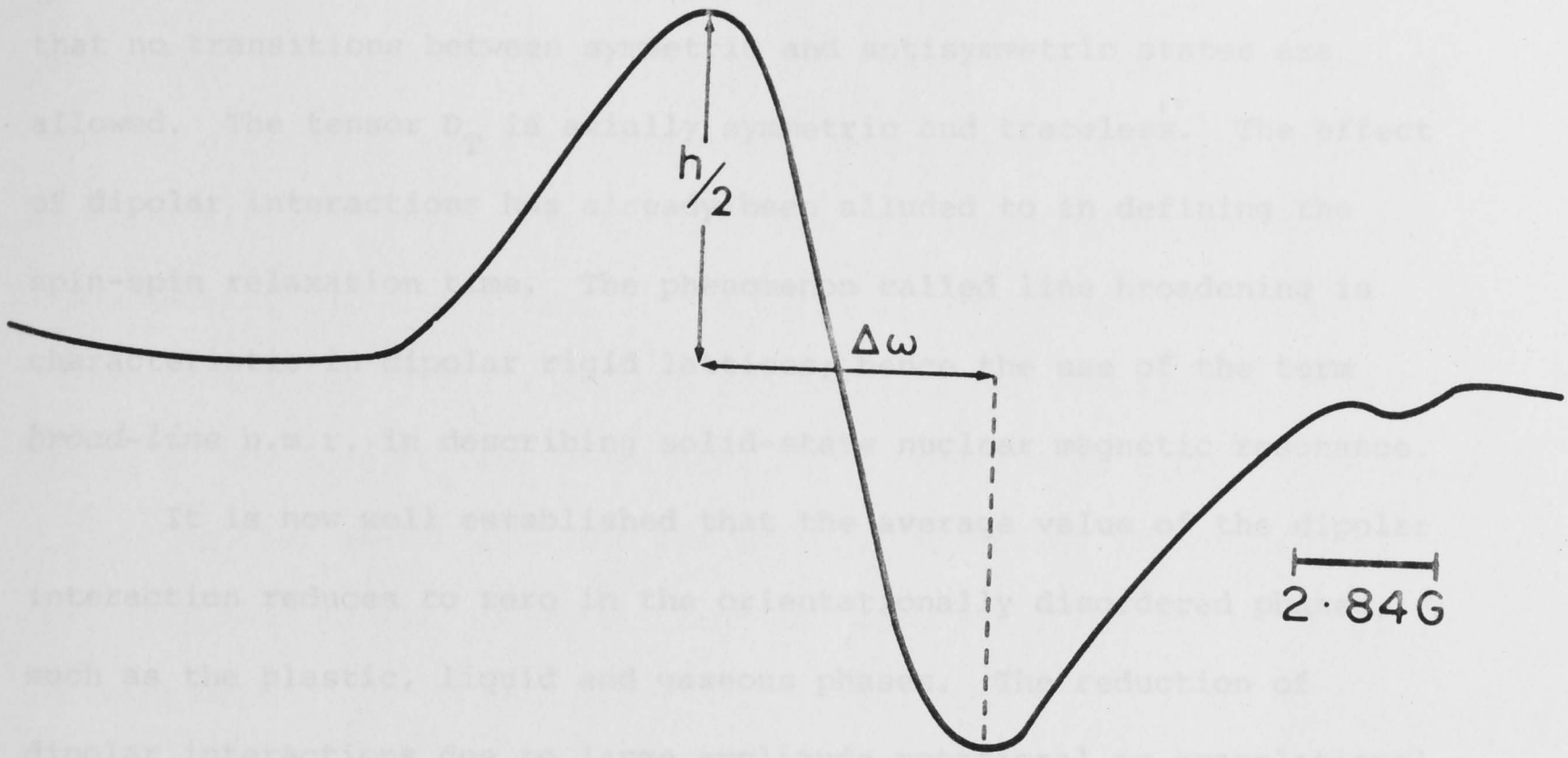

Fig 4.1: A typical solid-state n.m.r. signal obtained for *d*-camphoric anhydride at room temperature. $\Delta\omega$ and h/2 are the peak-to-peak line width and half signal amplitude respectively.

half power for a Lorentzian line as the points of inflection for this line shape function occurs at half the peak height.

The Hamiltonian which determines the n.m.r. spectra in rigid lattices is given by the following equation.

$$\underset{\sim}{H} = \underset{\sim Z}{H} + \underset{\sim D}{H} \qquad (4.7)$$

where $\underset{\sim Z}{H}$ is the Zeeman interaction between the nuclei and the applied magnetic field $\underset{\sim}{H_0}$. $\underset{\sim D}{H}$ is the truncated dipolar interaction and is given by

$$\underset{\sim D}{H} = h \sum_{i<j} \underset{\sim i}{I} . \underset{\sim t}{D} . \underset{\sim j}{I} \qquad (4.8)$$

where $\underset{\sim t}{D}$ is the truncated dipolar interaction tensor. All terms in this tensor contain the angular factor $(3\cos^2\theta_{ij} - 1)$, where θ_{ij} is the angle between the magnetic field $\underset{\sim}{H_0}$ and the internuclear vector r_{ij}. The truncation in H_D is governed by the quantum mechanical selection rule

that no transitions between symmetric and antisymmetric states are allowed. The tensor D_T is axially symmetric and traceless. The effect of dipolar interactions has already been alluded to in defining the spin-spin relaxation time. The phenomenon called line broadening is characteristic in dipolar rigid lattices; hence the use of the term *broad-line* n.m.r. in describing solid-state nuclear magnetic resonance.

It is now well established that the average value of the dipolar interaction reduces to zero in the orientationally disordered phases, such as the plastic, liquid and gaseous phases. The reduction of dipolar interactions due to large amplitude rotational or translational motion gives rise to line-narrowing, a phenomenon known as *motional narrowing*. Motional narrowing is generally associated with a change in the line shape from one that is near Gaussian in the rigid lattice to a Lorentzian line shape in the isotropic disordered phases. Thus both the line width and second moment of the line may be used to study motional narrowing processes. However, Andrew [45] has shown that the application of second moment procedures in the case of extremely rapid narrowing of the line width is inappropriate and that this procedure, in general, may obscure intermediate characteristics of the overall transition which may correspond to a different relaxation mechanism (with its own energy of activation) from the one causing the initial motional narrowing.

Similar observations to those of Andrew had been made by Waugh and Fedin [46] who derived the following approximate expression for the energy of activation E_a for motional narrowing.

$$E_a = 155\ T_c \text{ J/mole} \tag{4.9}$$

where T_c is the temperature at which the n.m.r. spectrum narrows. This equation provides reasonable estimates of the activation energies provided

the motional narrowing transition is continuous (i.e. the rigid lattice and the disordered phase spectra do not appear simultaneously during the transition) [45]. The equation has the advantage of describing intermediate characteristics of the motional narrowing transition. However equation (4.9) is defined for motional narrowing only and may not apply in the case of line broadening which occurs with rising temperature.

Another useful equation for motional narrowing in solids has recently been derived by Hendrickson and Bray [47], and may be written as follows.*

$$ln(1/\Delta\omega - 1/\Delta\omega_{max}) = -E_a/kT + ln(1/\Delta\omega_{min} - 1/\Delta\omega_{max}) \qquad (4.10)$$

where $\Delta\omega_{max}$ is the line width corresponding to the rigid lattice, $\Delta\omega$ is the line width in the region associated with motional narrowing and $\Delta\omega_{min}$ is the line width of the rotationally disordered phases. The theory is based on the concept of two possible states for each magnetic dipole: the excited state B (with $T_{2B} = 1/\Delta\omega_{min}$) and the non-excited state A (with $T_{2A} = 1/\Delta\omega_{max}$). It is then postulated that, due to the rapid exchange between the two states (the thermally activated and dynamic B, and the initial and static states), only a single line width $\Delta\omega$ is observed. This line width is related to a single transverse relaxation time T_2 by $T_2 = f_A T_{2A} + f_B T_{2B}$ where f_A and f_B represent average fractions of dipoles in states A and B respectively.

Equation (4.10) has the advantage of reducing to the Redfield theory [42] (where the activation energy is determined from an Arrhenius plot, i.e. it assumes a single relaxation time for the relaxation process and therefore is valid only at high temperatures). Unlike equation (4.9),

---

* The sign of the last term in the right hand side of equation (4.10) was given incorrectly in the original paper.

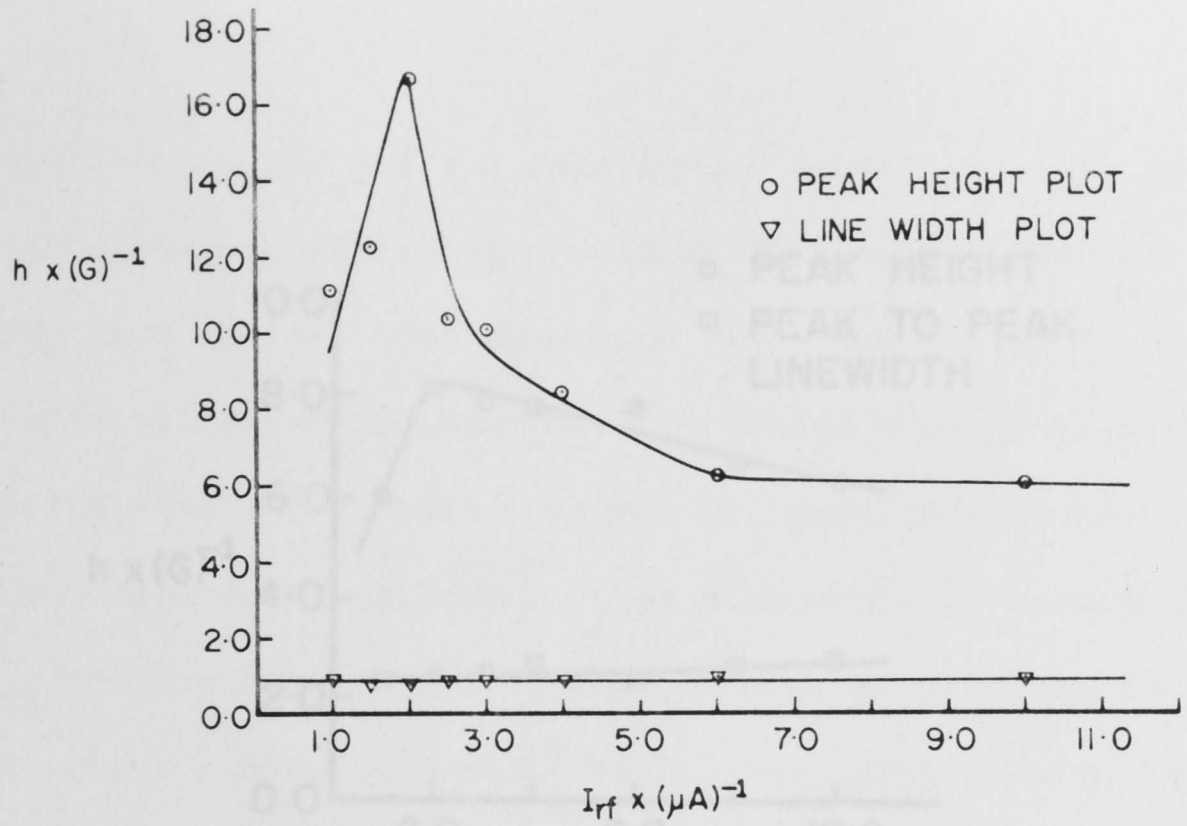

Fig 4.2: NMR SIGNAL SATURATION CURVES OF THE ROTATOR PHASE OF d-CAMPHORIC ANHYDRIDE

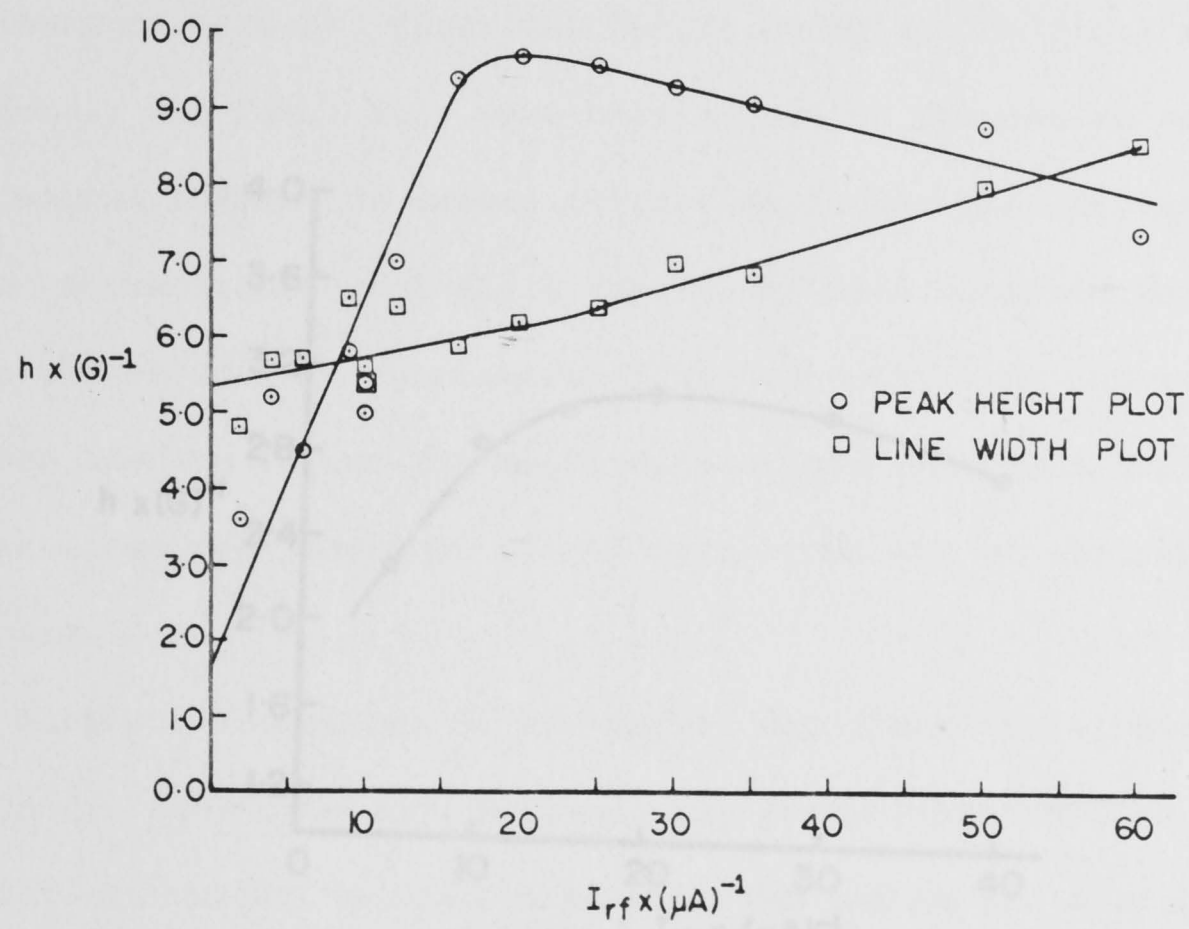

Fig 4.3: NMR SIGNAL SATURATION CURVES OF THE NON-ROTATOR PHASE OF d-CAMPHORIC ANHYDRIDE.

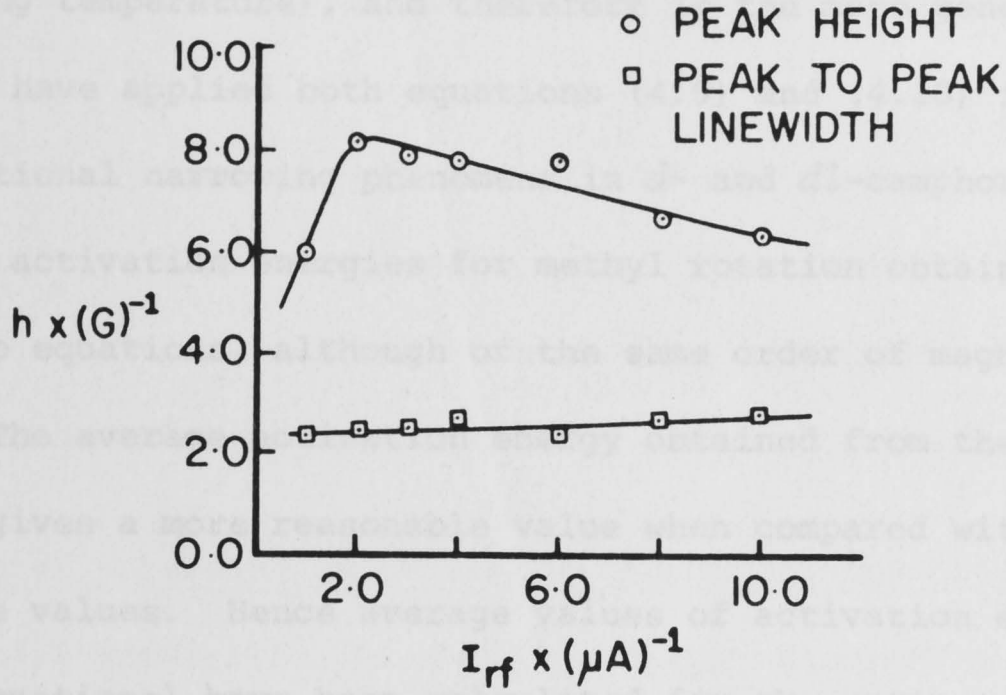

Fig 4.4: SOLID-STATE NMR SIGNAL SATURATION CURVES OF THE dl-CAMPHORIC ANHYDRIDE ROTATOR PHASE.

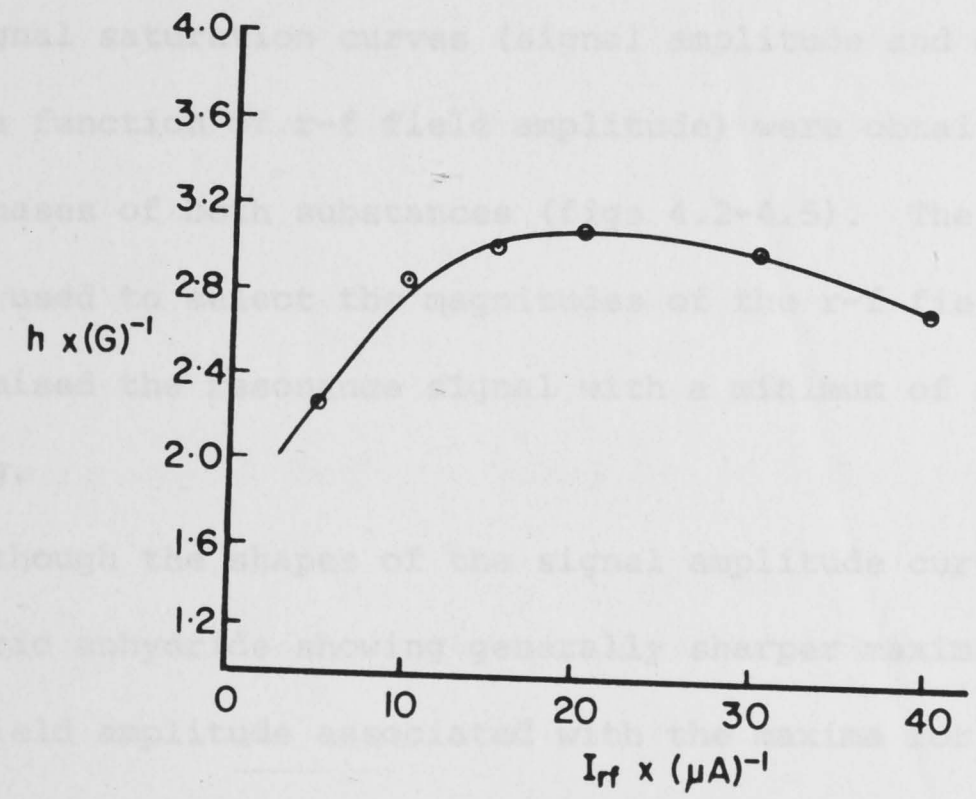

Fig 4.5: SOLID STATE NMR SIGNAL SATURATION CURVES OF THE dl-CAMPHORIC ANHYDRIDE NON-ROTATOR PHASE.

this equation may allow for a negative activation energy* (line broadening with rising temperature), and therefore is the more general.

We have applied both equations (4.9) and (4.10) in the analysis of the motional narrowing phenomena in *d*- and *dl*-camphoric anhydride. Values of activation energies for methyl rotation obtained by the use of the two equations, although of the same order of magnitude, generally differ. The average activation energy obtained from the two equations, however, gives a more reasonable value when compared with independent literature values. Hence average values of activation energies (from the two equations) have been calculated for the entire motional narrowing transition in *d*- and *dl*-camphoric anhydride.

4.4 Experimental

The n.m.r. experiments were performed on a Varian V2400 Wide Line NMR Spectrometer. Preliminary experiments were carried out using annealed racemate in the temperature range 295 K to 500 K, in order to establish the pattern of motional narrowing before defining the final experimental conditions. The final runs were carried out on unannealed samples and n.m.r. signal saturation curves (signal amplitude and derivative line width as a function of r-f field amplitude) were obtained for each of the two phases of both substances (figs 4.2-4.5). The saturation curves were then used to select the magnitudes of the r-f field amplitude that optimised the resonance signal with a minimum of saturation broadening.

Although the shapes of the signal amplitude curves differed (*d*-camphoric anhydride showing generally sharper maxima) the values of the r-f field amplitude associated with the maxima for corresponding phases were the same in both substances. Values of 20 μA and 2 μA were taken as the optimal r-f field amplitudes for the non-rotator and

---

* The physical significance of a process that requires a negative activation energy is difficult to visualise. All that can be said, for the present, is that such a process is more complicated than a simple passage over an energy barrier.

rotator phases respectively and these values were used throughout the experiment.

Both the annealed and unannealed samples of the racemate gave the same pattern of motional narrowing. When racemate samples were annealed in the course of measurement (the consequence of being held for several hours in the plastic phase (400 K)) results were unaltered.

4.5 Motional Narrowing in *d*- and *dl*-Camphoric Anhydride Crystals

Fig 4.6 summarises the results of the solid-state n.m.r. measurements for *d*- and *dl*-camphoric anhydride. It should be noted that both substances show a rapid decrease in their common line width at about 90 K and another fall at the temperature of the rotational transition. The racemate however shows an *anomalous increase in line width* from 160 K to a maximum at 290 K returning to the value for *d*-camphoric anhydride at 330 K. A rapid fall at the rotational transition follows in each case. Anderson and Slichter [25] did not observe this anomaly in their second moment study of camphor.

The activation energy 17 ± 4 kJ/mole associated with the low temperature motional narrowing commencing at 80 K was calculated using equations (4.9) and (4.10). This value is the same as the activation energy calculated for methyl group re-orientation in the non-rotator phase of *d*-camphor at 135 K [14]. Thus we attributed the low temperature motional narrowing in camphoric anhydride to methyl group re-orientation.

Fig. 4.7 is a plot of $ln(1/\Delta\omega - 1/\Delta\omega_{max})$ vs. 1/T. Regions with a common activation energy appear as straight lines. These activation energies, together with those obtained from the use of equation (4.9), are summarised in table 4.1. However equation (4.9) may not be applicable to the secondary line broadening process observed in the racemate, and therefore a calculation of the activation energy for this region has been

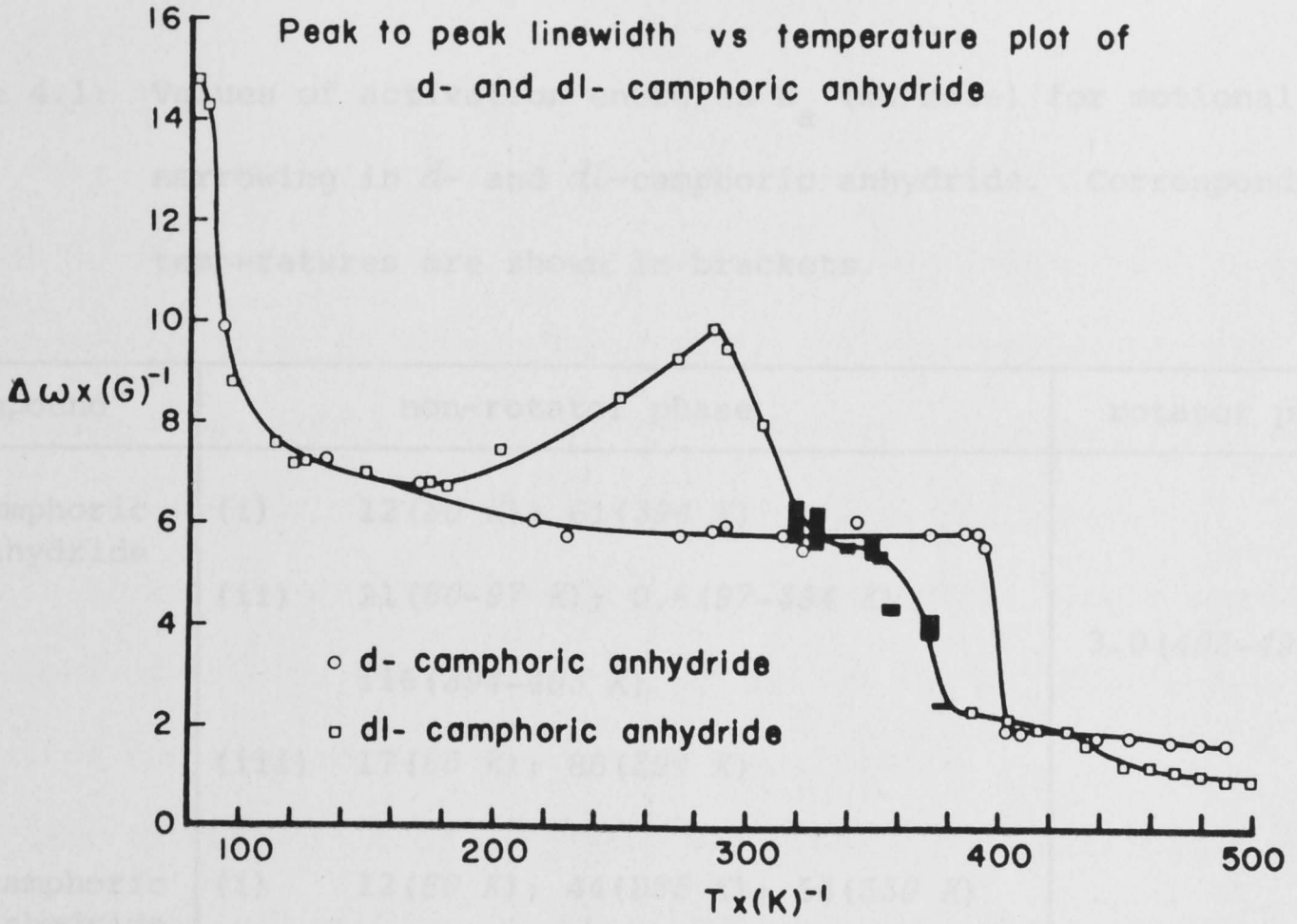

Fig 4.6: Motional narrowing in *d*- and *dl*-camphoric anhydride. There is a rapid decrease in their common line-width at low temperatures, and another fall at the rotational transition. An anomalous line broadening is observed in the racemate, but is absent in the optical isomer.

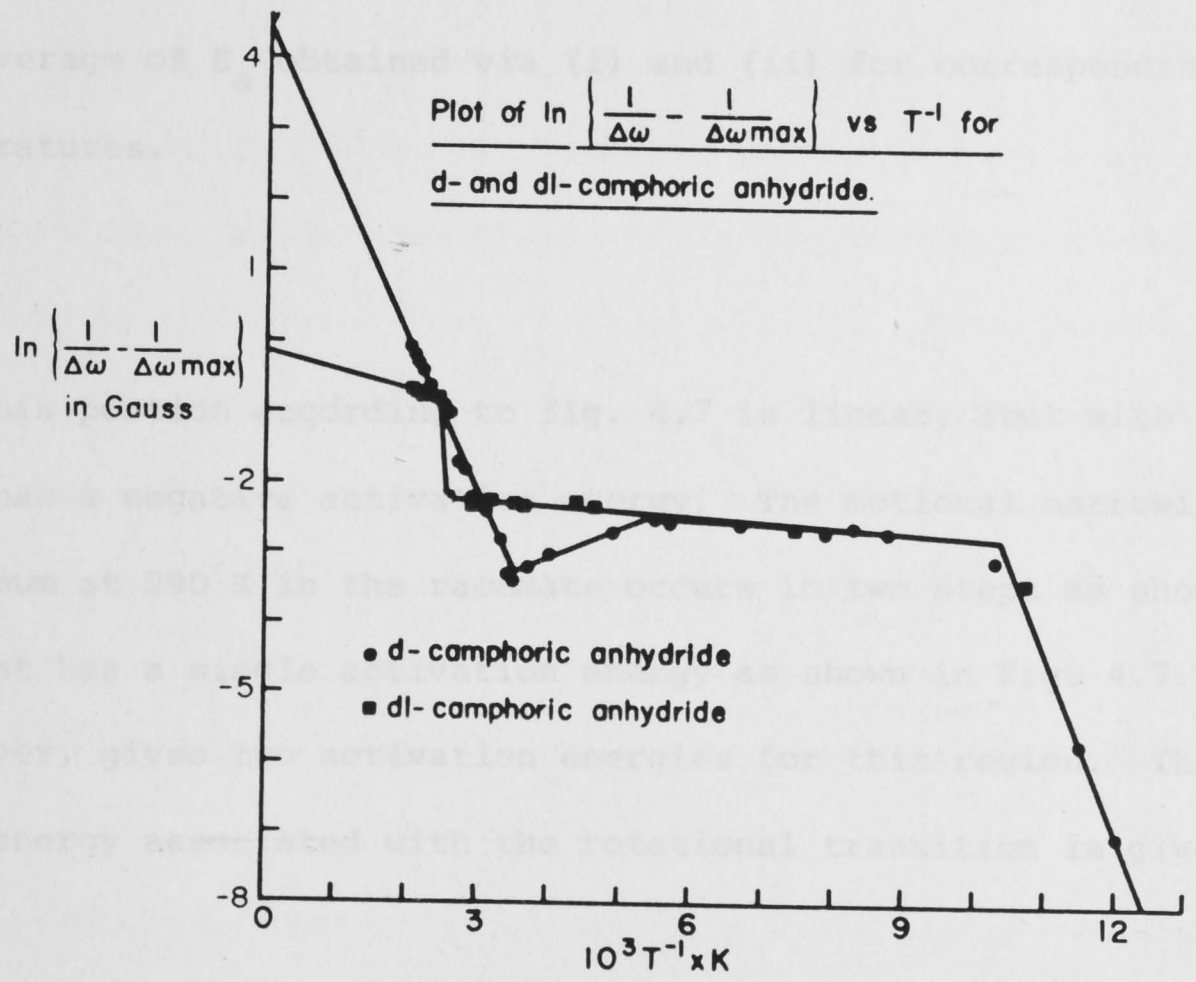

Fig 4.7: Analysis of the *d*- and *dl*-camphoric anhydride motional narrowing characteristics.

Table 4.1: Values of activation energies E_a (kJ/mole) for motional narrowing in *d*- and *dl*-camphoric anhydride. Corresponding temperatures are shown in brackets.

Compound	non-rotator phase	rotator phase
d-camphoric anhydride	(i) 12(*80 K*); 61(*394 K*)	
	(ii) 21(*80-97 K*); 0.6(*97-394 K*)	3.0(*403-495 K*)
	116(*394-403 K*)	
	(iii) 17(*80 K*); 88(*394 K*)	
dl-camphoric anhydride	(i) 12(*80 K*); 44(*285 K*); 54(*350 K*)	
	(ii) 21(*90-97 K*); 0.6(*97-182 K*)	18(*287-500 K*)
	-4(*182-287 K*); 18(*287-500 K*)	
	(iii) 17(*80 K*); 31(*285 K*); 36(*350 K*)	

(i) via equation (4.9)

(ii) via equation (4.10)

(iii) the average of E_a obtained via (i) and (ii) for corresponding temperatures.

omitted. This portion according to fig. 4.7 is linear, (but with positive slope) and has a negative activation energy. The motional narrowing from the submaximum at 290 K in the racemate occurs in two steps as shown in Fig. 4.6, but has a single activation energy as shown in Fig. 4.7. Equation (4.9), however, gives two activation energies for this region. The activation energy associated with the rotational transition is given in Table 4.1.

4.6 Discussion

The reproducibility of the n.m.r. anomaly observed in the racemate may not be doubted as several runs involving both annealed and unannealed samples gave similar results. This anomaly is observed over a wide temperature range (160-320 K), and indicates both an ordering and disordering of magnetic dipole moments of protons in the molecule. In contrast dielectric studies indicate that the electric dipole moments of the molecules (5.41D, see table 3.1) are locked in the lattice during the entire range before the rotational transition.

The initial motional narrowing has already been attributed to methyl rotation. Therefore, in agreement with dielectric results, molecular orientational disorder is absent in this temperature range; i.e. the anomaly is not attributable to an ordering process involving molecular reorientation. Thus the explanation of the anomaly being sought for must be consistent with dipolar ordering and should also allow for thermal expansion.

A *possible* explanation of the n.m.r. anomaly is that anisotropic thermal expansion brings protons on adjacent molecules into a more intimate disposition, which encourages proton magnetic dipole moment coupling. This in turn would cause line broadening. With increasing temperature a stage is reached where through further thermal expansion the intimate disposition between the protons and adjacent molecules is lost and the line width falls again to the value observed in *d*-camphoric anhydride just before the rotational transition. We shall attempt to identify the protons concerned with the anomaly in the next chapter.

We note that the magnitudes of the line width at low temperatures are the same in both *d*- and *dl*-camphoric anhydride. This implies that

the degree of molecular packing in both substances is very similar in this temperature range. The similarity between the crystal systems at room temperature (at around the peak of the n.m.r. anomaly in the racemate) has been alluded to in chapter 2. Thus it would seem to follow that the racemate crystal lattice is even closer to the orthorhombic lattice of the optical isomer at low temperatures.

5 predicted crystal structures of *d*- and *dl*-camphoric anhydride

The observed differences in the physical properties of the optical isomers and their mixtures in the solid state must arise from differences in molecular packing. This in turn is a function of discrimination energies between the two optical isomers. None of the crystal structures of interest here are known, but the calculation of crystal structures is now a fairly established technique. This chapter discusses calculations of crystal packing, of d- and dl-camphoric anhydride at room temperature, in an attempt to explain the anomalies observed in the plastic crystal-phase transitions of the d- and l-systems of the camphor-type compounds.

5.1 Introduction

In this chapter we consider mixtures of *d*- and *l*-molecules at the most microscopic level: What is the intrinsic difference between solid *d*- (or *l*-) and solid racemate? Is the latter in any sense a compound or is it merely Nature's solution to the problem of packing equal numbers of *d*- and *l*-molecules? Is there an intrinsic extra attraction between *d*- and *l*-, over and above the interaction energy between *d*- and *d*-?

5.2 Computational

The theory of chiral interaction over longish distances (e.g. in solution) has lately received attention from Craig and Schipper [3]. Potentials expressed in terms of multipole interactions are applicable in this domain. In solids, no point multipole expression is likely to be useful, but one may turn to the methods already established for calculating crystal energies in terms of atom-atom interactions, with multipole-multipole interactions superimposed if desired. Chirality is then built into the problem automatically, through the coordinates of the atoms. We therefore set out to calculate the sublimation energies of the crystal of *d*-* and *dl*-camphoric anhydride, the compound of our series for which the unit cell parameters were most easily measurable.

This intention was made possible through the availability of a remarkably powerful QCFF/PI (the quantum mechanical extension of the consistent force field to π-electrons) program package written by Warshell *et al* [49],[50]. This program optimises the molecular geometry of the free molecule; and for a crystal, optimises both the geometry and

---

* or *l*-: our definition of absolute configuration is necessarily arbitrary.

the crystal packing. The geometry is optimised with respect to a Urey-Bradley intramolecular force-field for σ bonds, with a quantum mechanically calculated potential for π bonds. The crystal packing calculation is effected through a systematic search procedure within the space defined by intramolecular parameters plus the degrees of freedom defined by the space group and the number of molecules per unit cell. In principle, the cell parameters also could be variables, but in practice the task of calculating a crystal structure *a priori* is too demanding of computer time. Intermolecular interactions are a sum of exp-6 atom potentials plus the charge-charge interactions of the dipolar regions.

The unit cell parameters of *d*- and *dl*-camphoric anhydride are listed in table 2.1. We recall our discussion in chapter 2 that the *dl*-crystal has a unit cell which may be regarded as a slightly deformed variation of the orthorhombic unit cell of the *d*-compound. Also the molecular volume in the racemate significantly exceeds that in the *d*-compound. There is now abundant evidence that crystal stability (i.e. sublimation energy) is largely determined by the efficiency of packing - i.e. crudely, by density. Thus this observation alone suggests that the calculations will show the *d*-compound to form more stable crystals. The experimental evidence for *d*- and *dl*-camphor from the work of Schäfer and Frey [51] confirms this view: $(\Delta E_s)_{d-}$ = 80.42 kJ/mole; $(\Delta E_s)_{dl-}$ = 76.15 kJ/mole; $(v_m)_{d-}$ = 223.8Å^3; $(v_m)_{dl-}$ = 233.8Å^3; and therefore a discrimination energy of 4.27 kJ/mole in favour of the *d*-compound. The sublimation energies were calculated from specific heat curves extrapolated to 0 K. The sublimation energy for *d*-camphor in the temperature range 273 K to 453 K (rotator phase) is given as 53.55 kJ/mole [52].

5.3 Molecular geometry

The initial geometry offered to the program was roughly measured in cartesian coordinates from a Dreiding model. The program was then

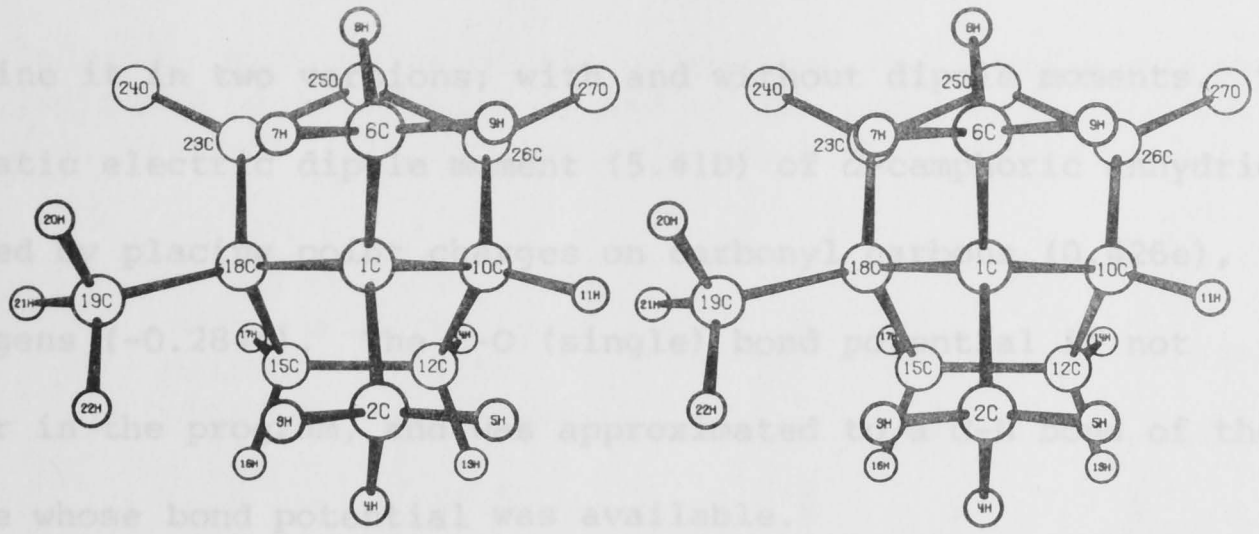

Fig 5.1: Equilibrium geometry of the free molecule of *d*-camphoric anhydride (with dipole moments)*.

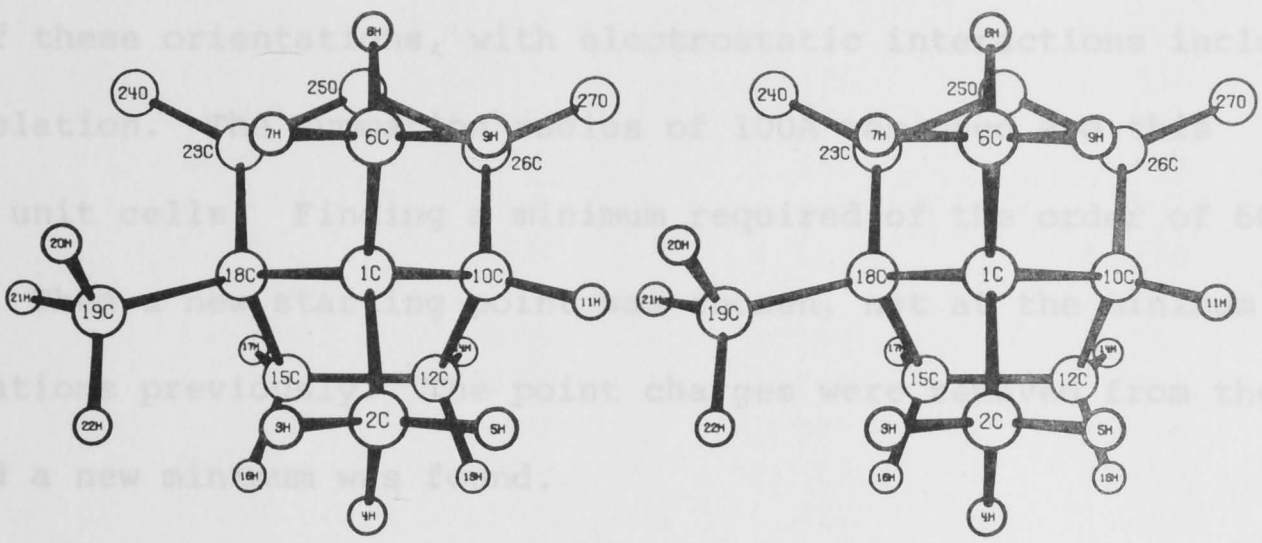

Fig 5.2: Equilibrium geometry of a *d*-molecule in the *d*-crystal of camphoric anhydride (with dipole moments).

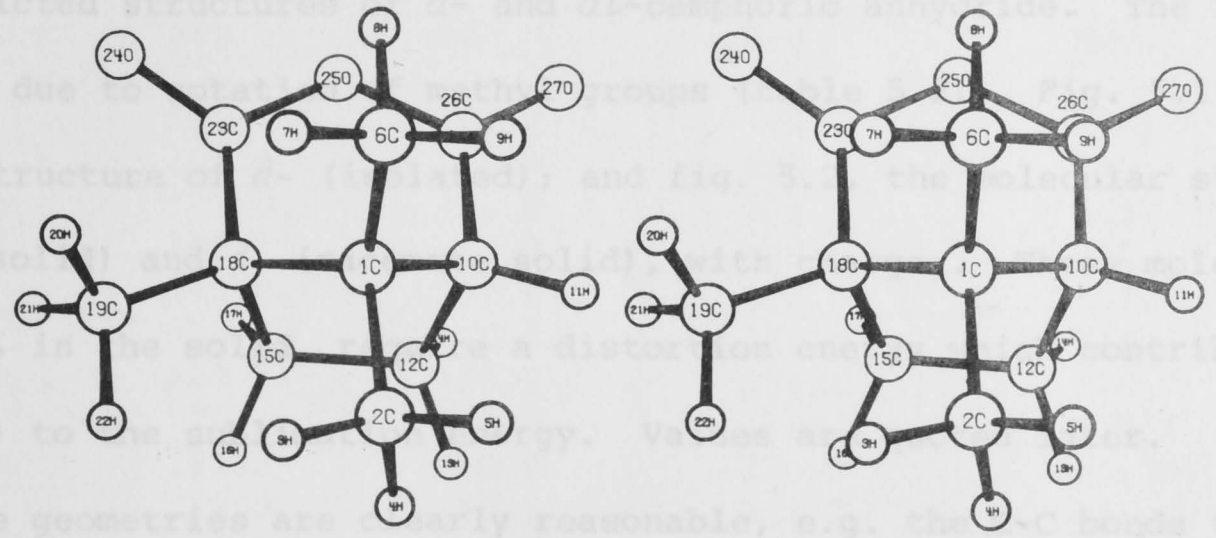

Fig 5.3: Equilibrium geometry of a *d*-molecule in the *dl*-crystal of camphoric anhydride (with dipole moments).

* All the diagrams in this chapter are stereoscopic, and were drawn with the use of ORTEP (the Oak-Ridge Thermal Ellipsoid Plot) program written by C.K. Johnson.

used to refine it in two versions; with and without dipole moments. The observed static electric dipole moment (5.41D) of *d*-camphoric anhydride was simulated by placing point charges on carbonyl carbons (0.426e), and the oxygens (-0.284e). The C-O (single) bond potential is not provided for in the program, and was approximated to a C-N bond of the pyrrole type whose bond potential was available.

In the case of crystal packing, finding a minimum involved first a systematic survey of initial molecular orientations (Williams' grid [53] of 12 rotational points was used) with no electrostatic interactions included. This was then followed by a search initiated from the most promising of these orientations, with electrostatic interactions included in the calculation. The summation radius of 100Å was used and this included 27 unit cells. Finding a minimum required of the order of 60 iterations. Then a new starting point was chosen, not at the minimum, say 20 iterations previously. The point charges were removed from the molecule and a new minimum was found.

Table 5.1, columns 1 and 2, list the geometrical parameters of these two optimised models of the free molecule. The crystal packing calculations allow for distortion of the geometry of the free molecule. Columns 3 and 4 of the table specify the distorted geometries of the polar model reached in the predicted structures of *d*- and *dl*-camphoric anhydride. The largest changes are due to rotation of methyl groups (table 5.2). Fig. 5.1 shows the molecular structure of *d*- (isolated); and fig. 5.2, the molecular structures of *d*- (isomer solid) and *d*- (racemate solid), with charges. These molecular distortions, in the solid, require a distortion energy which contributes (negatively) to the sublimation energy. Values are quoted later.

These geometries are clearly reasonable, e.g. the C-C bonds to the bridging $C(CH_3)_2$ group are long bonds, as considerations of ring strain would suggest. The only somewhat unexpected figures are the short

Table 5.1: Internal coordinates of the calculated equilibrium geometries (with and without charges) and of the *d*-molecule in *d*-, and *dl*-, crystals (electrostatic interactions included).

Internal coordinates	*d*- (free molecule without charges)	*d*- (free molecule with charges)	*d*-crystal	*dl*-crystal
bonds	Å	Å	Å	Å
C_1-C_2	1.546	1.548	1.543	1.541
C_1-C_6	1.526	1.525	1.521	1.512
C_1-C_{10}	1.567	1.564	1.558	1.564
C_1-C_{18}	1.560	1.559	1.555	1.555
C_2-H_3	1.104	1.104	1.100	1.102
C_2-H_4	1.100	1.100	1.099	1.095
C_2-H_5	1.105	1.105	1.102	1.098
C_6-H_7	1.105	1.115	1.104	1.106
C_6-H_8	1.102	1.110	1.100	1.097
C_6-H_9	1.106	1.117	1.104	1.106
C_{10}-H_{11}	1.102	1.102	1.095	1.097
C_{10}-C_{12}	1.554	1.555	1.550	1.551
C_{10}-C_{26}	1.495	1.495	1.492	1.499
C_{12}-H_{13}	1.104	1.103	1.101	1.099
C_{12}-H_{14}	1.098	1.098	1.092	1.093
C_{12}-C_{15}	1.556	1.556	1.550	1.552
C_{15}-H_{16}	1.101	1.101	1.100	1.093
C_{15}-H_{17}	1.100	1.100	1.093	1.094
C_{15}-C_{18}	1.563	1.563	1.561	1.566
C_{18}-C_{19}	1.504	1.505	1.498	1.499
C_{18}-C_{23}	1.512	1.511	1.506	1.506
C_{19}-H_{20}	1.107	1.107	1.103	1.105
C_{19}-H_{21}	1.107	1.107	1.104	1.103
C_{19}-H_{22}	1.106	1.106	1.105	1.105
C_{23}=O_{24}	1.327	1.325	1.317	1.322
C_{23}-O_{25}	1.465	1.461	1.459	1.457
O_{25}-C_{26}	1.458	1.454	1.449	1.450
C_{26}=O_{27}	1.319	1.318	1.320	1.318
bond angles	deg	deg	deg	deg
C_2-C_1-C_6	106.9	106.2	106.4	105.1
C_2-C_1-C_{10}	108.1	108.4	108.4	110.8
C_2-C_1-C_{18}	112.9	112.8	112.1	111.7
C_1-C_2-H_3	110.9	110.8	109.9	111.3
C_1-C_2-H_4	112.6	112.6	113.0	111.4
C_1-C_2-H_5	110.1	110.1	109.6	111.6
C_6-C_1-C_{10}	113.7	114.2	114.1	114.3
C_6-C_1-C_{18}	115.1	115.3	115.5	115.1
C_1-C_6-H_7	111.3	110.5	110.5	111.2
C_1-C_6-H_8	112.9	113.3	113.9	111.2
C_1-C_6-H_9	111.0	110.3	110.1	111.2
C_{10}-C_1-C_{18}	100.0	100.1	100.1	100.0
C_1-C_{10}-H_{11}	111.4	111.5	111.2	112.3
C_1-C_{10}-C_{12}	104.4	104.4	104.1	103.3
C_1-C_{10}-C_{26}	109.5	109.6	109.8	111.3
C_1-C_{18}-C_{15}	103.5	103.4	103.0	103.8

Table 5.1 continued

bond angles	deg	deg	deg	deg
C_1-C_{18}-C_{19}	114.6	114.7	114.5	115.5
C_1-C_{18}-C_{23}	109.1	109.0	108.6	108.5
H_3-C_2-H_4	107.6	107.7	107.8	108.5
H_3-C_2-H_5	107.7	107.7	108.4	105.8
H_4-C_2-H_5	107.8	107.7	108.0	107.9
H_7-C_6-H_8	106.6	107.2	107.3	108.0
H_7-C_6-H_9	107.3	107.9	107.3	107.5
H_8-C_6-H_9	107.5	107.4	107.5	107.6
H_{11}-C_{10}-C_{12}	111.8	111.9	112.1	111.1
H_{11}-C_{10}-C_{26}	112.1	112.2	111.9	112.4
C_{12}-C_{10}-C_{26}	107.2	107.0	107.4	105.9
C_{10}-C_{12}-H_{13}	110.2	110.3	110.7	109.2
C_{10}-C_{12}-H_{14}	112.3	112.3	112.3	112.3
C_{10}-C_{12}-C_{15}	105.2	105.1	104.9	104.5
C_{10}-C_{26}-O_{25}	116.8	117.1	117.4	117.7
C_{10}-C_{26}=O_{27}	121.9	121.8	121.2	122.4
H_{13}-C_{12}-H_{14}	109.2	109.3	109.4	108.4
H_{13}-C_{12}-C_{15}	108.6	108.6	109.1	110.0
H_{14}-C_{12}-C_{15}	111.2	111.2	110.3	112.4
C_{12}-C_{15}-H_{16}	109.7	109.7	110.0	111.8
C_{12}-C_{15}-H_{17}	110.5	110.5	109.9	110.3
C_{12}-C_{15}-C_{18}	106.1	106.1	106.3	106.4
H_{16}-C_{15}-H_{17}	108.2	108.2	108.2	106.6
H_{16}-C_{15}-C_{18}	110.9	110.9	111.2	110.8
H_{17}-C_{15}-H_{18}	111.4	111.4	111.3	111.0
C_{15}-C_{18}-C_{19}	112.1	112.0	111.2	110.2
C_{15}-C_{18}-C_{23}	105.3	105.4	106.8	105.5
C_{19}-C_{18}-C_{23}	111.6	111.6	112.2	112.4
C_{18}-C_{19}-H_{20}	111.5	111.5	112.2	112.5
C_{18}-C_{19}-H_{21}	111.5	111.4	112.0	109.5
C_{18}-C_{19}-H_{22}	112.0	112.1	111.0	112.6
C_{18}-C_{23}=O_{24}	123.5	123.4	123.4	124.2
C_{18}-C_{23}-O_{25}	117.7	118.0	118.0	117.2
H_{20}-C_{19}-H_{21}	107.6	107.6	107.3	108.3
H_{20}-C_{19}-H_{22}	107.4	107.4	107.5	107.7
H_{21}-C_{19}-H_{22}	106.5	106.5	106.5	106.0
O_{24}=C_{23}-O_{25}	118.6	118.4	118.5	118.3
C_{23}-O_{25}-C_{26}	120.1	119.8	119.6	119.6
O_{25}-C_{26}=O_{27}	121.2	121.0	121.3	119.7
torsional bond angles	deg	deg	deg	deg
C_6-C_1-C_2-H_3	58.0	56.7	56.1	69.7
C_6-C_1-C_2-H_4	178.6	177.4	176.5	190.9
C_6-C_1-C_2-H_5	298.9	297.7	297.1	311.6
C_{10}-C_1-C_2-H_3	180.7	179.6	179.4	193.6
C_{10}-C_1-C_2-H_4	301.3	300.4	299.8	314.9
C_{10}-C_1-C_2-H_5	61.2	61.7	60.4	75.6
C_{18}-C_1-C_2-H_3	290.4	289.5	289.0	304.1
C_{18}-C_1-C_2-H_4	51.0	50.3	49.4	65.4
C_{18}-C_1-C_2-H_5	171.3	170.5	170.0	186.1
C_2-C_1-C_6-H_7	332.5	304.3	298.8	297.8
C_2-C_1-C_6-H_8	212.7	183.9	177.9	177.5

Table 5.1 continued

torsional bond angles	deg	deg	deg	deg
C_2-C_1-C_6-H_9	91.9	63.5	57.1	57.6
C_{10}-C_1-C_6-H_7	213.3	185.0	179.2	176.1
C_{10}-C_1-C_6-H_8	93.5	64.6	58.3	55.8
C_{10}-C_1-C_6-H_9	332.7	304.2	297.5	295.9
C_{18}-C_1-C_6-H_7	98.7	69.9	63.9	61.2
C_{18}-C_1-C_6-H_8	338.9	309.6	303.0	300.8
C_{18}-C_1-C_6-H_9	218.1	189.1	182.2	180.9
C_2-C_1-C_{10}-H_{11}	314.0	313.7	312.2	311.8
C_2-C_1-C_{10}-C_{12}	74.9	74.7	73.1	71.6
C_2-C_1-C_{10}-C_{26}	189.4	188.9	187.9	184.8
C_6-C_1-C_{10}-H_{11}	72.5	71.8	70.7	70.3
C_6-C_1-C_{10}-C_{12}	193.4	192.7	191.6	190.1
C_6-C_1-C_{10}-C_{26}	307.9	306.9	306.3	303.3
C_{18}-C_1-C_{10}-H_{11}	195.8	195.5	194.7	193.8
C_{18}-C_1-C_{10}-C_{12}	316.7	316.4	315.6	313.6
C_{18}-C_1-C_{10}-C_{26}	71.2	70.7	70.3	66.8
C_2-C_1-C_{18}-C_{15}	288.5	288.3	289.0	284.3
C_2-C_1-C_{18}-C_{19}	50.8	50.5	49.8	45.1
C_2-C_1-C_{18}-C_{23}	176.7	176.5	176.0	172.4
C_6-C_1-C_{18}-C_{15}	165.4	166.1	166.9	164.6
C_6-C_1-C_{18}-C_{19}	287.8	288.3	287.7	285.4
C_6-C_1-C_{18}-C_{23}	53.6	54.3	53.9	52.6
C_{10}-C_1-C_{18}-C_{15}	43.1	43.3	43.7	41.6
C_{10}-C_1-C_{18}-C_{19}	165.5	165.5	164.5	162.4
C_{10}-C_1-C_{18}-C_{23}	291.3	291.5	290.7	289.7
C_1-C_{10}-C_{12}-H_{13}	269.9	270.1	270.1	275.4
C_1-C_{10}-C_{12}-H_{14}	147.9	148.0	147.6	155.2
C_1-C_{10}-C_{12}-C_{15}	26.8	27.0	27.8	33.1
H_{11}-C_{10}-C_{12}-H_{13}	30.5	30.8	30.4	36.0
H_{11}-C_{10}-C_{12}-H_{14}	268.5	268.8	267.9	275.8
H_{11}-C_{10}-C_{12}-C_{15}	147.4	147.7	148.1	153.7
C_{26}-C_{10}-C_{12}-H_{13}	153.8	154.0	153.7	158.4
C_{26}-C_{10}-C_{12}-H_{14}	31.8	31.9	31.2	38.1
C_{26}-C_{10}-C_{12}-C_{15}	270.7	270.9	271.4	276.1
C_1-C_{10}-C_{26}-O_{25}	319.0	319.2	320.9	322.7
C_{10}-C_{12}-C_{15}-H_{16}	240.5	240.5	239.4	232.0
C_{10}-C_{12}-C_{15}-H_{17}	121.3	121.2	120.4	113.6
C_{10}-C_{12}-C_{15}-C_{18}	.5	.4	359.9	353.2
H_{13}-C_{12}-C_{15}-H_{16}	358.5	358.5	358.1	349.1
H_{13}-C_{12}-C_{15}-H_{17}	239.3	239.2	239.1	230.7
H_{13}-C_{12}-C_{15}-C_{18}	118.4	118.3	118.6	110.3
H_{14}-C_{12}-C_{15}-H_{16}	118.7	118.7	118.2	110.0
H_{14}-C_{12}-C_{15}-H_{17}	359.5	359.5	359.2	351.6
H_{14}-C_{12}-C_{15}-C_{18}	238.7	238.6	238.8	231.2
C_1-C_{18}-C_{15}-C_{12}	332.4	332.4	332.5	338.0
C_1-C_{18}-C_{15}-H_{16}	91.6	91.5	93.2	92.3
C_1-C_{18}-C_{15}-H_{17}	212.2	212.2	212.9	218.0
C_{12}-C_{15}-C_{18}-C_{19}	208.4	208.4	209.5	213.6
C_{12}-C_{15}-C_{18}-C_{23}	86.9	86.9	86.8	92.0
H_{16}-C_{15}-C_{18}-C_{19}	327.6	327.5	329.2	335.4
H_{16}-C_{15}-C_{18}-C_{23}	206.1	206.0	206.5	213.9
H_{17}-C_{15}-C_{18}-C_{19}	88.2	88.1	89.9	93.7

Table 5.1 continued

torsional bond angles	deg	deg	deg	deg
H_{17}-C_{15}-C_{18}-C_{23}	326.7	326.6	327.2	332.1
C_1-C_{18}-C_{19}-H_{20}	61.9	62.6	52.0	64.6
C_1-C_{18}-C_{19}-C_{21}	182.2	182.8	172.7	185.0
C_1-C_{18}-C_{19}-H_{22}	301.4	302.1	291.7	302.6
C_{15}-C_{18}-C_{19}-H_{20}	179.5	180.0	168.2	181.8
C_{15}-C_{18}-C_{19}-H_{21}	299.7	300.3	288.9	302.3
C_{15}-C_{18}-C_{19}-H_{22}	59.0	59.5	47.8	59.9
C_{23}-C_{18}-C_{19}-H_{20}	297.3	298.0	287.7	299.3
C_{23}-C_{18}-C_{19}-H_{21}	57.6	58.2	48.4	59.7
C_{23}-C_{18}-C_{19}-H_{22}	176.9	177.5	167.3	177.3
C_1-C_{18}-C_{23}-O_{25}	37.5	38.1	38.7	45.8
C_{18}-C_{23}-O_{25}-C_{26}	356.7	355.9	356.4	348.2
O_{24}=C_{23}-O_{25}-C_{26}	181.1	180.6	179.6	163.0
C_{10}-C_{26}-O_{25}-C_{23}	5.0	5.5	3.7	7.2
C_{23}-O_{25}-C_{26}=O_{27}	182.5	183.0	180.6	182.2
C_{10}-O_{25}-C_{26}=O_{27}	177.5	177.5	177.0	174.9
C_{18}=O_{24}-C_{23}-O_{25}	175.4	175.1	176.7	185.6

C-C bond distances to the bridgehead methyl group. An example of the consequences of ring strain is the C-O-C angle of 120, which may be compared with an average value of 110±3 in dialkyl ethers [54].

5.4 Crystal packing

These are very heavy calculations, requiring a search (by steepest descent method followed by the modified Newton-Raphson method) for a minimum in the energy of the packed crystal. We cannot be sure that the energy minima here are global, but we have accepted them because they give eminently reasonable sublimation energies.

Table 5.3 lists the energy terms contributing to the sublimation energies of the resulting *predicted* crystal structures (Figs. 5.3 and 5.4)* of *d*- and *dl*-camphoric anhydride. The diagonal core contributions refer to the one-electron energy terms in the Pariser-Parr-Pople molecular

* Note that the racemate packing pattern consists of homogeneous layers of *d*- and *l*-molecules.

Table 5.2: Selected torsional bond angle changes $\Delta\phi_{d-}$ for methyl group rotation in a *d*-molecule of *d*-, and *dl*-, crystals, with the geometry of the free molecule taken as standard. Electrostatic interactions were included and angles are in degrees

methyl groups	torsional bond angle ϕ	ϕ_{d-} (free molecule)	$\Delta\phi_{d-}$ (*d*-crystal)	$\Delta\phi_{d-}$ (*dl*-crystal)
C_2	C_6-C_1-C_2-H_3	56.7	-0.6	13.0
	C_6-C_1-C_2-H_4	177.4	-0.9	13.5
	C_6-C_1-C_2-H_5	297.7	-0.6	13.9
C_6	C_2-C_1-C_6-H_7	304.3	-5.5	-6.5
	C_2-C_1-C_6-H_8	183.9	-6.0	-6.4
	C_2-C_1-C_6-H_9	63.5	-6.4	-5.9
C_{19}	C_1-C_{18}-C_{19}-H_{20}	62.6	-10.6	2.0
	C_1-C_{18}-C_{19}-H_{21}	182.8	-10.1	2.2
	C_1-C_{18}-C_{19}-H_{22}	302.1	-10.4	0.5

Table 5.3: Contributions to the potential energy of *d*- and *dl*-camphoric anhydride crystals (electrostatic interactions included). All quantities in units of 10^3 kJ/mole.

	interaction	free molecule	*d*-crystal	*dl*-crystal
	intramolecular			
	diagonal core	3.087	3.087	3.088
	bond	-11.745	-11.748	-11.747
	non-bond	0.003	0.009	0.010
	repulsive	1.777	1.778	1.777
	angle bending θ	0.042	0.044	0.049
	torsional ϕ	-0.169	-0.171	-0.167
A :	total intramolecular energy	-7.004	-7.001	-6.991
B :	intermolecular		-0.073	-0.049
A + B :	total energy	-7.004	-7.074	-7.040
	molecular distortion energy		0.003	0.013
	*sublimation energy		0.070	0.036

* Sublimation energy = - intermolecular energy - molecular distortion energy.
The molecular distortion energy is the difference the total intramolecular energies for the molecule in the crystal and the free molecule (line A).

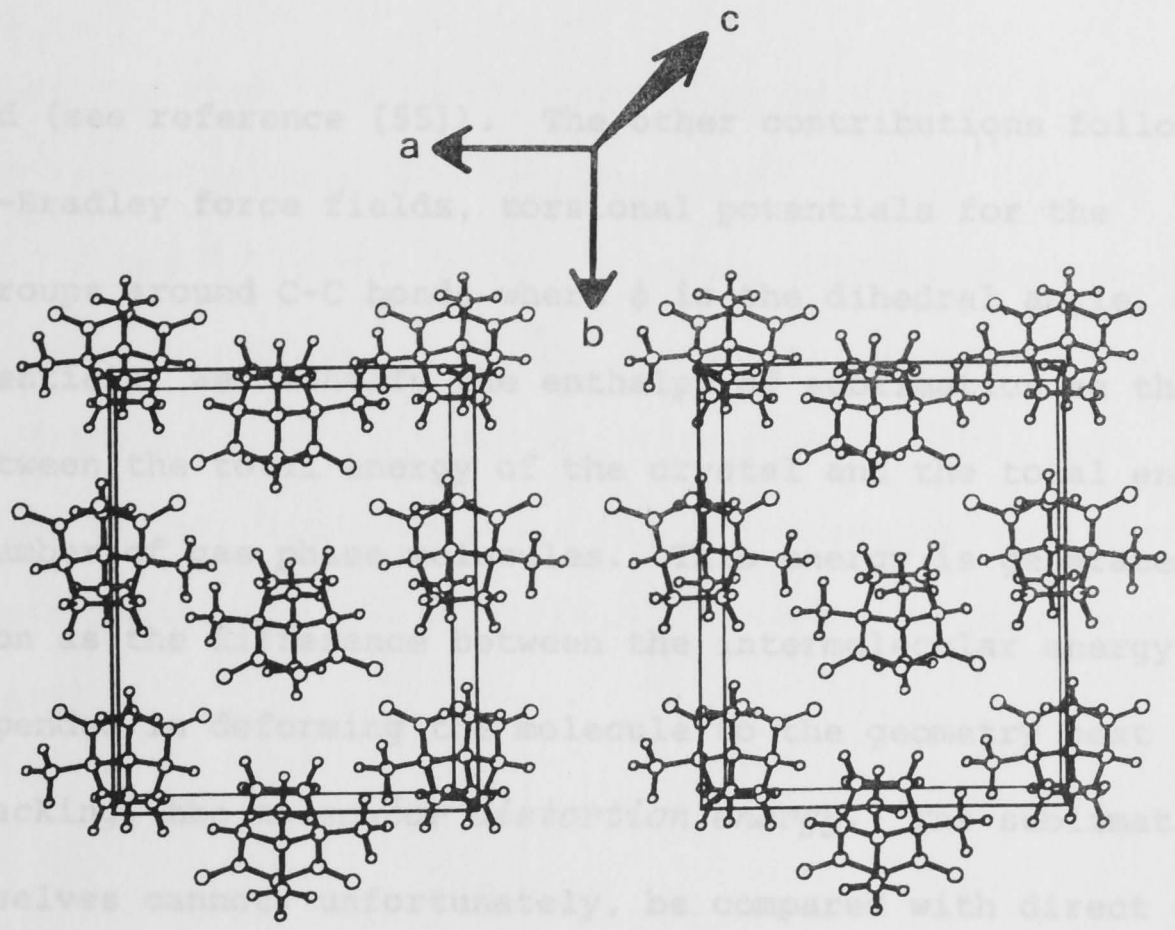

Fig 5.4: The predicted crystal structure of *d*-camphoric anhydride.

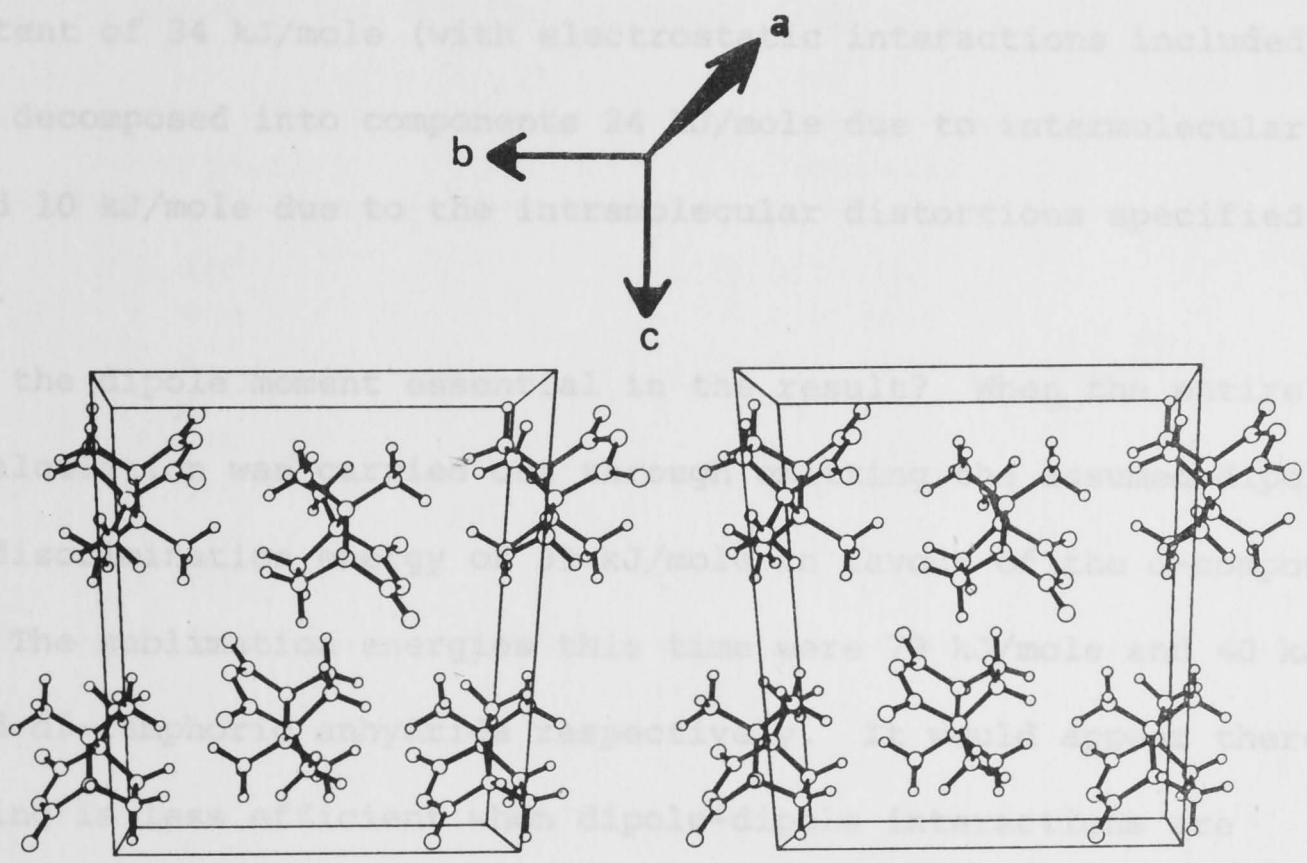

Fig 5.5: The predicted crystal structure of *dl*-camphoric anhydride

orbital method (see reference [55]). The other contributions follow from the Urey-Bradley force fields, torsional potentials for the rotation of groups around C-C bonds where ϕ is the dihedral angle, and the exp-6 potential. We identify the enthalpy of sublimation as the difference between the total energy of the crystal and the total energy of the same number of gas phase molecules. This energy is generated in the calculation as the difference between the intermolecular energy and the energy expended in deforming the molecule to the geometry best adapted for packing, the *molecular distortion energy*. The sublimation energies themselves cannot, unfortunately, be compared with direct experiment; but each lies within the range 20-100 kJ/mole, typical of organic crystals.

The discrimination energy (of sublimation) favours the *d*-compound to the extent of 34 kJ/mole (with electrostatic interactions included). It may be decomposed into components 24 kJ/mole due to intermolecular forces and 10 kJ/mole due to the intramolecular distortions specified in table 5.3.

Is the dipole moment essential in the result? When the entire packing calculation was carried out through omitting the assumed dipole moment a discrimination energy of 39 kJ/mole in favour of the *d*-compound emerged. The sublimation energies this time were 79 kJ/mole and 40 kJ/mole for *d*- and *dl*-camphoric anhydride respectively. It would appear therefore that packing is less efficient when dipole-dipole interactions are included, and that this destabilisation effect (which is in proportion to the sublimation energies themselves) is greatest in the *d*-compound. Thus, it would appear to follow that the discrimination energy is a difference between long-range (electrostatic) and short-range (exp-6) discrimination energies, the latter prevailing. It would also appear to follow that if the measurement of the unit cell parameters were performed at a lower temperature (reduced unit cell sizes), and the

calculation then repeated, the short-range contributions to the sublimation energies would become relatively more significant.

Tables 5.4 and 5.5 refer to the optimised crystal structures of *d*- and *dl*-camphoric anhydride. In these tables the emphasis is on the consequences of including electrostatic interactions. It is seen that the introduction of the dipoles changes the structures only moderately, with the largest changes in the *d*-,crystal. However, no atom is shifted by more than 0.3Å.

Table 5.6: Centre of mass distances (in Å) between a reference *d*-molecule and the first eight nearest neighbouring molecules in the calculated crystal structures of *d*- and *dl*-camphoric anhydride. The identities of the molecules involved are included in brackets in the entries for the racemate crystal only.

d-crystal	*dl*-crystal
6.440	5.829 (*d*-)
6.440	5.829 (*d*-)
6.617	6.386 (*l*-)
6.617	6.440 (*d*-)
6.620	6.440 (*d*-)
6.620	6.816 (*l*-)
7.144	6.838 (*l*-)
7.144	7.909 (*l*-)

Finally table 5.6 lists centre of mass distances between a reference *d*-molecule and the first eight nearest neighbours in the optimised *d*-, and *dl*-, crystals. In the case of the racemate, it is found that the nearest neighbrous are of the same type as the reference molecule and occur at a shorter distance than in the *d*-, crystal. The

Table 5.4: Calculated solid-state equilibrium geometries of *d*-camphoric anhydride with and without electrostatic interactions at room temperature. μ_D is the electric dipole moment. x, y, z are cartesian coordinates (in Å) in the orthorhombic unit cell of the *d*-crystal.

	μ_D = 5.41D			μ_D = 0		
atom	x	y	z	x	y	z
C_1	-0.316	-1.187	0.593	-0.325	-1.276	0.659
C_2	-0.355	-0.111	1.699	-0.366	-0.316	1.868
H_3	0.467	-0.278	2.411	0.461	-0.538	2.561
H_4	-0.258	0.912	1.307	-0.286	0.741	1.579
H_5	-1.309	-0.178	2.247	-1.315	-0.448	2.415
C_6	-0.372	-2.532	1.300	-0.394	-2.686	1.228
H_7	0.500	-2.655	1.965	0.461	-2.875	1.899
H_8	-0.388	-3.395	0.617	-0.390	-3.477	0.464
H_9	-1.277	-2.592	1.930	-1.312	-2.809	1.827
C_{10}	-1.500	-0.929	-0.386	-1.501	-0.912	-0.298
H_{11}	-2.437	-0.768	0.159	-2.439	-0.782	0.255
C_{12}	-1.066	0.329	-1.182	-1.046	0.399	-0.991
H_{13}	-1.405	1.246	-0.677	-1.387	1.280	-0.430
H_{14}	-1.442	0.320	-2.207	-1.401	0.473	-2.023
C_{15}	0.484	0.289	-1.176	0.504	0.356	-0.959
H_{16}	0.883	1.198	-0.702	0.892	1.211	-0.383
H_{17}	0.859	0.247	-2.202	0.892	0.423	-1.980
C_{18}	0.886	-0.989	-0.374	0.886	-0.998	-0.282
C_{19}	2.207	-0.807	0.308	2.202	-0.912	0.426
H_{20}	2.411	-1.606	1.042	2.413	-1.815	1.024
H_{21}	3.045	-0.799	-0.410	3.045	-0.780	-0.273
H_{22}	2.245	0.157	0.846	2.225	-0.050	1.115
C_{23}	0.905	-2.131	-1.356	0.903	-2.033	-1.378
O_{24}	2.013	-2.665	-1.826	2.007	-2.461	-1.958
O_{25}	-0.373	-2.621	-1.863	-0.382	-2.478	-1.913
C_{26}	-1.608	-2.057	-1.356	-1.617	-1.959	-1.355
O_{27}	-2.782	-2.483	-1.782	-2.794	-2.361	-1.797

Table 5.5: Calculated solid-state equilibrium geometries* of *dl*-camphoric anhydride with and without electrostatic interactions at room temperature. μ_D is the electric dipole moment.

	μ_D = 5.41D			μ_D = 0		
atom	x	y	z	x	y	z
C_1	1.576	-0.807	3.407	1.575	-0.802	3.396
C_2	1.102	0.353	4.304	1.105	0.356	4.297
H_3	1.749	0.465	5.189	1.750	0.461	5.185
H_4	1.092	1.302	3.759	1.103	1.308	3.756
H_5	0.091	0.176	4.693	0.091	0.185	4.681
C_6	1.276	-2.062	4.196	1.272	-2.058	4.182
H_7	1.846	-2.083	5.144	1.843	-2.085	5.129
H_8	1.537	-2.961	3.625	1.526	-2.957	3.608
H_9	0.202	-2.127	4.452	0.198	-2.118	4.440
C_{10}	0.882	-0.746	2.007	0.880	-0.737	1.996
H_{11}	-0.204	-0.607	2.086	-0.205	-0.595	2.077
C_{12}	1.553	0.476	1.328	1.555	0.485	1.321
H_{13}	1.034	1.393	1.638	1.038	1.403	1.634
H_{14}	1.520	0.413	0.237	1.522	0.426	0.230
C_{15}	3.005	0.476	1.876	3.007	0.481	1.869
H_{16}	3.284	1.448	2.288	3.288	1.452	2.283
H_{17}	3.714	0.263	1.071	3.716	0.269	1.064
C_{18}	3.061	-0.634	2.979	3.062	-0.631	2.970
C_{19}	4.006	-0.232	4.071	4.005	-0.232	4.065
H_{20}	4.100	-1.005	4.856	4.093	-1.003	4.851
H_{21}	5.006	-0.051	3.643	5.008	-0.056	3.640
H_{22}	3.710	0.712	4.563	3.712	0.714	4.554
C_{23}	3.503	-1.887	2.269	3.507	-1.882	2.260
O_{24}	4.595	-2.567	2.572	4.584	-2.577	2.582
O_{25}	2.602	-2.436	1.264	2.597	-2.431	1.256
C_{26}	1.246	-1.933	1.168	1.240	-1.923	1.154
O_{27}	0.416	-2.457	0.288	0.387	-2.481	0.316

* x, y, z are cartesian coordinates (in Å) in the monoclinic unit cell of the *dl*-crystal. The cartesian coordinates are related to the monoclinic unit cell axes a, b and c by the relations: $\bar{x} = \{x - z\cot\beta\}/a$; $\bar{y} = y/b$; $\bar{z} = z/c\sin\beta$; where $\bar{x}$, $\bar{y}$, $\bar{z}$ are the reduced coordinates.

molecules with the opposite handedness tend to be pushed out to larger distances.

5.5 Conclusions

The few *a priori* calculations of crystal structures so far reported have treated aromatic molecules - rigid and aspherical. A single energy minimum has generally been reached from different starting points, but difficulties in finding the same minimum have also been recorded [56],[57]. The present calculations are more ambitious than any so far described, not least since the molecules are spherical. The essential conclusions that we deduce are that reasonable structures have been found; that there is nothing special about the *dl*-structure, and that the discrimination energy is to be seen as a result simply of necessarily different patterns of atom-atom interactions, modified in this case by permanent dipole effects and by different extents of molecular deformation. In no sense is there any hint of a *dl*-compound - there is merely a *dl*-packing pattern, less stable (as it happens) than the packing pattern of *d*- or *l*-molecules alone, but stable enough to be thermodynamically advantageous for the racemate.

The *dl*-pattern that emerges is that of a superlattice (with the *d*- and *l*-molecules occupying unique positions in a systematic fashion)*. The stability of the *dl*-crystal in the presence of a large discrimination energy that acts against the mixing of *d*- and *l*-molecules is achieved by making the nearest neighbours to be of the same type as the reference molecule. The situation is different in camphor, where the discrimination energy (also of the same sense as in camphoric anhydride) is relatively low, and some miscibility between *d*- and *l*-molecules is expected. This explains why no eutectic behaviour is observed in the phase diagram of

*This is one manifestation of immiscibility of the *d*- and *l*-molecules, as the entropy of mixing is zero. Immiscibility can also be manifested through the separation of the components. Chapter 8 considers the problem of crystallisation in *dl*-systems further.

camphor, but is observed in the phase diagram of camphoric anhydride. The coupling effects between orientational and substitutional disorder in the neighbourhood of the rotational transition would be more pronounced in camphor than in camphoric anhydride. The consequences of this type of coupling is the subject of chapter 8. Also, and perhaps more significantly, in the rotator phase the discrimination energy would be much reduced. This in turn would enhance miscibility between *d*- and *l*-molecules in this phase.

The anomaly observed in the n.m.r. linewidth studies of *dl*-camphoric anhydride, reported in the preceding chapter, has been explained by postulating an anisotropic thermal expansion through which some magnetic moment coupling is enhanced. One possible direction of strong proton magnetic dipolar interaction in the *dl*-crystal (Fig. 5.4) occurs along the *d*- or *l*-layers in the b-direction (since the centre of mass distances (table 5.6) between adjacent molecules are least in this direction). These interactions involve one of the bridge methyl groups on one *d*- (or *l*-) molecule and two ring-side protons facing this methyl group on an adjacent *d*- (or *l*-) molecule. We have not attempted, for the present, to identify other possible directions of strong proton-proton interaction perpendicular to the plane of the paper. However, the fact that the neighbouring *d*-molecules are closer to each other in the *dl*-crystal than they are in the *d*-crystal at room temperature would strongly lead us to expect the racemate crystal to have the larger n.m.r. linewidth at this temperature.

We confirm the already established view [56],[58],[59] that electrostatic interactions, even those involving large dipole moments as in camphoric anhydride, are not prime determinants of the equilibrium crystal structures. Claims to the contrary, however have been made by Williams [60] and Morris [61] with regard to certain aromatic compounds.

The former observed trends of larger coulombic contributions to the lattice energy in the aromatics, with the largest observed contribution being in benzene (29%). The latter observes that quadrupole interactions may play an important role in aromatic crystal structures in which pairs of molecules have their planes parallel, e.g. anthracene dimers; but may not, in crystals in which the molecules lie with their planes approximately perpendicular.

Molecular packing analysis is still a young and lively field of crystal physics. Its success depends on the regularities of atomic and molecular properties such that the empirical force-field developed for one molecule is applicable to another molecule. Mirsky [62] has provided an interesting evaluation of the transferability of the empirical force-fields together with an illustration of how the technique of molecular packing analysis can be applied to study of plastic phase transitions, using adamantane as an example. It seems very promising that this technique will be called upon more frequently to elucidate solid state phenomena in the future.

The observation that the crystal of *dl*-camphoric anhydride does not consist of *dl*-molecules also applies to *dl*-camphor; since both have discrimination energies of the same sense. This observation calls for an entirely new approach to the interpretation of phase diagrams in general; and in particular, those of camphor and related compounds. The submaxima on the phase diagrams of camphor and camphoric anhydride can not be attributed to compound formation as a conventional thermodynamic approach would suggest. We return to this subject in chapter 8.

a theory of fusion of atomic and molecular crystals 6

To understand the plastic-phase transition we must first study the general melting transition of which it is a part. The observed relation between entropy and volume change at the melting transition for simple substances makes the entropy term in the free energy function for the transition the more useful parameter. This in turn implies that the most important feature of the melting transition in these simple substances is the increase in positional disorder. Fortunately the entropy of fusion can be computed with confidence from theory without empirical parameter fitting. This is not at all the case for the enthalpy, given the present knowledge of intermolecular forces. This chapter concerns itself with the development of a single-lattice model of fusion in atomic and molecular crystals, and a model which calculates the entropy of fusion without any parameter fitting. The enthalpy function can then be regressed on the calculated entropy and the experimental melting point to evaluate mean values for the interaction energies for positional disorder.

6.1 Introduction

We recall our discussion in chapter 1 of the relationship observed in crystals, consisting of atoms and globular molecules, between the entropy of fusion and the volume change at the melting point. This observation has been the basis for treating these transitions as order-disorder phenomena. The two-sublattice model used by Lennard-Jones and Devonshire [8] is one of the few most successful treatments of the melting process of inert gases. This model has been extended by Pople and Karasz [9] to cover the case of molecular crystals with plastic phases by allowing the molecules to take two distinguishable orientations in the orientationally disordered phase. Various improvements have been suggested [63], [64] to the Pople and Karasz model; but the most notable one is that due to Amzel and Becka [10]. In this treatment an extension of the Pople and Karasz model to cover the case of the general number of distinguishable molecular orientations on a lattice site was attempted with success.

Despite the success of the two-sublattice models in affording both quantitative and qualitative descriptions of real systems in some accord with experimental data, a number of the assumptions made have been shown to be contrary to experimental observations [65]. Also these models assume that melting in both atomic and molecular crystals occurs predominantly via the migration of constituent units from lattice sites to interstitial sites. Chadwick and Sherwood [66] observe both from theoretical and experimental evidence that vacancy migration is fundamentally responsible for self-diffusion phenomena in molecular crystals. Thus the application of a two-sublattice model to the melting phenomena in molecular crystals as proposed by Pople and Karasz, and Amzel and Becka may not be realistic.

Would the theory be improved by postulating more than two sublattices? We first examine the generalization of the theory to an arbitrary number of sublattices. The solid then is assumed to be represented by the configuration

that maximises the partition function of the general model with respect to the number of sublattices.

6.2 The Multi-Sublattice Model of a Lattice Gas (Ising Model)

Suppose we have m sublattices of N lattice sites each, N molecules with n allowed orientations. We define the ordered solid as consisting of all the N molecules in one of the m sublattices and one of the n distinguishable orientations. Then the liquid and gaseous states will correspond to the situation when the N molecules are distributed equally over a given number of sublattices and orientations; the situation corresponding more and more to the gaseous state as m is increased. The plastic phase then will be defined as *that state of aggregation of matter in which all the molecules are predominantly in one of the m sublattices and are equally distributed over the n distinguishable orientations.* Let ρ_i stand for the fraction of molecules in the ith sublattice and σ_j for the fraction of molecules in the jth orientation.

The crucial assumptions are those which relate the energies of molecules displaced from a site on the initial sublattice to a site on another sublattice, or else (on the same site) from a reference orientation to another orientation. Definitions are simple if the lattice is initially perfect, i.e. if all the molecules are on the same sublattice, in the same orientation. We then define E' as the energy required to shift one molecule to a site on *any* other sublattice (such 'other' sublattices being thus degenerate), and E" is the energy required to move one molecule from the reference orientation to *any* other orientation (these 'other' orientations being thus degenerate).

For higher degrees of disorder, decisions have to be taken about *interactions between displaced molecules.* The choice Pople and Karasz, and following them Amzel and Becka made is to say that E' and E" apply to

all neighbouring pairs of molecules that are not in the same position or orientation. However, there is no rotational disorder energy (E") between molecules in different orientations but on different sublattices. This last provision means that rotational disorder carries no energy penalty if molecules are positionally disordered, and thus the desired element of co-operation is brought into the model. The average configurational energy per molecule then takes the form.

$$\langle E(m,n,\rho,\sigma)\rangle = \sum_{i}^{m}\sum_{k>i}^{m} \rho_i\rho_k E' + \sum_{i}^{m} \rho_i^{\,2} \sum_{j}^{n}\sum_{\ell>j}^{n} \sigma_j\sigma_\ell E'' \qquad (6.1)$$

An alternative view is to regard *the initial positions and orientations as being so much deeper in energy that E' and E" pertain only to displacements from the original lattice (occupation fractions* ρ_1 *and* σ_1*); for interactions between disordered molecules different quantities, say* E_d' *and* E_d'' *must be used.* Then the mean configurational energy per molecule has the form.

$$\langle E(m,n,\rho,\sigma)\rangle = \sum_{k>1}^{m} \rho_1\rho_k E' + \sum_{i>1}^{m}\sum_{k>j}^{m} \rho_i\rho_k E_d' + \sum_{i} \rho_i\left(\sum_{\ell>1}^{n} \sigma_1\sigma_\ell E'' + \sum_{j>2}^{n}\sum_{\ell>j}^{n} \sigma_j\sigma_\ell E_d''\right) \qquad (6.2)$$

If this distinction is drawn, then a limiting case is $E_d' = E_d'' = 0$. In either situation, expressed through (6.1) and (6.2), there should be equal populations on all sites or orientations other than the initial ones. Then since $\sum\rho_i = 1$, $\sum\sigma_j = 1$;

$$\left.\begin{aligned} \rho_i &= (1 - \rho_1)/(m - 1) \qquad (i \neq 1) \\ \sigma_j &= (1 - \sigma_1)/(n - 1) \qquad (j \neq 1) \end{aligned}\right\} \qquad (6.3)$$

6.3 Properties of the Multi-Sublattice Model

The partition function, customarily written on the basis of an Einstein model, has the form

$$Q = (Q_m)^N . Q_c$$

where Q_m is the molecular partition function and

$$Q_c = \sum_{\rho,\sigma} \exp\{-E(m,n,\rho,\sigma)/kT\} \qquad (6.4)$$

is the configurational part; $Q_c = 1$ for a perfectly ordered state. Assuming that Q_m is independent of disorder (an assumption improved in the next chapter) equilibrium conditions associated with disordering depend solely on Q_c. To evaluate Q_c we resort to the Bragg-Williams approximation which simply requires replacing the argument of the exponential in equation (6.4) by its average, and identifying the total number of terms in the sum as $g(m,n,\rho,\sigma)$, the number of ways of arranging particles for given values of m,n,ρ,σ. Thus equation (6.4) is replaced by

$$Q_c = g(m,n,\rho,\sigma)\exp\{-\langle E(m,n,\rho,\sigma)\rangle/kT\} \qquad (6.5)$$

where

$$g(m,n,\rho,\sigma) = \left(\frac{N!}{\{N\rho_1\}! \prod_{i=2}^{m} \{N\rho_i\}!}\right)^m \cdot \frac{\{N\rho_1\}!}{\{N\rho_1\sigma_1\}! \prod_{j=2}^{n} \{N\rho_1\sigma_j\}!} \cdot \prod_{i=2}^{m} \frac{\{N\rho_i\}!}{\{N\sigma_1\rho_i\}! \prod_{j=2}^{n} N\rho_i\sigma_j} \qquad (6.6)$$

and $\langle E(m,n,\rho,\sigma)\rangle$ is identified either with the expression (6.1) or with (6.2). Using equation (6.3) to eliminate ρ_i,σ_j for $i,j \neq 1$ we have, for the more general case (equation (6.2))

$$\langle E(m,n,\rho,\sigma)\rangle = E'N\rho_1(1-\rho_1) + E''N\sigma_1(1-\sigma_1)(m\rho_1^2-2\rho_1+1)/(m-1)$$

$$+ \tfrac{1}{2}E'_d N(1-\rho_1)^2(m-2)/(m-1)$$

$$+ \tfrac{1}{2}E''_d N(1-\sigma_1)^2(m\rho_1^2-2\rho_1+1)(n-2)/(n-1)(m-1) \qquad (6.7)$$

Equations (6.6) and (6.7) reduce to the results of Amzel and Becka if m = 2, $E'_d = E'$ and $E''_d = E''$. Further it will be observed that the values of E'_d and E''_d are immaterial if m = 2 and n = 2 respectively. Also if m = n = 2, then the issue which exercised us in defining the elementary energy quantities is of no consequence. This case is of course the Pople-Karasz model. Thus it would seem that *the fortuitous choice** *of these parameters which L-J-D and Pople and Karasz made protects the theory, to some extent, from one of the more difficult physical issues.*

Using equation (6.3) again, and applying the Stirling approximation in equation (6.6), we have for the free energy

$$A_c/RT = m\rho_1 ln\rho_1 + m(1-\rho_1) ln\{(1-\rho_1)/(m-1)\} + \sigma_1 ln\sigma_1$$

$$+ (1-\sigma_1) ln\{(1-\sigma_1)/(n-1)\} + \langle E(m,n,\rho,\sigma)\rangle/RT \qquad (6.8)$$

We are interested in stationary values of A_c/RT, and so may differentiate equation (6.8) with respect to m, n, ρ, and σ. Illustratively, $\partial(A_c/RT)/\partial m = 0$ if

$$(m-1)^2[\rho_1 ln\rho_1 + (1-\rho_1)\{ln(1-\rho_1)/(m-1)\}] = m(m-1)(1-\rho_1)$$

$$+ \{\tfrac{1}{2}E'_d(1-\rho_1)^2 + (1-\sigma_1)(1-\rho_1)^2[E''\sigma_1+\tfrac{1}{2}E''_d(1-\sigma_1)(n-2)/(n-1)]\}/kT \qquad (6.9)$$

This condition is always satisfied if $\rho_1 = 1$, that is, by a single fully occupied lattice; if $\sigma_1 = 1/n$ we have the plastic phase. If $E'_d = 0$, then equation (6.9) is satisfied also by m = 1, $\sigma_1 = 1$ (and ρ_1 is arbitrary). That is the free energy is stationary if there is orientational order, and

---

* These parameters were chosen arbitrarily and the choice of m=2 was mainly encouraged by developments in the crystal statistics of alloys.

the number of sublattices (in which there may be vacancies) is specifically unity (liquid crystal). This result encourages us to proceed, in the next section, to employ the single lattice model, with vacancies. However, we note that for any $m > 1$, there is always an implied functional relationship between σ_1 and ρ_1 - between degrees of orientational and positional disorder - which will ensure that (6.9) is satisfied; and therefore *the model that we develop shortly ($m = 1$) and the Pople-Karasz and Amzel-Becka ($m = 2$) models are merely the first two of a series of models which might be called upon.* The relationship between these two models is of some interest, but will not be examined in the present exercise.

6.4 A Single-Lattice Model for the Evaluation of Thermodynamic Properties of Order-Disorder Transitions in Molecular Crystals

Having in mind the discussion above we now attempt to discuss melting in a way consistent with a *single-lattice model of positional order-disorder transitions* in atomic and molecular crystals. The theory will be modelled around argon and methane; substances which have received extensive studies and have the relevant experimental data. From the Significant Structure Theory of Liquids [67] we adopt the concept that melting is to be seen as a consequence of the creation of *fluidised vacancies* leading to a volume expansion characteristic to the melting process. According to this model the fluidised vacancies are, on the average, of molecular size so that the number of moles of such vacancies per mole of occupied sites is $(V-V_s)/V_s$ where V and V_s are the molar volumes of liquid and solid respectively. It is argued that the energy for the creation of a lattice vacancy is equal to the energy of sublimation. Since the fraction of neighbouring positions to a vacancy which are filled by molecules is V_s/V, there are $(V_s/V)\{(V-V_s)/V_s\}$ $= (V-V_s)/V$ moles of *gas-like molecules*. The rest V_s/V moles are *solid-like molecules*. It follows therefore that the molecular partition function is

constructed from the Einstein partition function of solids to account for the solid-like molecules, and from the partition function of an ideal gas for the gas-like molecules. The *locked lattice vacancies* present in solids at finite temperatures will be assumed to make a negligible contribution to the thermodynamic properties of the system; since according to this model, such vacancies will be present in both the solid and liquid and only a very small fraction of them will become fluidised. We shall deal with one component of the partition function at a time for convenience.

The significant structure theory of liquids gives the following partition function.

$$Q_m(\rho) = \{(Q_{ms}(\rho))^{NV_s/V} \cdot (Q_{mG}(\rho))^{N(V-V_s)/V}\}/\{N(V-V_s)/V\}! \qquad (6.10)$$

where

$$Q_{ms}(\rho) = \left(\frac{\exp[E_s/RT]}{\{1-\exp[-\theta_E/T]\}^3}\right)\left[1+n'\left(\frac{V-V_s}{V_s}\right)\exp\{-aE_sV_s/(V-V_s)RT\}\right] \qquad (6.11)$$

and

$$Q_{mG}(\rho) = (2\pi mkT)^{3/2}(V-V_s)/h^3 \qquad (6.12)$$

In (6.11) the expression in the brackets () is the Einstein partition function for the solid including the zero point energy and the last factor is the degeneracy factor that arises from $(V-V_s)/V_s$ moles of fluidised vacancies. Q_{mG} is the molecular partition function for the gas-like molecules. θ_E is the Einstein characteristic temperature measured in the crystal phase* and E_s is the sublimation energy in the neighbourhood of the melting transition. This sublimation energy is approximated by the energy of vapourisation of the melt.† The constants n and a are readily evaluated from theory at the freezing point if the coordination number of the crystal is known.

For our purpose we redefine the molecular partition function as

---

* Presumably θ_E is measured in the crystal phase close to the melting point.

† This is an approximation because it assumes that the vapourisation energy of the melt is equal to that of the solid during melting.

follows.

$$Q_m(\rho)/Q_m(1) = \{Q_{ms}(\rho).Q_{mG}(\rho)\}/Q_{ms}(1) \qquad (6.13)$$

where

$$Q_{ms}(\rho) = (Q_{mi})^{NV_s/V}$$

$$Q_{ms}(1) = (Q_{mi})^{N}$$

and

$$Q_{mG}(\rho) = \{(2\pi mkT)^{3/2}(V-V_s)/h^3\}^{N(V-V_s)/V}/\{N(V-V_s)/V\}!$$

where the molecular partition function has been defined relative to that of the positionally ordered solid at absolute zero including the zero point energy. Q_{mi} can be either the Einstein partition function or the Debye partition function, the subscript i denoting the ith mode in the case of the former or the mode corresponding to the Debye cut-off frequency in the latter case. We shall find later that both the Einstein and Debye thermodynamic functions lead to good agreement of the predicted properties of real systems with experimental data, though the Debye function appears to be a little better. If we let $\chi = 1 - V_s/V$, the number of moles of the gas-like molecules*, we have for the relative free energy the following expression

$$\{G_m(\rho) - G_m(1)\}/RT = \chi\{ln(Q_{mi}) + lnN\chi - ln[(2\pi mkT)^{3/2}V\chi/h^3] - 1\} \qquad (6.14)$$

We now turn to the problem of constructing the configurational partition function to take the place of the degeneracy factor in (6.11). For one mole of substance the total number of lattice sites in the melt is given by

$$N_T = n_v + N \qquad T \geq T_m \qquad (6.15)$$

where $n_v = N(V-V_s)/V_s$, number of fluidised vacancies.* Therefore ρ is

---

* per mole of substance.

defined as follows

$$\rho = N/N_T = V_s/V \tag{6.16}$$

and

$$(1-\rho) = n_v/N_T = 1 - V_s/V \tag{6.17}$$

where ρ, a long range positional order parameter, is the fraction of lattice sites occupied by molecules on average. We note that χ, the number of moles of gas-like molecules, and $(1-\rho)$, the fraction of vacant sites, are numerically identical. We retain both quantities, however, and use them according to what aspect of the problem we wish to emphasise; i.e. the population of gas-like molecules or vacant sites. Therefore the configurational partition function in the Bragg-Williams approximation takes the form

$$Q_c = \frac{N_T!}{\{\rho N_T\}!\{(1-\rho)N_T\}!} \cdot \frac{\{\rho N_T\}!}{\{N\sigma_1\}!\left\{\{N\frac{(1-\sigma_1)}{n-1}\}!\right\}^{n-1}} \cdot \exp\{-<E(\rho,\sigma)>/RT\} \tag{6.18}$$

where $\sigma_1 = 1$ for the ordered solid, and $\sigma_1 = 1/n$ for the plastic phase.

The energy term $<E(n,\rho,\sigma)>$ has a component attributable to the existence of vacancies *per se*, plus the usual interaction term for the reorientational disordering process (if present). In respect of the vacancy term, let $E_v^{(1)}$ be the energy needed to create an isolated vacancy. Vacancy pairs, triplets, etc. introduce new energy terms. The number density of n-fold vacancy clusters is proportional to $(1-\rho)^n$. Therefore the vacancy term which we designate $<E(\rho,1)>$ may be expanded as a power series in $(1-\rho)$:

$$<E(\rho,1)> = N_T\{(1-\rho)E_v^{(1)} + (1-\rho)^2E_v^{(2)} + (1-\rho)^3E_v^{(3)} + ...\}$$

$$= N_T(1-\rho)\{(E_v^{(1)}+E_v^{(2)}+E_v^{(3)}+...) - \rho(E_v^{(2)}+2E_v^{(3)}+...)+...\}$$

This expression may be written in the form

$$\langle E(\rho,1)\rangle = N_T(1-\rho)(E_s + \rho E_s' + \ldots.) \qquad (6.19)$$

where

$$E_s = E_v^{(1)} + E_v^{(2)} + E_v^{(3)} + \ldots.$$

Now, for a completely vacant lattice ($\rho = 0$),

$$\langle E(0,1)\rangle = N_T E_s \qquad (6.20)$$

and therefore E_s is the sublimation energy per molecule (since then $N_T = N$). The next term in the series has an interesting form, as it seems to depend on the number of hole-molecule pairs or gas-like and solid-like molecule pairs ($N_T(1-\rho)\rho$). Thus we may assume this term to include any interaction between the equilibrium number of vacancies and molecules, or that of gas-like and solid-like molecules.*

The orientational disordering term assumes a contribution from a disordered molecule next to an ordered molecule (but not next to a vacancy), and so is given by

$$\langle E(1,\sigma)\rangle = N_T E''\rho\sigma_1(1-\sigma_1) \qquad (6.21)$$

where it has been assumed that E_d'' (the interaction energy between molecules in the disordered orientations) is negligible. Then finally

$$\langle E(\rho,\sigma)\rangle = \langle E(\rho,1)\rangle + \langle E(1,\sigma)\rangle \qquad (6.22)$$

The configurational free energy, after applying Stirlings approximation in equation (6.18) is

$$\{G_c(\rho,\sigma) - G_c(1,1)\}/RT = \zeta_\ell[\rho \ln\rho + (1-\rho)\ln(1-\rho)] + \sigma_1 \ln\sigma_1$$
$$+ (1-\sigma_1)\ln\{(1-\sigma_1)/(n-1)\} + \langle E(\rho,\sigma)\rangle/RT \qquad (6.23)$$

---

* We have in effect accounted for some short-range order here.

where $\zeta_\ell = 1 + n_v/N$, the total number of moles of lattice sites (the subscript ℓ denotes lattice).

From (6.14) and (6.23), the Gibbs free energy of the system relative to the ordered solid* (omitting for the present the work done against the atmosphere) is given by the following expression.

$$\{G(\rho,\sigma) - G(1,1)\}/T = R\left[\{\ln(Q_{mi}) - \ln[(2\pi mkT)^{3/2} v_m/h^3] - 1\}\chi - \psi\right]$$
$$+ \zeta_\ell[(1-\rho)\{\Delta E_s + \rho\Delta E'\} + \rho\sigma_1(1-\sigma_1)\Delta E"]/T \qquad (6.24)$$

where

$$\psi = -\zeta_\ell \psi(\rho,\sigma)$$

$$\psi(\sigma,\sigma) = \rho\ln\rho + (1-\rho)\ln(1-\rho) + \sigma_1\ln\sigma_1 + (1-\sigma_1)\ln(1-\sigma_1)/(n-1)$$

$V_m = V/N$, the molecular volume

$\Delta E_s = NE_s$, sublimation energy per mole

$\Delta E'_s = NE'_s$

$\Delta E" = NE"$

and we have used the *truncated* positional configurational energy defined in (6.19).

Note that *this model introduces an explicit coupling between orientational and positional disordering processes* realised in the term $\rho\sigma_1(1-\sigma_1)\Delta E"$. The origin of this term is the energy term proposed in equation (6.21). No such coupling appears in previous models. The coupling vanishes, of course, when $\rho = 1$ and $\sigma_1 = 1$.

Conditions for stationary states in (6.24) with respect to ρ are complicated by the explicit dependence of ρ on volume and are omitted in the present discussion; but those with respect to σ_1 are given in the

* The definition of thermodynamic functions relative to their values at absolute zero is a conventional approach (see Fowler and Guggenheim [75]). Equilibrium values for a system of one phase can tell little about the phase transition when ΔG or ΔA is the quantity involved.

following equation.

$$ln\{(1-\sigma_1)/(n-1)\sigma_1\} = \zeta_\ell \rho(1-2\sigma_1)\Delta E''/RT \qquad (6.25)$$

In equation (6.25), if n = 2, the condition of minimum free energy is satisfied by $\sigma_1 = \frac{1}{2}$ (complete orientational disorder) at all temperatures T (>0). This corresponds to the Pople-Karasz model if $\rho = 1$ (positionally ordered solid). If $n > 2$ and $\sigma_1 = 1/n$ (complete orientational disorder), then it is necessary that $T \to \infty$. The state $\sigma_1 = 1/n$ has already appeared elsewhere as the plastic phase. For general n ($\neq 1$), $\sigma_1 \to 1$ (complete orientational order) requires $T \to +0$. The quantity ρ appearing on the left hand side of the equation does not seem to play an important role; except that when $\rho \to 0$ (in the gas phase), then the state $\sigma_1 = 1/n$ can be reached at any temperature T (>0) for any value of n (free rotation).

The model presented above amounts to assuming a *lattice structure for the melt*. Chen [68] has summarised the evidence for the structure of liquids based on the similarities between the thermodynamic properties of liquids and solids such as densities, specific heats and compressibilities. Also it is now established from X-ray diffraction studies that nearest neighbours in the melt are at essentially the same distance as the solid. The significant structure model, on which we base our theory, observes the similarity between liquids and solids, and views *the melt as a distorted fluctuating lattice caused by the addition of holes to the solid during the melting transition*. The addition of holes to the solid is manifested by the volume expansion at the melting point.

6.5 Thermodynamic Functions for the Melting Transition in Plastic Crystals

Although all thermodynamic functions are generated, no immediate use is made of the specific heat function. Also, we do not calculate

the enthalpy change at the melting transition, since such a calculation requires knowledge of the interaction constants or mean disordering energies. Instead, we shall regress the enthalpy function on the calculated entropies to evaluate these disordering energies. This task, however, shall be undertaken in the next section in respect to atomic crystals (e.g., argon) only. The general case of molecular crystals we postpone to the next chapter after the thermodynamic equations for the orientational disorder have been found, since the orientational disordering energy is involved in the enthalpy function for the melting transition.

The question may be raised of the appearance of the orientational term in the enthalpy function for the melting transition of plastic crystals. It may be suggested that the term is irrelevant here since $\sigma_1 = 1/n$ and all the allowed orientations become degenerate. However, this may not be the case, since complete orientational disorder may not occur before the melting transition; if so $\sigma_1 = 1/n$ is only an approximation.* This aspect has been observed in some systems, for example methane, where the plastic phase transition is associated with anomalous specific heat extending beyond the maximum on the C_p-curve. Thus the Gibbs free energy is given by

$$G(\rho)-G(1) = RT\left(\{ln(Q_{mi})-ln[(2\pi mkT)^{3/2}v_m/h^3]-1\}\chi-\psi_\rho\right)$$

$$+ \zeta_\ell(1-\rho)\{\Delta E_s+\rho\Delta E_s'-(n-1)\Delta E''/n^2\} + (V-V_s)P \qquad (6.26)$$

where P is the pressure and

$$\psi(\rho)=-\zeta_\ell\{\rho ln\rho + (1-\rho)ln(1-\rho)\}$$

and the remaining thermodynamic functions follow from (6.25);

$$U(\rho)-U(1) = \zeta_\ell\left((1-\rho)[\Delta E_s+\rho\Delta E_s']-(1-\rho)(n-1)\Delta E_0''/n^2\right) + RT\chi[3/2-E(x)] \quad (6.27)$$

---

* This, in our model, is a consequence of the fact that $E_d'' << E''$. When $E_d'' = E''$ (Amzel-Becka model), $\sigma_1 = 1/n$ is always a solution to the free energy function. In this case, the initial orientation may not be recovered in the non-rotator phase on lowering the temperature from the plastic phase through the transition.

where

$$E(x) = 3\{x/2 + x/[\exp(x)-1]\} \; ; \quad x = \theta_E/T$$

or

$$E(x) = (9/8)x + 3D(x) \; ; \quad x = \theta_D/T$$

$$S(\rho)-S(1) = R\left[\left(\ln\left\{\frac{(2\pi m)^{3/2}(ekT)^{5/2}}{ph^3}\right\} - S(x) + 1\right)\chi + \psi_\rho\right] \tag{6.28}$$

where

$$S(x) = -3\ln[1-\exp(-x)] + 3x/[\exp(x)-1] \; ; \quad x = \theta_E/T$$

or

$$S(x) = -3\ln[1-\exp(-x)] + 4D(x) \; ; \quad x = \theta_D/T$$

θ_E and θ_D are the Einstein and Debye characteristic temperatures respectively; and D(x) is the usual Debye function whose values are tabulated in standard textbooks. The application of equations involving θ_E and θ_D is simply a matter of choice between Einstein and Debye functions respectively. The specific heat is therefore given by the following equation.

$$C_p(\rho)-C_p(1) = \left\{(1-\rho)\left(\frac{\Delta E_s}{\rho} + \Delta E_s' - \frac{(n-1)}{\rho n^2}\Delta E''\right) + \rho\zeta_\ell\left(\Delta E_s - \Delta E_s'(1-2\rho) - \frac{(n-1)}{n^2}\Delta E''\right) + \frac{RT}{\zeta_\ell}[3/2-E(x)]\right\}\alpha + \chi\left(3/2R - C_v(x)\right) + P\left(\frac{\partial v}{\partial T}\right)_P \tag{6.29}$$

where

$$C_v(x) = 3Rx^2\exp(x)/[\exp(x)-1]^2 \; ; \quad x = \theta_E/T$$

or

$$C_v(x) = 3R\left(4D(x) - 3x/[\exp(x)-1]\right) \; ; \quad x = \theta_D/T$$

α is the thermal expansivity defined by the relation $\alpha = (1/V)\,\frac{\partial V}{\partial T}$.

6.6 Thermodynamic Functions for Melting Transitions in Atomic Crystals and Substances with Liquid-Crystal Phases

In substances with liquid-crystal phases positional disordering precedes orientational disordering; in atomic crystals, of course, only positional disordering is possible. The nett result in both these cases is that the coupling term in (6.26) vanishes and the free energy is now given by the following expression;

$$G(\rho)-G(1) = RT\left\{\{ln(Q_{mi})-ln[(2\pi mkT)^{3/2}v_m/h^3]-1\}\chi-\psi_\rho\right\}$$
$$+ \zeta_\ell(1-\rho)[\Delta E_s+\rho\Delta E'_s] + (V-V_s)p \qquad (6.30)$$

and the remaining thermodynamic functions follow from (6.30)

$$H(\rho)-H(1) = \zeta_\ell(1-\rho)[\Delta E_s+\rho\Delta E'_s] + RT\chi[3/2-E(x)] + (V-V_s)p \qquad (6.31)$$

The entropy is given by (6.28).

$$C_p(\rho)-C_p(1) = \{(1-\rho)[\frac{\Delta E_s}{\rho} + \Delta E'_s] + \rho\zeta_\ell[\Delta E_s - \Delta E'_s(1-2\rho) + \frac{RT}{\zeta_\ell}[3/2-E(x)]\}\alpha$$
$$+ \chi[3/2R - C_v(x)] + P(\frac{\partial v}{\partial T})_P \qquad (6.32)$$

6.7 Mean Positional Disordering Energies in Atomic Crystals

Since two energy terms, namely ΔE_0 and ΔE_s, are involved in the positional disordering process at the melting point it is reasonable to introduce a new term, the *effective positional disordering energy* $\Delta E'_{eff}$. We define the effective positional disordering energy as follows.

$$\Delta E'_{eff} = \frac{\Delta E_s}{\rho} + \Delta E'_s \qquad (6.33)$$

and $\Delta E'^{*}_{eff}$ is given by the following equation.

$$\Delta E'_{eff} = T_m[\Delta S_m(\rho) - R\chi(3/2-E(x))]/\zeta_\ell\rho(1-\rho) \qquad (6.34)$$

where $\Delta S_m(\rho)$ is the entropy change at the melting point. Using results

---

* Note that $\Delta E'_{eff}$ is a function of volume, and therefore of temperature, from its dependence on ρ.

Table 6.1: Predicted entropies of fusion for argon and methane.

Theory	Reduced entropy of fusion $\Delta S_M/R$	
	Argon	Methane
Present theory/classical	1.52	1.00
" " /Einstein	1.73	1.17
" " /Debye	1.74	1.24
LJ-D [69]	1.7	-
HSE [69]	1.0	-
LHW [69]	1.64	-
Observed	1.71 (a)	1.24 (b)

(a) Reference [70]

(b) From heat of fusion data in reference [52]

Key:

LJ-D ≡ Lennard-Jones, S.E., and Devonshire, A.F.

HSE ≡ Hirschfelder, J.O., Stevenson, D.P., and Eyring, H.

LHW ≡ Longuet-Higgins, H.C., and Widom, B.

All these theories are reviewed in reference [69].

Table 6.2: A summary of values for parameters used in the calculation of entropies of fusion. (All data from reference [67] except those asterisked.)

	argon	methane
T_m (K)	83.96	90.65
V_s (cc/mole)	24.98	31.06
V (cc/mole)	28.03	33.63
ΔE_s (kJ/mole)	79.019	9.209
θ_E (K)	60.0	71.34
θ_D (K)	*85	**136.7

* from reference [71]

** Calculated from spectroscopic data in reference [69] (which cross-references to [72]); ν_D was taken to be 95 cm^{-1}.

from our calculations for $\Delta S_M(\rho)$ in the Einstein approximation to be reported below the effective mean positional disordering energy for the case of argon is found to be 193 kJ/mole.*

6.8 Melting Transitions in Molecular Crystals with Complications

We have given here a treatment of melting transitions in molecular crystals which can be described solely as due to positional disordering process. The *ordinary melting transition* is in general associated with an increase in orientational (or rotational) disorder in addition to an increase in positional disorder. Further, intramolecular vibrations may also contribute appreciably to the thermodynamic properties of the transition in some cases. We consider the effect of orientational disorder on the melting transition in the next chapter after obtaining the thermodynamic functions for the plastic-phase transition.

6.9 Predicted Values of Entropy of Fusion

Values of entropy of fusion for argon and methane have been computed from equation (6.28). Table 6.1 summarises the numerical results. Three calculations for each substance were done assuming the classical limit of theories of lattice vibrations, the Einstein and Debye functions. Considering that the model does not involve any parameter fitting the agreement between predicted and experimental values of argon and methane is reasonable. Further the quality of its predictions depends on the accuracy of the experimental data used, i.e. V, V_s, θ_D, θ_E and T_M. Table 6.2 shows the data used in the computation.

---

* This gives 104 kJ/mole for $\Delta E'_s$.

7 theory of rotational and melting transitions in molecular crystals

The thermal entropy change at the rotational transition can be accounted for by simply attributing it to the changes in force constants associated with both intra- and inter-molecular vibrations due to thermal expansion at the transition. This chapter introduces a model for the evaluation of thermodynamic properties of the rotational transition which is a generalisation of a theory due to Aston and which gives an analytic expression for the relative disordering energies for the melting and the rotational transition. The melting transition involving both orientational and positional disordering processes in molecular crystals is also considered.

7.1 Introduction

Pople and Karasz [9] have shown from a two-sublattice model of order-disorder transitions that whether or not a rotational transition which gives rise to the plastic phase of the crystal will occur depends on the relative energy barriers for the orientational and positional disordering of a molecule in the solid state. Our purpose is to apply a similar approach to that of Pople and Karasz to a single-lattice model developed in chapter 6 and to generate thermodynamic functions of the plastic phase transition taking into account the frequency changes of the oscillating molecules at the transition as proposed by Aston [11]. Finally we complete the generation of thermodynamic functions for the general melting transitions that were omitted in the preceding chapter pending the treatment of orientational disordering of molecules in the solid state.

7.2 A Model for Orientational Order-Disorder Phenomena in Molecular Crystals

The model for orientational order-disorder phenomena associated with the plastic-phase transition has already been discussed in chapter 6. In particular, the configurational partition function is obtained from equation 6.18 by setting $\rho = 1$, and therefore $N_T = N$, and is given by the following equation.

$$Q_c = \frac{N!}{\{N\sigma_1\}!\left\{N\frac{(1-\sigma_1)}{n-1}\right\}!^{n-1}} \cdot \exp\{-\langle E(\sigma)\rangle/RT\} \qquad (7.1)$$

where, from equation 6.21,

$$\langle E(\sigma)\rangle = \Delta E''\sigma_1(1-\sigma_1) \qquad (7.2)$$

and $\Delta E'' = NE''$. Also the similarities between this model and the Pople-

Karasz and Amzel-Becka models have already been alluded to in Chapter 6.

The partition function of the system is again written in the form

$$Q = (Q_m)^N . Q_c$$

where Q_m is the molecular partition function. We now set out to derive Q_m whose function will be to account for all thermal properties (as opposed to configurational) associated with the rotational transition.

The effect of lattice vibrations on order-disorder transitions in plastic crystals has received the attention of Aston [11] lately. He allowed for thermal expansion by assuming that the I.R. and Raman frequencies observed above and below the transition are ascribed to molecules undergoing torsional lattice vibrations independently. We modify this hypothesis by assuming that these frequencies could be attributed to both intra- and intermolecular vibrations where the latter contain both the translational and torsional lattice vibrations. This assumption can be justified by observing that the volume of expansion and the entropy change at the rotational transition are of the same order of magnitude as those observed at the melting point of substances without plastic phases. This means that the translational lattice vibrations may be significantly affected also. Further a molecule with a general shape may be distorted in the non-rotator phase in order to acquire the geometry best adapted to packing in the crystal. The molecular packing analysis of camphoric anhydride reported in chapter 5 is a good example. Thus the volume expansion at the transition would allow the molecule to relax in the plastic phase with consequent changes in the force constants for intramolecular vibrations. These changes in the force constants would in turn be manifested in the thermal transition energy.

We assume that these intra- and intermolecular vibrations can be represented by the Einstein harmonic oscillators. Thus, on the basis of an Einstein model, *the disordered crystal consists of a locally distorted lattice* where the molecule in the reference orientation occupies a cell of the same size and is oscillating with the same frequency in the ith mode as it did before the transition. At the same time the molecule in any of the other orientations occupies an expanded cell and consequently oscillates with a lower frequency for the same mode than it did before the transition. The observed I.R. spectrum and Raman spectrum in the disordered phase therefore consists of the resultant of the averaging of the effects due to the two types of molecules, the reference-type and the disordered-type of molecules. The effect of the disorder, in this model, is to lower the frequency of the ith mode for those molecules transforming from the reference orientation to any of the other molecular orientations available in the plastic phase. Thus we define the molecular partition function relative to its value at absolute zero as follows.

$$Q_m(\sigma_1)/Q_m(1) = \prod_i (Q'_{mi})^{N\sigma_i} . (Q''_{mi})^{N \sum_{i=2}^{n} \sigma_i} / (Q'_{mi})^{N} \qquad (7.3)$$

for n orientations. Q'_{mi} and Q''_{mi} are molecular partition functions for the ith mode of lattice vibrations corresponding to the ordered and disordered phases respectively. Equation (7.3) simplifies to

$$Q_m(\sigma_1)/Q_m(1) = \prod_i \{Q''_{mi}/Q'_{mi}\}^{N(1-\sigma_1)} \qquad (7.4)$$

which is identical to the result obtained by Aston for n = 2. The full partition function is then defined by

$$Q(\sigma_1)/Q(1) = Q_m(\sigma_1) . Q_c(\sigma_1)/Q_m(1) . Q_c(1) \qquad (7.5)$$

Because the relative molecular partition function is an implicit function of volume we invoke the Gibbs free energy, which (after making the Stirling

approximation on equation (7.1)) becomes

$$\{G(\sigma)-G(1)\}/T = R[\sigma_1 ln\sigma_1 + (1-\sigma_1) ln\{(1-\sigma_1)/(n-1)\} + \{\Delta E''\sigma_1(1-\sigma_1) + (1-\sigma_1)\Delta G_m\}/T \quad (7.6)$$

where work done by the system against the atmosphere has been neglected for the present and $\Delta G_m = -kT\sum_i ln(Q''_{mi}/Q'_{mi})^N$. The term $(1-\sigma_1)\Delta G_m$ constitutes a coupling between configurational and thermal properties of the system. Stationary values for equation (7.6) with respect to σ_1 are defined in the following expression

$$\{\Delta E''(1-2\hat{\sigma}_1)-\Delta G_m\}/T = R ln\{(1-\hat{\sigma}_1)/(n-1)\hat{\sigma}_1\} \quad (7.7)$$

where $\hat{\sigma}_1$ is the equilibrium value of σ_1. We devise a means of getting at these stationary values below.

Our definition of $\Delta E''$ is different from that of Aston who defines this parameter as follows:- $\Delta E = NZE/4$, where Z is the coordination number of the crystal.* We find that this definition is not proper since the term 4 in the denominator arises from the usage of the degree of order s as the long range order parameter. For the case of two orientations the interaction energy term becomes; $NZE\sigma_1(1-\sigma_1) = NZE(1-s^2)/4$ since $\sigma_1 = (1+s)/2$. The term 4 therefore fundamentally belongs to the order parameters and not to the interaction energy. Consequently the term 4 disappears when we use mole fractions for long range order parameters. Further, as will be seen later, the factor 4 changes when n is changed and therefore is not a characteristic constant for all plastic phase transitions.

We now wish to obtain $G(1/n) - G(\hat{\sigma})$, the free energy change at the rotational transition, where $\sigma_1 = \hat{\sigma}_1$ at the transition temperature

---

* Note that the quantity corresponding to ΔE (of Aston) in our model is $\Delta E'' = NE''$ where $E'' = ZE$ (of Aston). We have not included Z explicitly because it is assumed to be invariant with order-disorder phase transitions.

and $\hat{\sigma}_1 \leqslant 1$. To do this we re-write equation (7.6) as follows

$$\{G(\hat{\sigma}_1)-G(1)\}/T = R\{\hat{\sigma}_1 ln\hat{\sigma}_1 + (1-\hat{\sigma}_1) ln\{(1-\hat{\sigma}_1)/(n-1)\}] + \{\Delta E''\hat{\sigma}_1(1-\hat{\sigma}_1) + (1-\hat{\sigma}_1)\Delta G_m\}/T \quad (7.8)$$

The total free energy change is given by

$$\{G(1/n)-G(1)\}/T = R ln(n) + \{(n-1)\Delta E''_0/n^2T + (n-1)\Delta G_m/n\}/T \quad (7.9)$$

subtracting equation (7.8) from (7.9) we have

$$-\{G(1/n)-G(\hat{\sigma})\}/T = R[\hat{\sigma}_1 ln\hat{\sigma}_1 + (1-\hat{\sigma}_1) ln\{(1-\hat{\sigma}_1)/(n-1)\} + lnn] + \{\Delta E''_0\{n^2\hat{\sigma}_1(1-\hat{\sigma}_1)-n+1\}/n^2 + (1-n\hat{\sigma})\Delta G_m/n\}/T \quad (7.10)$$

Both sides of equation (7.10) must equal zero for the phase with order parameter $\sigma_1 = \hat{\sigma}_1$ to be in equilibrium with the disordered phase with $\hat{\sigma}_1 = 1/n$. Figures 7.1 and 7.2 summarise the properties of this equation. We observe that the transitions become more isothermal (see chapter 1) with increase in n or the closer $\hat{\sigma}$ approaches 1/n for a fixed value of ΔG_m. Also the more isothermal transitions generally occur at lower temperatures with a common value of ΔG_m. The observation that solid-state transitions become more isothermal with large values of n may correspond to the observation made by Amzel and Becka that transitions with $n > 2$ are always first order. Substituting for $\Delta E''_0/T$ from (7.7) into (7.10) (with $\Delta G = 0$) and solving for ΔG_m we have

$$\frac{\Delta G_m}{RT} = -\left([n(1-n\hat{\sigma}_1^2)-1] ln\hat{\sigma}_1 + [1-n(1-\hat{\sigma}_1)^2)] ln\{(1-\hat{\sigma}_1)/(n-1)\}\right)/(1-n\hat{\sigma}_1)^2 \quad (7.11)$$

Equation (7.11) allows one to find $\hat{\sigma}_1$ once n and ΔG_m values are

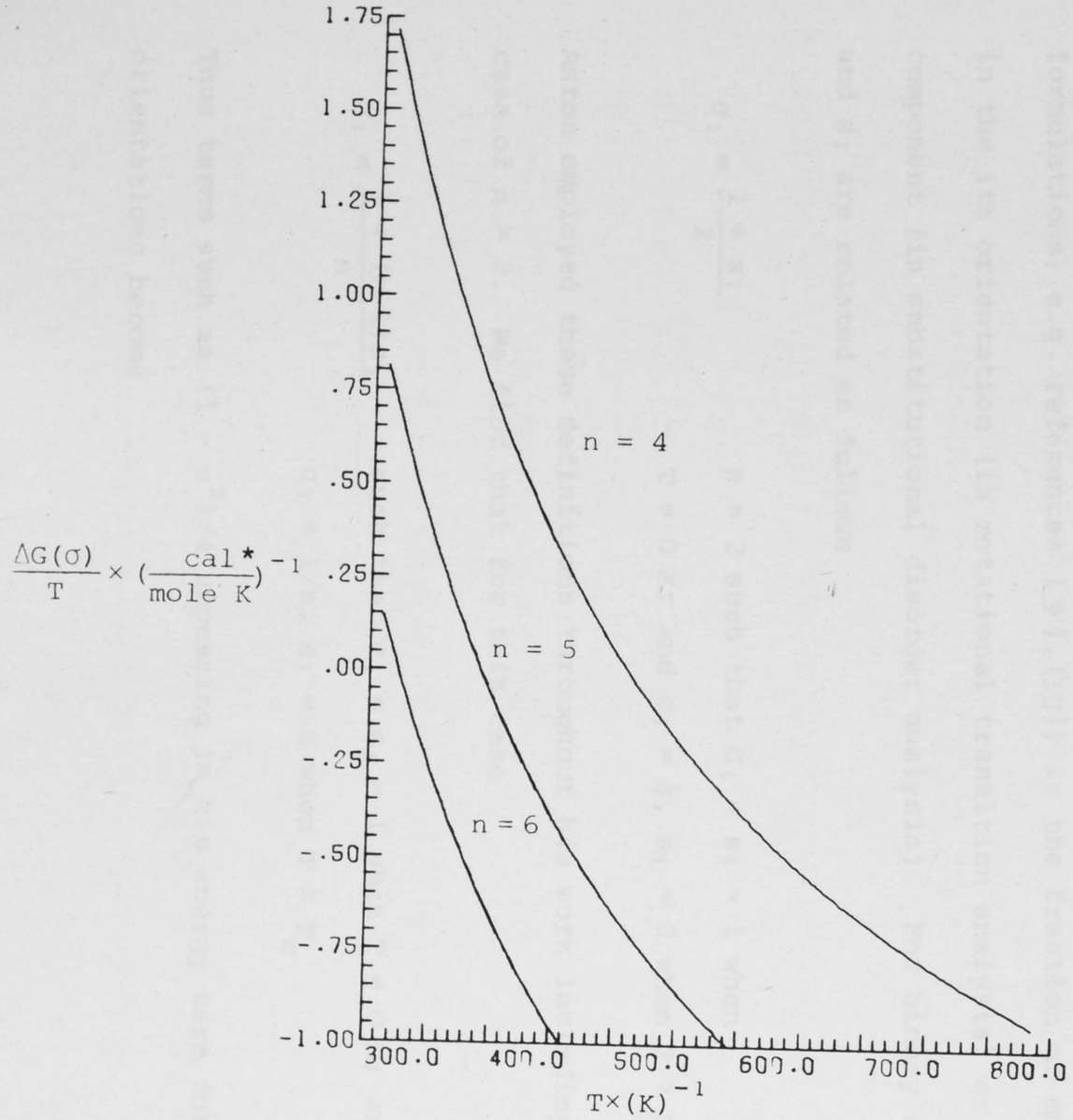

Figure 7.1: Properties of the free energy $\Delta G(\hat{\sigma}) = G(1/n)-G(\hat{\sigma})$, where $\hat{\sigma} = 0.95$, and n is varied. The transition occurs along the line $\Delta G = 0$.
Values of parameters used: $\Delta E'' = 6.34 \times 10^3$ cal/mole, $\tilde{\nu}'_{mi} = 221\ cm^{-1}$ and $\tilde{\nu}''_{mi} = 141\ cm^{-1}$. These frequency values are average values derived from our preliminary study of camphor.

* 1 cal = 4.184 J

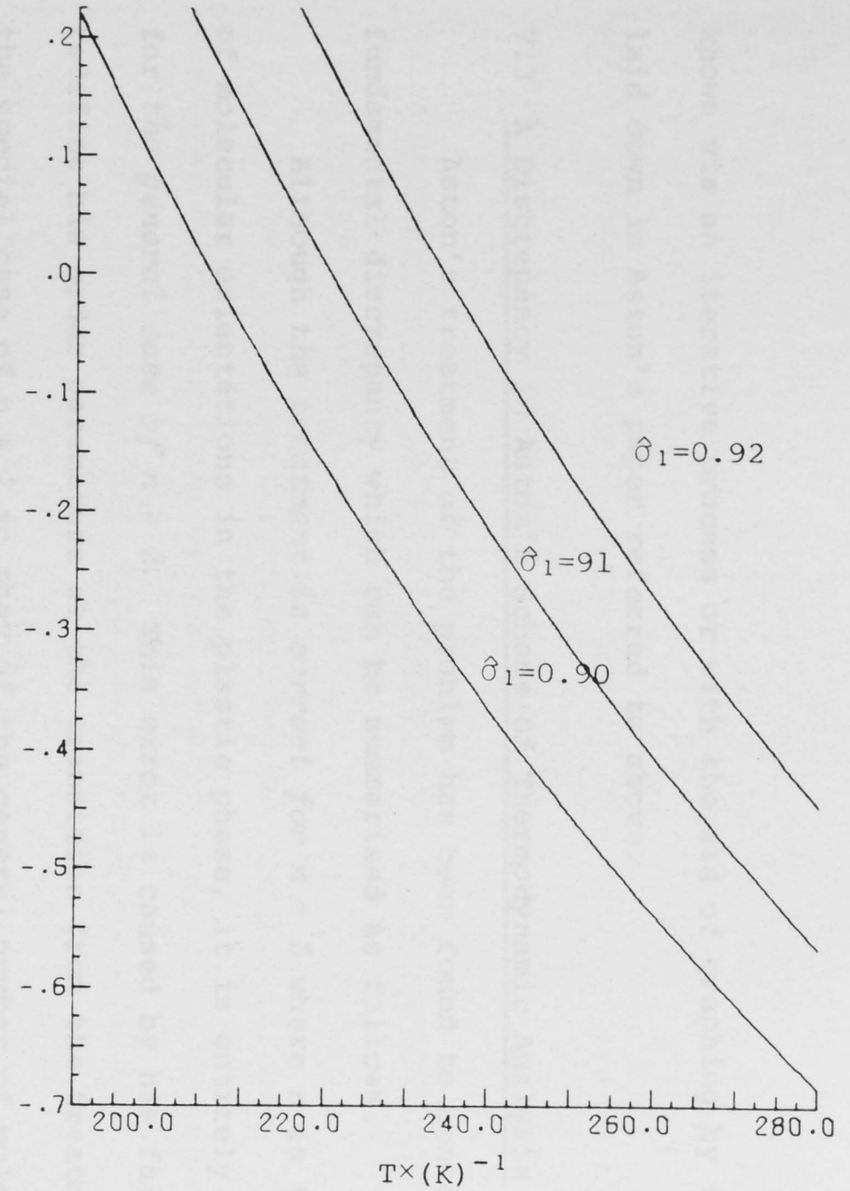

Figure 7.2: Properties of the free energy $\Delta G(\hat{\sigma}) = G(1/n)-G(\hat{\sigma})$, where n = 6, and $\hat{\sigma}$ is varied. The effect of the variation of $\hat{\sigma}_1$ on the free energy is not obvious from this figure because the values of $\hat{\sigma}$ are close together. However, the effect described in the text is observed at large separations of $\hat{\sigma}_1$ values.

known via an iterative process or with the aid of graphing by the method laid down in Aston's paper referred to above.

7.3 A Discrepancy in Aston's Scheme of Thermodynamic Analysis

Aston's treatment of the problem has been found to contain a fundamental discrepancy which can be summarised as follows.

Although *the treatment is correct for* $n = 2$ where n is the number of molecular orientations in the plastic phase, it is entirely in error for *the general case of* $n > 2$. This error is caused by his failure to redefine his order parameters at the transition from the treatment of the special case of n = 2 to that of the general number of molecular orientations. Order parameters are customarily defined as follows. The degree of long range order s_1 is a measure of order in the system and takes the value of unity at 0 K in the ordered phase, and zero in the disordered phase. The fractional long range order σ_i (S in most formulations; e.g. references [9],[10]) is the fraction of molecules in the ith orientation (in rotational transition analysis) or of the ith component (in substitutional disorder analysis). For binary systems σ_i and s_1 are related as follows

$$\sigma_1 = \frac{1 + s_1}{2}$$

n = 2 such that $\sigma_1 = s_1 = 1$ when T = 0 K; and $\sigma_1 = \frac{1}{2}$, $s_1 = 0$ when $T > T_c$

Aston employed these definitions throughout his work including the general case of n > 2. We find that for this case

$$\sigma_1 = \frac{1 + (n-1)s_1}{n}$$

such that $\sigma_1 = s_1 = 1$ when T = 0 K; and $\sigma_1 = 1/n$, $s_1 = 0$ when $T > T_c$

Thus terms such as $(1 - s^2)/4$ appearing in his energy term for 2n orientations become

$$(2n - 1)\{1 + s[(2n - 2) - (2n - 1)s]\}/(2n)^2$$

which returns to $(1 - s^2)/4$ when $n = 1$. The entropy term is also seriously affected (as can be expected).

7.4 Thermodynamic Functions for Solid State Order-Disorder Transitions in Molecular Crystals

The molecular partition function for the general model being discussed now is identical to that of Aston for $n = 2$; hence we adopt his result for the molecular free energy function which is

$$\Delta G_m = (Nhc/2)\sum_i\{\tilde{\nu}''_{mi} - \tilde{\nu}'_{mi}\} + \sum_i\{A''_{mi} - A'_{mi}\} \qquad (7.12)$$

where A'_{mi} and A''_{mi} are Einstein free energy functions. Applying the appropriate thermodynamic relations to equation (7.8) we obtain the following results

$$G(\hat{\partial}_1)-G(1) = RT[\hat{\partial}_1 ln\hat{\partial}_1+(1-\hat{\partial}_1) ln\{(1-\hat{\partial}_1)/(n-1)\}] + (1-\hat{\partial}_1)[\hat{\partial}_1\Delta E''$$
$$+ (Nhc/2)\sum_i\{\tilde{\nu}''_{mi}-\tilde{\nu}'_{mi}\} + \sum_i\{A''_{mi}-A'_{mi}\}] + \rho\Delta V_c \qquad (7.13)$$

$$U(\hat{\partial})-U(1) = (1-\hat{\partial}_1)[\hat{\partial}_1\Delta E''_0 + (Nhc/2)\sum_i\{\tilde{\nu}''_{mi}-\tilde{\nu}'_{mi}\} + \sum_i\{E''_{mi}-E'_{mi}\}] \qquad (7.14)$$

$$S(\hat{\partial})-S(1) = -R[\hat{\partial}_1 ln\hat{\partial}_1 + (1-\hat{\partial}_1) ln\{(1-\hat{\partial}_1)/(n-1)\}] + (1-\hat{\partial}_1)\sum\{S''_{mi}-S'_{mi}\} \qquad (7.15)$$

$$C_p(\hat{\partial})-C_p(1) = [\Delta E''(1-2\hat{\partial}_1)-(Nhc/2)\sum_i\{\tilde{\nu}''_{mi}-\tilde{\nu}'_{mi}\} - \sum_i\{E''_{mi}-E'_{mi}\}][\{(1-2\hat{\partial}_1)\Delta E''$$
$$- \Delta G_m\}/T - \sum_i\{S''_{mi}-S'_{mi}\}]/[RT/(1-\hat{\partial}_1)\hat{\partial}_1 - 2\Delta E'']$$
$$+ (1-\hat{\partial}_1)\sum_i\{C''_{mi}-C'_{mi}\} + P\left(\frac{\partial V}{\partial T}\right)_P \qquad (7.16)$$

where ΔV_c is the volume change at the rotational transition, V is the volume of substance during the transition and P is pressure. C_{mi}, E_{mi}

and S_{mi} are Einstein thermodynamic functions. Equation (7.14) gives the transition energy between the perfectly ordered solid (obtainable only at 0 K) and the partially disordered solid with $\sigma_1 = \hat{\sigma}_1$ at the transition temperature. The transition energy is then given by

$$U(1/n)-U(\hat{\sigma}) = [n-n^2(1-\hat{\sigma}_1)\hat{\sigma}-1]\Delta E''/n^2 + (n\hat{\sigma}-1)[Nhc/2)\sum_i\{\tilde{\nu}''_{mi}-\tilde{\nu}'_{mi}\} + \sum_i\{E''_{mi}-E'_{mi}\}]/n \quad (7.17)$$

and the total transition energy is given by

$$U(1/n)-U(1) = (n-1)[\Delta E''_0/n + (Nhc/2)\sum_i\{\tilde{\nu}''_{mi}-\tilde{\nu}'_{mi}\} + \sum_i\{E''_{mi}-E'_{mi}\}]/n \quad (7.18)$$

The transition temperature is defined as the temperature at which the partially disordered solid ($\sigma_1 = \hat{\sigma}_1$) is in equilibrium with the completely disordered solid ($\hat{\sigma}_1 = 1/n$). When $\hat{\sigma}_1$ is not known rough estimates can be achieved by setting it to unity and ignoring the contribution from the molecular partition function. For some molecular crystals this assumption may be valid provided there is no significant change in the vibrational frequencies at the transition. This approximation may be expected to apply for globular molecules such as methane where the potential barriers to molecular rotations are low. For transitions that occur at high temperatures it is the difference in the zero-point energies for both phases that makes the primary contribution to the thermodynamic properties from the molecular free energy point of view as terms such as $\{A''_{mi} - A'_{mi}\}$ vanish.

7.5 Estimation of the Number of Molecular Orientations in the Plastic Phase

In order to get at the number of molecular orientations it is helpful to consider the total entropy change of transition which, from equation (7.15), becomes

$$S(1/n)-S(1) = R\ln n + (n-1)\sum\{S''_{mi}-S'_{mi}\}/n \qquad (7.19)$$

From both (7.18) and (7.19) the following expression for ΔG_m is obtained.

$$\Delta E''/n - \{n/(n-1)\}RT\ln n = -\Delta G_m \qquad (7.20)$$

Note that when $\Delta G_m = 0$ then the system is adequately described by the configurational partition function only. It will be shown later that methane can be reasonably described by this procedure.

From (7.17) we find an expression for $\Delta E''/n$ which we substitute into (7.20) (if $\Delta G_m \neq 0$) and obtain

$$[n\Delta U(\sigma)-T(n\hat{\sigma}_1-1)\sum\{S''_{mi}-S'_{mi}\} - n/(n-1)\{n-[1+n^2\hat{\sigma}_1(1-\hat{\sigma}_1)]\}TR\ln n]/ \cdot$$

$$\cdot[(n\hat{\sigma}_1+1)(n\hat{\sigma}_1-n)-2] = \Delta G_m \qquad (7.21)$$

where $\Delta U(\sigma) = U(1/n) - U(\hat{\sigma}) = \Delta H_P(\sigma) - P\Delta V$

and $\Delta U(\sigma)$ is the experimental transition energy less work done against the atmosphere. Thus as we did with $\hat{\sigma}_1$ in (7.11) we search for n via an iteration procedure with known values of $\hat{\sigma}$, $\Delta U(\sigma)$ and ΔG_m. However we note that the value of n in (7.21) depends on knowledge of $\hat{\sigma}_1$ which in turn is evaluated in (7.11) from knowledge of n. We therefore propose the following iterative procedure for the case of $\omega \neq 0$.

(i) Compute the initial value of n from the relation

$$n = \exp[\{\Delta U(\sigma) - \Delta E_{Th}(\sigma)\}/RT_{MR}] \qquad (7.22)$$

where $\Delta E_{Th}(\sigma)$ is the thermal transition energy calculated from Einstein thermodynamic functions. $\Delta U(\sigma)$ is obtained from calorimetric measurements (e.g. C_P-curve) with allowances made for the work terms, if necessary. T_{MR} is the temperature at which transition is complete corresponding to the peak of a λ-transition and may be termed the *rotational melting*

temperature.*

(ii) With the known value of ΔG_m and the new value of n evaluate $\hat{\sigma}_1$ from (7.11).

(iii) With the new value of $\hat{\sigma}_1$ evaluate a new value of n from (7.21) using the same value of $\Delta U(\sigma)$ as in (i).

(iv) Return to (ii) until some degree of self-consistency is achieved between the two equations, (7.11) and (7.21). The final value is then converted into an integer by dropping the decimal point or by rounding-off. We shall hereafter denote the value of n found this way by $\hat{n}$ in correspondence with $\hat{\sigma}_1$.

Equation 7.22 applies the principal correction required to n, and the rest of the steps are merely a refinement of this quantity. However, we have not tested the convergence characteristics of this procedure as yet; but hope to do so when our spectroscopic studies of camphor and camphoric anhydride are completed. Also, as will be seen later, steps (ii) to (iv) may become less important for large values of n.

7.6 Configurational and Thermal Entropies of Transition

The transition energy, $\Delta U(\sigma)$, must be known before the number of molecular orientations associated with the plastic phase transition can be estimated. A method that is becoming more useful for the estimation of the number of molecular orientations in the plastic phase is due to Guthrie and McCullough [1]. In this method the experimental entropy of transition is attributed to configurational entropy change. This implies that the entropy of expansion, the thermal entropy, is negligible.

---

* The difficulties in defining characteristic transition temperatures in continuous transitions of the λ-type is discussed later in the text.

Reynolds [12] has calculated the entropy change in the plastic phase transition of diazabicyclo[2,2,2]octane(DABCO) through the use of empirical intermolecular potentials to be 60 per cent due to entropy of expansion and 40 per cent due to configurational entropy change. Schäfer *et al* [51] observed by applying the familiar thermodynamic identity (7.23) to the plastic phase transition of camphor that the thermal energy change due to lattice expansion associated with the transition was of the same order as the experimental transition energy.

$$C_V = C_P - \alpha^2 VT/K_T \qquad (7.23)$$

This leads us to conclude that the approximation of Guthrie *et al* is valid only for transitions with negligible thermal expansion such as may be expected for tetrahedral molecules like methane. In order to apply it in general it is necessary to isolate the configurational entropy change from the experimental entropy change. This will be attempted in the next section.

We proceed to show how the experimental entropy change can be broken down into its components. We define the transition energy at constant volume, $\Delta E(\sigma)$, as follows

$$\Delta E_v(\sigma) = \Delta U(\sigma) - \Delta E_{Th}(\sigma) \qquad (7.24)$$

We observe that $\Delta E_v(\sigma)$ is identical to the configurational transition energy. This is the quantity in the argument of the exponent in equation (5.22).

The work done by the system against the atmosphere is generally negligible and may be omitted. For example the increase in molar volume associated with the plastic phase transition in *d*-camphor is 10.2 cm^3/mole [51] and $P\Delta V$ is therefore 0.25 cal/mole whereas $\Delta H(\sigma) = 2700$ cal/mole. Thus $\Delta U(\sigma) \simeq \Delta H(\sigma)$. The transition entropy from theory is obtained by

subtracting equation (7.15) from equation (7.19). Thus

$$\Delta S(\sigma) = R[ln n + \hat{\sigma}_1 ln\hat{\sigma}_1 + (1-\hat{\sigma}_1) ln\{(1-\hat{\sigma}_1)/(n-1)\}]$$

$$+ \{(n\hat{\sigma}_1-1)/n\}\sum_i \{S''_{mi} - S'_{mi}\} \qquad (7.25)$$

where

$$\Delta S(\sigma) = S(1/n) - S(\hat{\sigma}).$$

We observe that the transition entropy is in general given by

$$\Delta S(\sigma) = [\Delta S_c(\sigma)]_{T_c, T_{MR}} + \{(n\hat{\sigma}-1)/n\}\Delta S_{Th}(\sigma) \qquad (7.26)$$

where

$$[\Delta S_c(\sigma)]_{T_c, T_{MR}} = [\Delta S_c(\sigma)]_{T_0, T_{MR}} - [\Delta S_c(\sigma)]_{T_0, T_c}$$

and is configurational entropy change. The temperature subscripts indicate the temperature ranges. T_c is the transition temperature; and T_0 = 0 K. If $\hat{\sigma}_1 = 1.0$ then $[\Delta S_c(\sigma)]_{T_0, T_c} = 0$ and $[\Delta S_c(\sigma)]_{T_c, T_{MR}} = [\Delta S_c(\sigma)]_{T_0, T_{MR}}$. In this case the entropy change is given by (7.19) and we can write

$$\Delta S(\sigma) = \Delta S_c(\sigma) + \eta \Delta S_{Th}(\sigma) \qquad (7.27)$$

where $\eta = (n-1)/n$ and $\Delta S_{Th}(\sigma)$ is the thermal entropy change. When n is large η approaches unity and lattice vibrations and configurational disorder can be considered separately. Reynolds calculation* on 'model DABCO' depends on this *separability of the entropies* and indicates that

---

* This calculation is based on the assumption that the configurational and thermal entropies are corrected only via volume changes; and a self-consistent calculation is adequate.

in DABCO the observed transition entropy of 7.2 cal mol^{-1} K^{-1} may be divided so that 2.9 cal mol^{-1} K^{-1} is from configurational disordering. This configurational entropy change gives a value of 4 for n in the plastic phase and $\eta = 3/4$. Therefore $\Delta S_{Th}(\sigma) \simeq 5.7$ cal mol^{-1} K^{-1}. If however $\hat{\sigma}_1 \neq 1.0$ the separability may not exist even if n is large. On the other hand, if $\hat{\sigma} \sim 1/n$ then the transition entropy is very small.

7.7 Configurational Entropy Change of Rotational Phase Transition from Experimental Transition Energies

We now describe an alternative approximate method which can be used to calculate the configurational thermodynamic properties from thermal data alone. In principle if we had a C_P-curve we would convert it to the C_V-curve by the fundamental thermodynamic identity, equation (7.23), and the area between C_V-curve maximum and the *baseline extrapolation* would give us the transition energy at constant volume, $\Delta E(\sigma)$. In practice, however, compressibility data are very difficult to obtain and for systems for which this type of data is not available one tends to use the approximate relation due to Nernst and Lindemann

$$C_V = C_P - \lambda \left(\frac{T}{T_M}\right) C_V^2 \qquad (7.28)$$

where $\lambda = 0.0214$ deg cal^{-1}.

Lord *et al* [73] have empirically demonstrated that this expression is applicable to molecular crystals. Although equation (7.28) is simple and widely used in the literature in the study of plastic crystals [based on a common reference to Lord's work] there appears to be some conflict in its application apparently due to some indecision on what values of T_M are to be used - the rotational melting or the ordinary melting temperature.

In applying equation (7.28) to the C_P data obtained through an order-disorder transition, we are assuming that equation (7.23) applies

during the transition. We note that many workers involved in the study of transitions of this nature have taken this fact for granted. We can see how this assumption can be arrived at even by assuming a more difficult theory - the domain theory of order-disorder transition. This theory supposes that the mechanism for an order-disorder transition involves the creation of the nucleus of the disordered phase within the ordered phase and that the nucleus spreads out with increase in temperature. We particularly choose this theory because it accounts for the commonly observed hysteresis and remarkable increase in specific conductivity at the phase transition [14]. The problem simply amounts to demonstrating that quantities of the kind $(\frac{\partial V}{\partial T})_P$ may be evaluated at the same pressure for the coexisting phases during the transition. It is argued here that for cooperative transitions conducted quasi-statically, the pressure $P = -(\partial A/\partial V)_T$ is constant throughout the crystal so that these quantities can be evaluated at the same pressure (~ 0) for both phases. We discuss this matter again in section (7.12).

We now expand equation (7.28) into its components and seek to get the contribution to the specific heat at constant volume due to the rotation of the molecules during the transition, $C_V(\sigma)$. This is necessary in order to get at the energy of the phase transition at constant volume, $\Delta E_V(\sigma)$. Let

$$C_P = C_P(v) + C_P(\sigma) \tag{7.29}$$

$$C_V = C_V(v) + C_V(\sigma) \tag{7.30}$$

and assume

$$C_V(v) = C_V(D) + C_V(I) \tag{7.31}$$

where $C_V(D)$ represents the contribution to the specific heat from

translational vibrations; $C_V(I)$, internal degrees of freedom of the molecules; and $C_V(\sigma)$, the rotational degrees of freedom during the transition. Then putting (7.29), (7.30) and (7.31) in (7.28) and solving for $C_V(\sigma)$ after ignoring small terms some of which cancel one another we have

$$C_V(\sigma) = \sqrt{\{C_V^2(v) + C_V(v)\frac{T_M}{\lambda T} + \frac{T_M}{\lambda T}[\frac{T_M}{4\lambda T} + C_P(\sigma)]\}} - C_V(v) + \frac{T_M}{\lambda T} \qquad (7.32)$$

Equation (7.32) enables one to convert a $C_P(\sigma)$-curve into a $C_V(\sigma)$-curve. Integration of the area under the $C_V(\sigma)$-curve should give the transition energy at constant volume. However, it is necessary to decide what T_M stands for at this stage. We will assume that T_M is the temperature at which the "rotational melting" is complete which should coincide with the temperature at which $C_P(\sigma)$ is a maximum for an ideal λ-transition. We have already called this temperature the rotational melting temperature T_{MR}. We arrive at this conclusion by noting that the dominant contribution to the specific heat at this temperature will be due to the rotational part of the specific heat, $C_P(\sigma)$, and that $C_V(v)$ in equation (7.32) simply arises from the coupling term $\frac{2\lambda T}{T_M} C_V(\sigma)C_V(v)$; since we have already neglected the contribution to the specific heat by the translational vibrations. In practice this is achieved by applying the method of baseline extrapolation on the C_P data to give $C_P(\sigma)$ data. Because rotational transitions are non-isothermal we shall assume hence-forth that both T_c and T_{MR} are characteristics of the transition which must be defined in computations of transition energies from thermal data.

In order to evaluate $C_V(v)$ around the transition temperature which, it will be recalled, contains translational and intramolecular components it is proper to assume the high temperature limit of the Debye heat capacity for the intermolecular vibrations, especially for molecular crystals where the characteristic temperature is relatively small. This however will not

be true for the high energy intramolecular vibrations. In this case the contribution to the specific heat should be done by a frequency assignment for each of the internal degrees of freedom and their thermodynamic properties evaluated from tabulated Einstein thermodynamic functions. However rough estimates of $C_V(v)$ can be achieved by the following relation which assumes a small difference between C_P and C_V and that the data is collected at lower temperatures before the transition.

$$C_V(v) = C_P\left(1 - \frac{\lambda T}{T_M} C_P\right) - 3R \qquad (7.33)$$

where T_M is the ordinary melting point (assuming that the melting point of the ordered solid can be approximated by the observed melting point occurring above the plastic phase).

In some circumstances the C_P-curve may not be available; but the experimental transition energy and the temperatures characterising it may be known. In this case we have to assume the form of $C_P(\sigma)$ in order to calculate the transition energy at constant volume. If we assume $C_P = a + bT$ and let $C_P(\sigma) = b(T-T_C)$ such that $T \geq T_C$ and $T \leq T_{MR}$, equation (7.32) takes the form

$$C_V(\sigma) = \sqrt{\left\{C_V^2(v) + C_V(v)\frac{T_{MR}}{\lambda T} + \frac{T_{MR}}{\lambda T}\left(\frac{T_{MR}}{4\lambda T} + \frac{2\Delta U(\sigma)\,(T-T_C)}{(T_{MR}-T_C)^2}\right)\right\}} - C_V(v) + \frac{T_{MR}}{\lambda T} \qquad (7.34)$$

and the area under $C_V(\sigma)$ gives the transition energy at constant volume. In obtaining $C_P(\sigma)$ we have assumed a standard empirical formula which expresses C_P as a power series in T, where we have used the formula up to the first term only. The values of $C_V(\sigma)$ in Figure 7.3 were obtained via equation (7.34) and $\Delta E_V(\sigma)$ was estimated to be 880 cal/mole from a literature value of 2700 cal/mole [24] for $\Delta H(\sigma)$ for camphor. Thus about 30 per cent of the experimental transition entropy in *d*-camphor is configurational and the rest, about 70%, is thermal entropy change due to

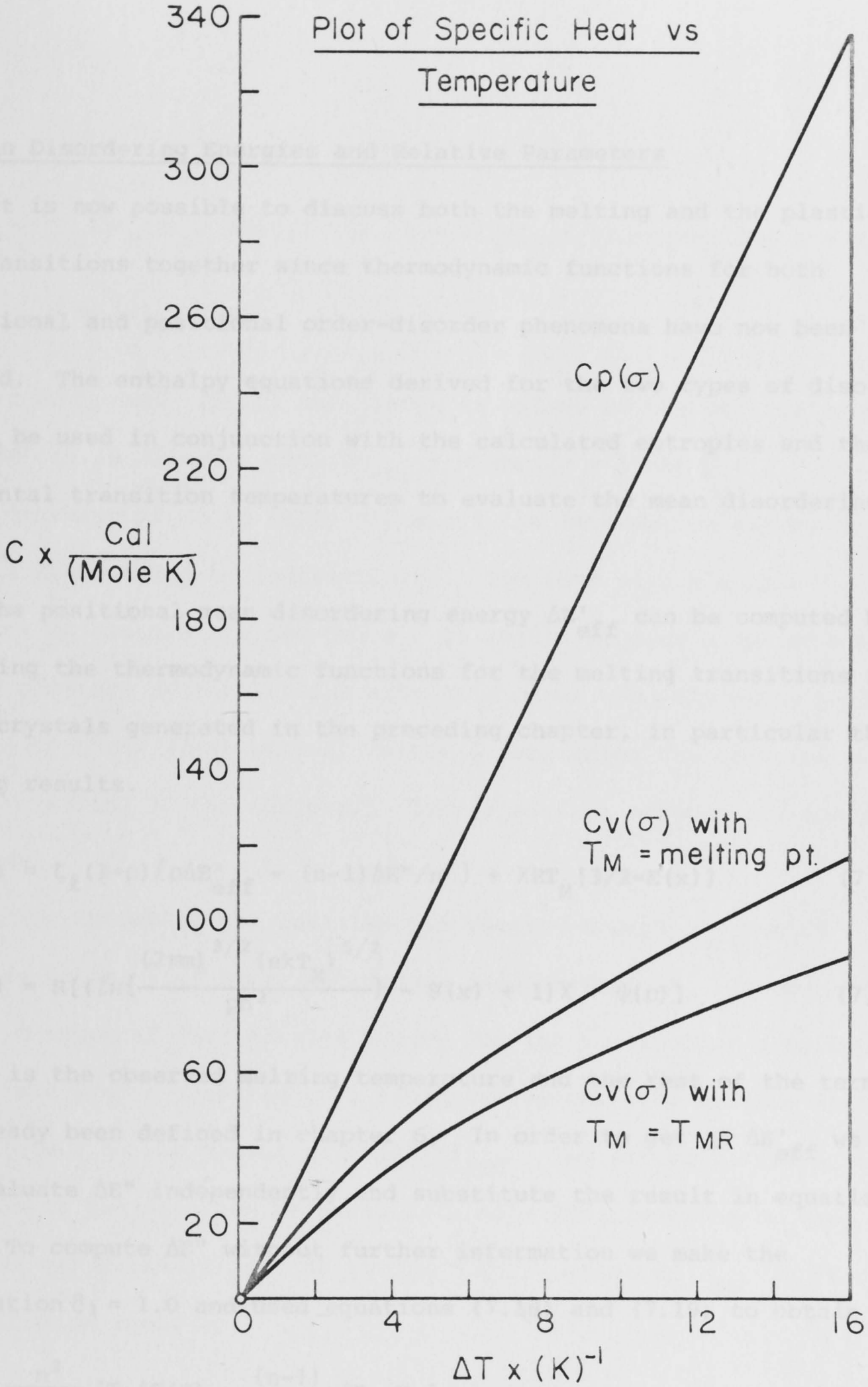

Figure 7.3: Specific heat curves from which the transition energy $\Delta E_v(\sigma)$ is calculated via numerical integration. $\Delta E_v(\sigma)$ obtained by the use of T_M (the ordinary melting point) is greater than the one obtained using T_{MR}. The text assumes the latter to apply.

expansion. This is in reasonable agreement with the results reported by Reynolds for DABCO. The configurational transition energy of 880 cal/mole gives a value of 6 for n in the plastic phase of camphor. It is interesting to note that the same value for n was found for camphor by Schäfer and Frey [51] from specific heat measurements at low temperatures.

7.8 Mean Disordering Energies and Relative Parameters

It is now possible to discuss both the melting and the plastic-phase transitions together since thermodynamic functions for both orientational and positional order-disorder phenomena have now been generated. The enthalpy equations derived for the two types of disorder will now be used in conjunction with the calculated entropies and the experimental transition temperatures to evaluate the mean disordering energies.

The positional mean disordering energy $\Delta E'_{eff}$ can be computed by considering the thermodynamic functions for the melting transitions in plastic crystals generated in the preceding chapter, in particular the following results.

$$\Delta U_M(\rho) = \zeta_\ell(1-\rho)\{\rho\Delta E'_{eff} - (n-1)\Delta E''/n^2\} + \chi RT_M[3/2-E(x)] \qquad (7.35)$$

$$\Delta S_M(\rho) = R[(\ell n\{\frac{(2\pi m)^{3/2}(ekT_M)^{5/2}}{ph^3}\} - S(x) + 1)\chi + \psi(\rho)] \qquad (7.36)$$

where T_M is the observed melting temperature and the rest of the terms have already been defined in chapter 6. In order to get at $\Delta E'_{eff}$ we must first evaluate $\Delta E''$ independently and substitute the result in equation (7.35). To compute $\Delta E''$ without further information we make the approximation $\hat{\sigma}_1 = 1.0$ and used equations (7.18) and (7.19) to obtain

$$\Delta E'' = \frac{n^2}{(n-1)}[T_c\Delta S(\sigma) - \frac{(n-1)}{n}\Delta E_{\tilde{\nu}} - W_c] \qquad (7.37)$$

where $\Delta S(\sigma) = S(1/n) = S(1)$, $\Delta E_{\tilde{\nu}}$ is given by the equation

$$\Delta E_{\tilde{\nu}} = (Nhc/2)\sum\{\tilde{\nu}''_{mi} - \tilde{\nu}_{mi}\} + \sum\{E''_{mi} - E'_{mi}\} \qquad (7.38)$$

and $W_c = P\Delta V_c$ where ΔV_c is the change in volume at the rotational transition. Substituting for $\Delta E''$ in (7.35) and solving for $\Delta E'_{eff}$ using equations (7.35) and (7.36) under equilibrium conditions we have

$$\Delta E'_{eff} = \{T_m[\Delta S_M(\rho) - \chi R(3/2-E(x))] + \chi\zeta_\ell[T_c\Delta S(\sigma) - (n-1)\Delta E_{\tilde{\nu}}/n - W_c] - W_M\}/\zeta_\ell\rho(1-\rho) \quad (7.39)$$

where $W_M = P\Delta V_M$, and ΔV_M is the change in volume at the melting transition. From (7.39) it is observed that $\Delta E_{eff} \to \infty$ when $\rho = 0$ and $\rho = 1$. The case of $\rho = 0$ corresponds to an empty space and the interaction energy for positional disordering is indeterminate. The case of $\rho = 1$ is a consequence of cooperative phenomena. It should require a lot of energy to move a molecule from a lattice site to another when all other molecules are occupying their sites without initially requiring the creation of a vacant site except at the surface. However surface effects are ignored in our model.

We now introduce the relative disordering energy ν_{eff} which corresponds to the ν of Pople and Karasz (see chapter 1). In our model ν_{eff} is a measure of the relative energy for the rotation of a molecule and the simultaneous creation of a fluidised vacant site and the diffusion of the molecule to the vacant site $\Delta E''/\Delta E'_{eff}$. The latter situation simply corresponds to the creation of a gas-like molecule according to the significant structure of liquids theory. This parameter ν_{eff} is given by the following equation.

$$\nu_{eff} = \{n^2T_c\Delta S(\sigma)/(n-1) - n\Delta E_{\tilde{\nu}}\}\zeta_\ell\rho(1-\rho)/\{T_M[\Delta S_M(\rho) - \chi R(3/2-E(x))] + \chi\zeta_\ell[T_c\Delta S(\sigma) - (n-1)\Delta E_{\tilde{\nu}}/n]\} \quad (7.40)$$

where we have ignored the work terms. Note that this parameter is generally defined for configurational energies as the thermal energies are subtracted out except for coupling terms. Further the critical relative disordering energy is defined as

$$(\nu_{eff})_c = \{\Delta E''/\Delta E'_{eff}\}_{T_c=T_M} \tag{7.41}$$

and corresponds to the case where both orientational and positional disordering processes occur at the same temperature. From (7.40) we obtain the following result for the melting temperature.

$$T_M = \frac{\chi\zeta_\ell\{\frac{n^2\rho}{n-1} - \nu_{eff}\}\Delta E_v(\sigma)}{\nu_{eff}\Delta E_v(\rho)} \tag{7.42}$$

where $\Delta E_v(\sigma) = (n-1)\Delta E''/n^2$, the orientational configurational energy; and $\Delta E_v(\rho) = \Delta S_M(\rho) - \chi R[3/2-E(x)]$, the positional configurational energy. The quantity $\Delta E_v(\rho)$ for plastic crystals is of the order of R since $\Delta S_M(\rho)$ is of the order of R, $\chi \simeq 0.1$ for substances such as methane and $E(x) = 3$ in the classical limit. The term under {} brackets is always positive since ν_{eff} is a small number and can be neglected; and $\rho \simeq 1$. Thus the melting temperature is directly proportional to the orientational configurational energy and inversely proportional to ν_{eff} for given values of n and ρ. Thus the melting temperature is higher if $\Delta E_v(\sigma)$ is large and ν_{eff} is small.

However equation (7.42) is simply an analytical expression standing for a well known principle - that phase transitions in the solid elevate the melting temperature roughly in proportion to the entropy changes associated with them. This then is established as the explanation for the high melting temperatures generally observed in plastic crystals.

7.9 Computational Results for Methane

Our task is to compute the mean disordering energies and relative parameters for methane, the simplest and probably the most well known of all plastic crystals. Although the value of n may be assumed to be 10, following the result for tetrahedral molecules reported by Guthrie *et al*

[1], the value of n in the computations shall be varied in order to estimate relative parameters for a number of molecular orientations.

For the present purpose we make the assumption that $\Delta G_m = 0$ at the rotational transition; since methane is a perfectly globular molecule. We recall that the term globular molecule refers to those molecules which have an overall repulsion envelope with approximate or actual spherical symmetry. Thus if $\Delta G_m = 0$ then terms involving E defined in (7.38) also vanish. From the argument presented above this assumption should not affect the magnitudes of ν_{eff} seriously. Thus (7.39) takes the form

$$\Delta E'_{eff} = \{T_M[\Delta S_M(\rho) - \chi R(3/2-E(x))] + \chi\zeta_\ell RT_c \ln n\}/\zeta_\ell\rho(1-\rho) \qquad (7.43)$$

where $\Delta S(\sigma)$ has been substituted with $R\ln n$. Also equation (7.40) becomes

$$\nu_{eff} = \{n^2RT_c \ln n/(n-1)\}\zeta_\ell\rho(1-\rho)/\{T_M[\Delta S_M(\rho) - \chi R(3/2-E(x))] + \chi\zeta_\ell RT_c \ln n\} \qquad (7.44)$$

and the critical relative energy is given by the following equation.

$$(\nu_{eff})_c = \frac{\{n^2R\ln n/(n-1)\}\zeta_\ell\rho(1-\rho)}{\Delta S_M(\rho) - \chi R[3/2 - E(x)] + \chi\zeta_\ell R\ln n} \qquad (7.45)$$

Table 7.1 summarises the results of the computation for the interactive energies and relative parameters for methane.

Table 7.1: A sample of mean disordering energies and relative parameters for methane with $\Delta E_s = 9.209$ kJ/mole (ΔE_s data from reference [67]).

ENERGIES*	$\nu_{eff} \times 10^2$	$(\nu_{eff})_c \times 10^2$	n
$\Delta E'_0 = 217$ kJ/mole	0.21	0.92	2
$\Delta E'_{eff} = 227$ kJ/mole	1.91	8.44	10
	18.7	81.9	60

*The energies vary very slowly with n, and can be assumed to be constant within the range n=2 to n=60. The values quoted are average values.

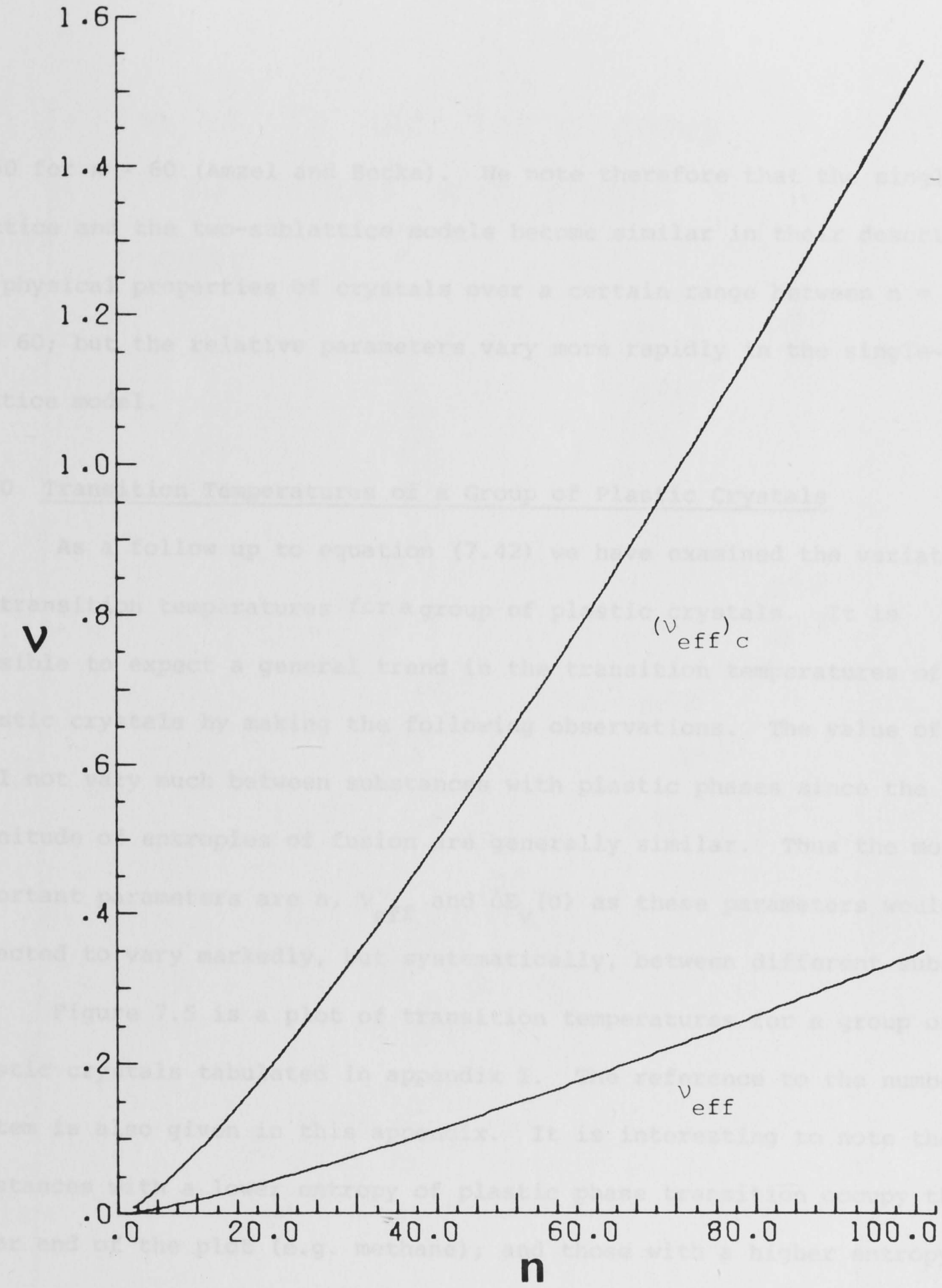

Figure 7.4: The variation of the relative energy parameter with n.

The properties of equations (7.44) and (7.45) for fixed values of ρ are summarised in Figure 7.4. Thus for every value of n there is a unique value for $(\nu_{eff})_c$ in agreement with Amzel and Becka. From table 7.1, for n = 2 the value of the critical relative parameter is 9.2×10^{-3}; and for n = 60, the value of this parameter is 0.82. The two-sublattice model gives the critical value of 0.325 for n = 2 (Pople and Karasz); and

0.50 for n = 60 (Amzel and Becka). We note therefore that the single-lattice and the two-sublattice models become similar in their description of physical properties of crystals over a certain range between n = 2 and n = 60; but the relative parameters vary more rapidly in the single-lattice model.

7.10 Transition Temperatures of a Group of Plastic Crystals

As a follow up to equation (7.42) we have examined the variation of transition temperatures for a group of plastic crystals. It is possible to expect a general trend in the transition temperatures of plastic crystals by making the following observations. The value of ρ will not vary much between substances with plastic phases since the magnitude of entropies of fusion are generally similar. Thus the most important parameters are n, ν_{eff} and $\Delta E_v(\sigma)$ as these parameters would be expected to vary markedly, but systematically, between different substances.

Figure 7.5 is a plot of transition temperatures for a group of plastic crystals tabulated in appendix I. The reference to the numbering system is also given in this appendix. It is interesting to note that substances with a lower entropy of plastic phase transition occupy the lower end of the plot (e.g. methane); and those with a higher entropy of transition, the upper end (e.g. camphoric anhydride). Also molecules in the camphor group (16, 38, 48, 50, 51) and the methane group (1-3) form their own patterns. The methane group is particularly interesting. It will be seen that the melting temperature decreases with molecular mass, while the rotational transition temperature increases. We do not attempt an explanation of this anomaly at the present.

It is seen that there is some correlation between the melting point and the rotational transition temperature. The correlation is governed by the constraint $T_M/T_C > 1$. Thus there is a forbidden region on the right side of the cluster of points bounded by a straight line (not

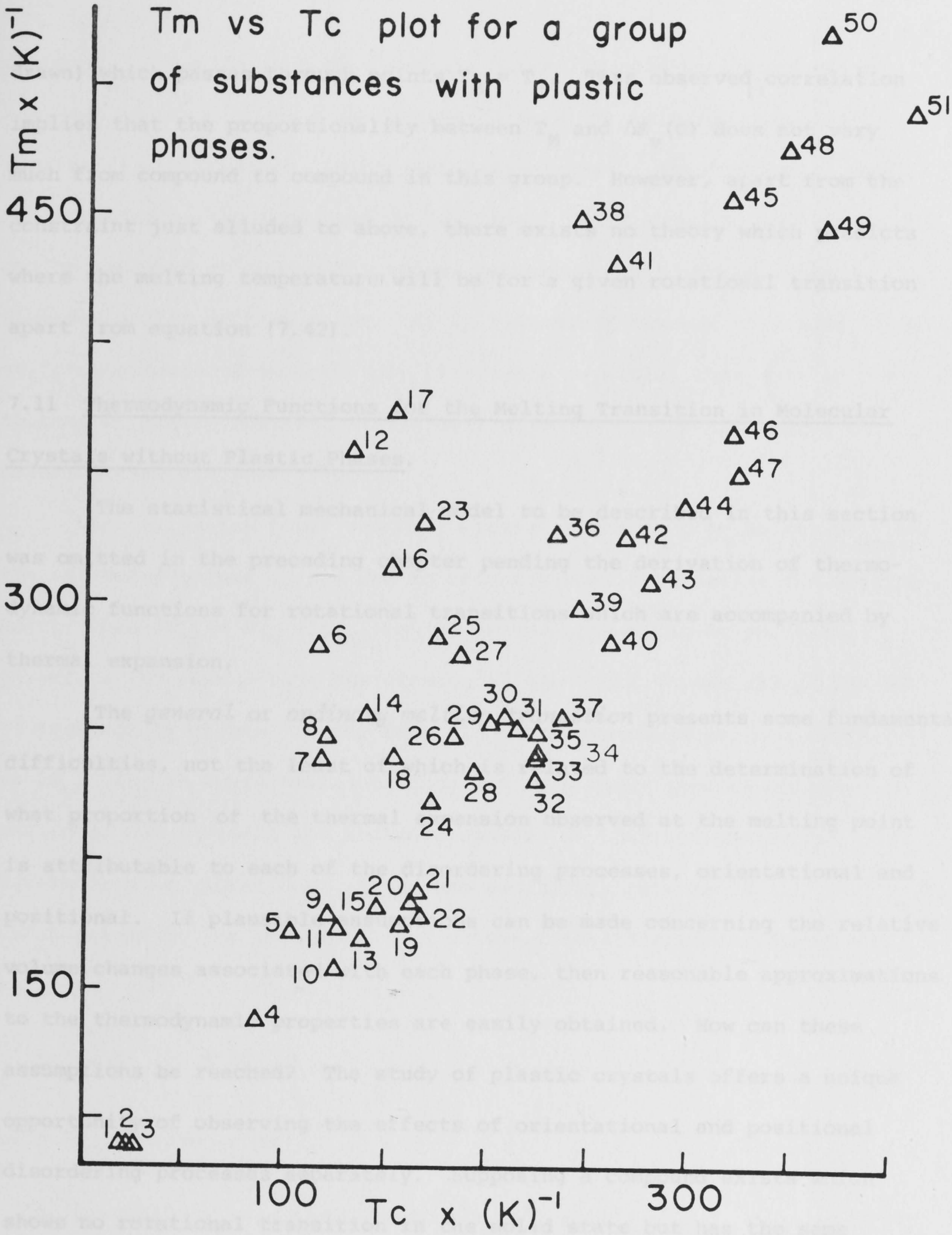

Fig 7.5: The variation of the melting temperature with the rotational transition temperature in a group of plastic crystals (see appendix 7.1 for a guide to the numbering scheme).

drawn) which passes through points $T_M = T_c$. This observed correlation implies that the proportionality between T_M and $\Delta E_v(\sigma)$ does not vary much from compound to compound in this group. However, apart from the constraint just alluded to above, there exists no theory which predicts where the melting temperature will be for a given rotational transition apart from equation (7.42).

7.11 Thermodynamic Functions for the Melting Transition in Molecular Crystals without Plastic Phases.

The statistical mechanical model to be described in this section was omitted in the preceding chapter pending the derivation of thermodynamic functions for rotational transitions which are accompanied by thermal expansion.

The *general* or *ordinary melting transition* presents some fundamental difficulties, not the least of which is related to the determination of what proportion of the thermal expansion observed at the melting point is attributable to each of the disordering processes, orientational and positional. If plausible assumptions can be made concerning the relative volume changes associated with each phase, then reasonable approximations to the thermodynamic properties are easily obtained. How can these assumptions be reached? The study of plastic crystals offers a unique opportunity of observing the effects of orientational and positional disordering processes separately. Supposing a compound exists which shows no rotational transition in the solid state but has the same molecular geometry as another compound with a plastic phase; then the volume expansion at the rotational transition of the latter may be used to deduce, at least roughly, the volume expansion due to the rotation of the former at the melting point. It is apparent that such compounds

do exist. Hexamine is a good example, where no rotational transition has been observed up to a few degrees before its melting point [74], whereas its hydrocarbon analog (adamantane) does. Alternatively, model calculations of the type used by Reynolds [12], alluded to in section 7.6 can be employed to deduce the volume expansion due to orientational disorder at the melting point. It is reasonable however to assume, from evidence gathered from the study of plastic crystals, that most of the thermal expansion observed at the melting point can be attributed to orientational disorder effects.

Let ΔV_M = the total volume increase at the melting point; $\Delta V_{M\sigma}$ = the estimated volume change due to orientational disorder at the melting point; then $\Delta V_{M\rho} = \Delta V_M - \Delta V_{M\sigma}$ is the volume change due to positional disorder. We assume that the effects of the total volume change can be represented by changes in the Einstein thermodynamic functions defined in ΔG_m. ΔG_m is again evaluated from I.R. and Raman spectra obtained in the solid and the melt and includes changes in both intramolecular and intermolecular vibrations. We assume additivity between $\Delta G_m(\rho)$ and $G_m(\sigma)$ which relate to the positional and orientational disorder respectively, i.e.

$$\Delta G_m = \Delta G_m(\rho) + \Delta G_m(\sigma) \tag{7.46}$$

Once $\Delta V_{M\rho}$ is known then

$$\Delta G_m(\rho) = \chi RT[\ln(Q_{mi}) - \{\ln[(2\pi mkT)^{3/2} v_m/h^3] + 1\}] \tag{7.47}$$

where $\chi = \dfrac{\Delta V_{M\rho}}{V_s + \Delta V_{M\rho}}$. Then $\Delta G_m(\sigma)$ is evaluated from the relation $\Delta G_m(\sigma) = \Delta G_m - \Delta G_m(\rho)$ where both ΔG_m and $\Delta G_m(\rho)$ are known. The internal energy change due to orientational disorder at the melting transition is given by $\Delta U_M(\sigma) = \Delta U_M(\rho,\sigma) - \Delta U_M(\rho)$. The orientational configurational energy change is given by $\Delta E_v(\sigma) = \Delta U_M(\sigma) - \Delta E_{Th}(\sigma)$, where $\Delta E_{Th}(\sigma)$ is evaluated from $\Delta E_{Th} - \Delta E_{Th}(\rho)$. ΔE_{Th}

is evaluated from ΔG_m; and $\Delta E_{Th}(\rho)$ from (7.47). $\Delta U_M(\rho,\sigma)$ is the observed melting transition energy less work done by the system against atmospheric pressure. $\Delta U_M(\sigma)$ is given by equation (6.31). Thus

$$n = \exp[\Delta E_v(\sigma)/RT_M]$$

as in equation (7.22), and may be refined further by the procedure following this equation using $\Delta G_m(\sigma)$ for ΔG_m in section 7.5.

Finally, thermodynamic functions for the general melting transition are given by the following equations.

$$G(\rho,1/n)-G(1,1) = \frac{1}{n}\{\Delta G_m(\rho)+(n-1)\Delta G_m\}-RT\psi + \zeta_\ell[(1-\rho)\{\Delta E_s + \Delta E'_s\} + \frac{n-1}{n^2}\rho\Delta E"] \quad (7.48)$$

$$U(\rho,1/n)-U(1,1) = \frac{1}{n}\left\{\chi RT[3/2-E(x)] + (n-1)[\frac{Nhc}{2}\sum_i\{\tilde{\nu}"_{mi}-\tilde{\nu}'_{mi}\} + \sum_i\{E"_{mi}-E'_{mi}\}]\right\}$$
$$+ \zeta_\ell[(1-\rho)\{\Delta E_s+\rho\Delta E'_s\} + \frac{n-1}{n^2}\rho\Delta E"] \quad (7.49)$$

$$S(\rho,1/n)-S(1,1) = R\ell nn + \frac{1}{n}\{\Delta S_M(\rho) + (n-1)\sum_i\{S"_{mi}-S'_{mi}\} \quad (7.50)$$

where $\Delta S_M(\rho)$ is given by equation (6.28).

$$C_P(\rho,\hat{\partial})-C_P(1,1) = \left((1-\rho)\{\frac{\Delta E_s}{\rho} + \Delta E'_s\} + \hat{\partial}_1(1-\hat{\partial}_1)\Delta E" + \rho\zeta_\ell[\Delta E_s-\Delta E'_s(1-2\rho)\right.$$
$$\left. - \hat{\partial}_1(1-\hat{\partial}_1)\Delta E"] + \frac{\hat{\partial}RT}{\zeta_\ell}\{3/2-E(x)\}\right)\alpha + \hat{\partial}\chi[3/2R-C_V(x)]$$
$$+ \left(\alpha\chi RT\{3/2-E(x)\} + \zeta_\ell\rho\Delta E"(1-2\hat{\partial}_1) - \frac{Nhc}{2}\sum_i\{\tilde{\nu}"_{mi}-\tilde{\nu}'_{mi}\}\right.$$
$$\left. - \sum_i\{E"_{mi}-E'_{mi}\}\right)\left(\{\zeta_\ell\rho(1-2\hat{\partial})\Delta E" - \Delta G_m\}/T - \sum_i\{S"_{mi}-S'_{mi}\}\right)/\cdot$$
$$\cdot\left(\frac{RT}{\hat{\partial}_1(1-\hat{\partial})} - 2\zeta_\ell\rho\Delta E"_0\right) + (1-\hat{\partial}_1)\sum_i\{C"_{mi}-C'_{mi}\} + P\left(\frac{\partial V}{\partial T}\right)_P \quad (7.51)$$

where $\rho = V_s/\{V_s + \Delta V_{M\rho}\}$. From equation (7.48) it is interesting to

note that the first term on the right hand side reduces to ΔG_m and the orientational configurational energy vanishes as $n \to \infty$ (free rotation).

7.12 The Effect of Short-Range Order

The model as presented so far does not allow for the existence of short-range order.* However, short-range order effects may be significant in some systems but are generally of secondary importance. In this section we make a brief survey of their significance in principle by examining their role in the specific heat function of the system. We do this by enquiring how equation (7.23) applies through a rotational transition characterised by a cooperative coexistence of domains of the non-rotator and rotator phases which are denoted by A and B respectively. Domain B has different physical properties from the plastic crystal phase. Its specific volume is varying with temperature during the transition in such a way that the specific volume approaches that of the plastic crystal phase at the end of the transition. It has already been argued that for a rotational transition conducted quasi-statically the pressure $P = -(\partial F/\partial V)_T$ is constant throughout the crystal, so that quantities of the kind $(\partial V/\partial T)_P$ may be evaluated at the same pressure (~ 0) for both coesixting phases.

Thus if f_0 is the mole fraction of phase A and δ is the volume increase of phase B relative to that of phase A, then (by appendix II)

$$\alpha = \frac{f_0\alpha_A + \delta(1-f_0)\alpha_B}{f_0 + \delta(1-f_0)} \tag{7.52}$$

$$K_T = \frac{f_0 K_{T_A} + \delta(1-f_0)K_{T_B}}{f_0 + \delta(1-f_0)} \tag{7.53}$$

where

$$\alpha_A = \alpha_A^\circ + \frac{1}{f_0}\left(\frac{\partial f_0}{\partial T}\right)_P \tag{7.54}$$

---

* We have allowed for some positional short-range order in obtaining ΔE's; but not for orientational short-range order.

$$\alpha_B = \alpha_B^\circ - \frac{1}{1-f_0}\left(\frac{\partial f_0}{\partial T}\right)_P \tag{7.55}$$

$$K_{T_A} = K_{T_A}^\circ - \frac{1}{f_0}\left(\frac{\partial f_0}{\partial P}\right)_T \tag{7.56}$$

$$K_{T_B} = K_{T_B}^\circ + \frac{1}{1-f_0}\left(\frac{\partial f_0}{\partial P}\right)_T \tag{7.57}$$

α_A° and $K_{T_A}^\circ$ are the thermal expansivity and isothermal compressibility before the transition; and α_B° and $K_{T_B}^\circ$ correspond to the plastic phase. The thermodynamic parameters before and after the transition are related by the following simple equations

$$\alpha_B^\circ = \alpha_A^\circ + \frac{1}{\delta}\left(\frac{\partial \delta}{\partial T}\right)_P \tag{7.58}$$

and

$$K_{T_B}^\circ = K_{T_A} - \frac{1}{\delta}\left(\frac{\partial \delta}{\partial P}\right)_T \tag{7.59}$$

It follows therefore from equation (7.52) that, since $C_P - C_V$ is proportional to α^2, the specific heat of the system is not a simple sum of contributions from the coexisting non-rotator and rotator phases. This effect has not been allowed for by the use of a long-range order parameter. Therefore a correction term which may be associated with the cross terms contained in α^2 has been ignored in the present treatment. However we allow for short-range order effects in the next chapter.

APPENDIX 7.1: Guide to the numbering of molecules in Fig 7.5.

	No	Substance		No	Substance
*	1	methane		27	cyclohexane
*	2	monodeuteromethane		28	t-butyl iodide
*	3	deuteromethane	*	29	cyclopentanol
	4	cyclopentene	*	30	t-butyl bromide
	5	hexafluoroethane		31	2-chloro-2-nitropropane
*	6	decafluorocyclopentane		32	1-chlorocyclohexane
	7	2,2-dichloropropane		33	methyl chloroform
	8	2,2,3-trimethylbutane		34	cyclohexanone
	9	cyclopentane		35	carbon tetrachloride
	10	t-butylethylene		36	succinotrile
	11	2,2-dimethylbutane		37	2-bromo-2-nitropropane
	12	norbonane	a	38	camphor
	13	cyclohexane	*	39	cyclohexanol
	14	tetramethylmethane		40	cyclohexyl cyanide
	15	cyclobutane		41	2,3-dichloro-2,3-dimethylbutane
	16	camphene		42	2,2-dinitropropane
	17	2,2,3,3-tetramethylbutane		43	pivalic acid
	18	1,1-dimethylcyclohexane	*	44	tetrakis-methane
	19	methanol	*	45	hexachloroethane
	20	1,3-cyclohexadiene		46	carbon tetrabromide
	21	cyclohexylfluoroform		47	1,4-cyclohexanedione
	22	1-chlorocyclopentane		48	borneol
	23	dodecafluorohexane		49	2,3-dibromo-2,3-dimethylbutane
	24	cis-1,2-dimethylcyclohexane		50	camphorimide
	25	tetranitromethane	a	51	camphoric anhydride
*	26	t-butyl chloride			

a From our own measurements.

All data (except those labelled a) are from a table in reference [29]. Transition temperatures given by defining a range have been modified to the average of the two extreme numbers.

* Two transitions occur before the melting transition and the rotational transition has been assumed to be one occurring at the lowest temperature following the pattern observed in camphor [24]; except for the case of the methane group where the rotational transition has been explicitly associated with the intermediate transition temperature [29].

APPENDIX 7.2

If f_0 is the mole fraction of phase A and δ is the volume increase of phase B relative to phase A then

$$V_A = f_0 V$$

$$V_B = \delta(1-f_0)V$$

$$V_T = f_0 V + \delta(1-f_0)V$$

where V is the volume of the ordered solid before the transition and V_T is the total volume during the transition. V_A and V_B are the volumes of the coexisting phases A and B. Then

$$\alpha_A = \{f_0(\frac{\partial V}{\partial T})_P + V(\frac{\partial f_0}{\partial T})_P\}/f_0 V \qquad (A7.2.1)$$

$$\alpha_B = \{\delta(1-f_0)(\frac{\partial V}{\partial T})_P + (1-f_0)V(\frac{\partial \delta}{\partial T})_P + \delta V(\frac{\partial (1-f_0)}{\partial T})_P\}/\delta(1-f_0)V \qquad (A7.2.2)$$

and finally

$$\alpha = \{[f_0(\frac{\partial V}{\partial T})_P + V(\frac{\partial f_0}{\partial T})_P] + [\delta(1-f_0)(\frac{\partial V}{\partial T})_P + (1-f_0)V(\frac{\partial \delta}{\partial T})_P + \delta V(\frac{\partial (1-f_0)}{\partial T})_P]\}/\cdot$$

$$\cdot[Vf_0 + \delta(1-f_0)]$$

where it is seen that

$$\alpha = \{f_0\alpha_A + \delta(1-f_0)\alpha_B\}/[f_0 + \delta(1-f_0)]$$

which is identified as equation (7.56) in the main text. Equations (A7.2.1) and (A7.2.2) can be written in the form given by equations (7.54), (7.58) and (7.55). The process is then repeated for K_T and remaining equations (7.53), (7.56) and (7.57) are generated.

8 theory of order-disorder phase equilibria in *d*- and *l*-systems of camphor-type compounds

The general features of the phase diagrams of d- and l-systems of camphor-type compounds must depend on the discrimination energy between optical isomers present in each system. These discrimination energies must be altered by the plastic crystal-phase transition as the directionally-sensitive components of this energy must be substantially reduced in the rotator phase. Thus the most important features in the phase diagram must arise from differences between intermolecular interactions present in the two phases, the non-rotator and rotator phases. For the low temperature transitions, the temperature dependent short-range order effects must be taken into account. This chapter discusses a statistical mechanical model that explains the phase diagrams with that of camphor taken as a model system.

8.1 Introduction

The phase diagrams of *d*- and *l*-systems of substances with plastic phases such as camphor occupy a unique position in solid-state phase equilibria. So far no detailed statistical explanation of these phase diagrams has been attempted and, as already alluded to elsewhere, there appear to be some conflicting explanations about the phase diagram of camphor in the literature.

The phase diagram of *d*- and *l*-camphor (Fig 2.4) has already been discussed in chapter 2. We particularly recall that the melting point is independent of composition. The reconstructive phase change is slightly, whilst the rotational transition is strongly, composition dependent. Also the absence of eutectic behaviour in the whole phase diagram is of fundamental importance in the present discussion.

The feature in the phase diagram that has caused some controversy is the appearance of the submaximum with respect to the plastic phase transition. This phenomenon is associated with compound formation by conventional thermodynamics and consequently led Schäfer *et al* to postulate about the existence of a pseudo-racemic compound or isomer pairing in *d*- and *l*-systems of camphor. Anderson and Slichter [25] have disagreed with this theory on the basis of a lack of true eutectoids at the melting point (i.e. minima on either side of the racemic composition) and the presence of long-range orientational disorder in *dl*-camphor revealed by their X-ray diffraction measurements at 77 K, about 130 K below the transition. This premonitory behaviour in *dl*-camphor has also been observed in their solid state NMR experiments and our dielectric relaxation studies as well as those of others [36]. On the basis of these facts Anderson *et al* concluded that the physical differences among the solid solutions in the vicinity of the rotational transition result from mutual short-range repulsion between different isomers rather than

from mutual attraction as was proposed by Schäfer and Wagner. An important observation in this theory which is due to Anderson and Slichter is that the X-ray diffraction patterns in the plastic phase of camphor do not vary with composition at the same (room) temperature.

In this chapter it will be shown that a detailed statistical mechanical analysis can lead to a similar conclusion as that of Anderson *et al.* A model that allows for the increased isotropy in the plastic phase explains the submaximum on the phase diagram and the associated premonitory behaviour as due to short-range order consistent with a discrimination energy in favour of identical molecules. Also the observed cusp or near-cusp on the phase diagram can be reproduced by a model which switches the mode of mixing of the two components at a certain composition.

8.2 The Requirements for the Acceptability of the Model

From the phase diagram of the binary system of *d*- and *l*-camphor it is obvious that for the model to be acceptable the following conditions must be satisfied.

(i) $\left(\frac{\partial T_c}{\partial x_d}\right)_{x_d \to 0,1} \to 0$, where T_c is the plastic-phase transition temperature. This condition is established by noting that the magnitude of the slope of the curve defining the phase diagram of camphor with respect to the rotational transition decreases as we approach composition $x_d = 0$ (or 1).

(ii) $\left(\frac{\partial T_c}{\partial x_d}\right)_{x_d=0.5} = 0$; and the composition $x_d = 0.5$ must be associated with a submaximum in T_c.

(iii) The model should be capable of generating a cusp, or near-cusp, at some compositions, e.g. 0.25.

In what follows it is shown that the *superlattice model*

of mixing by itself is not an acceptable model. An acceptable model, however, is found by a combination of two models, one of which is developed later in the discussion, in such a way that they are allowed to operate on the system at different composition ranges. We define the superlattice model as one in which the highly ordered state corresponds to a superlattice. The other model, which we shall call the *domain model of mixing* is defined as one in which the highly ordered state corresponds simply to a mechanical mixture of the two compounds which are not soluble.

8.3 Orientational Order-Disorder Phenomena in the Superlattice Model

The superlattice model has been developed for the study of substitutional order-disorder transitions in metal alloys. According to this model the crystal is viewed as consisting of two interpenetrating sublattices which are symmetrically related to each other. Unlike the two-sublattice model exploited by Lennard Jones and Devonshire and their followers (see [9],[10]), where one sublattice contains an empty basis for the description of a solid, both sublattices are filled with molecules in the present model. The total number of lattice sites N is equal to the total number of molecules. Further the numbers of d- and l-molecules are allowed to vary independently. We make the assumption that the pure substances of d- and l-molecules have identical crystal systems and their occupations on a lattice site are related to each other simply by symmetry. It is assumed that the effect of the substitution on a d-molecule by an l-molecule on a lattice is taken into account by the introduction of a substitutional interaction energy which would correspond to the discrimination energy. The coordination number is invariant with composition.

The case of unequal numbers of two types of atoms on two different sites has already been worked out by Fowler and Guggenheim [75]. In what

follows the treatment of the problem by these workers is briefly reviewed and modified for our purposes. Thus if we denote the number of d-molecules on the d-sublattice (standard or right occupation) by d_D, etc. where D refers to the sublattice; and if $d_D = Nx_d(1 + s)/2$, then the distribution of the two kinds of molecules on the two kinds of sites is given as follows.

$$d_D = \tfrac{1}{2}Nx_d(1 + s); \quad d_L = \tfrac{1}{2}Nx_d(1 - s); \quad l_D = \tfrac{1}{2}N[1 - x_d(1 + s)];$$

$$l_L = \tfrac{1}{2}N[1 - x_d(1 - s)] \qquad (8.1)$$

where $x_d \leqslant 0.5$* and is the mole fraction of d-molecules so that $x_d + x_l = 1$, and x_l is the mole fraction of the l-molecules; s is the degree of long range order satisfying the inequality $0 \leqslant s \leqslant 1$. The situation corresponds to the highest possible order when s = 1; and to complete disorder when s = 0. We are concerned with the pair-wise interactions between molecules on different sublattices; and therefore the average number of such pairs is given by

$$(d.d) = \tfrac{1}{2}zNx_d(1 - s^2);$$

$$(d.l) = zN[x_d(1 - x_d) + x_d^2 s^2];$$

$$(l.l) = \tfrac{1}{2}zN[1 - 2x_d + x_d^2(1 - s^2)]; \qquad (8.2)$$

where z is the number of nearest neighbours of one molecule.

To allow for the isotropy† observed in the plastic phases of the phase diagrams of d- and l-systems of camphor with identical crystal systems we make the following assumptions. We assume that the substitutional interaction energy between d- and l-molecules is related to the discrimin-

---

* The condition $x_d \leqslant 0$ ensures that all the terms involving factorials in the combinatorial factor to be derived below, are positive. All the expressions derived in this chapter will be consistent with this condition. Note that no loss of generality is incurred by this approach as similar expressions apply for $x_l \leqslant 0.5$ and either x_d or x_l is $\leqslant 0.5$ in any given binary mixture.

† Evidence for this isotropy is found in the diffraction experiments reported by Anderson *et al.*

ation energies observed in systems containing *d*- and *l*-molecules. From our calculations of molecular packing in camphoric anhydride, the discrimination energy has been shown to originate from both electrostatic and short-range (exp-6) interactions, with the latter making the largest contributions. The plastic phase, as it will be recalled, corresponds to the weakly coupled limit in the calculations of chiral intermolecular interactions by Craig *et al* [3]. Thus we would expect the substitutional interaction energy to average out to a negligible value in the plastic phase due to molecular rotation. For simplicity we assume that the molecular partition function is independent of composition; and the treatment for the plastic phase transition is identical to the one presented in chapter 7 for each composition. In particular, the configurational partition function for the transition will be given by equation (7.1). The value of n, the number of distinguishable molecular orientations in the plastic phase, is independent of composition. This follows from the fact that, with the exception of optical activity, the physical properties observed do not vary appreciably with composition in the plastic phase. Because of the complete range of solid solutions in both rotator and non-rotator phases of camphor we assume the same degree of substitutional disorder in both non-rotator and rotator phases.

8.4 Properties of the Superlattice Model in the Bragg-Williams Approximation

The configurational partition function of the system at any composition is given by

$$Q_c = \sum_{\sigma,s} \exp[-E(n,\sigma,s,x_d)/kT] \qquad (8.3)$$

where n and σ are the number of molecular orientations available in the plastic phase and the fractional orientational long range order parameter. The remaining parameters have already been defined above. Applying the

Bragg-Williams approximation (see section 6.3) we have for the configurational partition function

$$Q_c = g(n,\sigma,s,x_d)\ \exp\{-\langle E(n,\sigma,s,x_d)\rangle/kT\} \tag{8.4}$$

where

$$g(n,\sigma,s,x_d) = \frac{N!}{\{N\sigma_1\}!\prod_{j=2}^{n}\{N\sigma_j\}!} \cdot \frac{\{\frac{1}{2}N\}!}{\{\frac{1}{2}Nx_d(1+s)\}!\{\frac{1}{2}N[1-x_d(1+s)]\}!} \cdot$$

$$\cdot \frac{\{\frac{1}{2}N\}!}{\{\frac{1}{2}Nx_d(1-s)\}!\{\frac{1}{2}N[1-x_d(1-s)]\}!} \tag{8.5}$$

and

$$\langle E(n,\sigma,s,x_d)\rangle = \tfrac{1}{2}zN\{2E''\sigma_1(1-\sigma_1) + x_d^2(1-s^2)E_{dd} + [1-2x_d+x_d^2(1-s^2)]E_{ll}$$

$$+ 2[x_d-x_d^2(1-s^2)]E_{dl}\} \tag{8.6}$$

E_{dd}, E_{ll} and E_{dl} are the interaction energies between pairs of molecules shown in the subscript. Because of the necessary symmetry $E_{dd} = E_{ll}$. The combinatorial term $g(n,\sigma,s,x_d)$ has been arrived at by considering the orientational and substitutional disordering processes to be independent of each other; i.e. $g(n,\sigma,s,x_d) = g(n,\sigma)\cdot g(s,x_d)$, and the two combinatorial terms correspond to orientational and substitutional disorder respectively. Equation (8.6) can be re-written as follows.

$$\langle E(n,\sigma,s,x_d)\rangle = \Delta E_0''\sigma_1(1-\sigma_1) + s_1[\Delta E(1) + \Delta E x_d^2(1-s^2)] \tag{8.7}$$

where $\Delta E = zN\{\frac{1}{2}(E_{dd}+E_{ll}) - E_{dl}\} = zN(E_{dd}-E_{dl})$

$$\Delta E(1) = (zNE_{dd} - 2x_d\Delta E)/2$$

and s_1 = the orientational degree of order related to σ_1 by the relation

$$\sigma_1 = \{1 + (n-1)s_1\}/n$$

and satisfying the same inequality as s. The parameter s_1 functions as a coefficient for the energy term concerned with mixing and has been introduced into (8.7) arbitrarily. This parameter has the function of ensuring that the energy of mixing term vanishes in the plastic phase where it takes a value of zero to allow for ideal mixing. Similarly the orientational energy term vanishes in the ordered phase when $\sigma_1 = s_1 = 1$. The term $\Delta E(1)$ is the configurational energy of mixing corresponding to the state of perfect order, i.e. s = 1. The terms ΔE and $\Delta E_0''$ are the configurational energy of mixing in the non-rotator phase and the orientational energy of disordering at 0 K.

Defining the configurational free energy function relative to the orientationally and substitutionally ordered phase we have, after using Stirling's approximation in equation (8.5), the following result.*

$$A_c(\sigma,s,x_d) - A_c(1,1,x_d) = RT[\psi(\sigma) + \psi(s,x_d) - \psi(1,x_d)] + \Delta E_0''\sigma_1(1-\sigma_1)$$

$$- (1-s_1)\Delta E\, x_d^2(1-s^2) \qquad (8.8)$$

where

$$\psi(\sigma) = \sigma_1 ln\sigma_1 + (1-\sigma_1) ln\{(1-\sigma_1)/(n-1)\},$$

$$\psi(s,x_d) = \tfrac{1}{2}\Big\{x_d(1+s) ln\{x_d(1+s)\} + [1-x_d(1+s)] ln[1-x_d(1+s)]$$

$$+ x_d(1-s) ln\{x_d(1-s)\} + [1-x_d(1-s)] ln[1-x_d(1-s)]\Big\},$$

$$\psi(1,x_d) = \tfrac{1}{2}\{2x_d ln2x_d + (1-2x_d) ln(1-2x_d)\}$$

Stationary conditions for equation (8.8) are given by the following relationships with respect to σ_1, s and x_d respectively.

$$ln\left(\frac{(1-\sigma_1)}{(n-1)\sigma_1}\right) = \left(\frac{1}{RT}\right)\left((1-2\sigma_1)\Delta E_0'' + \frac{n(1-s^2)x_d^2\Delta E_0}{4(n-1)}\right) \qquad (8.9)$$

---

* Alternatively, we can obtain a similar expression to (8.8) with $\sigma_1=1/n$ and $s_1=0$ (plastic phase). Consider the free energy above and below the transition in which s is constant. $A_1=RT\{\psi(s,x_d)-\psi(1,x_d)\}+\Delta E_1 x_d^2(1-s^2)$; $A_2=RT\{\psi(s,x_d)-\psi(1,x_d)-ln n\}+(n-1)\Delta E''/n^2+\Delta E_2 x_d^2(1-s^2)$, where A_1 and A_2 refer to non-rotator and rotator phases. Then $\Delta A=-RT ln n+(n-1)\Delta E''/n^2-\Delta E x_d^2(1-s^2)$ where $\Delta E=-\{\Delta E_2-\Delta E_1\}$

$$ln\left[\frac{x_d(1+s)[1-x_d(1-s)]}{x_d(1-s)[1-x_d(1+s)]}\right] = \frac{-4(1-s_1)x_d\Delta E_0 s}{RT} \tag{8.10}$$

$$(1+s)\,ln\left[\frac{x_d(1+s)}{1-x_d(1+s)}\right] + (1-s)\,ln\left[\frac{x_d(1-s)}{1-x_d(1-s)}\right] + 2ln\left[\frac{2x_d}{1-2x_d}\right]$$
$$= \frac{4(1-s_1)\Delta E_0 x_d(1-s^2)}{RT} \tag{8.11}$$

From equation (8.9) we observe that stationary conditions are obtained at constant σ_1 when

a) $\sigma_1 = 1$ and $T = 0$ K provided $x_d = 0$ or ΔE_0 is negative, such that both sides of equation approach negative infinite values.

b) $\sigma_1 = \frac{1}{2}$, $n = 2$ and $x_d = 0$ or $s = 1$.

c) $\sigma_1 = 1/n$ and $T \to \infty$.

From equation (8.10) stationary conditions are obtained at constant s when

a) $s = 0$ and $T > 0$ K.

b) $s = 1$, $\Delta E_0 < 0$ and $T \to 0$ K so that both sides of equation approach positive infinite values.

Finally from equation (8.11) stationary values which minimise the configurational free energy require $x_d = 0.25$, $s \to 1$ and $T > 0$ K. Observe that this corresponds to the cusped minimum on the phase diagram of camphor. This solution, however, plays no significant role in the explanation of the phase diagram. It simply defines the most stable composition when $s = 1$. Observe that if s remains equal to unity during the rotational transition the substitutional free energy, equation (8.8), does not make any contribution to the free energy change at the transition.

Equation (8.11) is one of particular interest in this model and will be examined further with the simplifying assumption that $s = 0$ for

---

and $\Delta E_2 < \Delta E_1$ (due to increased isotropy in the rotator phase). The equation just obtained is identical to the one obtained from (8.8) when $\sigma_1 = 1/n$. Thus the expressions obtained apply even to cases where complete isotropy may not be observed.

both phases connected by a plastic phase transition. This amounts to assuming that the molecules occupy the same relative positions and substitutional long-range order is absent in both phases. The difference between the two phases depends solely on the degree of orientational long-range order. A further differentiation of equation (8.11) readily shows that the configurational free energy function generally has a minimum around the racemic composition irrespective of the sign of ΔE for any given temperature $T > 0$ K.

From equation (8.8) we observe that the transition energy to the plastic phase for any composition is given by

$$\Delta E(\sigma,x) = (n - 1)\Delta E_0''/n^2 - x_d^2 \Delta E_0 \qquad (8.13)^*$$

where $\Delta E(\sigma,x) = E_c(1/n,x) - E_c(1,x)$ and E_c is the configurational energy of the system. The substitutional long-range order parameter is now being treated as constant with respect to both composition and phases. Thus the composition with $x_d = 0.5$ also corresponds to a minimum in configurational energy change if a repulsive interaction energy of mixing is assumed. It follows therefore that under equilibrium conditions the transition temperature is a minimum at the racemic composition; since both the energy term and the free energy† take a minimum value at this composition. Observe that we obtain the general rotational transition energy by subtracting the energy of mixing from the rotational transition energy of the pure component. This implies that each molecule for any composition in the plastic phase appears to possess the same energy as a consequence of the isotropy acquired in the process of molecular rotation. Thus from an interactive point of view *d*- and *l*-molecules are similar. In other words we have subtracted any differences between *d*- and *l*-molecules that existed in the non-rotator solid but which does not exist in the rotator phase. This can be shown schematically in fig. 8.1. This model explains

---

* Equation (8.12) does not exist.

† This implies that the low temperature phase is most unstable at this composition since we are dealing with ΔA.

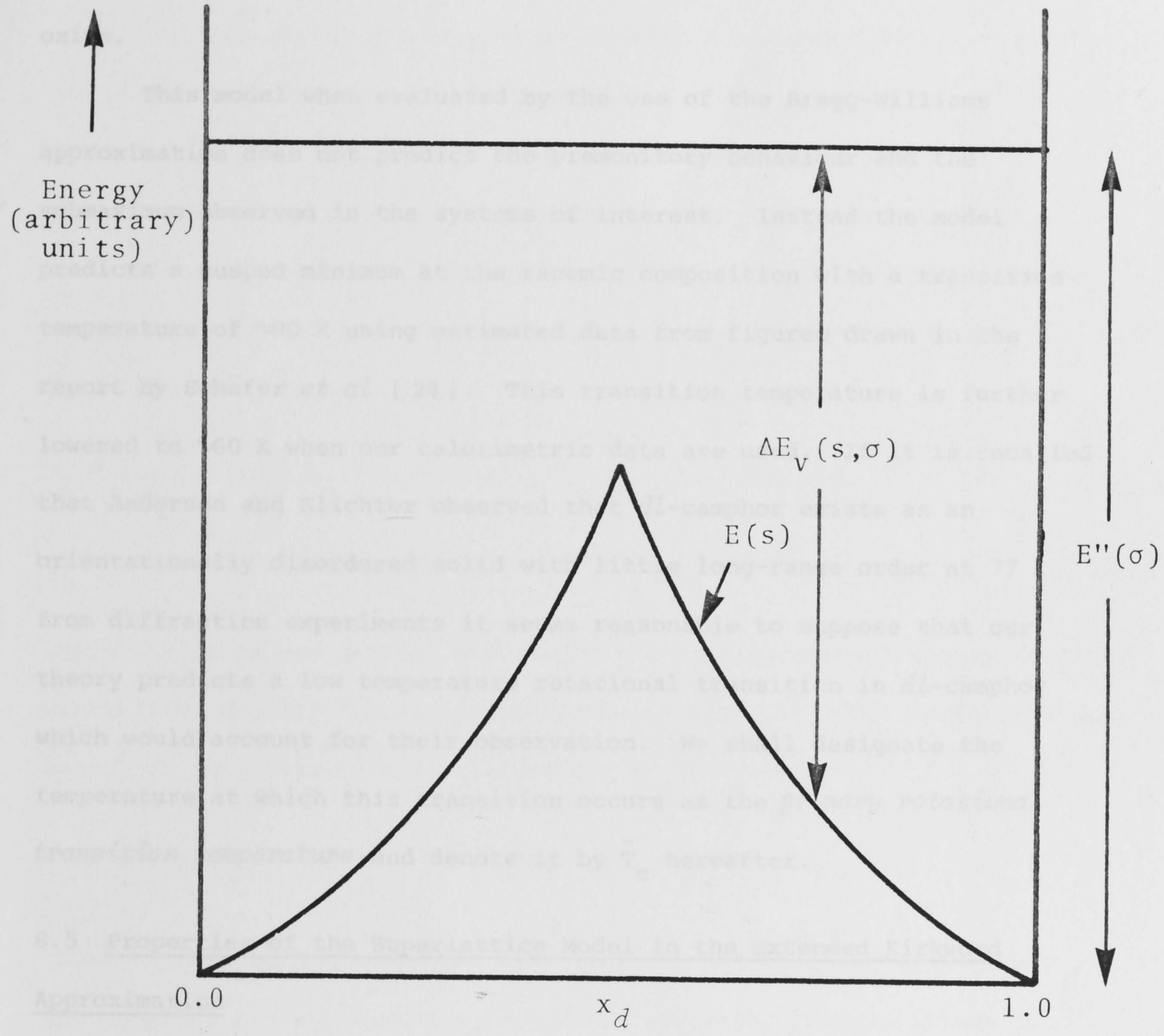

Fig 8.1: A schematic diagram showing the variation of E(s), E''(σ) and $\Delta E_v(s,\sigma)$ with composition. The energy parameters are the energy of mixing, the energy of a molecule in the plastic phase relative to an arbitrary point of origin, and $\Delta E(s,\sigma)$ is the transition energy; i.e. $\Delta E_v(s,\sigma) = E''(\sigma) - E(s)$. These quantities refer to configurational properties only. Note the cusped maximum in E(s) which corresponds to the cusped minima in $\Delta E_v(s,\sigma)$ and (therefore) the transition temperature.

the general pattern observed in the phase diagrams of camphor and related compounds if the submaximum is ignored except in the case of camphor oxime.

This model when evaluated by the use of the Bragg-Williams approximation does not predict the premonitory behaviour and the submaximum observed in the systems of interest. Instead the model predicts a cusped minimum at the racemic composition with a transition temperature of ∿90 K using estimated data from figures drawn in the report by Schäfer *et al* [24]. This transition temperature is further lowered to ∿60 K when our calorimetric data are used. If it is recalled that Anderson and Slichter observed that *dl*-camphor exists as an orientationally disordered solid with little long-range order at 77 K from diffraction experiments it seems reasonable to suppose that our theory predicts a low temperature rotational transition in *dl*-camphor which would account for their observation. We shall designate the temperature at which this transition occurs as the *primary rotational transition temperature* and denote it by $\hat{T}_c$ hereafter.

8.5 Properties of the Superlattice Model in the Extended Kirkwood Approximation

An elegant method due to Kirkwood expresses the configurational energy of the system by a series expansion in terms of moments of energy probability distributions [75],[76]. Therefore the configurational energy of the system can in principle be evaluated to any desired degree of accuracy. The Kirkwood approximation differs from the Bragg-Williams approximation in that the former allows for fluctuations of energy within states of fixed degree of long-range order which are ignored in the latter. In other words the higher order terms appearing in the Kirkwood approximation may be associated with short-range order effects. We have already

hinted at the role of short range order in section 7.12, where a simple model revealed that the specific heat of a substance going through a rotational transition via cooperative domain interaction is not a simple sum of the specific heat of the co-existing phases.

It is not surprising therefore that inclusion of higher order terms in the configurational energy may account for short-range order effects.

The configurational energy of the system may be written in terms of the configurational energy calculated in the Bragg-Williams approximation as follows (see Hiroshi Sato [76]).

$$\hat{E}(s,x_d) = \langle E(s,x_d)\rangle - (1/2!kT)\{\langle E^2(s,x_d)\rangle - \langle E(s,x_d)\rangle^2\}$$

$$+ (1/3!kT)\{\langle E^3(s,x_d)\rangle - 3\langle E(s,x_d)\rangle\langle E^2(s,x_d)\rangle + 2\langle E(s,x_d)\rangle^3\} + \ldots . \quad (8.14)$$

Where the terms are central moments of the configurational energy probability density function with the mean $\langle E(s,x_d)\rangle$. The configurational energy of the system $\hat{E}(s,x_d)$ is defined by the relation

$$\sum_s \exp[-E(s,x_d)/kT] = g(s,x_d)\exp[-\hat{E}(s,x_d)/kT] \quad (8.15)$$

Thus the retention of only the first term in equation (8.14) leads to the equality $\hat{E}(s,x_d) = \langle E(s,x_d)\rangle$ and therefore the Bragg-Williams approximation. This amounts to assuming that the configurational energy distribution within states of fixed degree of long-range order has the form of a delta function $\delta[E(s,x_d) - \langle E(s,x_d)\rangle]$. The result obtained by Kirkwood for the configurational energy of binary systems corresponding to the case $x_d = x_l = 1/2$ may be written as follows.

$$\{\hat{E}(s,\tfrac{1}{2}) - \Delta E(1,\tfrac{1}{2})\}/RT = \mu_1\frac{\Delta E}{RT} - \tfrac{1}{2}\left(\frac{\mu_2}{2!z}\left(\frac{2\Delta E}{RT}\right)^2 + \frac{\mu_3}{3!z^2}\left(\frac{2\Delta E}{RT}\right)^3 + \ldots\right) \quad (8.16)$$

where

$\Delta E(1,\tfrac{1}{2}) = E(1)$ (for the case $x_d = \tfrac{1}{2}$),

and $\mu_1,\mu_2\ldots$ are central moments. These moments are given by the

following equations

$$\mu_1 = (1 - s^2)/4$$
$$\mu_2 = \mu_1^2$$
$$\mu_3 = \mu_1^2 s^2 \qquad (8.17)$$

If equation (8.16) is compared with equation (8.8) we see that the first moment as given by equation (8.17) is simply the coefficient of the energy of mixing ΔE in the Bragg-Williams approximation for the case $x_d = \frac{1}{2}$ when $s_1 = 0$. Thus by a simple analogy the central moments for any composition $x_d \leqslant \frac{1}{2}$ should be given by the following equations

$$\mu_1 = x_d^2(1-s^2)$$
$$\mu_2 = \mu_1^2$$
$$\mu_3 = \mu_1^2 s^2 \qquad (8.18)$$

From now onwards it will be assumed that the Kirkwood approximation of the substitutional configurational energy can be generalised to cover all cases including orientational configurational energy provided the configurational energy in the Bragg-Williams approximation can be evaluated. With these results the configurational free energy function to the third central moment in the energy of mixing term, is given by

$$A_c(\sigma,s,x_d) - A_c(1,1,x_d) = RT[\psi(\sigma) + \psi(s,x_d) - \psi(1,x_d)] + \Delta E_0''\sigma_1(1-\sigma_1)$$
$$- (1-s_1)\{\mu_1\Delta E - \frac{\mu_2\Delta E^2}{zRT} - \frac{2\mu_3\Delta E^3}{3(zRT)^2}\} \qquad (8.19)$$

Equilibrium values of order parameters σ_1, s, and x_d are those values which minimise equation (8.19) given by the following equations respectively.

$$ln\left(\frac{(1-\sigma_1)}{(n-1)\sigma_1}\right) = \left(\frac{1}{RT}\right)\left((1-2\sigma_1)\Delta E_0'' + \frac{n\{\mu_1\Delta E - \frac{\mu_2\Delta E^2}{zRT} - \frac{2\mu_3\Delta E^3}{3(zRT)^2}\}}{4(n-1)}\right) \qquad (8.20)$$

$$ln\left(\frac{(1+s)[1-x_d(1-s)]}{(1-s)[1-x_d(1+s)]}\right) = -4(1-s_1)sx_d\left(\frac{\Delta E}{RT} - \frac{2\mu}{z}\left(\frac{\Delta E}{RT}\right)^2 + \frac{2(1-s^2)}{3z^2}\cdot\right.$$

$$\left.\cdot\{\mu_1 - 2s^2\}\left(\frac{\Delta E}{RT}\right)^3\right) \qquad (8.21)$$

$$(1+s)ln\left(\frac{x_d(1+s)}{1-x_d(1+s)}\right) + (1-s)ln\left(\frac{x_d(1-s)}{1-x_d(1-s)}\right) + 2ln\left(\frac{2x_d}{1-2x_d}\right)$$

$$= \frac{4x_d(1-s_1)(1-s^2)}{RT}\left(\Delta E_0 - 2\mu_1\{\frac{\Delta E^2}{zRT} + \frac{2}{3}\frac{s^2\Delta E^3}{(zRT)^2}\}\right) \qquad (8.22)$$

It is seen that conditions for stationary values of the free energy function in the extended Kirkwood approximation are generally similar to those obtained from a free energy function evaluated with the use of the Bragg-Williams approximation for the cases where the order parameters take extreme values, e.g. $s = 0,1$; $\sigma_1 = \frac{1}{n},1$; and $x_d = 0,0.5$. It is, however, important to note that in both equations (8.9) and (8.20) stationary values of σ_1 are not independent of s. This implies some coupling between orientational and substitutional disorder.

The configurational free energy of the completely orientationally disordered phase ($s_1 = 0$) with respect to the ordered phase is given by the equation

$$A_c(1/n,s,x_d) - A(1,1,x_d) = -RTlnn + (n-1)\frac{\Delta E_0''}{n^2} - \mu_1\Delta E + \frac{\mu_2\Delta E^2}{zRT} + \frac{2\mu_3\Delta E^3}{3(zRT)^2} \qquad (8.23)$$

where it has been assumed that s and x_d are the same in both phases*, and $\psi_\sigma = -lnn$. Both sides of equation (8.23) must equal zero so that the plastic phase with $\sigma_1 = 1/n$ is in equilibrium with the ordered phase with $\sigma_1 = 1$. Equation (8.23) defines the relative stability of the plastic phases between different compositions. Since $Rlnn$ is independent of composition it is the energy term only that is important in establishing the pattern of the phase diagram with respect to the plastic crystal-phase

---

* Note that this assumption may be expected to hold in second order transitions. In other words the transitions are not isothermal for any composition. Therefore a change of composition between two phases of the type observed in the liquid-vapour transition is not allowed for even in the standard treatments of Fowler and Guggenheim.

transition.

Observe that after $\mu_1\Delta E$ in the energy term the rest of the terms are temperature dependent. These are the energy terms due to short-range order which are sharply centred around the racemate composition where they have a maximum effect mainly due to the symmetry properties of μ_2 since $\mu_3 = 0$ when $s = 0$, and the fact that the primary transition temperature (predicted by the Bragg-Williams approximation) is a minimum around the racemate composition for a positive value of ΔE. Observe also that these new terms have the nett effect of increasing the transition energy from their sign. Thus for low temperature transitions once the primary transition temperature is reached the short-range order terms begin to oppose the transition by setting new equilibrium conditions for each new temperature until a temperature is reached where they become insignificant and the transition goes to completion in the conventional way. Clearly therefore, the temperature range between the primary transition temperature and the *secondary or final transition temperature* will be characterised by non-isothermal progressive changes in the state of disorder of the system which should be detected in NMR, dielectric and calorimetric measurements. Thus the submaximum observed in the phase diagrams of *d*- and *l*-systems of camphor and related compounds around the racemate composition and the associated premonitory behaviour may be attributed to short-range order effects. The primary and secondary transition temperatures under equilibrium conditions may be approximated by the following equations which are derived from the transition configurational free energy function in equation (8.23), i.e.

$$A_c(1/n,s,x_d) - A(1,1,x_d) = 0.$$

$$\hat{T}_c = \{(n-1)\Delta E_0''/n^2 - \mu_1\Delta E\}/R\ln n \qquad (8.24)$$

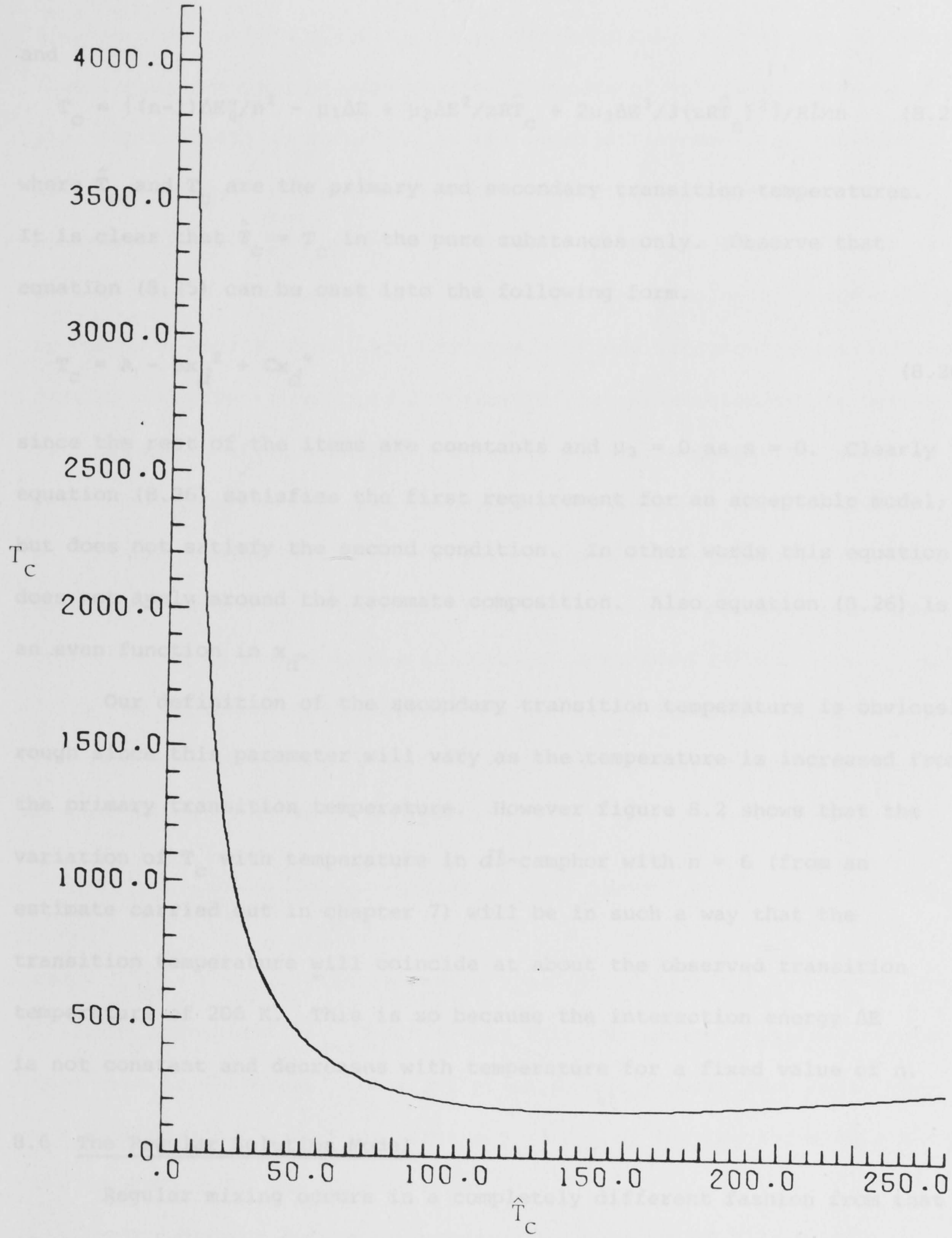

Figure 8.2: The variation of the secondary transition temperature T_c with the primary transition temperature $\hat{T}_c$ for n = 6 and $\Delta E'' = 880$ cal/mole (1 cal = 4.184J).

and

$$T_c = \{(n-1)\Delta E_0''/n^2 - \mu_1\Delta E + \mu_2\Delta E^2/zR\hat{T}_c + 2\mu_3\Delta E^3/3(zR\hat{T}_c)^2\}/Rlnn \qquad (8.25)$$

where $\hat{T}_c$ and T_c are the primary and secondary transition temperatures. It is clear that $\hat{T}_c = T_c$ in the pure substances only. Observe that equation (8.25) can be cast into the following form.

$$T_c = A - Bx_d^2 + Cx_d^4 \qquad (8.26)$$

since the rest of the items are constants and $\mu_3 = 0$ as $s = 0$. Clearly equation (8.26) satisfies the first requirement for an acceptable model; but does not satisfy the second condition. In other words this equation does not apply around the racemate composition. Also equation (8.26) is an even function in x_d.

Our definition of the secondary transition temperature is obviously rough since this parameter will vary as the temperature is increased from the primary transition temperature. However figure 8.2 shows that the variation of T_c with temperature in dl-camphor with $n = 6$ (from an estimate carried out in chapter 7) will be in such a way that the transition temperature will coincide at about the observed transition temperature of 206 K. This is so because the interaction energy ΔE is not constant and decreases with temperature for a fixed value of n.

8.6 The Regular Solution Model

Regular mixing occurs in a completely different fashion from that of the superlattice models. Consider an assembly of Nx_d d-molecules and Nx_l l-molecules such that $N = Nx_d + Nx_l$ is equal to the number of molecules and lattice sites. When the system is in the highly ordered state a superlattice is formed if the two types of molecules alternate each other regularly throughout the crystal, or, alternatively, the mixture consists of homogeneous domains of either d- or l-molecules forming a polycrystalline material. The latter mode of mixing gives rise to regular

solution as the components of the domains exchange their molecules. However, the configurational entropy corresponding to complete disorder (regular mixing) is the same whether the mode of interaction assumed for the ordered state is according to the superlattice model or the *domain model of mixing*. If, however, the *molecular interchange energy* E_{dl} between molecules in the d- and l-domains is zero an ideal solution will be formed. We define an *ideal solution* as a solution characterised by complete mixing at all temperatures. In our treatment we regard the *regular solution* as an upper temperature phase characterised by complete mixing (s = 0) after a substitutional transition accompanied by a positive energy change. The low temperature phase is characterised by complete immiscibility (s = 1), i.e. a mechanical mixture. On the other hand when ΔE_{dl} is negative then the solution may have a tendency to form a superlattice as the temperature decreases [77].

An approximate configurational partition function which has received a wide application in the study of regular solutions is given by the following equation [77].

$$Q_c(x_d) = \frac{N!}{\{Nx_d\}!N\{1-x_d\}!} \exp\{-\Delta E_{dl} x_d(1-x_d)/kT\} \qquad (8.27)$$

where $\Delta E_{dl} = NzE_{dl}$. This expression is derived with the use of the Bragg-Williams approximation. Observe that this expression contains an energy term that is different to the one given by the superlattice model when s = 0; although the entropy terms are identical for the two models under the conditions of complete disorder.

The obvious difficulty confronting equation (8.27) is that it defines conditions of critical phenomena associated with regular mixing without any knowledge of the mode of mixing below the critical temperature. It predicts the same *critical temperatures** as the superlattice model

---

* Following Fowler and Guggenheim, we define the critical temperature for mixing as the substitutional transition temperature for a given composition x_d. In chemical nomenclature, this term is defined as the temperature at which complete solubility is independent of composition. This would correspond to the maximum value of the critical temperature for a given system in our treatment.

despite the difference in the configurational energy function. Because of this we may consider equation (8.27) as representing a totally different model with the observed agreement with the superlattice model taken as coincidental. In fact it is an improper model for studying critical behaviour.

One form of improvement to equation (8.27) is the quasi-chemical treatment [76] in which the pair consisting of d- and l-molecules would be treated as a compound in equilibrium with d- and l-molecules in the gaseous phase [77]. Although this model is fairly respectable it is rather inappropriate for the purpose of our discussion and therefore will be abandoned. The quasi-chemical approximation also known as the cluster-variation method, can be expected to apply if atomic or molecular pairs are considered to be independent units of the assembly (see Hiroshi Sato). Instead we shall introduce a new model with a familiar structure and which can be evaluated easily by the use of the Bragg-Williams approximation. We shall then expand the configurational energy in the Kirkwood approximation and expect the model to be as good as the superlattice model in its own right.

8.7 The Regular Solution via the Domain Interaction Model

We make the assumption that substitutional disorder associated with the interchange of molecules from co-existing domains homogeneous in molecular species can be described by a long range degree of order parameter of the type used in the superlattice model. In this case the state s = 1 now corresponds to a state where the components are completely immiscible to each other and the assembly may exist as a conglomerate of d- and l-crystallites. This model leads to a similar distribution of molecules on the lattice sites as in equation (8.1) with D and L representing the sum of domains of d- and l-molecules respectively.

The configurational energy for the assembly is arrived at by the

following considerations. Since our interest lies in the excess values of thermodynamic quantities relative to those of the substitutionally ordered system, the interchange energies E_{dd} and E_{ll} cancel out. Thus the effective interchange energy is E_{dl} which we define as the energy required to move a d-molecule from the D-domain to an L-domain and vice versa. Therefore the configurational energy is simply equal to $N_{dl}E_{dl}$, where N_{dl} is the number of dl-pairs. We then apply the Bragg-Williams approximation to obtain $\langle N_{dl} \rangle$ as follows. When the number of d-molecules in the proper occupation is $Nx_d(1 + s)/2$ there must be $Nx_d(1 - s)/2$ d-molecules with an improper occupation which will be interacting with $N(1 - x_d)(1 + s)/2$ l-molecules with a proper occupation. The average number of pairs therefore is $Nx_d(1 - x_d)(1 - s^2)/4$ in the L-domain. The same number of pairs will be formed in the D-domain at the same time. Since the process can commence from either of the two domains $\langle N_{dl} \rangle = Nx_d(1 - x_d)(1 - s^2)$, and the excess configurational energy is given by $\Delta E_{dl}x_d(1 - x_d)(1 - s^2)$, where $\Delta E_{dl} = NE_{dl}$. In general, however, ΔE_{dl} includes the excess vibrational free energy function relative to that of the pure components and is a complex function of temperature [78]. In that form ΔE_{dl} is an interchange free energy. We make the simplifying assumption that ΔE_{dl} is independent of temperature and will be treated as an energy term. Finally the configurational partition function of the assembly takes the form

$$Q_c = g(s,x_d)\exp\{-\Delta E_{dl}x_d(1 - x_d)(1 - s^2)/RT\}^{*} \tag{8.28}$$

where

$$g(s,x_d) = \frac{\{\frac{1}{2}N\}!}{\{\frac{1}{2}Nx_d(1+s)\}!\{\frac{1}{2}N[1-x_d(1+s)]\}!} \cdot$$

$$\cdot\frac{\{\frac{1}{2}N\}!}{\{\frac{1}{2}Nx_d(1-s)\}!\{\frac{1}{2}N[1-x_d(1-s)]\}!} \tag{8.29}$$

---

* Note that the configurational energy is now symmetrical about x_d=0.5 unlike in the superlattice model where it is quadratic in composition. However we find later that the symmetry characteristics are interchanged in the expressions for critical temperatures of mixing.

We note that when s = 0 expression (8.28) reduces to the regular solution partition function equation (8.27). This reduction can be seen by comparing the entropy function $\psi(s,x_d)$ in equation (8.8) when s = 0 and with the one derived from (8.27).

The excess configurational free energy relative to the substitutionally ordered phase is given by applying Stirling's approximation on (8.28).

$$A_c(s,x_d) - A_c(1,x_d) = RT[\psi_s(s,x_d) - \psi_s(1,x_d)] + \Delta E_{dl} x_d(1-x_d)(1-s^2) \quad (8.30)$$

where $\psi_s(s,x_d)$ and $\psi_s(1,x_d)$ are given in equation (8.8).

Stationary conditions for equation (8.30) are given by those values of s and x_d that satisfy the following equations respectively.

$$ln\left(\frac{(1+s)\{1-x_d(1-s)\}}{(1-s)\{1-x_d(1+s)\}}\right) = \frac{4\Delta E_{dl}(1-x_d)s}{RT} \quad (8.31)$$

$$(1+s)\,ln\left(\frac{x_d(1+s)}{1-x_d(1+s)}\right) + (1-s)\,ln\left(\frac{x_d(1-s)}{1-x_d(1-s)}\right) + 2ln\left(\frac{2x_d}{1-2x_d}\right)$$
$$= -\frac{4\Delta E_{dl}(1-2x_d)(1-s^2)}{RT} \quad (8.32)$$

From equation (8.31) stationary conditions require that s = 0 at any composition provided T > 0 K. This solution corresponds to a minimum in the free energy if $\Delta E_{dl} > 0$. The conditions for *critical mixing* are determined by s = 0, $\frac{\partial A_c}{\partial s} = 0$ and $\frac{\partial^2 A_c}{\partial s^2} = 0$ (see Fowler and Guggenheim) and *the critical temperature of mixing in the domain model* $T_c^{(D)}$ is given by the following equation.

$$RT_c^{(D)} = 2(1-x_d)^2\Delta E_{dl} \quad (8.33)$$

The *critical temperature of mixing in the superlattice* model $T_c^{(s)}$ has already been obtained by Guggenheim and Fowler and is given by the following

equation.

$$RT_c^{(s)} = 2x_d(1 - x_d)\Delta E \qquad (8.34)$$

Thus the two models predict similar thermodynamic properties at $x_d = 0.5$ if $\Delta E = \Delta E_{dl}$. If this is not the case then the system has a choice of two different critical temperatures by which to be characterised. Theoretically the system (in a given composition) is expected to assume the model that will have a lower free energy, and therefore a lower critical temperature to correspond to a lower configurational energy since the entropy terms are identical.

We note that equation (8.33) is quadratic in x_l and states that the critical temperature of an assembly with x_d-mole fraction of d-molecules is a function of x_l-mole fraction of l-molecules. Thus the critical temperature of the system is decided upon by the population of molecules in the majority (since $x_l \geq 0.5$) and the critical temperature approaches a maximum as $x_d \to 0$. On the other hand the variation of the critical temperature defined by equation (8.34) is symmetrical about $x_d = 0.5$. Figure 8.3 depicts the relationship between the two critical temperatures. Note that the superlattice mode precedes the domain mode when $\Delta E > \Delta E_{dl}$. For $\Delta E \leq \Delta E_{dl}$, domain mode of mixing is not expected to apply. Both mixing modes may appear together if the ratio $\Delta E_{dl}/\Delta E \sim x_d/(1-x_d)$ and the interaction energies themselves are very small. Equation (8.33) is meaningless when $x_d = 0$ since ΔE_{dl} is not defined in pure substances. Also, it will be noted from Figure 8.3, that (generally) the domain mode becomes important at higher concentrations ($x_d > 0$).

Finally, from equation (8.32) stationary conditions require that $x_d = 0.25$, and $s = 1$; and this corresponds to a minimum in the free energy.

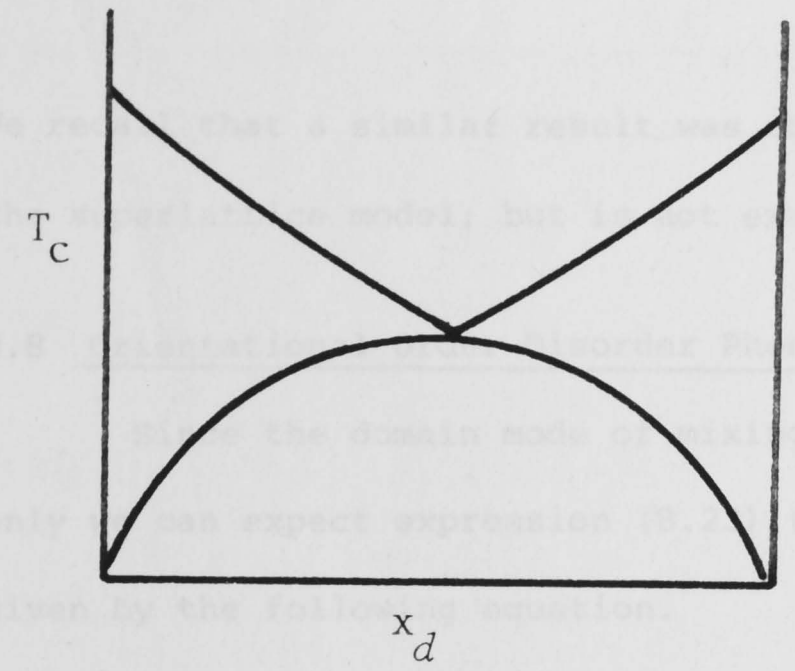

$\Delta E = \Delta E_{dl}$
mixed mode at $x_d = 0.5$
otherwise superlattice mode

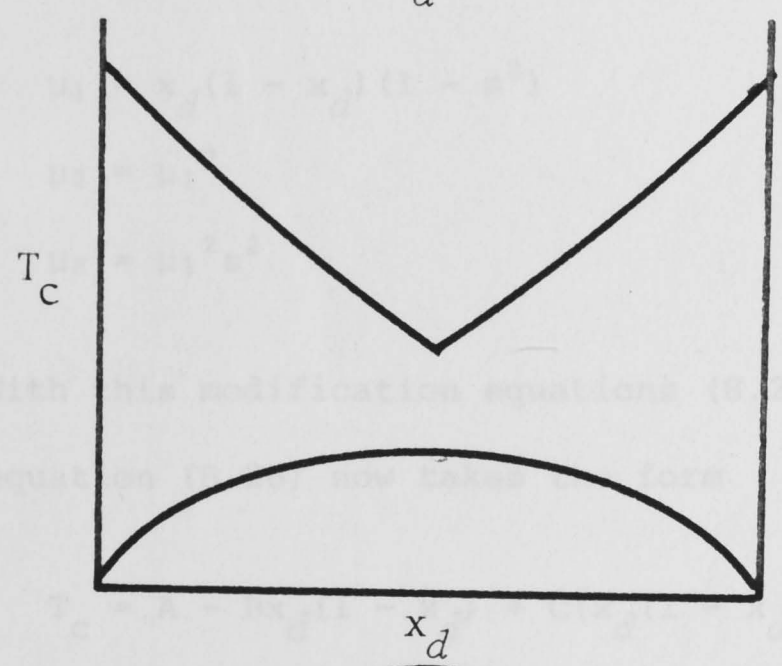

$\Delta E << \Delta E_{dl}$
superlattice mode

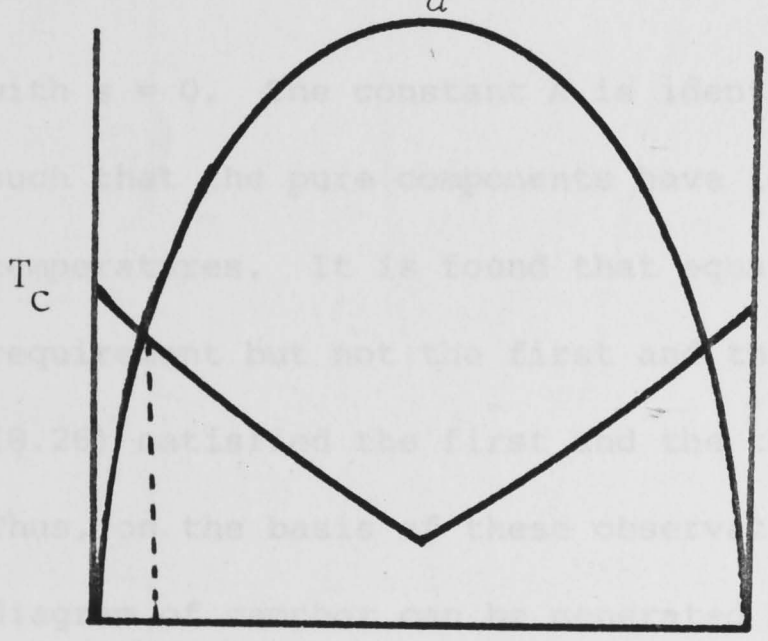

$\Delta E >> \Delta E_{dl}$
superlattice mode $0 < x_d < x_{d_1}$;
domain mode $x_{d_1} < x_d < (1-x_{d_1})$;
superlattice mode $(1-x_{d_1}) < x_d < 1$.

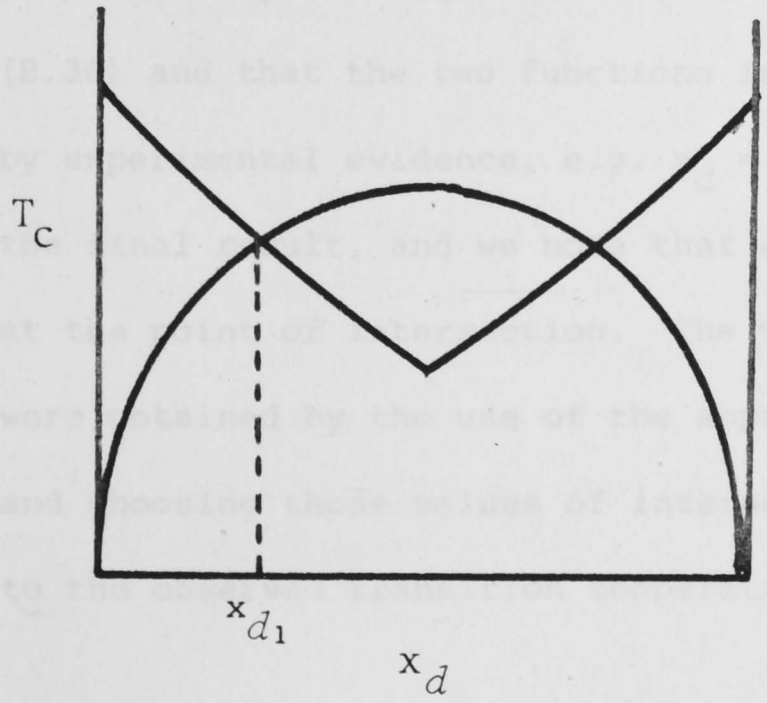

$\Delta E > \Delta E_{dl}$
superlattice mode $0 < x_d < x_{d_1}$;
domain mode $x_{d_1} < x_d < (1-x_{d_1})$;
superlattice mode $(1-x_{d_1}) < x_d < 1$.

Fig 8.3: Schematic diagrams of critical temperatures vs. x_d. The smooth curve corresponds to the superlattice mode of mixing; and the quadratic curve, to the domain mode of mixing. Where the curves intersect $\Delta E/\Delta E_{dl} = (1-x_d)/x_d$, and the values of the free energies for both models are the same.

We recall that a similar result was obtained from equation (8.11) in the superlattice model; but is not examined further for the present.

8.8 Orientational Order-Disorder Phenomena in the Regular Solution Model

Since the domain mode of mixing alters the configurational energy only we can expect expression (8.23) to apply with the central moments given by the following equation.

$$\mu_1 = x_d(1 - x_d)(1 - s^2)$$
$$\mu_2 = \mu_1^2$$
$$\mu_3 = \mu_1^2 s^2 \qquad (8.35)$$

With this modification equations (8.24) and (8.25) also apply and equation (8.26) now takes the form

$$T_c = A - Bx_d(1 - x_d) + C\{x_d(1 - x_d)\}^2 \qquad (8.36)$$

with s = 0. The constant A is identical in equations (8.26) and (8.36) such that the pure components have identical rotational transition temperatures. It is found that equation (36) satisfies the second requirement but not the first and the third. We recall that equation (8.26) satisfied the first and the third requirements but not the second. Thus, on the basis of these observations, we assume that the phase diagram of camphor can be generated by a combination of the two functions in such a way that equation (8.26) is allowed to operate before equation (8.36) and that the two functions intersect at any value of x_d as guided by experimental evidence, e.g. $x_d = 0.25$ in our case. Figure 8.4 depicts the final result, and we note that a cusp or a near cusp is generated at the point of intersection. The values of interaction energies used were obtained by the use of the approximate relations (8.24) and (8.25) and choosing those values of interaction energies that gave T_c closest to the observed transition temperature from the lowest primary transition

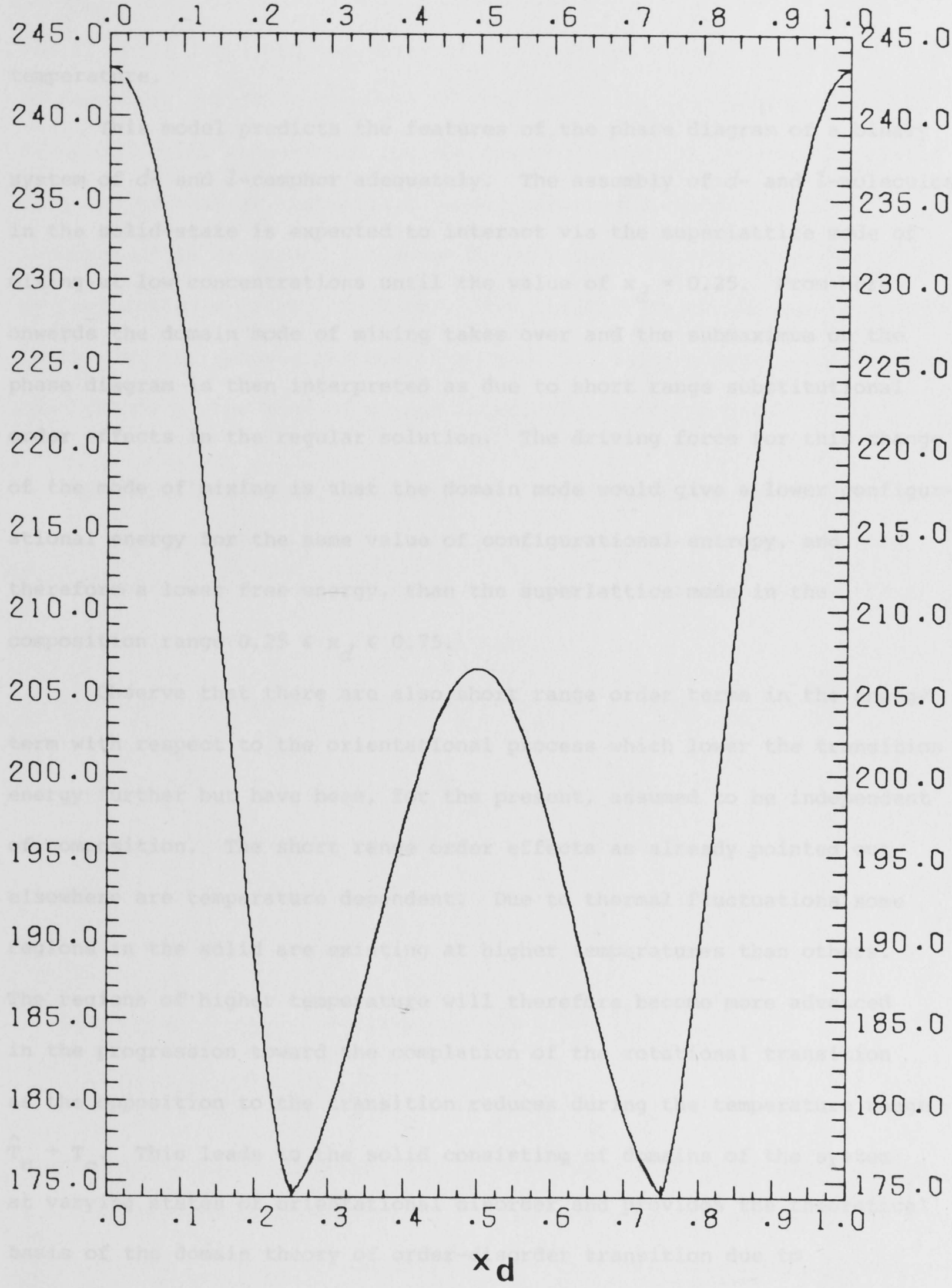

Figure 8.4: A theoretical phase diagram of *d*- and *l*-camphor (with respect to the III-II rotational transition) as predicted by equations (8.26) and (8.36). The cusps, or near-cusps at x_d = 0.25 and x_d = 0.75 correspond to points at which the two functions from the superlattice and domain models intersect.

temperature.

This model predicts the features of the phase diagram of a binary system of *d*- and *l*-camphor adequately. The assembly of *d*- and *l*-molecules in the solid-state is expected to interact via the superlattice mode of mixing at low concentrations until the value of $x_d = 0.25$. From here onwards the domain mode of mixing takes over and the submaximum on the phase diagram is then interpreted as due to short range substitutional order effects in the regular solution. The driving force for this change of the mode of mixing is that the domain mode would give a lower configurational energy for the same value of configurational entropy, and therefore a lower free energy, than the superlattice mode in the composition range $0.25 \leq x_d \leq 0.75$.

Observe that there are also short range order terms in the energy term with respect to the orientational process which lower the transition energy further but have been, for the present, assumed to be independent of composition. The short range order effects as already pointed out elsewhere are temperature dependent. Due to thermal fluctuations some regions in the solid are existing at higher temperatures than others. The regions of higher temperature will therefore become more advanced in the progression toward the completion of the rotational transition as the opposition to the transition reduces during the temperature range $\hat{T}_c \rightarrow T_c$. This leads to the solid consisting of domains of the system at varying states of orientational disorder and provides the theoretical basis of the domain theory of order-disorder transition due to Ubbelohde [14] which accounts for hysteresis commonly observed in plastic crystals.

Finally since the domain mode of mixing is expected to operate around the racemate composition from this model with $\Delta E_{dl} > 0$ it follows that *d*- and *l*-molecules interact with a repulsive force in this composition

range. This observation is in agreement with the postulate of Anderson and Slichter [25] and our observations from the crystal packing analysis of camphoric anhydride reported in chapter 5. It also accounts for the large molecular volumes and low sublimation energy of the racemic mixture relative to that of the optical isomer reported by Schäfer *et al*. Anderson *et al* explained the cusps or near cusps in the phase diagram by postulating a change of lattice from the lattice of the pure components to that of the racemic mixture at $x_d = 0.25$. This, however, corresponds to a change of the mode of mixing interaction in our model.

8.9 Critical Temperatures of Mixing in the Extended Kirkwood Approximation*

We consider first critical mixing in the domain mode. Equation (8.30) takes the following form in the Kirkwood expansion to the third term (see equation (8.16) for reference).

$$A_c(s,x_d) - A_c(l,x_d) = RT[\psi_s(s,x_d) - \psi_s(l,x_d)] + \mu_1 \Delta E_{dl} - \frac{\mu_2 \Delta E_{dl}^2}{zRT} - \frac{2\mu_3 \Delta E_{dl}^3}{3(zRT)^2} + \ldots. \qquad (8.37)$$

where the central moments are defined in equation (8.35). Stationary conditions for equation (8.37) with respect to s are defined by the following equation.

$$ln\left(\frac{(1+s)\{1-x_d(1-s)\}}{(1-s)\{1-x_d(1+s)\}}\right) = 4(1-x_d)s\left\{\frac{\Delta E_{dl}}{RT} - \frac{2\mu_1}{z}\left(\frac{\Delta E}{RT}\right)^2 + \frac{2(1-s^2)}{3z^2}\{\mu_1 - 2s^2\}\left(\frac{\Delta E}{RT}\right)^3 + \ldots.\right\} \qquad (8.38)$$

Observe that, as in equation (8.31), stationary conditions require that $s = 0$ at any composition provided $T > 0$. Applying the conditions, $s = 0$, $\frac{\partial A_c}{\partial s} = 0$ and $\frac{\partial^2 A_c}{\partial s^2} = 0$, for determining the critical temperature of mixing

---

* Since, to our knowledge, the superlattice model of mixing for the general composition has been evaluated to the Kirkwood Approximation for the first time and a new model, the domain model, has been developed, it is necessary to complete the analysis of substitutional order-disorder phenomena for the two models according to the established tradition.

we have

$$\frac{RT_c^{(D)}}{2(1-x_d)^2\Delta E_{dl}} = 1 - 2x_d(1-x_d)\frac{\Delta E_{dl}}{zRT_c^{(D)}} + \frac{2x_d(1-x_d)}{3}\left(\frac{\Delta E_{dl}}{zRT_c^{(D)}}\right)^2 + \ldots \quad (8.39)$$

which reduces to equation (8.34) when the second and third terms on the right hand side of equation (8.39) are ignored. Similarly for the superlattice model, the excess free energy relative to that of the substitutionally ordered solid is given by (8.37) but with the central moments given by equation (8.18). In this case the equation for stationary conditions is given by the following.

$$ln\left(\frac{(1+s)\{1-x_d(1-s)\}}{(1-s)\{1-x_d(1+s)\}}\right) = 4x_d s\left(\frac{\Delta E}{RT} - \frac{2\mu_1}{z}\left(\frac{\Delta E}{RT}\right)^2 + \frac{2(1-s^2)}{3z^2}\{\mu_1-2s^2\}\left(\frac{\Delta E}{RT}\right)^3\right) + \ldots \quad (8.40)$$

Equation (8.40) has similar characteristics as (8.38) for the state s = 0. The expression for the critical temperature of mixing now becomes

$$\frac{RT_c^{(s)}}{2x_d(1-x_d)\Delta E_{dl}} = 1-2x_d^2\frac{\Delta E_{dl}}{zRT_c^{(s)}} + \frac{2x_d^2}{3}\left(\frac{\Delta E_{dl}}{zRT_c^{(s)}}\right)^2 + \ldots. \quad (8.41)$$

Both equations (8.39) and (8.40) reduce to the standard result when $x_d = \frac{1}{2}$ given by the following equation [75]

$$\frac{2RT'^{*}_c}{\Delta E_{dl}} = 1 - \frac{1}{2}\frac{\Delta E_{dl}}{zRT'_c} + \frac{1}{6}\left(\frac{\Delta E_{dl}}{zRT'_c}\right)^2 + \ldots. \quad (8.42)$$

Stationary conditions for the case $x_d = \frac{1}{2}$ in the Kirkwood approximation have been studied in detail [75]. The equation always has one solution s = 0; but at sufficiently low temperature there is also a non-zero root if $\Delta E > 0$. This non-zero root corresponds to a minimum in the free energy; and the zero-root, to a maximum. When there is only one root, s = 0, the root corresponds to a minimum in the free energy. We assume the same applies to all other compositions.

---

* T'_c is either $T_c^{(D)}$ or $T_c^{(s)}$.

From the foregoing discussion it is obvious that the schematic phase diagrams depicted in figure 8.3 are simply first-order approximations. The effects of the higher order terms in configurational energy is to lower the critical temperature of mixing. The essential arguments related to figure (8.3), however, remain unaltered. We make use of these equations in section 8.13 when discussing specific cases.

8.10 Comparison with Other Methods of Approximation

We have shown that the extended Kirkwood approximation reduce to the Bragg-Williams approximation when the higher order terms are ignored. Fowler and Guggenheim have shown that for an assembly containing equal numbers of two types of atoms (or molecules in our case), the Kirkwood and the quasi-chemical methods have similar expressions for the critical temperature of mixing. The quasi-chemical method has briefly been hinted at elsewhere in this chapter and is equivalent to Bethe's method. In the latter, from the statistical mechanical point of view, the treatment is equivalent to dealing with the grand partition function of a sample group of sites from the lattice which represents the system. The sample is assumed to be small enough to allow accurate calculations of all possible configurations with the short-range order, as opposed to long-range order, taken into account. The effect of the surroundings is allowed for by a factor which is equivalent to the chemical potential acting differently for atoms or molecules with proper and improper occupations.

In order to make the comparison clearer we shall write down the expressions for the critical temperature in the same way as Fowler and Guggenheim have done.

$$\text{B - W}(x_d=\tfrac{1}{2}) \qquad 1 - \frac{2}{z} = 1 - \frac{\Delta E}{zRT_c} \tag{8.43}$$

$$\text{K}(x_d=\tfrac{1}{2}) \qquad 1 - \frac{2}{z} = 1 - \frac{\Delta E}{zRT_c} + \frac{1}{2}\left(\frac{\Delta E}{zRT_c}\right)^2 - \frac{1}{6}\left(\frac{\Delta E}{zRT_c}\right)^3 + \ldots \tag{8.44}$$

$$\left.\begin{matrix}\text{Q-C}\\ \text{B}\end{matrix}\right\}(x_d=\tfrac{1}{2}) \qquad 1 - \frac{2}{z} = \exp\left(-\frac{\Delta E}{zRT_c}\right) \tag{8.45}$$

$$\text{B-W}(x_d \neq x_l) \qquad 1 - \frac{1}{zx_d} - \frac{1}{z(1-x_d)} = 1 - \frac{2\Delta E}{zRT_c} \qquad \text{(S-mode)} \tag{8.46}$$

$$\text{Modified B-W}(x_d \neq x_l) \qquad 1 - \frac{1}{z(1-x_d)^2} = 1 - \frac{2\Delta E}{zRT_c} \qquad \text{(D-mode)} \tag{8.47}$$

$$\text{Extended K}(x_d \neq x_l) \qquad 1 - \frac{1}{zx_d} - \frac{1}{z(1-x_d)} = 1 - \frac{2\Delta E}{zRT_c} + 4x_d^2\left(\frac{\Delta E}{zRT_c}\right)^2 - \frac{4x_d^2}{3}\left(\frac{\Delta E}{zRT_c}\right)^3 + \ldots \qquad \text{(S-mode)} \tag{8.48}$$

$$\text{Extended K}(x_d \neq x_l) \qquad 1 - \frac{1}{z(1-x_d)^2} = 1 - \frac{2\Delta E}{zRT_c} + 4x_d(1-x_d)\left(\frac{\Delta E}{zRT_c}\right)^2 - \frac{4x_d(1-x_d)}{3}\left(\frac{\Delta E}{zRT_c}\right)^3 + \ldots \qquad \text{(D-mode)} \tag{8.49}$$

$$\text{Extended } \left.\begin{matrix}\text{Q-C}\\ \text{B}\end{matrix}\right\}(x_d \neq x_l) \qquad \frac{(x_d z-1)[(1-x_d)z-1]}{z^2 x_d(1-x_d)} = \exp\left(-\frac{2\Delta E}{zRT_c}\right) \tag{8.50}$$

where K, Q-C, B and B-W stand for the Kirkwood, quasi-chemical, Bethe and Bragg-Williams methods. Equation (8.50) is due to Easthope [79] who obtained it from the equicomponent equation (8.45) in much the same way as we have derived equations (8.48) and (8.49); that is by obtaining the entropy term explicitly for the general case $x_d \neq x_l$ and deriving the configurational energy for the general case by analogy of the expression for the equicomponent binary system. It is found that the general forms

of the Kirkwood equations ($x_d \neq x_l$) do not reduce into an exponential form easily, whilst the equation for $x_d = \frac{1}{2}$ does. The relationship between the extended Bethe's treatment and the extended Kirkwood method is not obvious; and it would seem that the two methods are fundamentally different. This is not surprising since the former can be interpreted as assuming atomic or molecular pairs as units of the assembly, whilst the other has atoms and molecules as units. The cluster variation or the quasi-chemical treatment has been extended by Guggenheim [78] to treat the cases in which triangles and tetrahedra are units of the assembly.

8.11 Orientational and Substitutional Disorder Coupling

So far we have introduced a coupling between orientational and substitutional disordering processes in a manner that ignores any variation of the orientational configurational energy with composition. This has been achieved by ignoring orientational short-range order effects in the model. We now wish to expand the model to allow for these short range order effects, at least qualitatively.

We have already established the fact that the temperature range over which the rotational transition occurs varies with composition. That is the primary transition temperature is a minimum at the racemic composition where the transition temperature range is the greatest. Substitutional short range effects are found to be inversely proportional to temperature and proportional to the product $x_d(1-x_d)$. Orientational short-range order effects, on the other hand, would appear with the same temperature dependence; but would not contain the product $x_d(1 - x_d)$. Their variation with composition would arise indirectly particularly from the variation of the primary transition temperature with composition. Thus the orientational short-range order effects should vary relatively slowly with composition with a maximum effect at the racemic composition.

Expanding the orientational configuration energy in the Kirkwood

approximation we have

$$\{\hat{E}(\sigma_1) - \Delta E_0''(1)\}/RT = \mu_1''\frac{\Delta E_0''}{RT} - \tfrac{1}{2}\left(\frac{\mu_2''}{2!z}\left(\frac{2\Delta E_0''}{RT}\right)^2 + \frac{\mu_3''}{3!z^2}\left(\frac{2\Delta E_0''}{RT}\right)^3 + \ldots\right) \quad (8.51)$$

where

$$\mu_1'' = \sigma_1(1-\sigma_1)$$

$$\mu_2'' = \mu_1''^2$$

$$\mu_3'' = \frac{(n\sigma_1-1)^2\mu_1''^2}{n-1} \quad (8.52)$$

and $\Delta E(1) = 0$. The identity $s_1 = (n\sigma_1-1)/(n-1)$ has been used in obtaining μ_3''. Equation (8.51) is similar to equation (8.16). Thus equation (8.19) takes the form (to the third central moments)

$$A_c(\sigma,s,x_d) - A_c(1,1,x_d) = RT[\psi_\sigma+\psi_s(s,x_d)-\psi_s(1,x_d)] + \mu_1''\Delta E_0'' - \mu_2''\frac{\Delta E''^2}{zRT}$$

$$- \frac{2\mu_3''}{3}\frac{\Delta E_0''^3}{(zRT)^2} - (1-s_1)\{\mu_1\Delta E - \mu_2\frac{\Delta E^2}{zRT} - 2\mu_3\frac{\Delta E^3}{(zRT)^2}\} \quad (8.53)$$

Stationary conditions with respect to orientational disorder must satisfy the following equation.

$$ln\left(\frac{(1-\sigma_1)}{(n-1)\sigma_1}\right) = \left(\frac{1-2\sigma_1}{RT}\right)\left(\Delta E_0'' - 2\mu_1\frac{\Delta E_0''^2}{zRT} - \{\frac{2(n\sigma_1-1)\mu_1''}{n-1} + \frac{2n\mu''^2}{3(n-1)(1-2\sigma_1)}\}\cdot\right.$$

$$\left.\cdot\frac{\Delta E''^3}{(zRT)^3}\right) + \left(\frac{n\{\mu_1\Delta E - \mu_2\Delta E^2/zRT - 2\mu_3\Delta E^3/3(zRT)^2\}}{4(n-1)RT}\right) \quad (8.54)$$

The stationary conditions with respect to s, and x_d are still governed by equations (8.17) and (8.21), and appear to be independent of σ_1. Values of σ_1, s, and x_d that minimise the free energy (for the simple cases only) are still similar to those defined by equation (8.9), which turn out to correspond to situations in which the coupling vanishes.

The inclusion of orientational short-range order in our model has the effect of lowering the secondary plastic-phase transition temperature if the primary transition temperature is fixed and vice versa. The

orientational short-range order effects cancel out some of the substitutional short-range order effect. In the case of the phase diagram of camphor it is the substitutional order effects that are dominant around the racemate composition, and the effect of short-range orientational order is to flatten the submaximum. The effects from both short-range orientational and substitutional disorder take maximum values at the racemate composition because this is where the primary transition temperature is least for the same values of the long-range order parameters. However, since the orientational short-range order effects vary more slowly relative to the substitutional order effects the former is not expected to change the shape of the phase diagram significantly. The primary transition temperature, concerned with the disappearance of long-range order is still approximated by equation (8.24) and the secondary transition temperature is given by the following equation.

$$T_c = \hat{T}_c + \left(zR\hat{T}_c \{\mu_2 \Delta E^2 - \mu_2'' \Delta E_0''^2\} + \frac{2}{3}\{\mu_3 \Delta E^3 - \mu_3'' \Delta E_0''^3\} \right) / (zR\hat{T}_c)^2 R^3 \ell n n \quad (8.55)$$

where $\hat{T}_c$ is the primary transition temperature. It is again stressed that the use of equations (8.24) and (8.55) only gives rough estimates of the temperatures concerned. A better treatment would involve an iterative search of the secondary transition temperatures from temperatures below, but in the vicinity of the plastic-phase transition. This iterative search would take into account contributions from short-range order effects at both temperatures. In doing this a more applicable value of the substitutional disordering energy could be found for that temperature range, which in turn would be used to generate the phase diagram.

When the computation of the phase diagram was repeated using equations (8.34) and (8.55), and fixing the secondary transition temperature a phase diagram was found very similar to figure 8.4 except that the temperature at the cusp and the primary transition temperature were

slightly lowered. It should also be noted that the forms of equations (8.26) and (8.36) are not affected by the present extension.

8.12 Mole Fraction and the Degree of Substitutional Long-Range Order

There exists a discrepancy in the usage of the degree of substitutional long-range order in the literature. The definition of the substitutional long-range order parameter we have employed here is according to references [75] and [76], and was also the one adopted in the original paper by Kirkwood [80]. The degree of substitutional long-range order can be defined as follows [76].

$$s = (R - W)/(R + W) \tag{8.57}$$

where R is the total number of d-molecules occupying a D-lattice (proper lattice) and W is the total number of d-molecules occupying an L-lattice (an improper lattice). Clearly, s = 1 when W = 0 corresponding to a superlattice or complete separation of components from the mixture; and s = 0 when W = R corresponding to the substitutionally disordered phase. It follows from this definition that there is no direct functional relationship between s and the mole fraction x_d except through equations (8.10) and (8.11), and also that s = 1 (always) in pure substances (e.g. $x_d = 0$). The last aspect simply arises from the indistinguishability of the two-sublattices and constituent atoms or molecules.

Guggenheim [13], however, uses the following functional relationship between mole fraction and the degree of substitutional long-range order, which he attributes to Bragg and Williams.

$$s = 2x_d - 1$$

or

$$x_d = \tfrac{1}{2}(1 + s) \tag{8.58}$$

He argues further that the usage of the variable s instead of x by pioneer workers in this field is merely a historical accident. This observation is obviously a result of a misunderstanding and the relationship he refers to between s and x_d is not valid. For example this would mean that when $x_d = \frac{1}{2}$, the long-range order parameter s would always be zero. Thus an equicomponent system consisting of two types of atoms or molecules could never form a superlattice. In fact the superlattice phenomena could only be associated with the pure components. These implications derived from equation (8.58) are contrary to experimental evidence. Therefore the following equations which are Guggenheim's interpretation [77] of the central moments of the configurational energy distributions derived by Kirkwood for an equicomponent system in a two-sublattice crystal do not apply.

$$\mu_2 = x_d^2(1 - x_d)$$
$$\mu_3 = x_d^2(1 - x_d)^2(1 - 2x_d)^2 \qquad (8.59)$$

These results are readily obtained by applying the identities (8.58) on equation (8.17). We comment in passing that the theoretical treatment of co-operative phenomena presented in his textbook [13] must be interpreted with care. Equations with mole fraction as a parameter describe chemical systems in the absence of long-range order so that fractions of molecules in any state are simply proportional to mole fractions. When he uses degree of substitutional long-range order s the equations describe an equicomponent system of two molecular species with the degree of order varying. The former gives the relative thermodynamic stability between systems of different compositions whilst the latter is an analysis of substitutional order-disorder transition and gives, among other things, the Curie temperature for the system with mole fraction equal to $\frac{1}{2}$.* Guggenheim discusses these two aspects of crystal statistics without

---

* For example, the former treatment would give $RT_c^{(s)} = 2x_d(1-x_d)\Delta E$ as in equation (8.33) with $R(T_c^{(s)})_{max} = \frac{1}{2}\Delta E$ corresponding to $x_d = \frac{1}{2}$. The latter would give $RT_c^{(s)} = \frac{1}{2}\Delta E$ for all compositions and therefore defines the maximum critical temperature only (see footnote on page 152).

distinguishing the difference between them.

8.13 Discussion

8.13.1 Camphor

Our model explains the phase diagram of camphor with respect to the rotational III → II phase transition as a result of coupling between orientational and substitutional disorder which vanishes in the plastic phase due to isotropy. The general features of the phase diagram are generated by two modes of mixing with the superlattice mode preceding the domain mode in the mole fraction coordinate where the cusp represents the composition at which the mixing modes change. Our observation in connection with the cusp corresponds to the postulate due to Anderson *et al* which attributes it to a change of lattice.

The model has taken a too extreme view for the case of camphor in one respect. The molecular partition function for the rotational transition as defined in chapter 7 has been assumed to be independent of composition. This may not be true for mixtures since in this case the temperature range over which the phase transition occurs varies with composition, and the effects of short-range order on the molecular partition function have not been allowed for by assuming an Einstein model for the solid in which they are irrelevant.

The discrimination energy between *d*- and *l*-molecules of camphor does not completely vanish in the plastic phase due to isotropic molecular fields. This fact is reflected by a rather small depression in the transition temperature at the reconstructive II → I phase transition before the melting point (Fig. 2.4). It has, however, been shown elsewhere in this chapter that essentially the same expressions are obtained whether or not complete isotropy is assumed after the rotational transition.

The interaction energies of mixing, ΔE and ΔE_{dl} must be positive in order to explain the phase diagram of camphor. We recall from equation (8.7) that $\Delta E = zN(E_{dd} - E_{dl})$. If we identify zE_{dd} and zE_{dl} as sublimation energies per molecule then ΔE is the *substitutional discrimination energy* identical to the chiral discrimination energy which we have defined in chapter 5. On the other hand the interchange energy ΔE_{dl} between molecules on *d*- and *l*-domains may not be related to a discrimination energy of the type encountered so far.

Our analysis, however, does not allow for the reconstructive transition associated with the rotational transition in camphor. This introduces difficulties in the estimation of substitutional interaction energies directly from the phase diagram of camphor. Thus the values of the interaction energies used for the prediction of the phase diagram are likely to be rather large as they include the effect of the reconstructive transition. However the interaction energy for the superlattice mode of mixing is known from the calculation of discrimination energies in chapter 5. Using this value in equation (8.41) we have calculated T_c^s at $x_d = 0.25$ (where the functions intersect) to be 179 K. Solving for the interchange energy in equation (8.33) at this temperature and composition we obtained the following result, $\Delta E_{dl} = 1.32$ kJ/mole. Using this result in equation (7.39), the value of T_c^D at $x_d = 0.5$ was found to be 59 K. This implies that the assumption of complete substitutional disorder in the phase stable below the rotational transition is reasonable. This also accounts for the lack of eutectic behaviour on the phase diagram of camphor.

8.13.2 Camphoric Anhydride

The phase diagram of camphoric anhydride is shown in figure 2.8. It is seen that the conditions which must be fulfilled by the appropriate model are different from those applicable in the case of camphor and may be summarised as follows. The model must allow for phase separation as implied by the existence of eutectic behaviour. The eutectic line is discontinued in the region of the submaximum as the experimental points indicate. However, the discontinuity of the eutectic line is not highly definite because of the difficulty of magnifying a vanishing peak on the shoulder of a large endotherm on a DSC thermogram (see Chapter 2). The model should again generate a submaximum in the phase diagram at the racemic composition. The characteristics of this submaximum are difficult to establish because of its diminished size on the actual submaximum, although it is still large enough to be significant even if experimental errors are taken into account.

The fact that a monoclinic centrosymmetric crystal lattice is observed for *dl*-camphoric anhydride at room temperature implies that the racemic mixture exists as a distorted superlattice in this temperature range. Dielectric studies reveal some similarity in the relaxation mechanisms present in the non-rotator phases of *d*- and *dl*-camphoric anhydride. The relatively higher dielectric absorption observed in the latter would seem to suggest that the solid of the racemic mixture is slightly more orientationally disordered than the optical isomer. The presence of some disorder is also revealed in the diffraction patterns of the non-rotator phases of *d*- and *dl*-camphoric anhydride obtained by Dr. M. Sterns in which the latter was associated with considerably more background radiation than the former. Thus the racemic composition in the non-rotator phase II (above room temperature) may be considered as a special arrangement of equal numbers of the two

types of molecules forming a slightly imperfect superlattice with little long-range disorder ($s \sim 1$)*.

Assuming an excess repulsion between molecules of different types relative to that between identical molecules, then (for $x_d \neq x_l$) regions in which d- and l-molecules make nearest neighbours are relatively unstable. These pockets of instabilities transform into the plastic phase earlier than regions in which identical molecules make neighbours to each other. The proportion of the unstable regions will increase with $x_D \rightarrow 0.5$ and the energy change associated with their transition increases as well. On the other hand the number of molecules in the pure regions decreases as $x_d \rightarrow 0.5$ with a consequent decrease of this part of the transition energy. This process is discontinued in the composition range $0.4 < x_d < 0.6$ when the perturbation on the lattice due to repulsion between different molecules is so dominant that even the minority pure component-regions begin to transform at the same temperatures as the mixed regions. At the same time contributions from short-range order effects begin to show their effect in much the same way as they did in camphor. However, their effect in this case is negligible mainly because of the fact that the magnitudes of the central moments are very small (since $s \sim 1$, see equation (8.18)) and the transitions occur at high temperatures. The constancy of the transition energy (the sum of the two transitions in the case of the composition ranges $0 < x_d < 0.4$ and $0.4 < x_d < 1$) simply implies that the configurational energy of mixing (including the sum of the substitutional short-range order terms) is insignificant relative to that of the plastic phase transition energy for the pure components.

The conventional way [81],[82] of looking at the phase diagram of camphoric anhydride would be to observe the differences between the observed crystal systems and molecular volumes of the isomers and the

---

* T_C^S for the non-rotator phase has been calculated using (8.41) with x_d=0.5 to be 4.2×10^3 K. Note that complete isotropy is achieved in the rotator phase, in this case, as T_M is invariant with composition.

racemate, where the composition $x_d = \frac{1}{2}$ is now treated as a compound. The discontinuous eutectic line would then imply partial miscibility between the molecules on an orthogonal lattice of the optical isomers and the monoclinic lattice of the racemate. The region under the submaximum would then be treated as the miscibility gap, a region in which the optical isomers make solid solutions with the racemate. However, all evidence accumulated so far refutes the existence of a racemic compound,* and therefore the conventional approach does not apply in this phase diagram.

8.13.3 Camphor Oxime

The phase diagram of camphor oxime has already been discussed in chapter 2. This system presents new features not present in the camphor and camphoric anhydride systems. These new features include the apparent discontinuity of the strongly composition dependent and low energy III → II reconstructive transition and the marginal dependence of composition of the rotational II → I transition. We also recall that the III → II reconstructive transition carries the unknown racemate lattice below the transition to the monoclinic lattice of the isomer. It is also evident that this transition introduces complete mutual solubility in phase II which is reflected by the reduced composition dependence of the II → I rotational transition. The discontinuity in the reconstructive transition marks the composition at which the crystal lattice begins to change from that of the isomer to that of the racemate below the III → II transition. The maximum on the phase diagram can also be explained as due to short-range order effects of the type defined in an equation of the form of (8.36) with the constant A containing the reconstructive transition energy of the pure component, where the reconstructive transition is of the type present at the racemate composition but absent in the pure components.

---

* Note that the existence of a racemic compound would be consistent with negative values of ΔE or ΔE_{dl}. In such cases the phase diagram would be characterised by a rise in the transition temperature to a maximum about

8.13.4 Some Observations on Phase Diagrams of Camphor-type Compounds

In general, it is found that although the phase diagrams of *d*- and *l*-systems of camphor-type compounds are similar there are gross differences in the fundamentals involved. The three systems studied seem to define the rule that the low temperature transitions are generally more composition dependent that those at high temperatures. This applies to both reconstructive and rotational transitions, and would be expected to apply at the melting transition also if no other transition generally of greater entropy occurs in the solid state. The effect of any phase transition with rising temperature is to increase the entropy and isotropy in the molecular potential surface. The independence of the melting point with composition is a consequence of the isotropy acquired by the system consisting of any composition through a series of solid state transitions of both the reconstructive and rotational types. This is a very important feature which is common to all the three systems studied.

Some isotropy is achieved at each phase transition. It is therefore necessary to allow for their effects explicitly in the analysis of phase diagrams. Observe that treatments analogous to the one used to analyse the portion of the phase diagram concerned with the rotational transition would be applied to the melting transition if the melting point were composition dependent. This could be done by simply replacing the partition function for orientational disorder by that of positional disorder developed in chapter 6.

Short-range order effects depend on the magnitude of the interaction energies of the system, the magnitude of the corresponding long-range order parameter, temperature and, for the case of substitutional disorder only, composition. Thus if the acquired isotropy after a phase transition alters the interaction energies, then these short-range order effects are altered also. The most important of these short-range order effects in

---

x_d = 0.5, provided the degree of substitutional order does not vary within each phase. Short range order effects, in this case, would tend to promote the maximum. This is how the well known phase diagram of *d*- and *l*-carvoxime can be explained according to our model.

the systems studied are of the substitutional-type and these have been found to be of varying significance in the phase diagrams. The magnitude of the changes in the substitutional short-range order effects vary with composition at any given temperature with the largest value obtained at the 50% composition for symmetric mixtures. It is found that the submaxima found in the phase diagrams of camphor-type compounds can in the main be attributed to changes in the substitutional short-range order effects.

In conclusion, chapters 4 and 5, have succeeded in providing some theoretical explanations concerning solid-state phase equilibria from both crystal packing and statistical mechanical points of view. Still further theoretical consideration is required in the following directions. How can the substitutional interaction energy in the domain model be evaluated independently? We have shown that the substitutional interaction energy in the superlattice model can be evaluated directly from sublimation energies. What factors determine the relative magnitudes of the two interaction energies? These are some of the questions that have to be answered before much progress is achieved in the theory of solid-state phase equilibria.

bibliography

1. Guthrie G.B. and McCullough J.P., *J.Phys.Chem.Solids* 18(1), 53 (1961).

2. Timmermans J.T., *J.Phys.Chem.Solids* 18(1), 1 (1961).

3. Craig D.P. and Schipper P.E., *Proc.R.Soc.Lond.* A342, 19 (1975).

4. Craig D.P., Ladon L. and Stiles P.J., *Proc.R.Soc.Lond.* A343, 11 (1975).

5. Darmon I. and Brot C., *J.Mol.Cryst.* 2, 301 (1967).

6. Fyfe C.A., *Faraday Transactions II* 10, 1633 (1974); 10, 1642 (1974).

7. Kohler F., 'The Liquid State', Section 6.4, Verlag Chemie, (1972).

8. Lennard-Jones J.E. and Devonshire A.F., *Proc.Roy.Soc.* A169, 317 (1939); A170, 464 (1939).

9. Pople J.A. and Karasz F.E., *J.Phys.Chem.Solids* 18, 28 (1961); Karasz F.E. and Pople J.A., *J.Phys.Chem.Solids* 20, 294 (1961).

10. Amzel L.M. and Becka L.N., *J.Phys.Chem.Solids* 30, 521 (1969); 30, 2495 (1969).

11. Aston J.G., *J.Chem.Therm.* 1, 241 (1969).

12. Reynolds P.A., *Mol.Phys.* 28(3), 633 (1974).

13. Guggenheim E.A., 'Thermodynamics', Ch. 7, pp 320-334, North Holland Publishing Co., (1959).

14. Ubbelohde A.R., *British J.Appl.Physics* 7, 313 (1956).

15. Westrum E.F. and McCullough J.P., 'Physics and Chemistry of the Organic Solid-State', V. 1, Ch. 1, edited by Fox *et al*, Interscience (1963).

16. Buerger M.J., *Sov.Phys.-Crystallography* 16(6), 959 (1972).

17. Ubbelohde A.R., 'Melting and Crystal Structure', pp 201-213, Oxford University Press (1965).

18. O'Neil M.J., *J.Anal.Chem.* 36(7), 1238 (1964).

19. 'Instructions - Differential Scanning Calorimeter', Perkin-Elmer Corporation, Norwalk, Conn., Rev. Sept. 1967.

20. Thermal Analysis Newsletter No. 5, Anal. Div., Perkin-Elmer Corporation, Norwalk, Conn.

21. Williams H.W. and Chamberland B.L., *J.Anal.Chem.* 41(14), 2084 (1969).

22. Thermal Analysis Newsletter No. 2, Anal. Div., Perkin-Elmer Corporation, Norwalk, Conn.

23. Huntress E.H. and Mulliken S.P., 'Identification of Pure Organic Compounds', p.373, John Wiley & Sons (1941).

24. Schäfer K.L. and Wagner, U., *Z.Electrochem.* 62, 328 (1958).

25. Anderson J.E. and Slichter W.P., *J.Chem.Phys.* 41(7), 1922 (1964).

26. Adriani J.H., *Z.Physik.Chem.* 33, 469 (1900).

27. Komorov P., Likhter A. and Ruhemann M., *Z.Tech.Fisik* 5, 1723 (1935).

28. Oonk H.A.J. and Hulscher J.B., *Acta Cryst.* 13, 851 (1960).

29. Aston J.G., 'Physics and Chemistry of the Organic Solid State', Vol. 1, edited by Fox *et al*, Interscience (1963).

30. Yager W.A. and Morgan S.O., *J.Am.Chem.Soc.* 57, 2072 (1935).

31. Meakins R.J., 'Progress in Dielectrics', V.3, pp 150-202.

32. Kittel C., 'Introduction to Solid State Physics', 3rd edition, John Wiley and Sons (1968).

33. Hill N.E., Vaughan W.E., Price A.H. and Davies M., 'Dielectric Properties and Molecular Behaviour', Van Nostrand (1969).

34. Smyth C.P., 'Dielectric Behaviour and Structure', McGraw-Hill (1955).

35. Thompson A.M., *Proc.Inst.Elect.Eng.* 103B(12), 704 (1956).

36. Williams D.E. and Smyth C.P., *J.Am.Chem.Soc.* 84, 1808 (1962).

37. Rossiter V., *J.Phys.C: Solid State Phys.* 5, 1969 (1972).

38. Williams J.O., Cox G.A. and Thomas J.M., *J.Phys.Chem.* 71(5), 1542 (1967).

39. Clemmett C. and Davies M., *Trans.Far.Soc.* 58, 1718 (1962).

40. Le Fèvre C.G. and Le Fèvre R.J.W., 'Physical Methods of Organic Chemistry', Ch. XXXVI, Edited by A. Weissberger, 3rd edition, Interscience.

41. Hecht H.G., 'Magnetic Resonance Spectroscopy', Ch. 3 and 4, John Wiley and Sons (1967).

42. Slichter C.P., 'Principles of Magnetic Resonance', Ch. 3 and 5, Harper and Row (1963).

43. Andrew E.R., 'Magnetic Resonance', p. 163, editors: Coogan *et al*, Plenum Press (1970).

44. The NMR-EPR Staff of Varian Associates, 'NMR and EPR Spectroscopy', Pergamon Press (1960).

45. Andrew E.R., 'Magnetic Resonance', Rehovolt and Jerusalem, p.41 editor: Fiat D., I.U.P.A.C. (1971).

46. Waugh J.S. and Fedin E.I., *Soviet Physics - Solid State* 4(8), 1633 (1963).

47. Hendrickson J.R. and Bray P.J., *J.Mag.Res.* 9, 341 (1973).

48. Moskalev V.V. and Petrov M.P., *Soviet Physics - Solid State* 5(5), 1018 (1963).

49. Warshel A. and Lifson S., *J.Chem.Phys.* 53(2), 582 (1970).

50. Warshel A. and Karplus M., *J.Am.Chem.Soc.* 94(16), 5612 (1972).

51. Schäfer K. and Frey O., *Z.Electrochem.* 56(9), 882 (1952).

52. CRC Handbook of Chemistry and Physics, 54th ed. (1973), CRC Press.

53. Williams D.E., *Acta Cryst.* A29, 408 (1973).

54. Gordon A.J. and Richard A.F., 'The Chemist's Companion', J. Wiley and Sons (1972).

55. Salem L., 'The Molecular Orbital Theory of Conjugated Systems', W.A. Benjamin N.Y. (1966).

56. Robey M.J., Sterns M., Morris H.M., and Ross I.G., *J.Cryst.Mol.Struct.* 1, 401 (1971).

57. Williams D.E., *Acta Cryst.* A25, 464 (1969).

58. Craig D.P., Mason R., Pauling P. and Santry D.P., *Proc.Roy.Soc.* A286, 98 (1965).

59. Kitaigorodskii A.I., *Acta Cryst.* 18, 585 (1965).

60. Williams D.E., *Acta Cryst.* A30, 71 (1974).

61. Morris J.M., *Molecular Physics* 28(5), 1167 (1974).

62. Mirsky K., *Acta Cryst.* section A, in press.

63. Chandrasekhar S., Shashidar R. and Tara N., *J.Phys.Chem.Solids* 10, 337 (1970); *J.Mol.Cryst. and Liquid Cryst.* 12, 245 (1971).

64. Webster D.S. and Hoch M.J.R., *J.Phys.Chem.Solids* 32, 2663 (1971).

65. Rowlinson J.S., *J.Phys.Chem.Solids* 18(1), 78 (1961).

66. Chadwick A.V. and Sherwood J.N., 'Diffusion Processes', V.2, Ch.6.1, Gordon and Breach (1971).

67. Jhon M.S. and Eyring H., 'Physical Chemistry - An Advanced Treatise', Vol. VIIIA, Ch.5, editors: Eyring *et al*, Academic Press (1971).

68. Chen Sow-Hein, 'Physical Chemistry - An Advanced Treatise', Vol.VIIIA, Ch.2, editors: Eyring *et al*, Academic Press (1971).

69. Bondi A., 'Physical Properties of Molecular Crystals, Liquids and Glasses', John Wiley and Sons (1968).

70. Flubacher P., Leadbetter A.J. and Morrison J.A., *Proc.Phys.Soc. (London)* 78, 1449 (1961).

71. Hirschfelder J.O., Stevenson D.P. and Eyring H., *J.Chem.Phys.* 5, 896 (1937).

72. Stiler H. and Haulecler S., *Proc. AEA Conf. Inelastic Scattering of Neutrons in Solids and Liquids*, p. 281 (1962).

73. Lord R.C., Ahlberg J.E. and Andrews D.H., *J.Chem.Physics* 5, 649 (1937).

74. Dunning W.J., 'Physics and Chemistry of the Organic Solid State', Vol. 1, editors: Fox *et al*, Interscience (1963).

75. Fowler R. and Guggenheim E.A., 'Statistical Thermodynamics', pp 566-582, Cambridge University Press (1949).

76. Sato H., 'Physical Chemistry - An Advanced Treatise', Vol. X, Ch.10 editors: Eyring *et al*, Academic Press, (1970).

77. Guggenheim E.A., 'Mixtures', Ch. IV, Oxford University Press (1952).

78. Guggenheim E.A., 'Applications of Statistical Mechanics', Ch. 6, Oxford University Press (1966).

79. Easthope C.E., *Proc.Camb.Soc.* 33, 502 (1937).

80. Kirkwood J.G., *J.Chem.Phys.* 6, 70 (1938).

81. Kitaigorodskii A.T., 'Organic Chemical Crystallography', English Translation by Consultants Bureau Inc, New York, p.231 (1961).

82. Robinson P.M., Rosell H.J. and Scott H.G., *J. Mol.Cryst.Liq.Cryst.* 10, 61 (1970).